AWARD NUMBER: W81XWH-15-1-0228

TITLE: Characterizing Myeloid Cell Activation in NF1 Vasculopathy

PRINCIPAL INVESTIGATOR: Brian Stansfield

CONTRACTING ORGANIZATION: Augusta University

REPORT DATE: March 2019

TYPE OF REPORT: Final Report

PREPARED FOR: U.S. Army Medical Research and Materiel Command
Fort Detrick, Maryland 21702-5012

REPORT DOCUMENTATION PAGE

Form Approved
OMB No. 0704-0188

1. REPORT DATE	2. REPORT TYPE	3. DATES COVERED
March 2019	Final Report	1 July 2015 – 31 Dec 2018

4. TITLE AND SUBTITLE

Characterizing Myeloid Cell Activation in NF1 Vasculopathy

5a. CONTRACT NUMBER
W81XWH-15-1-0228

5b. GRANT NUMBER
W81XWH-14-NFRP-NIA

5c. PROGRAM ELEMENT NUMBER

6. AUTHOR(S)
Brian Stansfield

E-Mail: bstansfield@augusta.edu

5d. PROJECT NUMBER

5e. TASK NUMBER

5f. WORK UNIT NUMBER

7. PERFORMING ORGANIZATION NAME(S) AND ADDRESS(ES)
Augusta University 1120 15th St, Augusta, GA 30912

8. PERFORMING ORGANIZATION REPORT NUMBER

9. SPONSORING / MONITORING AGENCY NAME(S) AND ADDRESS(ES)

U.S. Army Medical Research and Materiel Command
Fort Detrick, Maryland 21702-5012

10. SPONSOR/MONITOR'S ACRONYM(S)

11. SPONSOR/MONITOR'S REPORT NUMBER(S)

12. DISTRIBUTION / AVAILABILITY STATEMENT

Approved for Public Release; Distribution Unlimited

13. SUPPLEMENTARY NOTES

14. ABSTRACT

Our original proposal seeks to understand the mechanisms underlying macrophage recruitment and activation in NF1-related vasculopathy. We have developed two mouse models that closely recapitulate NF1-related arterial stenosis and aortic aneurysm formation and propose to examine the contribution of MCP-1/CCR2 signaling and redox biology to these pathologies. As aneurysm and arterial stenosis represent two ends of a continuum, perturbations in macrophage recruitment and redox biology may underlie both pathologies; therefore, we have attempted to take a broad approach to both models in regards to these mechanisms. We have completed all proposed experiments, which have been described in several high-impact publications with multiple manuscripts undergoing Editorial Review for publication.

15. SUBJECT TERMS
neurofibromatosis, NF1, aneurysm, stenosis, smooth muscle, macrophages, MCP1, CCR2, ROS

16. SECURITY CLASSIFICATION OF:			17. LIMITATION OF ABSTRACT	18. NUMBER OF PAGES	19a. NAME OF RESPONSIBLE PERSON
a. REPORT	b. ABSTRACT	c. THIS PAGE			USAMRMC
Unclassified	Unclassified	Unclassified	Unclassified	131	19b. TELEPHONE NUMBER *(include area code)*

Table of Contents

	Page
1. Introduction……	**4**
2. Keywords……	**4**
3. Accomplishments……	**4**
4. Impact……	**6**
5. Changes/Problems……	**6**
6. Products……	**7**
7. Participants & Other Collaborating Organizations……	**8**
8. Special Reporting Requirements……	**9**
9. Appendices……	**10**

Introduction:

The overarching theme of our NF1YI proposal is to gain mechanistic insight and develop therapeutic targets for the prevention/treatment of neurofibromatosis type 1 (NF1) related cardiovascular diseases. Cardiovascular disease affects upwards of 10% of the more than 2,000,000 persons with NF1 worldwide and presents with lesions in the proximal arteries such as arterial stenosis and aneurysm formation. We have developed murine models that closely resemble NF1 arterial stenosis and aneurysm formation, which are both primarily mediated through the infiltration of bone marrow-derived myeloid cells into the vascular wall in *Nf1* heterozygous mice. However, the pathological consequences of these cells are somewhat opposed, wherein arterial stenosis is the result of smooth muscle cell proliferation and inward remodeling and aneurysms are the result of smooth muscle cell apoptosis and outward remodeling. To better understand how neurofibromin-deficient myeloid cells can lead to different pathological outcomes, we propose to interrogate the recruitment of macrophages via monocyte chemotactic peptide-1 (MCP-1) stimulation of its receptor (CCR2) and the generation of reactive oxygen species, which are generated in excessive quantities by neurofibromin-deficient macrophages in our arterial stenosis and aneurysm models, respectively.

Keywords:

neurofibromatosis; stenosis; aneurysm; MCP-1; CCR2; reactive oxygen species; superoxide; macrophages; monocytes; arteries; cardiovascular disease

Major Goals and Accomplishments:

We have completed all of the major goals and experiments outlined in our DOD YI proposal. Outlined below are the original aims and a summary of experimental results and progress to date.

Aim 1: Test the hypothesis that upregulated MCP-1/CCR2 signaling drives macrophage homing and augments arterial stenosis in $Nf1^{+/-}$ mice.

We have completed the proposed experiments in Aim 1. We reported in a previous publication that compound mutant *Nf1+/-;CCR2-/-* do not develop neointima formation and arterial remodeling closely resembles our observations in WT C57Bl/6 mice. This is in stark contrast to *Nf1*+/- mice with intact CCR2 expression, which develop a robust neointima with marked macrophage infiltration. We also showed that treatment of *Nf1*+/- mice with a potent CCR2 inhibitor following carotid artery ligation rescues the phenotype and may be a viable therapeutic option for NF1 patients with arterial stenosis.

We have also completed the bone marrow transplant studies, which introduce *CCR2* knockout marrow into *Nf1*+/- animals. Following engraftment, *Nf1*+/- mice with CCR2-deficient and intact bone marrow cells were subjected to carotid artery ligation and neointima formation was studied as described. We showed that CCR2 signaling in bone marrow cells is required to produce the enhanced neointima observed in *Nf1*+/- mice. These findings are included in a forthcoming manuscript to be submitted in April 2019. Collectively, these data strongly implicate that CCR2 expression is required for NF1-arterial stenosis.

As mentioned in the previous report, we have completed *in vitro* studies to assess MCP-1 induced *Nf1*+/- SMC proliferation and migration. The results of these experiments were published in *Hum Molec. Genet.* in 2016. We observed that MCP-1 appears to preferentially activate Ras-Akt signaling in *Nf1*+/- macrophages, which is surprising considering our previous observation that Mek-Erk inhibition showed a dose-responsive reduction in *Nf1*+/- neointima formation (American Journal of Pathology, 2014). In follow up experiments, we have identified that inflammatory *Nf1* knockout macrophages display enhanced Akt activation; whereas, patrolling macrophages demonstrate more Erk activation. MCP-1, largely thought to mobilize inflammatory monocytes, appears to enhance M1 (inflammatory) macrophage mobilization. As a future direction, we are working to understand differential activation of Ras kinases in these macrophage subpoulations.

Major Goals for SA1:

1. Generation of experimental mice (0-12 months)

a. We have generated the experimental compound mutant mice outlined in SA1 and have completed the proposed experiments using these mice. A manuscript describing these results was published in *Human Molecular Genetics* in 2016.

2. Generation of chimeric mice (0-12 months)
    a. We have generated the appropriate experimental and control mice as outlined in the proposal and have completed experiments in these mice. Please see **Figure 1 and Figure 2** in the appendix for experimental results.

3. Carotid artery ligation (6-18 months)
    a. We have performed carotid artery ligation on our compound mutant mice and chimeric mice generated for this proposal.

4. Analysis of SMC proliferation and migration *in vitro* (0-12 months)
    a. We have completed experiments in cultured SMC as outlined in SA 1

5. Analysis of macrophage recruitment *in vivo* (6-12 months)
    a. We have completed experiments proposed to study $Nf1^{+/-}$ macrophage function *in vivo* using a peritonitis model. To provide more mechanistic insight, we studied cultured $Nf1^{+/-}$ and WT macrophage response to MCP-1. Cells were harvested from the bone marrow and derived with macrophage colony stimulating factor (M-CSF). Proliferation and migration along with Ras activity were studied in similar assays proposed in our SMC *in vitro* studies. We showed that MCP-1 is a potent agonist of $Nf1^{+/-}$ macrophage proliferation and migration via Erk and Akt activation.
    b. Please see **Figure 3** in the appendix for results of *in vivo* macrophage recruitment in *Nf1*+/- and WT mice.

Aim 2: Test the hypothesis that enhanced ROS production by $Nf1^{+/-}$ macrophages induces SMC proliferation, thus promoting inward arterial remodeling.

We have generated all cohorts of *Nf1*+/-; *p47*-/- mice and completed all proposed experiments. We show that deletion of the NOX2 subunit suppresses aneurysm formation in response to AngII (**Figure 4)**. Moreover, we provide evidence that the severity of aneurysms is reduced along with markers of inflammation. These phenotypic changes are supported mechanistically by our observations that reactive oxygen species production is increased in the arterial wall of *Nf1*+/- mice when compared to WT mice and this relationship is exacerbated in response to continuous AngII infusion.

In vitro experiments have substantiated our preliminary data that neurofibromin-deficient macrophages generate excessive quantities of ROS and that ROS production is largely dependent on downstream Ras kinase activation. Further, we show that nitritive stress, a common form of free radical formation, is enhanced in neurofibromin-deficient macrophages via a Ras-dependent mechanism (**Figure 5**).

Finally, we have identified that AngII infusion upregulates Ras kinase activity in smooth muscle cells (SMC) via a neurofibromin-regulated mechanism. Interestingly, we identify that cleaved caspase-3 is highly upregulated in response to oxidative stress, which suggests that the excessive ROS produced by neurofibromin-deficient macrophages in response to AngII appears to upregulate SMC apoptosis (**Figure 6**). This may be an underlying mechanism for aneurysm formation in these animals although directly linking ROS to SMC apoptosis in *Nf1*+/- animals remains to be demonstrated.

Major Goals for SA2:

1. Generation of $Nf1^{+/-}$;$p47^{phox-/-}$ mice (12-36 months)
    a. We have generated the experimental compound mutant mice outlined in SA2 and have completed the proposed experiments using these mice.

2. Angiotensin II infusion

a. We have completed all experiments using angiotensin II infusion. We identified that p47 deletion blocks aneurysm formation in *Nf1*+/- animals following AngII infusion. We are completing the final manuscript detailing these findings and will submit for publication in April 2019

3. Analysis of *Nf1*+/- SMC apoptosis
    a. We have completed experiments in *Nf1*+/- and WT smooth muscle cells (SMC). Interestingly, we found that Erk activity is markedly increased in *Nf1*+/- SMC in response to AngII and that hydrogen peroxide enhances *Nf1*+/- SMC apoptosis. We have included these findings in the forthcoming manuscript.

Opportunities for training and professional development

Nothing to report

Dissemination of Results

Results from this proposal have been published in high-impact, peer-reviewed journals (see appendix). Further, we have presented preliminary data from this proposal and results from the experimental approach at international meetings including the Children's Tumor Foundation, American Heart Association, and Pediatric Academic Societies. In addition, we held an informal town hall-style meeting with community members affected by neurofibromatosis and other rasopathies in December 2018. This was a unique opportunity to speak directly with family members and those with neurofibromatosis about our research, future directions, and opportunities for community participation.

Plan for reporting in coming fiscal year

Nothing to report

Impact:

Our experimental results from this proposal are critical to forming a comprehensive understanding of arterial stenosis and aneurysm formation in persons with NF1. We provide preclinical evidence that CCR2 expression is critical for $Nf1^{+/-}$ neointima formation and deletion of *CCR2* limits neointima formation and arterial stenosis in $Nf1^{+/-}$ mice. In contrast to arterial stenosis, aneurysm formation results from a thinning of the arterial wall that is characterized by excessive oxidative stress, inflammatory cell infiltration, and degradation of the extracellular matrix. As neurofibromin-deficiency in macrophages is sufficient to cause both pathologies, we have identified that oxidative stress generated by NOX2 activation is responsible for the outward remodeling observed in aneurysm formation. These formative studies allow us to understand why persons with NF1 are predisposed to both pathologies and why they may occur together in the same person. In broader context, a greater understanding of how neurofibromin controls macrophage function directly informs other manifestations of Nf1 for which macrophages participate in disease initiation or progression including myeloid leukemias, neurofibromas, and MPNST.

Technology impact

Nothing to report

Impact on Society

Nothing to report

Changes to Report:

Nothing to report

Products:

Published Manuscripts (*denotes federal support)

1. *Bessler WK, Kim G, Hudson FZ, Mund JA, Mali R, Menon K, Kapur R, Clapp DW, Ingram DA, **Stansfield BK**. "Nf1+/- Monocytes/Macrophages Induced Neointima Formation via CCR2 Activation". *Human Molecular Genetics*. 2016 Mar 1:25(6):1129-1139. PMCID: PMC4764194.
2. *Bessler WK, Hudson FZ, Zhang H, Harris V, Wang Y, Mund JA, Downing B, Ingram DA, Case J, Fulton DJ, **Stansfield BK**. "Neurofibromin Regulates Reactive Oxygen Species Production and Arterial Remodeling". *Free Radical Biology and Medicine*. 2016 Aug;97:212-22. PMID: 27266634.
3. *Kim HW, **Stansfield BK**. "Genetic and Epigenetic Regulation of Aortic Aneurysms". *Biomed Research International.* 2017;2017:7268521. PMCID: PMC5237727.
4. Yiew KH, Chatterjee TK, Tang YL, Pellenberg R, **Stansfield BK**, Bagi Z, Fulton DJ, Stepp DW, Chen W, Patel V, Kamath VM, Litwin SE, Hui DY, Rudich SM, Kim HW, Weintraub NL. "Novel role for Wnt inhibitor APCDD1 in adipocyte differentiation: implications for diet-induced obesity". *J Biol Chemist.* Apr 14;292(15):6312-6324. PMCID: PMC5391760.
5. Kim HW, Blomkalns AL, Ogbi M, Thomas M, Gavrila D, Neltner BS, Cassis LA, Thompson RW, Weiss RW, Lindower PD, Blanco VM, McCormick ML, Daugherty A,Fu X, Hazen SL, **Stansfield BK**, Huo Y, Chatterjee T, Weintraub NL. Role of myeloperoxidase in abdominal aortic aneurysm formation: mitigation by taurine. Am J Physiol - Heart Circ Physiol. *In Press*
6. Benson TW, Chatterjee TK, Weintraub DS, Popoola O, Joseph J, **Stansfield BK**, Crowe M, Yiew KH, Unruh D, Pillai A, Williams J, Mintz J, Stepp DW, Brittain J, Bogdanov V, Weintraub NL. "Duffy Antigen Receptor for Chemokines Regulates Insulin Signaling and Adipocyte Maturation". *Submitted*.
7. *Zhang H, Hudson FZ, Xu Z, Tritz R, Rojas M, Patel C, Haigh SB, Bordan Z, Ingram DA, Fulton DJ, Weintraub NL, Caldwell RB, **Stansfield BK.** "Neurofibromin Deficiency Induces Endothelial Cell Proliferation and Retinal Neovascularization." *Invest Ophthalmol Vis Sc*. Submitted

Abstracts

1. ***Stansfield BK**, Ingram DA. *CCR2 Signaling is Necessary for Nf1$^{+/-}$ Neointima Formation*, Southern Society for Pediatric Research, New Orleans, LA
2. Benson TW, Chatterjee TK, Weintraub DS, Popoola O, **Stansfield BK**, Crowe M, Pillai A, Mintz J, Stepp D, Brittain J, Bogdanov V, Weintraub NL. *Duffy Antigen Receptor for Chemokines Modulates Adipose Inflammation in Obesity Related Metabolic Disease*, American Diabetes Association, Boston, MA
3. *Bessler,WK, Hudson FZ, Fulton DJ, Ingram DA, **Stansfield BK***. *Neurofibromin Regulates Oxidative Stress and Arterial Remodeling*, Children's Tumor Foundation, Monterey, CA ***Award for Basic Science Poster**
4. Benson TW*, Chatterjee TK, Weintraub DS, Popoola O, Joseph J, **Stansfield BK**, Crowe M, Yiew N, Unruh D, Pillai A, Williams j, Mintz J, Stepp D, Brittain J, Bogdanov V, Weintraub NL. *The Role of the Duffy Antigen Receptor for Chemokines in Metabolic Disease*, Experimental Biology, San Diego, CA
5. Tritz R, Zhang H, Fulton DJ, **Stansfield BK**. *Metabolic Characterization of Circulating Human Endothelial Colony Forming Cells*. Southern Society for Pediatric Research, New Orleans, LA
6. *Tritz R, Zhang HB, Hudson FZ, Benson TW, Kim HW, Fulton DJ, Weintraub NL, **Stansfield BK.** *Neurofibromin is a Novel Regulator of Macrophage Polarization via PFKFB3 Activation.* Children's Tumor Foundation, Washington D.C.

7. Zhang H, Hudson FZ, Caldwell RB, **Stansfield BK*.** "Neurofibromin is a novel regulator of endothelial cell proliferation and retinal neovascularization" Southern Society for Pediatric Research, New Orleans, LA. ***Young Faculty Travel Award**

Participants:

Name:	Brian Stansfield, MD
Project Role:	Principal Investigator
Person Months:	1.8
Contribution:	Carried out experiments, results interpretation, data management
Funding Source:	W81XWH-15-1-022

Name:	Farlyn Hudson
Project Role:	Research Associate
Person Months:	6
Contribution:	Carried out experiments, colony management, breeding
Funding Source:	W81XWH-15-1-022

Name:	Val Harris
Project Role:	Research Associate
Person Months:	4.8
Contribution:	Carried out experiments, animal surgeries
Funding Source:	W81XWH-15-1-022

Funding changes for PI or key personnel:

Brian Stansfield
New Grant Added
5R01DK112874-02 (Birch/Lavner) 09/01/2017 – 07/31/2021 0.6 Calendar Months
University of Georgia/NIDDK Annual Direct Costs
"Responsive Parenting, Sleep, and Rapid Weight Gain Among African American Infants"
Role: Co-Investigator/Site PI of a MPI Grant

New Grant Added
1R01HL142097-01 (Weintraub) 05/01/2018 – 04/30/2022 2.4 Calendar Months
NIH/NHLBI Annual Direct Costs
"Mechanisms of myeloperoxidase and Nox4 interactions in abdominal aortic aneurysm"
Role: Principal Investigator

New Grant Added
1R01EY029318-01A1 (Stansfield) 05/01/2019 – 04/30/2024 3.0 Calendar Months
NIH/NEI Annual Direct Costs
"Inflammation and retinopathy of prematurity"
Role: Principal Investigator

Collaborators/Consultants

Neal Weintraub
Grant Ended
4R01HL112640-05 (Weintraub) 07/13/2012 – 11/30/2017 (NCE) 2.4 Calendar Months

NIH/NHLBI Annual Direct Costs
"Perivascular adipose tissue and vascular remodeling"
Role: Principal Investigator

New Grant Added
1R01HL142097-01 (Weintraub) 05/01/2018 – 04/30/2022 2.4 Calendar Months
NIH/NHLBI Annual Direct Costs
"Mechanisms of myeloperoxidase and Nox4 interactions in abdominal aortic aneurysm"
Role: Principal Investigator

David Fulton
Grant Extended to a No-Cost-Extension
5R01HL124773-04 (Stepp/Fulton) 04/01/2015 – 02/28/2020 2.4 Calendar Months
NIH/NHLBI Annual Direct Costs
"Novel mechanistic pathways of cardiovascular disease in obesity"
Role: Principal Investigator of MPI grant

Grant Ended
1-16-IBS-196 (Lucas – PI) 01/01/2016 – 12/31/2018 0.36 Calendar Months
American Diabetes Association Annual Direct Costs
"Increased pneumonia-associated pulmonary barrier dysfunction in type 2 diabetes"
Role: Co-Investigator

New Grant Added
1R01HL142097-01 (Weintraub) 05/01/2018 – 04/30/2022 0.6 Calendar Months
NIH/NHLBI Annual Direct Costs
"Mechanisms of myeloperoxidase and Nox4 interactions in abdominal aortic aneurysm"
Role: Co-Investigator

New Grant Added
W81XWH-17-1-0043 (Hecker) 09/01/2018 – 08/31/2019 0.12 Calendar Months
University of Arizona – (DoD) Annual Direct Costs
"Preclinical Development of Small-Molecule Inhibitors Targeting Nox4 for Pulmonary Fibrosis"
Role: Co-Investigator on a subcontract

New Grant Added
1R01HL147159-01 (Stepp/Fulton) 04/01/2019 – 03/31/2024 2.4 Calendar Months
NIH/NHLBI Annual Direct Costs
"Circadian origins of vascular disease in obesity"
Role: Principal Investigator of MPI grant

Other organizations involved in the project:
None to report

Special reporting:
None to report

Free Radical Biology and Medicine 97 (2016) 212–222

Contents lists available at ScienceDirect

Free Radical Biology and Medicine

journal homepage: www.elsevier.com/locate/freeradbiomed

Original article

Neurofibromin is a novel regulator of Ras-induced reactive oxygen species production in mice and humans

Waylan K. Bessler [a,b,c,1], Farlyn Z. Hudson [d,e,1], Hanfang Zhang [d,e], Valerie Harris [d,e], Yusi Wang [e,f], Julie A. Mund [a,b,g], Brandon Downing [a,b], David A. Ingram Jr. [a,b,c], Jamie Case [a,g,h], David J. Fulton [e,f], Brian K. Stansfield [d,e,*]

[a] Herman B. Wells Center for Pediatric Research, Indiana University School of Medicine, Indianapolis 46202, United States
[b] Department of Pediatrics and Neonatal-Perinatal Medicine, Indiana University School of Medicine, Indianapolis 46202, United States
[c] Department of Biochemistry and Molecular Biology, Indiana University School of Medicine, Indianapolis 46202, United States
[d] Department of Pediatrics and Neonatal-Perinatal Medicine, Augusta University, Augusta, GA 30912, United States
[e] Vascular Biology Center, Augusta University, Augusta, GA 30912, United States
[f] Department of Pharmacology and Toxicology, Augusta University, Augusta, GA 30912, United States
[g] Melvin and Bren Simon Cancer Center, Indiana University School of Medicine, Indianapolis 46202, United States
[h] Scripps Clinic Medical Group, Center for Organ and Cell Transplantation, La Jolla, CA 92037, United States

ARTICLE INFO

Article history:
Received 1 February 2016
Received in revised form
25 May 2016
Accepted 2 June 2016
Available online 3 June 2016

Keywords:
Neurofibromatosis
Neointima
Reactive oxygen species
Macrophage
Monocyte
Smooth muscle cell
Superoxide
NADPH oxidase
Apocynin
Ras

ABSTRACT

Neurofibromatosis type 1 (NF1) predisposes individuals to early and debilitating cardiovascular disease. Loss of function mutations in the *NF1* tumor suppressor gene, which encodes the protein neurofibromin, leads to accelerated $p21^{Ras}$ activity and phosphorylation of multiple downstream kinases, including Erk and Akt. *Nf1* heterozygous ($Nf1^{+/-}$) mice develop a robust neointima that mimics human disease. Monocytes/macrophages play a central role in NF1 arterial stenosis as *Nf1* mutations in myeloid cells alone are sufficient to reproduce the enhanced neointima observed in $Nf1^{+/-}$ mice. Though the molecular mechanisms underlying NF1 arterial stenosis remain elusive, macrophages are important producers of reactive oxygen species (ROS) and Ras activity directly regulates ROS production. Here, we use compound mutant and lineage-restricted mice to demonstrate that $Nf1^{+/-}$ macrophages produce excessive ROS, which enhance $Nf1^{+/-}$ smooth muscle cell proliferation *in vitro* and *in vivo*. Further, use of a specific NADPH oxidase-2 inhibitor to limit ROS production prevents neointima formation in $Nf1^{+/-}$ mice. Finally, mononuclear cells from asymptomatic NF1 patients have increased oxidative DNA damage, an indicator of chronic exposure to oxidative stress. These data provide genetic and pharmacologic evidence that excessive exposure to oxidant species underlie NF1 arterial stenosis and provide a platform for designing novels therapies and interventions.

1. Introduction

Neurofibromatosis type 1 (NF1) is a common genetic disorder resulting from germline mutations in the *NF1* tumor suppressor gene and affects over 2 million people worldwide [1]. Neurofibromin, the protein product of *NF1*, functions as a catalyst for the slow, intrinsic hydrolysis of active $p21^{Ras}$ (Ras) [1]. Thus, loss of neurofibromin expression increases Ras-dependent kinase activity in response to growth factor stimulation of receptor tyrosine kinases. The downstream Ras kinases Erk and Akt turn on multiple molecular switches to promote a pro-survival phenotype in neurofibromin-deficient cells.

Persons with NF1 have a strong predisposition for cardiovascular disease, which often presents in adolescence and early adulthood [2–4]. Upwards of 8% of NF1 patients will develop hypertension, arterial stenosis, aortic aneurysms, or moyamoya,

Abbreviations: EEL, external elastic lamina; IEL, internal elastic lamina; I/M ratio, intima/media ratio; MNC, peripheral blood mononuclear cells; NF1, neurofibromatosis type 1; $Nf1^{+/-}$, heterozygous for the *Nf1* allele; $Nf1^{+/-}$;$p47^{-/-}$, heterozygous for the *Nf1* allele and homozygous deletion of $p47^{phox}$; $Nf1^{flox/+}$;$LysM^{cre}$, heterozygous for the *Nf1* allele in myeloid cells alone; $Nf1^{flox/flox}$;$LysM^{cre}$, homozygous for the *Nf1* allele in myeloid cells alone; $Nf^{flox/+}$;$gp91^{flox/flox}$;$LysM^{cre}$, heterozygous for the *Nf1* allele and homozygous deletion of $gp91^{phox}$ in myeloid cells alone; NOX2, NADPH oxidase 2; PMA, phorbol myristate acid; Ras, $p21^{Ras}$ pathway; ROS, reactive oxygen species; SMC, smooth muscle cell; SOD, superoxide dismutase; WT, wild type

* Correspondence to: Department of Pediatrics, Augusta University, 1120 15th St, BIW 6033, Augusta, GA 30912, United States.
E-mail address: bstansfield@augusta.edu (B.K. Stansfield).
[1] W.B. and F.H. contributed equally to this work.

http://dx.doi.org/10.1016/j.freeradbiomed.2016.06.002
0891-5849/

though universal screening has not been adopted and may underestimate the true prevalence of disease [4–6]. The distribution of NF1 vasculopathy within a single patient is often patchy and affects multiple vessels [4]. The varied presentation of arterial lesions suggests that NF1 patients may require a "second hit" mutation in the normal *NF1* allele or, more likely, a local insult in the vessel wall leading to dysregulation of normal repair mechanisms. Constitutional homozygosity for *NF1* mutations is embryonic lethal in humans and mice; therefore, inherited mutations in a single *NF1* allele are likely sufficient for the increased disease prevalence and provide a platform for investigation [7].

We have developed a mouse model of NF1 arterial stenosis using *Nf1* heterozygous ($Nf1^{+/-}$) mice that phenotypically resembles human NF1 arterial lesions [8–12]. Following carotid artery injury, $Nf1^{+/-}$ mice develop a robust neointima when compared with WT mice, which is characterized by α-SMA positive smooth muscle cells (SMC) and a predominance of bone marrow-derived macrophages within the neointima [10–12]. Disruption of PDGF-Ras-Erk signaling inhibits $Nf1^{+/-}$ SMC proliferation and prevents neointima formation in $Nf1^{+/-}$ mice[9]; however, SMC-specific *Nf1* heterozygosity failed to replicate the enhanced neointima observed in $Nf1^{+/-}$ mice and provides evidence that other cell populations are required to initiate neointima formation in $Nf1^{+/-}$ mice [8,10]. In support of this hypothesis, WT mice reconstituted with $Nf1^{+/-}$ bone marrow developed a pronounced neointima following carotid artery ligation while $Nf1^{+/-}$ mice reconstituted with WT bone marrow developed a modest neointima similar in size to WT lesions [8]. Further, we recently showed that loss of a single *Nf1* gene copy in myeloid cells is sufficient to reproduce the exaggerated arterial lesions observed in $Nf1^{+/-}$ mice [11]. These experiments in lineage-restricted and chimeric mice provide strong evidence that neurofibromin-deficient monocytes and macrophages are critical mediators of $Nf1^{+/-}$ arterial stenosis. However, the mechanisms through which $Nf1^{+/-}$ monocytes and macrophages directly influence $Nf1^{+/-}$ SMC proliferation and arterial stenosis is completely unknown.

Emerging evidence suggests that Ras kinases directly regulate reactive oxygen species (ROS) production and, in turn, ROS may modulate Ras activity [13–15]. Constitutive activation of Ras in hematopoietic progenitor and cancer cells dramatically increases ROS production via activation of the NADPH oxidase complex [16–19]. Also, *Drosophila* harboring mutations in the *Nf1* gene exhibited shortened lifespan and increased production of and vulnerability to ROS [20,21], while overexpression of neurofibromin prolonged lifespan and reduced ROS production [22]. More recently, neurofibromin deficiency or Ras activation significantly increased oligodendrocyte ROS production and disrupted endothelial tight junctions, which was restored by daily administration of the antioxidant N-acetyl cysteine [23]. These findings are intriguing since neurofibromin occupies a unique position in the regulation of kinases that activate ROS production and enhance SMC proliferation [24–26]. For example, the Ras-dependent kinases Akt and Erk directly phosphorylate the $p47^{phox}$ subunit of NADPH oxidase 2 (NOX2) and facilitate Rac2-dependent recruitment of $p67^{phox}$ to the transmembrane component of NOX2 to increase superoxide production in phagocytes [27–29]. Overproduction of ROS in infiltrating leukocytes via NOX2 therefore may augment SMC function and participate in the pathogenesis of arterial lesions in NF1 patients. Therefore, we hypothesize that loss of neurofibromin in monocytes/macrophages enhances ROS production via NOX2 activation and amplifies $Nf1^{+/-}$ SMC proliferation leading to occlusive arterial disease. As a corollary to our experimental murine work, we seek to identify whether NF1 patients experience chronic oxidative stress.

2. Materials and methods

2.1. Animals

Protocols were approved by Laboratory Animal Services at Augusta University and Indiana University. $Nf1^{+/-}$ mice were obtained from Tyler Jacks (Massachusetts Institute of Technology, Cambridge, MA) and backcrossed 13 generations into the C57BL/6J strain. $p47^{phox}$ (4742) knockout mice ($p47^{-/-}$) were purchased from The Jackson Laboratory and maintained on C57BL/6 strain. $Nf1^{+/-}$ mice were intercrossed with $p47^{-/-}$ mice to produce $Nf1^{+/-}$;$p47^{-/-}$ mice. $Nf1^{flox/flox}$ mice were obtained from Luis Parada (University of Texas Southwestern Medical Center, Dallas, TX) and maintained on C57BL/6 background. $gp91^{flox/flox}$ mice were obtained from Abay Shah (King's College, London, UK). *LysMcre* (4781) mice were purchased from The Jackson Laboratory and maintained on C57BL/6 background. $Nf1^{flox/flox}$ mice were crossed with $gp91^{flox/flox}$ and *LysMcre* mice to generate $Nf^{flox/+}$;$gp91^{flox/flox}$;*LysMcre* mice (heterozygous loss of *Nf1* and homozygous loss of $gp91^{phox}$ in myeloid cells only). LysM is expressed in neutrophils and macrophages. *Cre*-mediated recombination was confirmed by PCR as previously described [11]. Inbreeding of $Nf1^{flox/flox}$ mice with *LysMcre* mice yielded $Nf1^{flox/+}$;*LysMcre* (heterozygous loss of *Nf1* in myeloid cells alone) and $Nf1^{flox/+}$ (WT) controls. Male mice, between 12 and 15 weeks of age, were used for experiments.

2.2. Carotid artery ligation

Carotid artery injury was induced by ligation of the right common carotid artery as previously described [11]. Briefly, mice were anesthetized by inhalation of an isoflurane (2%)/oxygen (98%) mixture. Under a dissecting scope, the right carotid artery was exposed through a midline neck incision and ligated proximal to the bifurcation using a 6-0 silk suture. The contralateral carotid artery was sham ligated as a control. Mice were administered 15 μg of buprenorphine (IP) following the procedure and recovered for 28 days. Whole ligated and control arteries were harvested from experimental mice for analysis as previously described.

2.3. Morphometric analysis

Van Gieson-stained arterial cross Sections 400, 800, and 1200 μm proximal to the ligation were analyzed for neointima formation using Image J (NIH, Bethesda, MD). Lumen area, area inside the internal elastic lamina (IEL), and area inside the external elastic lamina (EEL) were measured for each cross section. To account for potential thrombus formation, arteries containing significant thrombus (> 50% lumen occlusion) at 400 μm proximal to the ligation were excluded from analysis. The number of excluded arteries was not different between experimental groups. Representative photomicrographs for each figure are taken from arterial cross sections between 600 and 1200 μm proximal to the bifurcation. Intima area was calculated by subtracting the lumen area from the IEL area, and the media area was calculated by subtracting the IEL area from the EEL area. Intima/media (I/M) ratio was calculated as intima area divided by media area.

2.4. Arterial ROS detection in vivo

Carotid arteries from $Nf1^{+/-}$ and WT mice were injured as described above. Forty-eight hours after injury, dihydroethidium (20 mg/kg) was provided via IP injection. After an additional 24-h recovery period, mice were sacrificed and whole control and injured carotid arteries were perfused with heparinized saline and flash frozen in OCT compound. Arterial cross sections (20 μm)

were analyzed for fluorescence using an EVOS FL microscope. In a second set of experiments, whole arteries from *Nf1*$^{+/-}$ and WT mice were harvested 72 h after injury and pooled, minced into a single cell suspension, and placed in boiling sodium dodecyl sulfate (SDS) buffer. NOX2 and β-actin expression were analyzed by western blot.

2.5. Isolation of bone marrow-derived macrophages, characterization, and ROS determination

Bone marrow-derived macrophage isolation and characterization was performed as described [8]. To assess ROS production, WT, *Nf1*$^{flox/+}$*;LysMcre*, and *Nf1*$^{flox/flox}$*;LysMcre* macrophages (5×10^5 cells) were suspended in 0.5 mL Hank's Balanced Salt Solution (HBSSS) and stimulated with 100 nM phorbol myristate acid (PMA). L-012 (2 μM) with and without 50 units/mL superoxide dismutase (SOD) was added to the suspension and luminescence was measured at 15-s intervals in a luminometer. In some experiments, macrophages were incubated with PD0325901 (10 nM) or wortmannin (50 nM) to specifically inhibit Erk and Akt activity, respectively. All experiments were performed in triplicate in four distinct cohorts.

2.6. Smooth muscle cell isolation and proliferation

Smooth muscle cell isolation and proliferation assays were performed as described [26]. SMC were obtained by outgrowth from explants of WT and *Nf1*$^{+/-}$ thoracic aortas. SMC were cultured in DMEM supplemented with 20% fetal bovine serum and 100 U/ml penicillin/streptomycin in a 37 °C, 5% CO_2-humidified incubator. For cell proliferation, SMC (5000 cells/cm^2) were placed in a 96-well plate and deprived of growth factors for 12–18 h. Quiescent SMC were stimulated with H_2O_2 (1 and 100 μM) for 24 h and pulse-labeled with 1 μCi/ml of [^{3}H] thymidine for 6 h. β emission was measured and reported as counts per minute. Cell counts using a hemocytometer were performed to confirm radioisotope results. Under the same conditions, cell viability was assessed by MTT assay and light absorbance was measured using a plate reader (570 nm). All experiments were performed in triplicate in four distinct cohorts.

2.7. Patient recruitment

NF1 patients were recruited by the Indiana University NF1 Clinic at Riley Hospital for Children. All patients received a physical examination and a medical history was taken to confirm the diagnosis of NF1 according to the NIH clinical criteria [30]. Patients with a history of cancer, on anti-cancer drugs or pregnant were excluded from the study. All patients gave informed consent prior to participation in the study.

2.8. Isolation of human peripheral blood mononuclear cells and analysis

Blood samples were collected from NF1 patients (37.6 ± 9.7 years) and age- and sex-matched healthy controls (40.2 ± 8.1 years) into EDTA Vacutainer tubes (BD Biosciences). Peripheral blood mononuclear cells (MNCs) were isolated from 16 ml of peripheral blood by density centrifugation using Ficoll-Paque Plus (GE Healthcare) as previously described [31]. A total of 1×10^6 MNCs were resuspended in PBS with 2% FBS and incubated with human FcR Blocking Reagent (Miltenyi Biotec) for 10 min at 4 °C. After blocking, MNCs were incubated for 30 min at 4 °C with the following primary conjugated monoclonal antibodies: anti–human CD14–PECy5.5 (Abcam), anti–human CD45–allophycocyanin–Alexa Fluor 750 (Invitrogen), and anti-human CD16–PECy7 (BD Biosciences — Pharmingen), as well as the live/dead marker ViVid (Invitrogen). After staining, MNCs were washed 2 times with PBS with 2% FBS and fixed in 1% formaldehyde (Sigma-Aldrich) for a minimum of 24 h. Stained MNC samples were acquired on a BD LSRII flow cytometer equipped with a 405-nm violet laser, 488-nm blue laser, and 633-nm red laser. At least 300,000 events were collected for each sample. Data were collected uncompensated and analyzed using FlowJo software version 8.7.3 (Tree Star).

2.9. Modified comet assay in human mononuclear cells

MNCs were assayed for oxidative DNA damage as previously described, with modification [32]. Following cell lysis, slides were treated with formamidopyrimidine DNA glycosylase (FPG), which recognized and removed oxidized purines, causing a DNA break. For each sample, 100 cells were analyzed. The Institutional Review Board of the Indiana University School of Medicine approved all protocols using human tissue samples.

2.10. Statistics

All values are presented as mean ± S.E.M. unless otherwise noted. Human monocyte frequency and leukocyte oxidative-DNA damage was analyzed using Student's *t*-test and sample distribution was analyzed by *F*-test. Macrophage ROS production and SMC proliferation and viability was analyzed using 2-way ANOVA with Tukey's post-hoc test for multiple comparisons. Intima area and I/M ratio analysis was assessed by 1-way ANOVA with Tukey's post-hoc test for multiple comparisons. Murine experiments using apocynin treatment were assessed using 2-way ANOVA with Tukey's post-hoc test for multiple comparisons. Analysis was performed using GraphPad Prism version 5.0 d. $P < 0.05$ were considered significant.

3. Results

3.1. Neurofibromin-deficient macrophages produce excessive superoxide via p21^{Ras} activation

The p21^{Ras} pathway directly, but not completely, regulates intracellular and extracellular oxidant species concentration; therefore, Ras activation in neurofibromin-deficient leukocytes may increase ROS production. To examine the role of neurofibromin-deficiency in leukocyte-mediated ROS production, we utilized cre/lox technology to isolate *Nf1* heterozygous and homozygous macrophages. As *Nf1* nulzygosity results in embryonic lethality, we isolated bone marrow macrophages from *Nf1*$^{flox/+}$*;LysM*^{cre} (*Nf1* heterozygous in myeloid cells) and *Nf1*$^{flox/flox}$*;LysM*^{cre} (*Nf1* homozygous in myeloid cells) and subjected them to stimulation with phorbol myristate acetate (PMA) to provoke ROS production. In response to PMA stimulation, neurofibromin-deficient macrophages generated greater quantities of ROS when compared to WT macrophages (Fig. 1). In fact, a gene-dosage response was observed in neurofibromin-deficient macrophages (Fig. 1A and B). The addition of superoxide dismutase (SOD) effectively quenched ROS production, indicating that *Nf1* mutant macrophages produce excessive superoxide primarily (Fig. 1B).

To examine whether Ras activation in neurofibromin-deficient macrophages directly regulates ROS production, we elicited ROS production in WT and *Nf1*$^{+/-}$ macrophages with PMA in the presence of PD0325901, an inhibitor of Ras-Mek-Erk, and wortmannin, an inhibitor of Ras-PI-3K. In response to PMA, *Nf1*$^{+/-}$ macrophages produced significantly more ROS when compared with WT macrophages and this response was completely inhibited in the presence of either Erk or Akt inhibitors (Fig. 1C). WT macrophages

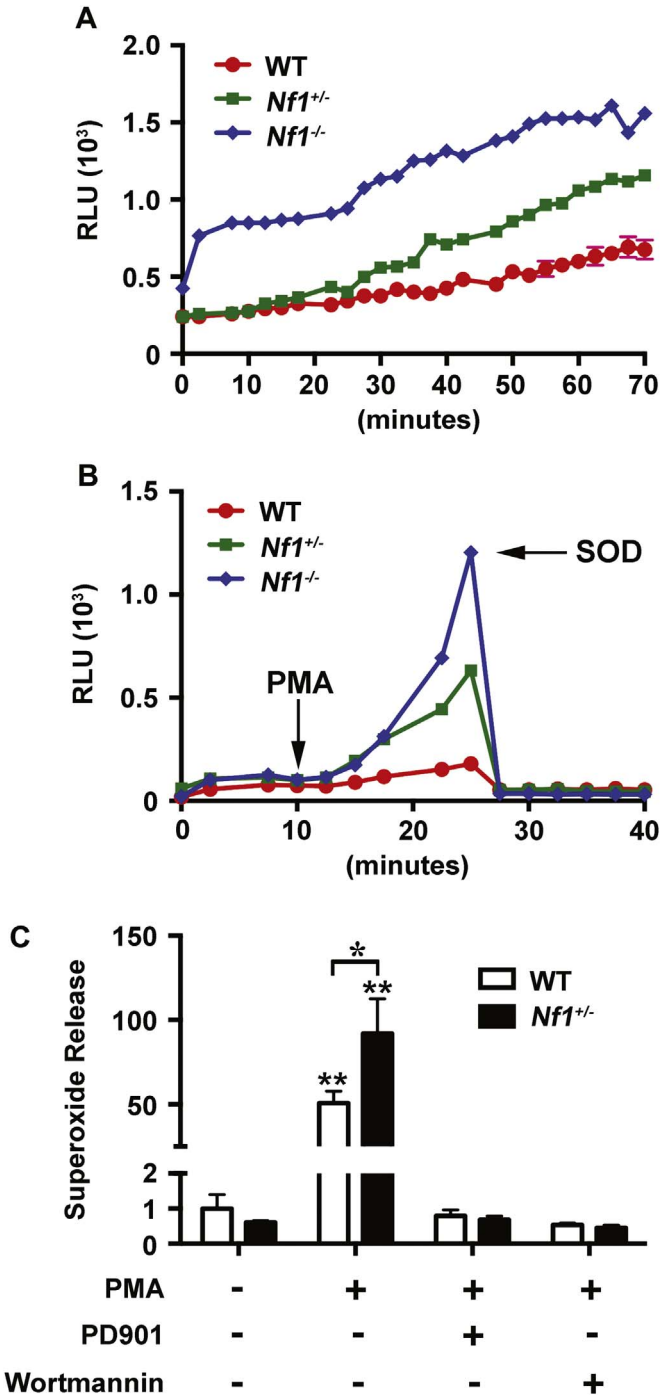

Fig. 1. Neurofibromin regulates ROS production via $p21^{Ras}$. WT (red), $Nf1^{+/-}$ (green), and $Nf1^{-/-}$ (blue) macrophage ROS production in response to phorbol myristate acid (PMA) in the presence or absence of $p21^{Ras}$ inhibitors. A and B. Data represent relative light units in response to PMA (A) and in response to PMA with the addition of superoxide dismutase (B) at indicated time point. C. Data represent fold change ± S.E.M. (n=4) for WT (white bars) and $Nf1^{+/-}$ (black bars) macrophage maximal superoxide production in response to PMA (30 min) in the presence or absence of PD0325901 (10 nM) and wortmannin (50 nM). All comparisons are referred are in reference to unstimulated WT macrophages. $^{*}P<0.01$ for WT versus $Nf1^{+/-}$ macrophages stimulated with PMA. $^{**}P<0.001$ for WT and $Nf1^{+/-}$ macrophages stimulated with PMA versus WT and $Nf1^{+/-}$ macrophages stimulated with PMA in the presence of either PD0325901 or wortmannin.

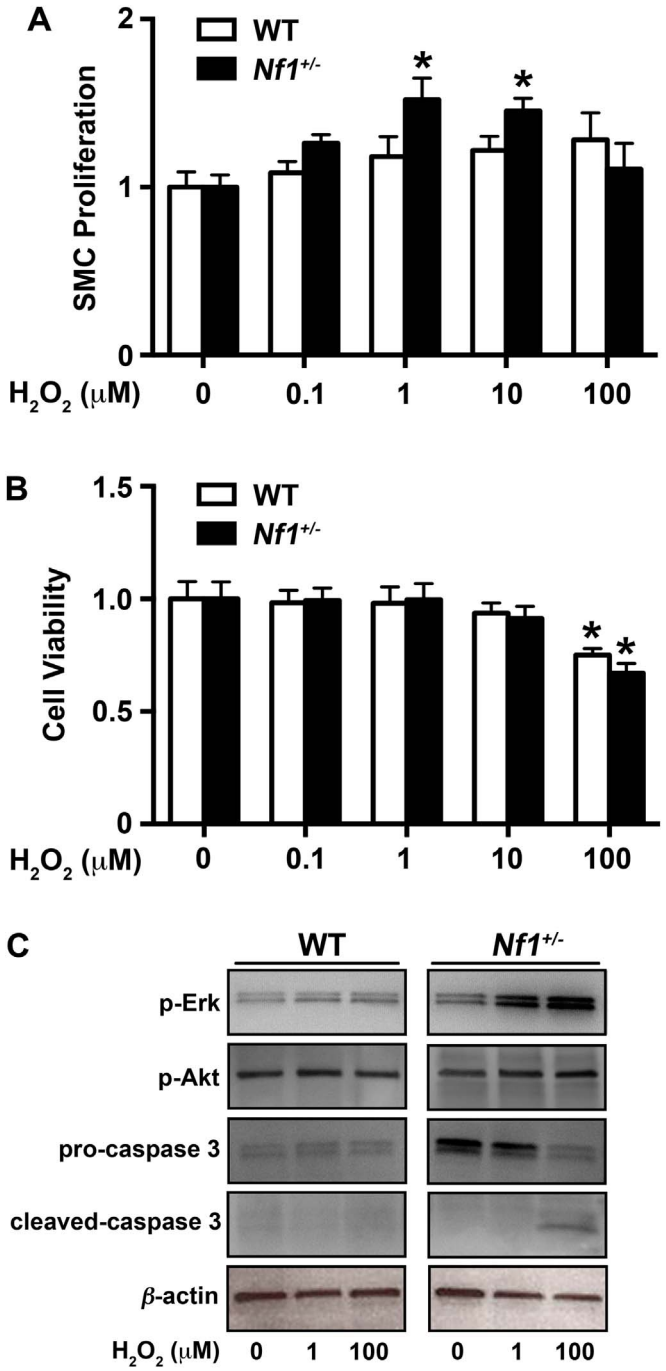

Fig. 2. Low dose H_2O_2 induces $Nf1^{+/-}$ SMC proliferation and Erk activation. WT (white bars) and $Nf1^{+/-}$ (black bars) SMC proliferation in response to stimulation with indicated concentration of H_2O_2 (μM). A. Data represent genotype-specific fold change ± SEM, n=4. $^{*}P<0.05$ for $Nf1^{+/-}$ SMC versus $Nf1^{+/-}$ SMC stimulated with indicated concentration of H_2O_2. B. Data represent genotype-specific SMC viability ± SEM (n=4) in the presence of H_2O_2. $^{*}P<0.01$ for $Nf1^{+/-}$ SMC versus $Nf1^{+/-}$ SMC stimulated with indicated concentration of H_2O_2. C. Representative western blots of phospho-Erk, phospho-Akt, pro-caspase 3, cleaved caspase 3, and β-actin in WT and $Nf1^{+/-}$ SMC treated with indicated concentration of H_2O_2 (n=4).

also produced little ROS when co-incubated with PD0325901 or wortmannin, which suggests that PMA likely induces ROS production via Ras activation.

3.2. $Nf1^{+/-}$ SMC are sensitive to oxidative stress

Reactive oxygen species modify the response of intracellular signaling pathways, including $p21^{Ras}$, and may exaggerate the response of extracellular growth signals to induce cell proliferation and survival. More specifically, superoxide and its primary by-product hydrogen peroxide (H_2O_2) are important mitogens for SMC [33–36]. Based on the observation that neurofibromin-

deficient macrophages produce excessive ROS, we isolated SMC from the aortas of WT and *Nf1*$^{+/-}$ mice to interrogate the potential paracrine effects of local ROS production by infiltrating *Nf1*$^{+/-}$ macrophages on arterial SMC *in vitro*. Under growth-restrictive conditions, *Nf1*$^{+/-}$ SMC exhibit increased proliferation when compared with WT SMC [11,12,26]. To account for this inherent advantage, we compared quiescent *Nf1*$^{+/-}$ and WT SMC incubated with/without H_2O_2 to mimic exposure to vascular oxidative stress. In response to low micromolar concentrations of H_2O_2, *Nf1*$^{+/-}$ SMC exhibited a dose-responsive increase in thymidine incorporation, while higher concentrations of H_2O_2 failed to stimulate *Nf1*$^{+/-}$ SMC proliferation (Fig. 2A). Thymidine incorporation was also dose-responsive in WT SMC, though higher H_2O_2 concentrations were required to induce the same proliferative response and statistical significance was not achieved. Interestingly, WT and *Nf1*$^{+/-}$ SMC viability dropped significantly in response to stimulation with 100 μM H_2O_2 as determined by MTT assay (Fig. 2B). Both low and high concentrations of H_2O_2 preferentially activated Erk in *Nf1*$^{+/-}$ SMC when compared to WT SMC, while Ras-PI-3K activity remained largely unchanged (Fig. 2C). Consistent with decreased cell viability, incubation of *Nf1*$^{+/-}$ SMC with 100 μM H_2O_2 induced the cleavage of caspase-3, an indicator of apoptosis (Fig. 2C). These data suggest that low-level ROS amplifies Erk activity in *Nf1*$^{+/-}$ SMC and potentiates *Nf1*$^{+/-}$ SMC proliferation, while higher concentrations of H_2O_2 may induce *Nf1*$^{+/-}$ SMC apoptosis. The latter is an important observation since SMC apoptosis is a critical step in the development of aortic aneurysms, which is a less common manifestation of NF1 vasculopathy [2,37]. Additionally, we examined *Nf1*$^{+/-}$ and WT SMC for native ROS production in response to incubation with H_2O_2 to identify particular advantages that neurofibromin-deficiency and/or Ras activation might have on ROS production. Quiescent *Nf1*$^{+/-}$ and WT SMC exhibited similar basal ROS production and the addition of H_2O_2 (10 and 100 μM) did not confer additional ROS production in *Nf1*$^{+/-}$ SMC when compared with WT SMC (data not shown). Thus, it is unlikely that *Nf1*$^{+/-}$ SMC produce sufficient quantities of ROS to autonomously induce SMC proliferation and arterial stenosis *de novo*, but may confer an additive effect to local ROS production by infiltrating macrophages.

3.3. NOX2 expression is upregulated in *Nf1*$^{+/-}$ carotid arteries

Previously, we showed that *Nf1*$^{+/-}$ mice develop exaggerated neointimas and excessive remodeling when compared with WT mice, which is largely mediated by neurofibromin-deficient monocytes/macrophages [9,11]. While loss of neurofibromin expression leads to increase Ras signaling and enhances macrophage survival and function, the inciting mechanism(s) leading to rampant SMC proliferation and neointima formation are poorly understood. To examine the potential role of excessive ROS production by *Nf1*$^{+/-}$ macrophages on the vascular wall, we harvested control and ligated arteries from *Nf1*$^{+/-}$ and WT mice 3 days after injury. Prior to tissue harvest, animals were provided dihydroethidium (DHE) via IP injection to detect ROS in the vascular wall. In comparison to control vessels, injured arteries from both genotypes exhibited increase DHE staining indicating an upregulation in ROS production (Fig. 3A). However, injured *Nf1*$^{+/-}$ arteries showed only a modest increase in ROS expression compared to injured WT arteries at this early time point. Next, control and injured carotid arteries from *Nf1*$^{+/-}$ and WT mice were pooled and analyzed for NOX2 expression. Interestingly, control *Nf1*$^{+/-}$ arteries have increased expression of NOX2 compared to WT control arteries (Fig. 3B). In response to arterial ligation, both WT and *Nf1*$^{+/-}$ carotid arteries have enhanced expression of NOX2 compared to genotype-specific controls, though injured *Nf1*$^{+/-}$ arteries exhibited the highest NOX2 expression of all conditions tested. Although examination of an early time point after arterial injury did not detect significant differences in ROS production in the vessel wall between *Nf1*$^{+/-}$ and WT arteries, NOX2 expression in whole artery lysates suggest that neurofibromin regulates the expression of NOX2 and NOX2 expression is increased during early inward arterial remodeling.

3.4. NOX2 activation is required for *Nf1*$^{+/-}$ neointima formation

Excessive ROS production by infiltrating leukocytes in the vascular wall contributes to SMC proliferation and arterial stenosis [34,38] and therapeutic attempts to scavenge excess ROS or interrupt ROS production have proven efficacious in preclinical models of neointima formation [39]. Superoxide production in leukocytes is largely mediated via NADPH oxidase 2 (NOX2), which is activated, in part, by the Ras-dependent kinases Erk and Akt [17,28,40]. Based on our observation that neurofibromin-deficient macrophages produce excessive superoxide and *Nf1*$^{+/-}$ SMC proliferation is dose-responsive to ROS species, we intercrossed *Nf1*$^{+/-}$ mice with *p47*^{phox} knockout mice to understand the role of NOX2 activation in *Nf1*$^{+/-}$ neointima formation. In response to carotid artery ligation, *Nf1*$^{+/-}$

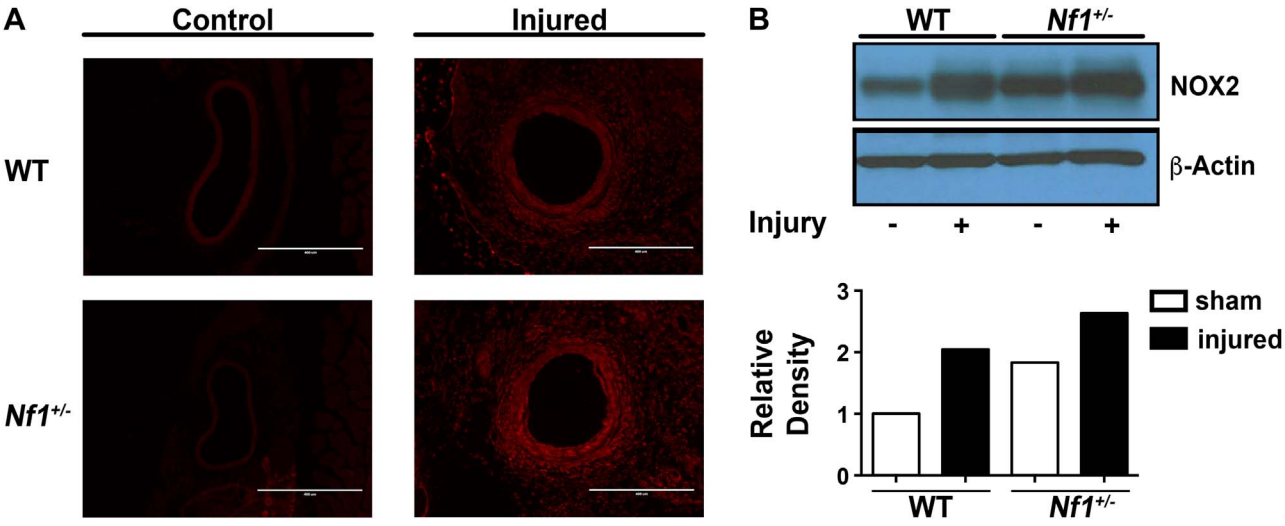

Fig. 3. Loss of neurofibromin enhances NOX2 expression in carotid arteries. Representative photomicrographs (A) and NOX2 expression (B) in control and injured carotid arteries from WT and *Nf1*$^{+/-}$ mice (n=3). A. Fluorescence indicating DHE staining in control and injured WT and *Nf1*$^{+/-}$ arterial cross sections. Scale bars: 400 μm. B. Representative western blot and quantitative densitometry for NOX2 and β-actin in pooled samples from WT *Nf1*$^{+/-}$ carotid arteries.

mice developed an enhanced neointima, which was phenotypically and histologically similar to our previous observations (Fig. 4). Genetic deletion of *p47^{phox}*, a cytosolic component of NOX2 that is required for NOX2 activation, reduced neointima formation in *Nf1$^{+/-}$* mice to levels observed in the background strain. Quantitative analysis of arterial cross sections from each cohort demonstrated a 65% reduction in neointima area and 80% reduction in intima/media (I/M) ratio (Fig. 4B and C). Thus, p47^{phox} expression is required for *Nf1$^{+/-}$* neointima formation and NOX2 activation may be mechanistically responsible for the enhanced ROS production observed in *Nf1* mutant macrophages.

Previously, we utilized *LysM^{cre}* mice to demonstrate that loss of a single *Nf1* gene copy in monocytes/macrophages is sufficient to reproduce the enhanced neointima observed in neurofibromin-deficient mice [11]. In order to specifically interrogate the role of macrophage-specific ROS production in the pathogenesis of *Nf1* arterial stenosis, we intercrossed *Nf1$^{flox/+}$;LysM^{cre}* mice with *gp91$^{flox/flox}$* mice to generate *Nf1$^{flox/+}$;gp91$^{flox/flox}$;LysM^{cre}* mice with specific deletion of both *gp91^{phox}* alleles in *Nf1$^{+/-}$* monocytes and macrophages. gp91^{phox} is the glycosylated membrane-bound component of NOX2 and is required for electron transfer to molecular oxygen in the generation of superoxide [41]. Cre^{+} and Cre^{-} mice were subjected to carotid artery ligation to induce neointima formation. Lineage-restricted inactivation of a single *Nf1* allele in myeloid cells alone was sufficient to induce a robust neointima that is an exact phenocopy of neointimas observed in *Nf1$^{+/-}$* mice after arterial injury (Fig. 5). In contrast, genetic deletion of both *gp91^{phox}* alleles in *Nf1$^{flox/+}$;LysM^{cre}* mice resulted in a 75% reduction in neointima formation after arterial injury when compared to *Nf1$^{flox/+}$;LysM^{cre}* mice (Fig. 5B and C). Collectively, these data provide genetic evidence that the presence and activation of NOX2 is necessary for *Nf1$^{+/-}$* neointima formation and limiting ROS production may be a viable therapeutic target for the prevention and/or treatment of NF1 arterial stenosis.

3.5. Apocynin inhibits neointima formation in *Nf1$^{+/-}$* mice

The proximity of invading *Nf1$^{+/-}$* macrophages to vascular wall SMC and their propensity for superoxide production may be pathologically linked to neointima formation in *Nf1$^{+/-}$* mice.

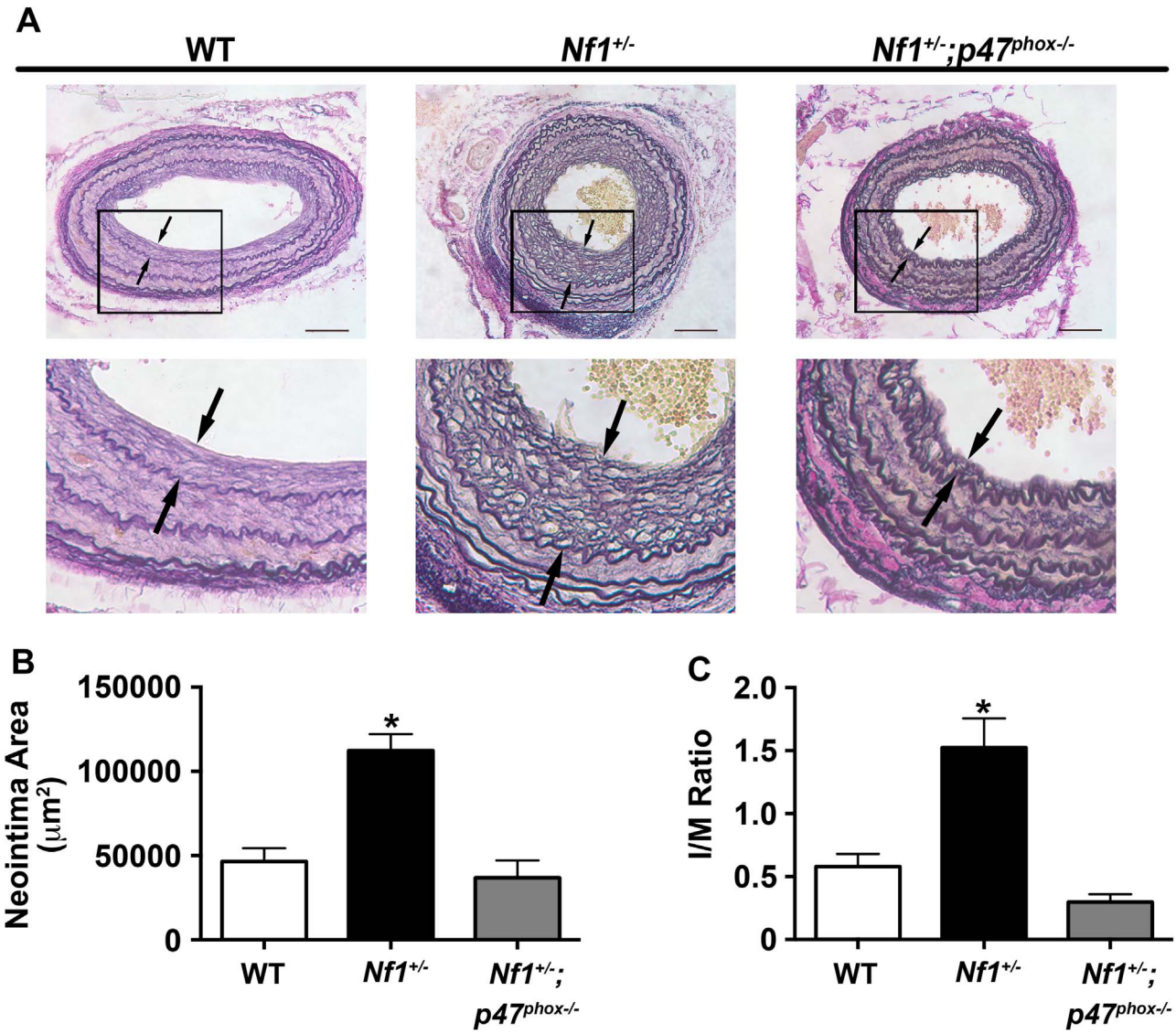

Fig. 4. Genetic deletion of *p47^{phox}* inhibits *Nf1$^{+/-}$* neointima formation. Representative photomicrographs (A) and quantification of neointima area (B and C) of injured carotid arteries from WT, *Nf1$^{+/-}$*, and *Nf1$^{+/-}$;p47$^{phox-/-}$* mice. A. Black arrows indicate neointima boundaries. Black boxes identify area of injured artery that is magnified below. Scale bars: 100μm. B and C. Quantification of neointima area (B) and I/M ratio (C) of injured carotid arteries from WT, *Nf1$^{+/-}$*, and *Nf1$^{+/-}$;p47$^{phox-/-}$* mice. Data represent mean neointima area or I/M ratio ± SEM, $n=8$–11. *$P<0.001$ for WT and *Nf1$^{+/-}$;p47$^{phox-/-}$* mice versus *Nf1$^{+/-}$* mice.

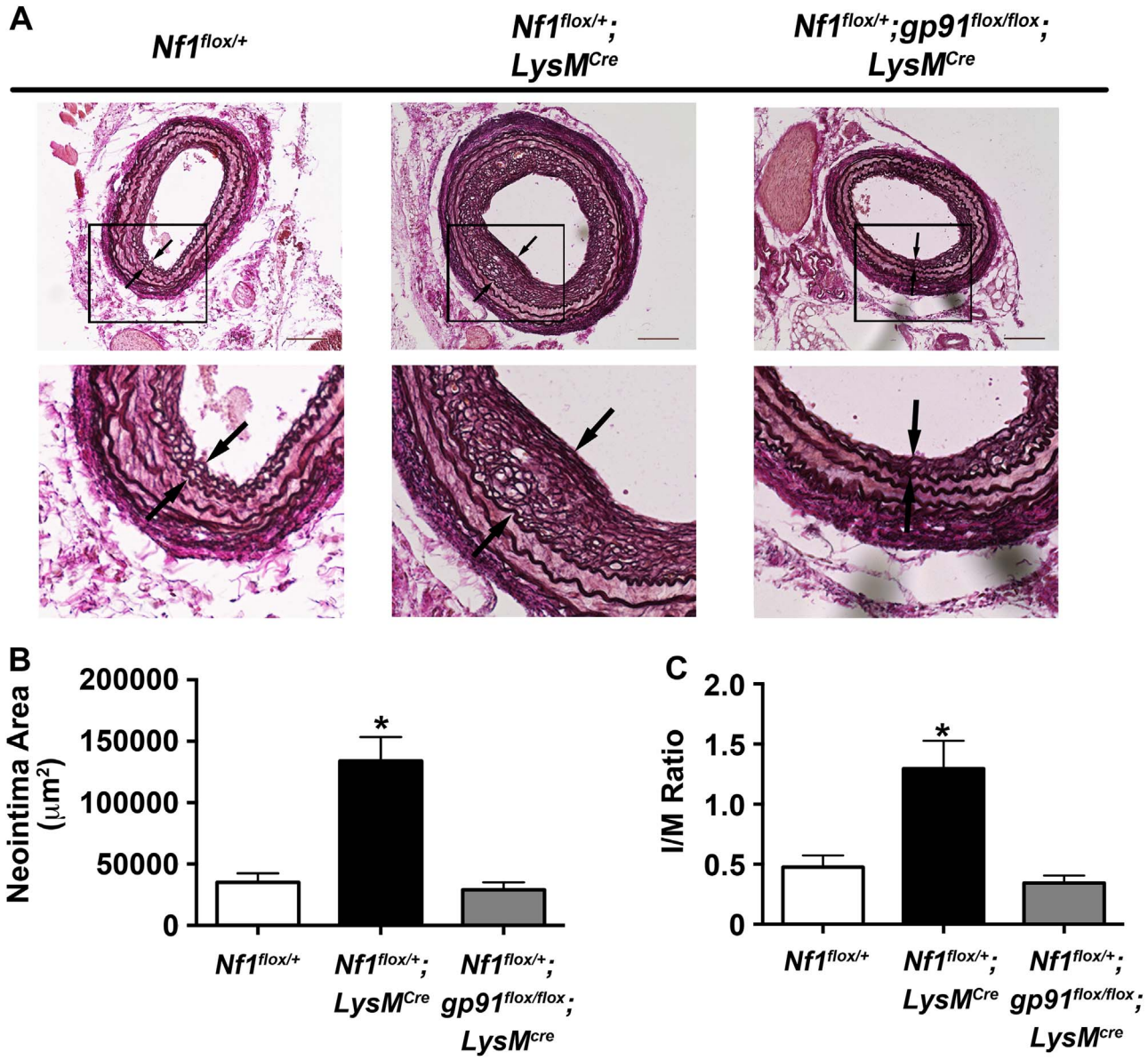

Fig. 5. Lineage restricted deletion of *gp91*^{phox} in myeloid cells inhibits *Nf1*$^{+/-}$ neointima formation. Representative photomicrographs (A) and quantification of neointima area (B and C) of injured carotid arteries from WT, *Nf1*$^{flox/+}$;*LysM*^{cre}, and *Nf1*$^{flox/+}$;*gp91*$^{flox/flox}$;*LysM*^{cre} mice. A. Black arrows indicate neointima boundaries. Black boxes identify area of injured artery that is magnified below. Scale bars: 100 μm. B and C. Quantification of neointima area (B) and I/M ratio (C) of injured carotid arteries from WT, *Nf1*$^{flox/+}$;*LysM*^{cre}, and *Nf1*$^{flox/+}$;*gp91*$^{flox/flox}$;*LysM*^{cre} mice. Data represent mean neointima area or I/M ratio ± SEM, $n = 10$–12. *$P < 0.001$ for WT, and *Nf1*$^{flox/+}$;*gp91*$^{flox/flox}$;*LysM*^{cre} mice versus *Nf1*$^{flox/+}$;*LysM*^{cre}.

Sequestering ROS production provides an attractive therapeutic option since anti-oxidants are well tolerated and may be particularly effective in NF1 patients with evidence of oxidative stress. The antioxidant apocynin is intriguing since it binds the p47 subunit in the cytosol and interferes with NOX2 activation [42–44]. Therefore, we subjected *Nf1*$^{+/-}$ and WT mice to carotid artery ligation to induce arterial stenosis and provided drinking water containing or lacking apocynin (100 mg/kg/day) for 28 days until the arteries were harvested and analyzed for neointima formation. In response to carotid artery injury, WT mice developed a modest neointima while *Nf1*$^{+/-}$ mice developed a severe arterial stenosis, which was similar to our previous observations (Fig. 6). In contrast, daily administration of apocynin reduced *Nf1*$^{+/-}$ neointima area and I/M ratio by 75% in comparison with control *Nf1*$^{+/-}$ mice (Fig. 6A and B). WT mice experienced a modest, but non-significant reduction in neointima formation, which is likely due to their resistance to neointima formation.

3.6. NF1 patients have increased pro-inflammatory monocytes and evidence of chronic oxidative stress

Loss of *Nf1* may increase the susceptibility of whole organisms and primary cells to oxidative stress, and previous studies have suggested interplay between chronic oxidative stress and inflammation in tissue derived from NF1 patients. However, evidence of oxidative stress has not been demonstrated in persons with NF1 [8,45–47]. Therefore, we isolated peripheral blood MNCs to examine them for evidence of oxidative stress. In comparison with age- and sex-matched controls, total monocyte count was elevated in asymptomatic NF1 patients. Examination of monocyte subpopulation frequency showed that some healthy persons with NF1 had a substantial increase in the frequency of a monocyte subpopulation ($CD14^+CD16^{++}$) associated with inflammatory conditions and oxidative stress [48–50] (Fig. 7 A and B). The mean frequency of $CD14^+CD16^{++}$ monocytes in the NF1 cohort was

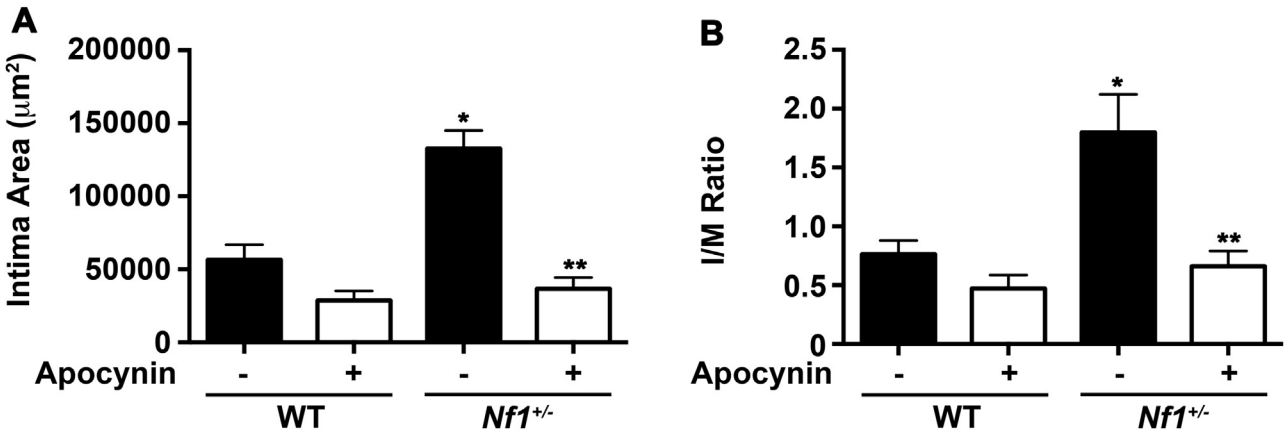

Fig. 6. Apocynin, a NOX2 inhibitor, reduces *Nf1*$^{+/-}$ neointima formation. Quantification of neointima area (A) and I/M ratio (B) of injured carotid arteries from WT and *Nf1*$^{+/-}$ mice treated with apocynin (100 mg/kg/day) or water. Data represent mean neointima area or I/M ratio ± SEM, $n=8$–10. *$P<0.001$ for WT versus *Nf1*$^{+/-}$ mice treated with water. **$P<0.001$ for *Nf1*$^{+/-}$ mice treated with apocynin versus *Nf1*$^{+/-}$ mice treated with water. No statistical difference was observed between WT mice treated with apocynin and WT mice treated with water.

2.5 times higher than the mean frequency of $CD14^+CD16^{++}$ monocytes in the control cohort (40.8 ± 14 vs. 15.73 ± 4.3 cells/μL, $P=0.06$). Within the NF1 cohort, we observed that some NF1 patients exhibited a significant elevation in the frequency of circulating $CD14^+CD16^{++}$ monocytes, which may cause a positive skew in the sample distribution. To determine if the sample distribution in these two cohorts could occur by random chance, we performed an *F*-test of variance. This secondary analysis revealed a significant difference in $CD14^+CD16^{++}$ monocyte frequency variance between NF1 and control patients ($P<0.001$). Monocyte subpopulation frequencies must be interpreted in relationship to controls since normal values do not presently exist. While nearly 60% of healthy controls had a $CD14^+CD16^{++}$ monocyte frequency of less than 10,000 cells/μL in their peripheral blood, less than 45% of healthy persons with NF1 met the same cutoff value. In fact, the highest $CD14^+CD16^{++}$ monocyte frequency observed in persons with NF1 were 2–3 fold higher than the highest observed frequencies in control patients (Fig. 7B). In comparison, the frequency of patrolling or "classical" monocytes did not differ between control and NF1 patients Fig. 7C. Since $CD14^{++}CD16^-$ classical

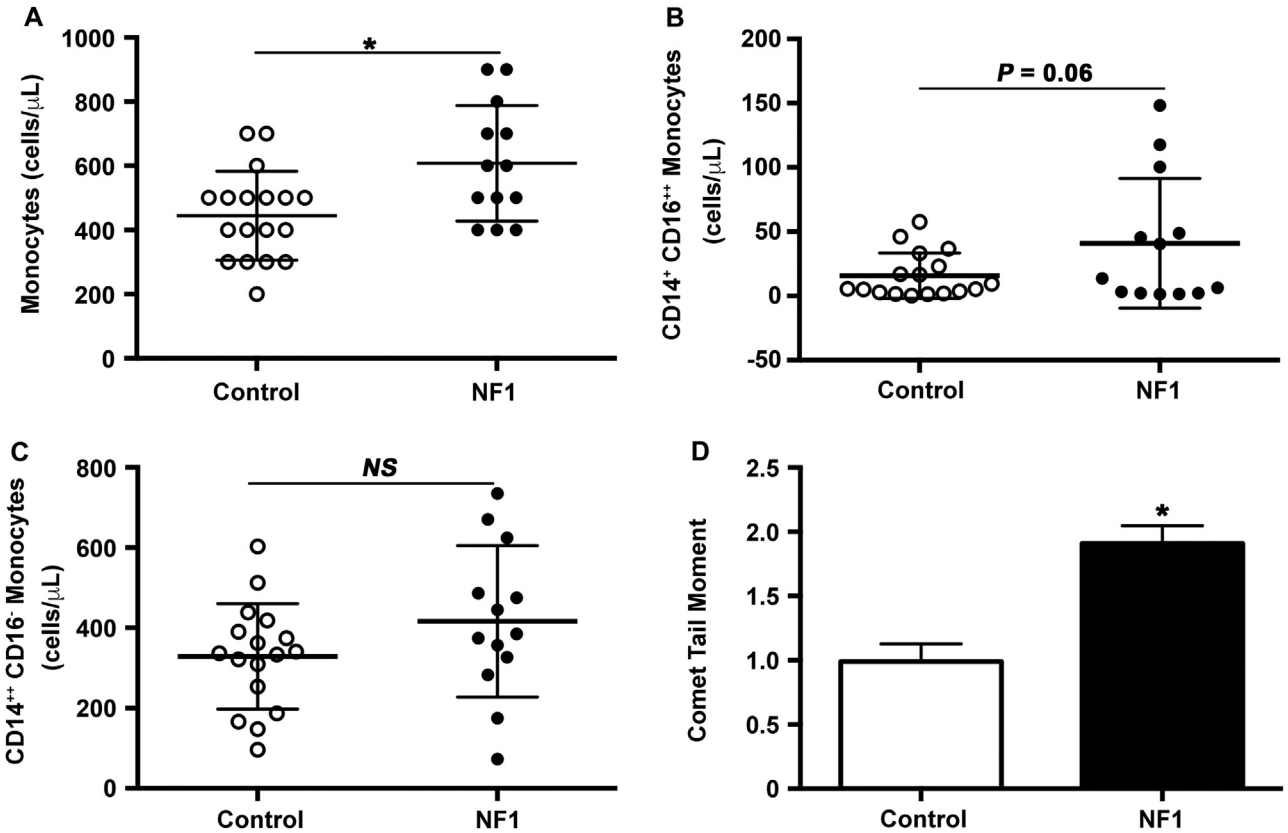

Fig. 7. NF1 patients have evidence of chronic inflammation and oxidative stress. Quantification of total monocyte count (A), $CD14^+CD16^{++}$ monocyte count (B), and peripheral blood MNC comet tail moment (C) in NF1 patients and age-, sex-matched controls. A. Data represent total monocyte count (cells/μL) for NF1 patients ($n=13$) and controls ($n=18$). $P<0.01$ for NF1 patients versus control patients. B. Data represent $CD14^+CD16^{++}$ monocytes (cells/μL) for NF1 patients ($n=13$) and controls ($n=17$). C. Data represent $CD14^{++}CD16^-$ monocytes (cells/μL) for NF1 patients ($n=13$) and controls ($n=17$). D. Data represent mean comet tail moment ± S.D. for NF1 patients ($n=10$) versus controls ($n=28$). $P<0.05$ for NF1 versus control patients.

monocytes arise from the bone marrow and give rise to $CD14^{++}CD16^{+}$ intermediate and $CD14^{+}CD16^{++}$ non-classical monocytes, this data suggests that the increased frequency of $CD14^{+}CD16^{++}$ monocytes is the result of signaling inputs outside the bone marrow compartment and do not arise from alterations in developmental maturation [50].

Next, we examined peripheral blood MNCs for evidence of oxidative stress using a modified comet assay to analyze for oxidative DNA damage. Monocytes isolated from NF1 patients displayed a 2-fold increase in oxidative DNA damage when compared with control patients (Fig. 7D Thus, NF1 patients have evidence of chronic oxidative stress and inflammation, which may predispose them to premature and/or severe forms of cardiovascular disease.

4. Discussion

Despite a high propensity for severe forms of cardiovascular disease, tailored therapies for NF1 patients with vasculopathy are nonexistent. The lack of a concise therapeutic approach to NF1 vasculopathy is largely due to a poor understanding of disease pathogenesis and latency in disease presentation. To date, most therapeutic studies have targeted downstream Ras kinases as their activity is deregulated and amplified in persons with NF1. While Ras pathway inhibitors are mechanistically plausible for the treatment of cardiovascular manifestations in NF1 patients, long-term treatment of cardiovascular diseases with Mek-Erk or Ras-PI-3K inhibitors is not practical due to the necessity of this highly conserved pathway in normal cell growth and differentiation. Thus, the need for highly efficacious and well-tolerated compounds for persons with NF1 vasculopathy must leverage the unique biochemistry found in neurofibromin-deficient tissue while maintaining a favorable side-effect profile.

Emerging evidence suggests that oxido-reductive balance is disturbed in active Ras mutants and neurofibromin-deficient tissues and humans. The interaction between ROS and Ras is multifaceted, but reactive oxygen and nitrogen species have been identified as upstream modulators and downstream targets of several Ras kinases [13]. Active Ras mutations or upregulation of Ras signaling leads to increased expression of NADPH oxidases to enhance ROS production in multiple cell types [17,51–53]. Ras activation through growth factor binding of various receptor tyrosine kinases may cooperate with small molecule modulators, such as ROS, to enhance phosphorylation of the downstream kinases Erk and Akt [54]. In turn, inhibition of ROS production appears to decrease Erk and Akt activity so that signaling feedback between ROS and Ras is critical for cell homeostasis [55–57]. The physiologic interaction of ROS and $p21^{Ras}$ may turn pathologic in the setting of neurofibromin-deficiency as evidenced by recent studies. Oligodendrocytes containing either inactivating *Nf1* or active *HRAS* mutations produce excessive ROS leading to disruption of local endothelial tight junctions and increased vascular permeability, which is restored with the administration of the antioxidant N-acetyl cysteine [23]. Neurofibromin may also express a more direct relationship with mitochondrial ROS production via protein kinase A (PKA). Mutations in the *Drosophila Nf1* homolog increased mitochondrial ROS production, shortened lifespan, and sensitized flies to oxidative stress [22]. Overexpression of PKA restored a normal response to oxidative stress in *Nf1* mutant *Drosophila* [58]. Conversely, overexpression of neurofibromin in *Drosophila* provided resistance to oxidant injury and prolonged mean lifespan. Here, we show that superoxide production by differentiated macrophages is directly regulated by neurofibromin via a gene-dosage dependent mechanism.

In support of neurofibromin's role in ROS production, we provide the first evidence of chronic oxidative stress in NF1 patients, as demonstrated by increased comet tail moment, an indicator of oxidative DNA damage [59]. Recent studies suggest that neurofibromin also regulates cell cycle and DNA repair pathways; therefore, loss of neurofibromin may prevent normal DNA repair to occur and may be an alternative explanation for the enhanced oxidative DNA damage [60]. However, measurement of direct DNA damage did not differ between NF1 and control patients (data not shown). Regardless, the implications of these findings may be broad-based since excessive ROS production and oxidative DNA damage may participate in several manifestations of NF1, including cancer, impaired learning and cognition, and musculoskeletal diseases. Further, modulating ROS production is an attractive therapeutic alternative for NF1 patients and may have additive effects since neurofibromin restrains ROS production directly and indirectly.

Monocytes and macrophages appear to play a critical role in the pathogenesis of NF1 vasculopathy. Lineage-restricted inactivation of *Nf1* in myeloid cells leads to a pro-inflammatory monocyte profile in mice and is sufficient to recapitulate the arterial stenosis phenotype observed in persons with NF1 [11]. *Nf1* mutant macrophages are readily recruited to sites of vascular injury and the excessive ROS production by $Nf1^{+/-}$ macrophages appears to promote a proliferative SMC response *in vitro* and *in vivo*. Interestingly, PMA elicited more ROS in *Nf1* mutant macrophages as compared to WT macrophages, which was effectively blocked by co-incubation with inhibitors of Ras. PMA is a potent stimulus for NADPH via Ras-Erk dependent and independent mechanisms and may explain the exaggerated response of $Nf1^{+/-}$ and $Nf1^{-/-}$ macrophages to PMA [61–64]. Increased production of ROS may propagate a pro-survival macrophage phenotype and increase the generation and secretion of pro-inflammatory cytokines, although this has yet to be demonstrated [65]. Neurofibromin's role in regulating monocyte/macrophage-mediated ROS is further emphasized by the observation that apocynin significantly inhibited neointima formation in $Nf1^{+/-}$ mice while having little effect on WT neointima formation. Although apocynin is generally recognized as a nonspecific antioxidant in vascular wall cells, Heumuller et al. concluded that apocynin dimerizes in myeloperoxidase-expressing cells, including macrophages, and suppresses superoxide production in leukocytes by inhibiting the binding of the cytosolic $p47^{phox}$ subunit to the transmembrane NOX2 complex [42]. Apocynin's dual roles as an antioxidant and specific inhibitor of NOX2 activity likely contribute to the reduced neointima formation observed in $Nf1^{+/-}$ mice. These observations are supported by our findings that genetic deletion of $p47^{phox}$ or myeloid cell specific inactivation of $gp91^{phox}$ inhibited neointima formation in $Nf1^{+/-}$ mice. Further, the activation of $p47^{phox}$ is highly regulated by the Ras dependent kinases Erk and Akt, which is required for NOX2 activation and superoxide production in circulating phagocytes [66–68]. Directly targeting NOX2 for the prevention and/or treatment of NF1-related arterial stenosis may not be viable as NOX2 is critical for respiratory burst and phagocytosis, though clinical trails of small molecule NOX inhibitors are forthcoming [40].

Antioxidants, on the other hand, have yielded promising results in multiple preclinical models of arterial stenosis, but human clinical trials have demonstrated only a modest effect [69–71]. Inhibition of ROS production or sequestering its activity via antioxidant therapy may provide a greater beneficial effect in patients with active Ras mutations, including NF1, than that observed in the general population since small perturbations in kinase activity precipitate a dramatic increase in downstream signaling. For example, anti-oxidant therapy significantly reduced vascular wall ROS in $Nf1^{+/-}$ aortas exposed to angiotensin II (AngII) while having minimal effect on ROS in WT aortas [72]. The preferential effect of antioxidant therapy in $Nf1^{+/-}$ mice may be explained by the high numbers of macrophages observed in $Nf1^{+/-}$ aortas exposed to

AngII resulting in an abundance of oxidant species. Interestingly, low dose simvastatin, an HMG-CoA reductase inhibitor with antioxidant properties, effectively blocked ROS production in *Nf1*$^{+/-}$ aortas exposed to AngII with only a modest treatment effect observed in WT aortas exposed to AngII. While the pleiotropic effects of statins are widely studied, their function as an inhibitor of prenylation has made them an attractive therapy for NF1 patients since prenylation is required for Ras activation [73]. The ability of statins to modulate Ras activity and scavenge oxidative species may cooperate to limit the production and local concentration of ROS within the vascular wall. Statins have proven beneficial for a variety of NF1 manifestations including cognitive deficits, behavioral impairment, bone dysplasia and healing in preclinical models, but randomized trials in NF1 patients have yielded mixed results [11,74–77]. To date, no clinical trials for NF1 vasculopathy have been performed.

In summary, our study identifies a novel role for neurofibromin signaling in the generation of reactive oxygen species and provides genetic and pharmacologic evidence that excessive ROS is linked to NF1 vasculopathy. Further, we provide the first human data to suggest that NF1 patients experience chronic oxidative stress. As neurofibromin-deficient myeloid cells are critical cellular mediators of multiple manifestations of NF1, our findings provide a framework for interrogating ROS in NF1 biology and the rational design of clinical trials using antioxidants for NF1 vasculopathy.

Conflict of interest

The authors have declared that no conflict of interest exists.

Acknowledgements

This work is supported by the Department of Defense (NF140031, B.K.S. and NF073122, D.A.I.), the American Heart Association (15SDG25500005, B.K.S.), the Department of Pediatrics at Augusta University (B.K.S.), and the National Institutes of Health (P50 NS052606, D.A.I.). Additionally, the authors thank Emily Sims and Matthew Repass of the Angio BioCore at the Melvin and Bren Simon Cancer Center for processing the human blood samples for this study, and the assistance of the Flow Cytometry Resource Facility.

References

[1] N. Ratner, S.J. Miller, A RASopathy gene commonly mutated in cancer: the neurofibromatosis type 1 tumour suppressor, Nat. Rev. Cancer 15 (5) (2015) 290–301.
[2] J.M. Friedman, J. Arbiser, J.A. Epstein, D.H. Gutmann, S.J. Huot, A.E. Lin, B. McManus, B.R. Korf, Cardiovascular disease in neurofibromatosis 1: report of the NF1 cardiovascular task force, Genet. Med. 4 (3) (2002) 105–111.
[3] A.E. Lin, P.H. Birch, B.R. Korf, R. Tenconi, M. Niimura, M. Poyhonen, K. Armfield Uhas, M. Sigorini, R. Virdis, C. Romano, et al., Cardiovascular malformations and other cardiovascular abnormalities in neurofibromatosis 1, Am. J. Med. Genet. 95 (2) (2000) 108–117.
[4] G.S. Oderich, T.M. Sullivan, T.C. Bower, P. Gloviczki, D.V. Miller, D. Babovic-Vuksanovic, T.A. Macedo, A. Stanson, Vascular abnormalities in patients with neurofibromatosis syndrome type I: clinical spectrum, management, and results, J. Vasc. Surg. 46 (3) (2007) 475–484.
[5] D. Rea, J.F. Brandsema, D. Armstrong, P.C. Parkin, G. deVeber, D. MacGregor, W. J. Logan, R. Askalan, Cerebral arteriopathy in children with neurofibromatosis type 1, Pediatrics 124 (3) (2009) e476–e483.
[6] T.L. Rosser, G. Vezina, R.J. Packer, Cerebrovascular abnormalities in a population of children with neurofibromatosis type 1, Neurology 64 (3) (2005) 553–555.
[7] S.A. Rasmussen, J.M. Friedman, NF1 gene and neurofibromatosis 1, Am. J. Epidemiol. 151 (1) (2000) 33–40.
[8] E.A. Lasater, F. Li, W.K. Bessler, M.L. Estes, S. Vemula, C.M. Hingtgen, M. C. Dinauer, R. Kapur, S.J. Conway, D.A. Ingram Jr., Genetic and cellular evidence of vascular inflammation in neurofibromin-deficient mice and humans, J. Clin. Invest. 120 (3) (2010) 859–870.
[9] E.A. Lasater, W.K. Bessler, L.E. Mead, W.E. Horn, D.W. Clapp, S.J. Conway, D. A. Ingram, F. Li, Nf1+/- mice have increased neointima formation via hyperactivation of a Gleevec sensitive molecular pathway, Hum. Mol. Genet. 17 (15) (2008) 2336–2344.
[10] B.K. Stansfield, W.K. Bessler, R. Mali, J.A. Mund, B.D. Downing, R. Kapur, D. A. Ingram Jr., Ras-mek-erk signaling regulates nf1 heterozygous neointima formation, Am. J. Pathol. 184 (1) (2014) 79–85.
[11] B.K. Stansfield, W.K. Bessler, R. Mali, J.A. Mund, B. Downing, F. Li, K.N. Sarchet, M.R. DiStasi, S.J. Conway, R. Kapur, et al., Heterozygous inactivation of the Nf1 gene in myeloid cells enhances neointima formation via a rosuvastatin-sensitive cellular pathway, Hum. Mol. Genet. 22 (5) (2013) 977–988.
[12] W.K. Bessler, G. Kim, F. Hudson, J.A. Mund, R. Mali, K. Menon, R. Kapur, D.W. Clapp, D.A. Ingram, Jr., B.K. Stansfield, Nf1$^{+/-}$ monocytes/macrophages induce neointima formation via CCR2 activation. Hum. Mol. Genet., 2016.
[13] D.I. Brown, K.K. Griendling, Regulation of signal transduction by reactive oxygen species in the cardiovascular system, Circ. Res. 116 (3) (2015) 531–549.
[14] E. Ferro, L. Goitre, E. Baldini, S.F. Retta, L. Trabalzini, Ras GTPases are both regulators and effectors of redox agents, Methods Mol. Biol. 1120 (2014) 55–74.
[15] L. Mitchell, G.A. Hobbs, A. Aghajanian, S.L. Campbell, Redox regulation of Ras and Rho GTPases: mechanism and function, Antioxid. Redox Signal. 18 (3) (2013) 250–258.
[16] P.S. Hole, L. Pearn, A.J. Tonks, P.E. James, A.K. Burnett, R.L. Darley, A. Tonks, Ras-induced reactive oxygen species promote growth factor-independent proliferation in human CD34+ hematopoietic progenitor cells, Blood 115 (6) (2010) 1238–1246.
[17] Y. Adachi, Y. Shibai, J. Mitsushita, W.H. Shang, K. Hirose, T. Kamata, Oncogenic Ras upregulates NADPH oxidase 1 gene expression through MEK-ERK-dependent phosphorylation of GATA-6, Oncogene 27 (36) (2008) 4921–4932.
[18] X.J. Li, C.B. Goodwin, S.C. Nabinger, B.M. Richine, Z. Yang, H. Hanenberg, H. Ohnishi, T. Matozaki, G.S. Feng, R.J. Chan, Protein-tyrosine phosphatase Shp2 positively regulates macrophage oxidative burst, J. Biol. Chem. 290 (7) (2015) 3894–3909.
[19] N.Y. Bhatt, T.W. Kelley, V.V. Khramtsov, Y. Wang, G.K. Lam, T.L. Clanton, C. B. Marsh, Macrophage-colony-stimulating factor-induced activation of extracellular-regulated kinase involves phosphatidylinositol 3-kinase and reactive oxygen species in human monocytes, J. Immunol. 169 (11) (2002) 6427–6434.
[20] F. Hannan, I. Ho, J.J. Tong, Y. Zhu, P. Nurnberg, Y. Zhong, Effect of neurofibromatosis type I mutations on a novel pathway for adenylyl cyclase activation requiring neurofibromin and Ras, Hum. Mol. Genet. 15 (7) (2006) 1087–1098.
[21] J. Tong, F. Hannan, Y. Zhu, A. Bernards, Y. Zhong, Neurofibromin regulates G protein-stimulated adenylyl cyclase activity, Nat. Neurosci. 5 (2) (2002) 95–96.
[22] J.J. Tong, S.E. Schriner, D. McCleary, B.J. Day, D.C. Wallace, Life extension through neurofibromin mitochondrial regulation and antioxidant therapy for neurofibromatosis-1 in Drosophila melanogaster, Nat. Genet. 39 (4) (2007) 476–485.
[23] D.A. Mayes, T.A. Rizvi, H. Titus-Mitchell, R. Oberst, G.M. Ciraolo, C.V. Vorhees, A.P. Robinson, S.D. Miller, J.A. Cancelas, A.O. Stemmer-Rachamimov, et al., Nf1 loss and Ras hyperactivation in oligodendrocytes induce NOS-driven defects in myelin and vasculature, Cell Rep. 4 (6) (2013) 1197–1212.
[24] D.A. Ingram, K. Hiatt, A.J. King, L. Fisher, R. Shivakumar, C. Derstine, M. J. Wenning, B. Diaz, J.B. Travers, A. Hood, et al., Hyperactivation of p21(ras) and the hematopoietic-specific Rho GTPase, Rac2, cooperate to alter the proliferation of neurofibromin-deficient mast cells in vivo and in vitro, J. Exp. Med. 194 (1) (2001) 57–69.
[25] J. Yan, S. Chen, Y. Zhang, X. Li, Y. Li, X. Wu, J. Yuan, A.G. Robling, R. Kapur, R. J. Chan, et al., Rac1 mediates the osteoclast gains-in-function induced by haploinsufficiency of Nf1, Hum. Mol. Genet. 17 (7) (2008) 936–948.
[26] F. Li, A.M. Munchhof, H.A. White, L.E. Mead, T.R. Krier, A. Fenoglio, S. Chen, X. Wu, S. Cai, F.C. Yang, et al., Neurofibromin is a novel regulator of RAS-induced signals in primary vascular smooth muscle cells, Hum. Mol. Genet. 15 (11) (2006) 1921–1930.
[27] A. Panday, M.K. Sahoo, D. Osorio, S. Batra, NADPH oxidases: an overview from structure to innate immunity-associated pathologies, Cell. Mol. Immunol. 12 (1) (2015) 5–23.
[28] G. Berton, M.A. Castaldi, M.A. Cassatella, W.M. Nauseef, Editorial: celebrating the 50th anniversary of the seminal discovery that the phagocyte respiratory burst enzyme is an NADPH oxidase, J. Leukoc. Biol. 97 (1) (2015) 1–2.
[29] K.K. Griendling, D. Sorescu, M. Ushio-Fukai, NAD(P)H oxidase: role in cardiovascular biology and disease, Circ. Res. 86 (5) (2000) 494–501.
[30] D.H. Gutmann, A. Aylsworth, J.C. Carey, B. Korf, J. Marks, R.E. Pyeritz, A. Rubenstein, D. Viskochil, The diagnostic evaluation and multidisciplinary management of neurofibromatosis 1 and neurofibromatosis 2, JAMA: J. Am. Med. Assoc. 278 (1) (1997) 51–57.
[31] M.C. Yoder, L.E. Mead, D. Prater, T.R. Krier, K.N. Mroueh, F. Li, R. Krasich, C. J. Temm, J.T. Prchal, D.A. Ingram, Redefining endothelial progenitor cells via clonal analysis and hematopoietic stem/progenitor cell principals, Blood 109 (5) (2007) 1801–1809.
[32] A. Azqueta, K.B. Gutzkow, G. Brunborg, A.R. Collins, Towards a more reliable comet assay: optimising agarose concentration, unwinding time and electrophoresis conditions, Mutat. Res. 724 (1-2) (2011) 41–45.
[33] P.F. Li, R. Dietz, R. von Harsdorf, Differential effect of hydrogen peroxide and superoxide anion on apoptosis and proliferation of vascular smooth muscle cells, Circulation 96 (10) (1997) 3602–3609.
[34] T. Ashino, M. Yamamoto, T. Yoshida, S. Numazawa, Redox-sensitive transcription factor Nrf2 regulates vascular smooth muscle cell migration and neointimal hyperplasia, Arterioscler. Thromb. Vasc. Biol. 33 (4) (2013) 760–768.

[35] R.E. Clempus, K.K. Griendling, Reactive oxygen species signaling in vascular smooth muscle cells, Cardiovasc. Res. 71 (2) (2006) 216–225.
[36] A.N. Lyle, K.K. Griendling, Modulation of vascular smooth muscle signaling by reactive oxygen species, Physiology 21 (2006) 269–280.
[37] S.J. Hamilton, J.M. Friedman, Insights into the pathogenesis of neurofibromatosis 1 vasculopathy, Clin. Genet. 58 (5) (2000) 341–344.
[38] Y. Chen, J. Jiang, H. Miao, X. Chen, X. Sun, Y. Li, Hydrogen-rich saline attenuates vascular smooth muscle cell proliferation and neointimal hyperplasia by inhibiting reactive oxygen species production and inactivating the Ras-ERK1/2-MEK1/2 and Akt pathways, Int. J. Mol. Med. 31 (3) (2013) 597–606.
[39] S.L. Liu, Y.H. Li, G.Y. Shi, S.H. Tang, S.J. Jiang, C.W. Huang, P.Y. Liu, J.S. Hong, H. L. Wu, Dextromethorphan reduces oxidative stress and inhibits atherosclerosis and neointima formation in mice, Cardiovasc. Res. 82 (1) (2009) 161–169.
[40] S. Altenhofer, K.A. Radermacher, P.W. Kleikers, K. Wingler, H.H. Schmidt, Evolution of NADPH oxidase inhibitors: selectivity and mechanisms for target engagement, Antioxid. Redox Signa. 23 (5) (2015) 406–427.
[41] L. Yu, M.T. Quinn, A.R. Cross, M.C. Dinauer, Gp91(phox) is the heme binding subunit of the superoxide-generating NADPH oxidase, Proc. Natl. Acad. Sci. USA 95 (14) (1998) 7993–7998.
[42] S. Heumuller, S. Wind, E. Barbosa-Sicard, H.H. Schmidt, R. Busse, K. Schroder, R.P. Brandes, Apocynin is not an inhibitor of vascular NADPH oxidases but an antioxidant, Hypertension 51 (2) (2008) 211–217.
[43] R.P. Brandes, N. Weissmann, K. Schroder, Nox family NADPH oxidases: molecular mechanisms of activation, Free Radic. Biol. Med. 76 (2014) 208–226.
[44] R.P. Brandes, N. Weissmann, K. Schroder, Redox-mediated signal transduction by cardiovascular Nox NADPH oxidases, J. Mol. Cell. Cardiol. 73 (2014) 70–79.
[45] S.J. Park, B. Sawitzki, L. Kluwe, V.F. Mautner, N. Holtkamp, A. Kurtz, Serum biomarkers for neurofibromatosis type 1 and early detection of malignant peripheral nerve-sheath tumors, BMC Med. 11 (2013) 109.
[46] G.A. Mashour, P.H. Driever, M. Hartmann, S.N. Drissel, T. Zhang, B. Scharf, U. Felderhoff-Muser, S. Sakuma, R.E. Friedrich, R.L. Martuza, et al., Circulating growth factor levels are associated with tumorigenesis in neurofibromatosis type 1, Clin. Cancer Res. 10 (17) (2004) 5677–5683.
[47] K. Sullivan, J. El-Hoss, K.G. Quinlan, N. Deo, F. Garton, J.T. Seto, M. Gdalevitch, N. Turner, G.J. Cooney, M. Kolanczyk, et al., NF1 is a critical regulator of muscle development and metabolism, Hum. Mol. Genet. 23 (5) (2014) 1250–1259.
[48] E.C. O'Brien, W.H. Abdulahad, A. Rutgers, M.G. Huitema, V.P. O'Reilly, A. M. Coughlan, M. Harrington, P. Heeringa, M.A. Little, F.B. Hickey, Intermediate monocytes in ANCA vasculitis: increased surface expression of ANCA autoantigens and IL-1beta secretion in response to anti-MPO antibodies, Sci. Rep. 5 (11888) (2015).
[49] L. Ziegler-Heitbrock, Blood monocytes and their subsets: established features and open questions, Front. Immunol. 6 (423) (2015).
[50] B.K. Stansfield, D.A. Ingram, Clinical significance of monocyte heterogeneity, Clin. Transl. Med. 4 (5) (2015).
[51] D. Komatsu, M. Kato, J. Nakayama, S. Miyagawa, T. Kamata, NADPH oxidase 1 plays a critical mediating role in oncogenic Ras-induced vascular endothelial growth factor expression, Oncogene 27 (34) (2008) 4724–4732.
[52] A.Y. Alexandrova, P.B. Kopnin, J.M. Vasiliev, B.P. Kopnin, ROS up-regulation mediates Ras-induced changes of cell morphology and motility, Exp. Cell Res. 312 (11) (2006) 2066–2073.
[53] M.T. Park, M.J. Kim, Y. Suh, R.K. Kim, H. Kim, E.J. Lim, K.C. Yoo, G.H. Lee, Y. H. Kim, S.G. Hwang, et al., Novel signaling axis for ROS generation during K-Ras-induced cellular transformation, Cell Death Differ. 21 (8) (2014) 1185–1197.
[54] S. Svegliati, R. Cancello, P. Sambo, M. Luchetti, P. Paroncini, G. Orlandini, G. Discepoli, R. Paterno, M. Santillo, C. Cuozzo, et al., Platelet-derived growth factor and reactive oxygen species (ROS) regulate Ras protein levels in primary human fibroblasts via ERK1/2. Amplification of ROS and Ras in systemic sclerosis fibroblasts, J. Biol. Chem. 280 (43) (2005) 36474–36482.
[55] R.S. Keshari, A. Verma, M.K. Barthwal, M. Dikshit, Reactive oxygen species-induced activation of ERK and p38 MAPK mediates PMA-induced NETs release from human neutrophils, J. Cell. Biochem. 114 (3) (2013) 532–540.
[56] S. Luanpitpong, P. Chanvorachote, U. Nimmannit, S.S. Leonard, C. Stehlik, L. Wang, Y. Rojanasakul, Mitochondrial superoxide mediates doxorubicin-induced keratinocyte apoptosis through oxidative modification of ERK and Bcl-2 ubiquitination, Biochem. Pharmacol. 83 (12) (2012) 1643–1654.
[57] F. Mologoni, F.H. de Melo, C.T. da Silva, M.G. Jasiulionis, Ras and Rac1, frequently mutated in melanomas, are activated by superoxide anion, modulate Dnmt1 level and are causally related to melanocyte malignant transformation, PLoS One 8 (12) (2013), e81937.
[58] I. The, G.E. Hannigan, G.S. Cowley, S. Reginald, Y. Zhong, J.F. Gusella, I.K. Hariharan, A. Bernards, Rescue of a Drosophila NF1) mutant phenotype by protein kinase A, Science 276 (5313) (1997) 791–794.
[59] A.R. Collins, Measuring oxidative damage to DNA and its repair with the comet assay, Biochim. Biophys. Acta. 1840 (2) (2014) 794–800.
[60] A. Pemov, C. Park, K.M. Reilly, D.R. Stewart, Evidence of perturbations of cell cycle and DNA repair pathways as a consequence of human and murine NF1-haploinsufficiency, BMC Genom. 11 (194) (2010).
[61] A. Karlsson, J.B. Nixon, L.C. McPhail, Phorbol myristate acetate induces neutrophil NADPH-oxidase activity by two separate signal transduction pathways: dependent or independent of phosphatidylinositol 3-kinase, J. Leukoc. Biol. 67 (3) (2000) 396–404.
[62] J.A. Frost, T.D. Geppert, M.H. Cobb, J.R. Feramisco, A requirement for extracellular signal-regulated kinase (ERK) function in the activation of AP-1 by Ha-Ras, phorbol 12-myristate 13-acetate, and serum, Proc. Natl. Acad. Sci. USA 91 (9) (1994) 3844–3848.
[63] D. Buscher, R.A. Hipskind, S. Krautwald, T. Reimann, M. Baccarini, Ras-dependent and -independent pathways target the mitogen-activated protein kinase network in macrophages, Mol. Cell. Biol. 15 (1) (1995) 466–475.
[64] M.E. Smith, K. van der Maesen, F.P. Somera, R.A. Sobel, Effects of phorbol myristate acetate (PMA) on functions of macrophages and microglia in vitro, Neurochem. Res. 23 (3) (1998) 427–434.
[65] A. Anwar, A.K. Keating, D. Joung, S. Sather, G.K. Kim, K.K. Sawczyn, L. Brandao, P.M. Henson, D.K. Graham, Mer tyrosine kinase (MerTK) promotes macrophage survival following exposure to oxidative stress, J. Leukoc. Biol. 86 (1) (2009) 73–79.
[66] K. Winiarska, R. Jarzyna, J.M. Dzik, A.K. Jagielski, M. Grabowski, A. Nowosielska, D. Focht, B. Sierakowski, ERK1/2 pathway is involved in renal gluconeogenesis inhibition under conditions of lowered NADPH oxidase activity, Free Radic. Biol. Med. 81 (2015) 13–21.
[67] L. Vergori, E. Lauret, A. Gaceb, C. Beauvillain, R. Andriantsitohaina, M. C. Martinez, PPARalpha regulates endothelial progenitor cell maturation and myeloid lineage differentiation through a NADPH oxidase-dependent mechanism in mice, Stem Cells 33 (4) (2015) 1292–1303.
[68] J. Kučera, L. Binó, K. Štefková, J. Jaroš, O. Vašíček, J. Večeřa, L. Kubala, J. Pacherník, Apocynin and diphenyleneiodonium induce oxidative stress and modulate PI3K/Akt and MAPK/Erk activity in mouse embryonic stem cells, Oxid. Med. Cell. Longev. 2016 (2015).
[69] S.B. Kritchevsky, T. Shimakawa, G.S. Tell, B. Dennis, M. Carpenter, J.H. Eckfeldt, H. Peacher-Ryan, G. Heiss, Dietary antioxidants and carotid artery wall thickness. The ARIC study. Atherosclerosis risk in communities study, Circulation 92 (8) (1995) 2142–2150.
[70] M. Aviram, M. Rosenblat, D. Gaitini, S. Nitecki, A. Hoffman, L. Dornfeld, N. Volkova, D. Presser, J. Attias, H. Liker, et al., Pomegranate juice consumption for 3 years by patients with carotid artery stenosis reduces common carotid intima-media thickness, blood pressure and LDL oxidation, Clin. Nutr. 23 (3) (2004) 423–433.
[71] K.K. Griendling, G.A. FitzGerald, Oxidative stress and cardiovascular injury: Part II: animal and human studies, Circulation 108 (17) (2003) 2034–2040.
[72] F. Li, B.D. Downing, L.C. Smiley, J.A. Mund, M.R. Distasi, W.K. Bessler, K. N. Sarchet, D.M. Hinds, L.M. Kamendulis, C.M. Hingtgen, et al., Neurofibromin-deficient myeloid cells are critical mediators of aneurysm formation in vivo, Circulation 129 (11) (2014) 1213–1224.
[73] A.D. Cox, C.J. Der, M.R. Philips, Targeting RAS membrane association: back to the future for Anti-RAS drug discovery? Clin. Cancer Res. 21 (8) (2015) 1819–1827.
[74] L.C. Krab, A. de Goede-Bolder, F.K. Aarsen, S.M. Pluijm, M.J. Bouman, J.N. van der Geest, M. Lequin, C.E. Catsman, W.F. Arts, S.A. Kushner, et al., Effect of simvastatin on cognitive functioning in children with neurofibromatosis type 1: a randomized controlled trial, JAMA: J. Am. Med. Assoc. 300 (3) (2008) 287–294.
[75] W. Wang, J.S. Nyman, H.E. Moss, G. Gutierrez, G.R. Mundy, X. Yang, F. Elefteriou, Local low-dose lovastatin delivery improves the bone-healing defect caused by Nf1 loss of function in osteoblasts, J. Bone Miner. Res. 25 (7) (2010) 1658–1667.
[76] M. Kolanczyk, J. Kuhnisch, N. Kossler, M. Osswald, S. Stumpp, B. Thurisch, U. Kornak, S. Mundlos, Modelling neurofibromatosis type 1 tibial dysplasia and its treatment with lovastatin, BMC Med. 6 (21) (2008).
[77] M.T. Acosta, P.G. Kardel, K.S. Walsh, K.N. Rosenbaum, G.A. Gioia, R.J. Packer, Lovastatin as treatment for neurocognitive deficits in neurofibromatosis type 1: phase I study, Pediatr. Neurol. 45 (4) (2011) 241–245.

Human Molecular Genetics, 2016, Vol. 25, No. 6 1129–1139

doi: 10.1093/hmg/ddv635
Advance Access Publication Date: 5 January 2016
Original Article

ORIGINAL ARTICLE

Nf1$^{+/-}$ monocytes/macrophages induce neointima formation via CCR2 activation

Waylan K. Bessler[1,2,3,†], Grace Kim[4,5,†], Farlyn Z. Hudson[4,5], Julie A. Mund[1,2], Raghuveer Mali[1,2,3], Keshav Menon[1,2], Reuben Kapur[1,2,3], D. Wade Clapp[1,2,3], David A. Ingram Jr[1,2,3] and Brian K. Stansfield[4,5,*]

[1]Herman B. Wells Center for Pediatric Research, [2]Department of Pediatrics and Neonatal-Perinatal Medicine and [3]Department of Biochemistry and Molecular Biology, Indiana University School of Medicine, Indianapolis, IN 46202, USA, [4]Department of Pediatrics and Neonatal-Perinatal Medicine and [5]Vascular Biology Center, Augusta University, Augusta, GA 30912, USA

*To whom correspondence should be addressed at: Department of Pediatrics, Augusta University, 1120 15th Street, BIW 6033, Augusta, GA 30912, USA. Tel: +1 7067212331; Fax: +1 7067217531; Email: bstansfield@gru.edu

Abstract

Persons with neurofibromatosis type 1 (NF1) have a predisposition for premature and severe arterial stenosis. Mutations in the *NF1* gene result in decreased expression of neurofibromin, a negative regulator of p21^{Ras}, and increases Ras signaling. Heterozygous *Nf1* (*Nf1*$^{+/-}$) mice develop a marked arterial stenosis characterized by proliferating smooth muscle cells (SMCs) and a predominance of infiltrating macrophages, which closely resembles arterial lesions from NF1 patients. Interestingly, lineage-restricted inactivation of a single *Nf1* allele in monocytes/macrophages is sufficient to recapitulate the phenotype observed in *Nf1*$^{+/-}$ mice and to mobilize proinflammatory CCR2+ monocytes into the peripheral blood. Therefore, we hypothesized that CCR2 receptor activation by its primary ligand monocyte chemotactic protein-1 (MCP-1) is critical for monocyte infiltration into the arterial wall and neointima formation in *Nf1*$^{+/-}$ mice. MCP-1 induces a dose-responsive increase in *Nf1*$^{+/-}$ macrophage migration and proliferation that corresponds with activation of multiple Ras kinases. In addition, *Nf1*$^{+/-}$ SMCs, which express CCR2, demonstrate an enhanced proliferative response to MCP-1 when compared with WT SMCs. To interrogate the role of CCR2 activation on *Nf1*$^{+/-}$ neointima formation, we induced neointima formation by carotid artery ligation in *Nf1*$^{+/-}$ and WT mice with genetic deletion of either *MCP1* or *CCR2*. Loss of MCP-1 or CCR2 expression effectively inhibited *Nf1*$^{+/-}$ neointima formation and reduced macrophage content in the arterial wall. Finally, administration of a CCR2 antagonist significantly reduced *Nf1*$^{+/-}$ neointima formation. These studies identify MCP-1 as a potent chemokine for *Nf1*$^{+/-}$ monocytes/macrophages and CCR2 as a viable therapeutic target for NF1 arterial stenosis.

Introduction

Neurofibromatosis type 1 (NF1) is an autosomal dominant disorder affecting 1 in 3000 persons and is the result of inactivating mutations in the *NF1* tumor suppressor gene. Neurofibromin, the protein product of *NF1*, functions as a GTPase activating protein for p21^{ras} (Ras) and accelerates the slow, intrinsic hydrolysis of active Ras-GTP to its inactive diphosphate conformation (1). Inherited mutations of *NF1* affect a single gene copy and result in disease with complete penetrance and a broad range of clinical features.

Cardiovascular disease represents a common, yet understudied, manifestation of NF1 that contributes to the early mortality observed in this patient population (2). NF1 vasculopathy

[†]These authors contributed equally to this work.

Received: October 26, 2015. **Revised:** December 7, 2015. **Accepted:** December 30, 2015

primarily affects the arterial network with a strong predilection for the renal artery and proximal branches of the carotid artery. The exact frequency of vasculopathy in NF1 patients is unknown; however, multiple case series and large patient cohorts suggest the prevalence of arterial disease approaches 10% (3–7). The insidious and progressive clinical presentation of these lesions in early adulthood likely places the true incidence much higher. In fact, histologic evidence of cardiovascular disease was identified in nearly 50% of young adults with NF1 in one case series (8), whereas a comprehensive review of 3253 death certificates revealed a diagnosis of vasculopathy was listed 7.2 times more frequently than expected among NF1 patients less than 30 years of age at the time of death (4).

Arterial lesions associated with NF1 are characterized by smooth muscle cell (SMC) hyperplasia, leukocyte infiltration and arterial remodeling leading to vasoocclusion and tissue ischemia (2,9–11). Previously, we developed a mouse model of NF1 arterial stenosis using *Nf1* heterozygous ($Nf1^{+/-}$) mice that completely recapitulates the human phenotype (12). Although neointima formation is the result of complex interactions between vascular wall cells and circulating leukocytes, we showed that loss of a single *Nf1* allele in bone marrow cells is both necessary and sufficient to induce arterial stenosis (13). These results were somewhat surprising, because neurofibromin-deficient SMC have increased proliferation and migration in response to multiple growth factors and $Nf1^{+/-}$ macrophages (13,14). Neurofibromin-deficient macrophages are the dominant hematopoietic cell within the neointima of $Nf1^{+/-}$ mice and likely secrete cytokines and chemokines that stimulate SMC proliferation and migration (13,15). Thus, it is plausible that loss of neurofibromin in bone marrow and circulating hematopoietic cells, particularly monocytes and macrophages, may predispose NF1 patients to develop exaggerated responses to acute and chronic inflammation or insult. Emerging evidence in NF1 patients is supportive of this hypothesis. Asymptomatic NF1 patients have increased circulating proinflammatory cytokines and monocytes ($CD14^+CD16^+$) in the peripheral blood compared with controls (13). Similar to NF1 patients, $Nf1^{+/-}$ mice have increased circulating $Ly6C^{hi}CCR2^+$ monocytes, which are the murine correlate of human proinflammatory monocytes (15,16). Murine $Ly6C^{hi}CCR2^+$ leukocytes are primitive bone-marrow-derived monocytes that are actively recruited to sites of inflammation and differentiate into macrophages and inflammatory dendritic cells (17,18). In support of our hypothesis that neurofibromin regulates inflammatory cascades in circulating leukocytes, we recently showed that loss of a single *Nf1* gene copy in myeloid cells was sufficient to mobilize $Ly6C^{hi}CCR2^+$ monocytes and induce arterial stenosis following carotid artery ligation (15). Interestingly, genetic deletion of both *Nf1* gene copies in myeloid cells alone resulted in a 4-fold increase in circulating $Ly6C^{hi}CCR2^+$ monocytes and nearly complete arterial occlusion following carotid ligation (15).

Based on these observations, we generated compound mutant mice to test the hypothesis that CCR2 activation is critical for $Nf1^{+/-}$ macrophage recruitment to sites of vascular injury and necessary for $Nf1^{+/-}$ neointima formation. Further, we sought to understand how CCR2 activation by its primary ligand, monocyte chemotactic protein-1 (MCP-1/CCL2), mediates neurofibromin-deficient macrophage function and SMC proliferation. Finally, we use our murine model system to test the efficacy of a potent and specific inhibitor of the CCR2 receptor as a potential therapeutic intervention in the treatment of NF1 arterial stenosis.

Results

MCP-1 is a potent chemokine for $Nf1^{+/-}$ macrophages and SMC

MCP-1 is a monomeric polypeptide anchored to the endothelial monolayer of blood vessels and secreted by SMC and circulating leukocytes (19,20). The chemotactic properties of MCP-1 are primarily mediated through its activation of the CCR2 receptor (19,21–23). Importantly, the expression of CCR2 in the cardiovascular system is restricted to endothelial cells (ECs), SMC and monocytes/macrophages and is not a mediator of granulocyte chemotaxis (24–26). Therefore, we derived $Nf1^{+/-}$ and WT macrophages from $Nf1^{+/-}$ and WT mice to assess their functional response to MCP-1 stimulation. At baseline, $Nf1^{+/-}$ macrophages demonstrate a 2-fold increase in migration, but do not exhibit enhanced proliferation. In response to MCP-1 incubation, $Nf1^{+/-}$ macrophages exhibited a dose-dependent increase in chemotaxis and proliferation when compared with WT macrophages (Fig. 1A and B). Although MCP-1 also increased WT macrophage migration and proliferation in a dose-dependent manner, MCP-1 stimulated a 2- to 3-fold increase in $Nf1^{+/-}$ macrophage migration and proliferation when compared with WT macrophages at the same concentration of MCP-1. Interestingly, analysis of culture media from growth-arrested $Nf1^{+/-}$ and WT macrophages revealed an increased concentration of MCP-1 in the media of cultured $Nf1^{+/-}$ macrophages when compared with WT macrophage media (Fig. 1C). Cell counts of growth-arrested macrophages did not differ between genotypes (data not shown). Next, we analyzed neurofibromin-regulated Ras kinase activity to determine which pathway may be preferentially activated in in $Nf1^{+/-}$ macrophages in response to MCP-1 (Fig. 1D). While phosphorylation of both Erk and Akt was demonstrated in $Nf1^{+/-}$ macrophages incubated with MCP-1, the increase in p-Erk/Erk ratio did not differ between $Nf1^{+/-}$ and WT macrophages incubated with MCP-1 and likely represents an increase in Erk activity that is independent of neurofibromin expression. Akt phosphorylation, on the other hand, was dramatically higher in $Nf1^{+/-}$ macrophages stimulated with MCP-1 when compared with WT macrophages stimulated with MCP-1. Thus, $Nf1^{+/-}$ macrophages exhibit an exaggerated response to MCP-1 stimulation that corresponds with preferential activation of the PI3-K–Akt pathway.

Infiltrating macrophages secrete growth factors and cytokines to induce SMC proliferation and inward remodeling, which are hallmarks of arterial stenosis. Although genetic deletion of *Nf1* in SMC is not required for $Nf1^{+/-}$ neointima formation, $Nf1^{+/-}$ SMCs demonstrate enhanced proliferation in response to multiple growth factors and co-incubation with $Nf1^{+/-}$ and WT macrophages (14,15,27). Based on the observation that $Nf1^{+/-}$ macrophages exhibit increased production of MCP-1 and that SMC express CCR2, we isolated SMC from WT, $Nf1^{+/-}$ and $Nf1^{+/-}$; $CCR2^{-/-}$ mice to assess their proliferative response to MCP-1. Similar to previous published reports, WT SMC showed a modest proliferative response to MCP-1 (28–31) (Fig. 2A). While $Nf1^{+/-}$ SMCs are more proliferative at baseline, $Nf1^{+/-}$ SMC exhibited a nearly 2-fold increase in proliferation in response to MCP-1 stimulation when compared with untreated $Nf1^{+/-}$ SMC. MCP-1 expression in cultured $Nf1^{+/-}$ SMC and secretion into growth media was similar to WT SMC (data not shown). Genetic deletion of CCR2 in $Nf1^{+/-}$ SMC completely abolished the proliferative response mediated by MCP-1 and demonstrates that MCP-1 is primarily activating CCR2 on $Nf1^{+/-}$ SMC (Fig. 2A). Examination of Ras-dependent kinase activity revealed a profound increase in Erk signaling in $Nf1^{+/-}$ SMC stimulated with MCP-1 when

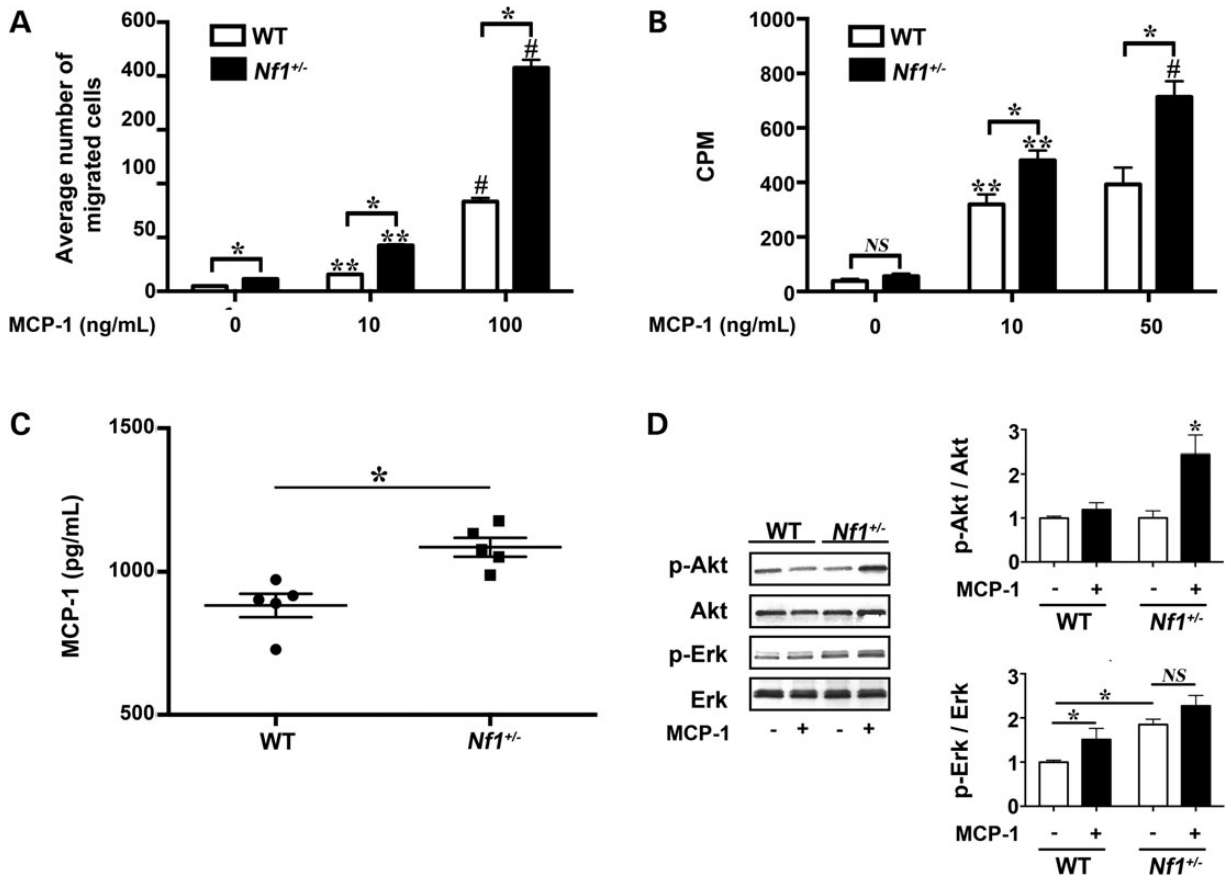

Figure 1. MCP-1 enhances $Nf1^{+/-}$ macrophage function. WT (white bars) and $Nf1^{+/-}$ (black bars) macrophage migration and proliferation, in response to MCP-1. (**A**) Data represent average number of migrated cells per HPF ± SEM, $n = 5$. *$P < 0.001$ for WT versus $Nf1^{+/-}$ macrophages at indicated concentration of MCP-1. **$P < 0.001$ for unstimulated WT and $Nf1^{+/-}$ macrophages versus MCP-1 (10 ng/ml) stimulated WT and $Nf1^{+/-}$ macrophages. #$P < 0.0001$ for MCP-1 (10 ng/ml) stimulated WT and $Nf1^{+/-}$ macrophages versus MCP-1 (100 ng/ml) stimulated WT and $Nf1^{+/-}$ macrophages. (**B**) Data represent thymidine incorporation reported as mean counts per minute (cpm) ± SEM, $n = 5$. *$P < 0.001$ for WT versus $Nf1^{+/-}$ macrophages at indicated concentration of MCP-1. **$P < 0.001$ for unstimulated WT and $Nf1^{+/-}$ macrophages versus MCP-1 (10 ng/ml) stimulated WT and $Nf1^{+/-}$ macrophages. #$P < 0.001$ for MCP-1 (10 ng/ml) stimulated $Nf1^{+/-}$ macrophages versus MCP-1 (50 ng/ml) stimulated $Nf1^{+/-}$ macrophages. (**C**) Data represent MCP-1 concentration reported as pg/ml ± SEM, $n = 5$. *$P < 0.01$ for WT versus $Nf1^{+/-}$ macrophage-conditioned media. (**D**) Representative western blots of Akt and Erk phosphorylation in WT and $Nf1^{+/-}$ macrophages treated with/without MCP-1 (10 ng/ml), $n = 4$. Quantitative densitometry ± SEM is reported as ratio of phosphorylated-Akt to total Akt or phosphorylated-Erk to total Erk density and corrected to unstimulated WT macrophages. *$P < 0.001$ for pAkt/Akt ratio in all conditions versus $Nf1^{+/-}$ macrophages stimulated with MCP-1. *$P < 0.01$ for pErk/Erk ratio for unstimulated WT macrophages versus MCP-1 stimulated WT macrophages and unstimulated $Nf1^{+/-}$ macrophages.

compared with unstimulated $Nf1^{+/-}$ SMC (Fig. 2B). MCP-1 did not alter Akt activity in $Nf1^{+/-}$ SMC (data not shown). Based on the substantial increase in Erk activity in response to MCP-1, we incubated $Nf1^{+/-}$ and WT SMC with MCP-1 (10 ng/ml) in the presence or absence of PD0325901, a potent inhibitor of Mek–Erk signaling. At low nanomolar concentrations of PD0325901, MCP-1 failed to evoke a proliferative response in *Nf1*+/– SMC (Fig. 2C). Not surprisingly, blockade of Erk signaling also reduced WT SMC proliferation and strengthens the argument that Erk activation is critical for MCP-1 elicited SMC proliferation. Collectively, these data suggest that $Nf1^{+/-}$ SMC exhibit enhanced proliferation in response to MCP-1 via Erk activation.

Genetic deletion of MCP-1 or CCR2 abrogates $Nf1^{+/-}$ neointima formation

Based on our observations that MCP-1 is a potent stimulus for $Nf1^{+/-}$ macrophage and SMC, we sought to interrogate the role of MCP-1/CCR2 signaling in the pathogenesis $Nf1^{+/-}$ arterial stenosis. $Nf1^{+/-}$ mice were intercrossed with $MCP1^{-/-}$ mice to generate compound mutant $Nf1^{+/-}$;$MCP1^{-/-}$ mice. WT, $MCP1^{-/-}$, $Nf1^{+/-}$ and $Nf1^{+/-}$; $MCP1^{-/-}$ mice underwent surgical ligation of the right common carotid artery to induce neointima formation. In response to arterial injury, WT mice developed a modest neointima, whereas $Nf1^{+/-}$ mice developed a robust neointimal layer after arterial injury (Fig. 3). Genetic deletion of MCP-1 completely inhibited neointima formation in $Nf1^{+/-}$ mice. Morphometric analysis of serial cross sections revealed a 70% reduction in neointima area (Fig. 3B) and a 55% reduction in intima/media (I/M) ratio (Fig. 3C). Corresponding with the reduced neointima in $Nf1^{+/-}$ mice lacking MCP-1 expression, Mac-3+ macrophage staining in the neointimas of $Nf1^{+/-}$; $MCP1^{-/-}$ mice were significantly reduced when compared with $Nf1^{+/-}$ neointimas (10.4 ± 3.0% versus 17.3 ± 3.4% of total cell number, $P = 0.1$; Fig. 3D).

Although MCP-1 primarily binds to CCR2, recent evidence suggests that MCP-1 has non-CCR2-mediated effects in SMC including binding of the CCR4 receptor (32,33). Therefore, we intercrossed $Nf1^{+/-}$ and $CCR2^{-/-}$ mice to examine the role of CCR2 activation on $Nf1^{+/-}$ neointima formation and macrophage infiltration into the vascular wall. The common carotid arteries of

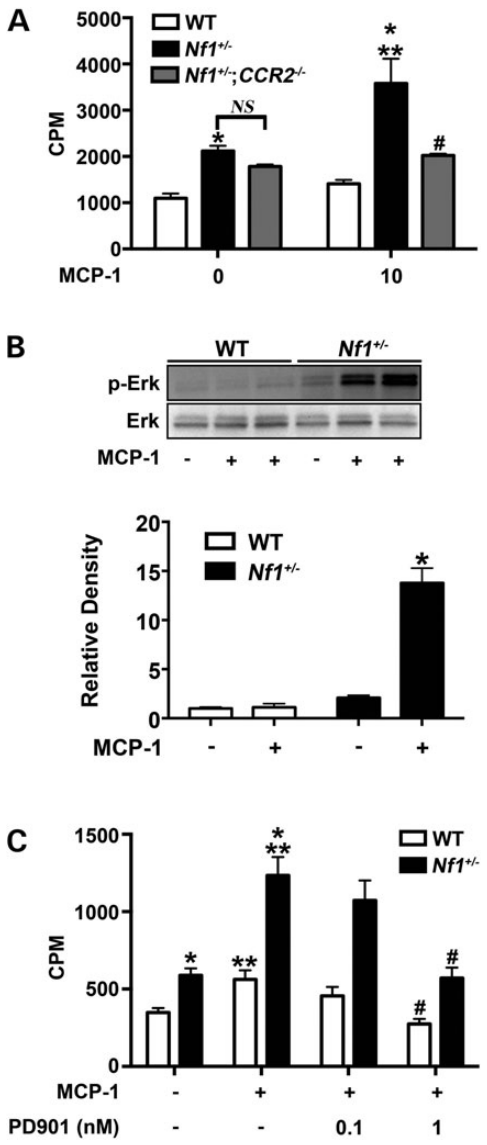

Figure 2. MCP-1 enhances $Nf1^{+/-}$ SMC proliferation via Erk activation. WT (white bars), $Nf1^{+/-}$ (black bars) and $Nf1^{+/-}$;$CCR2^{-/-}$ (gray bars) SMC proliferation in response to stimulation with MCP-1. (**A**) Data represent thymidine incorporation as mean cpm ± SEM, $n = 4$. *$P < 0.05$ for WT SMC versus $Nf1^{+/-}$ SMC at indicated concentrations of MCP-1. No statistical difference was observed between unstimulated $Nf1^{+/-}$ and $Nf1^{+/-}$;$CCR2^{-/-}$ SMC. **$P < 0.001$ for unstimulated $Nf1^{+/-}$ SMC versus MCP-1 stimulated $Nf1^{+/-}$ SMC. #$P < 0.001$ for MCP-1 stimulated $Nf1^{+/-}$ SMC versus MCP-1 stimulated $Nf1^{+/-}$;$CCR2^{-/-}$ SMC. (**B**) Representative western blot and quantitative densitometry of Erk phosphorylation in WT and $Nf1^{+/-}$ SMC treated with/without MCP-1 (10 ng/ml), $n = 3$. Quantitative densitometry ± SEM is reported as ratio for phosphorylated-Erk to total Erk density and corrected to unstimulated WT SMC. *$P < 0.0001$ for all conditions versus $Nf1^{+/-}$ SMC stimulated with MCP-1. (**C**) Data represent thymidine incorporation as mean cpm ± SEM, $n = 3$. *$P < 0.05$ for WT SMC versus $Nf1^{+/-}$ SMC at indicated concentrations of MCP-1. **$P < 0.01$ for unstimulated $Nf1^{+/-}$ and WT SMC versus MCP-1 stimulated $Nf1^{+/-}$ and WT SMC. #$P < 0.01$ for MCP-1 stimulated $Nf1^{+/-}$ and WT SMC versus MCP-1 stimulated $Nf1^{+/-}$ and WT SMC in the presence of PD0325901 at indicated concentration.

WT, $CCR2^{-/-}$, $Nf1^{+/-}$ and $Nf1^{+/-}$; $CCR2^{-/-}$ mice were ligated and analyzed for neointima formation after a 28-day recovery period. Similar to our previous experiment, $Nf1^{+/-}$ mice form a large neointima when compared with WT mice. Homozygous deletion of *CCR2* in $Nf1^{+/-}$ mice completely abrogated neointima formation and quantitative analysis of arterial cross sections demonstrated that arterial remodeling and neointima size were similar to WT arteries (Fig. 4A–C). Consistent with these observations, Mac-3+ macrophage infiltration into the neointima was reduced in $Nf1^{+/-}$;$CCR2^{-/-}$ mice when compared with $Nf1^{+/-}$ mice (12.2 ± 2.9% versus 21.53 ± 3.5% of total cell number, $P < 0.05$; Fig. 4D). Thus, MCP-1 and CCR2 expression are critical for neointima formation in $Nf1^{+/-}$ mice.

Pharmacologic inhibition of CCR2 inhibits $Nf1^{+/-}$ neointima formation

Pharmacologic inhibition of CCR2 could provide an attractive therapeutic target for NF1 patients with evidence of vasculopathy. Therefore, we utilized a specific CCR2 antagonist (INCB3284) for preclinical testing in our murine model system of NF1 arterial stenosis (34). $Nf1^{+/-}$ and WT mice were administered INCB3284 or vehicle via intraperitoneal injection immediately after arterial injury and once daily for 10 days as rescue therapy. This regimen was selected based on published pharmacokinetics for INCB3284 and specific targeting of macrophages during the early phase of arterial remodeling (34). In response to carotid artery ligation, vehicle-treated $Nf1^{+/-}$ mice developed significant intimal hyperplasia, whereas WT mice developed a more modest neointima, which was grossly and quantitatively similar to our previous observations (Fig. 5A–C). Daily administration of INCB 3284 as a rescue therapy significantly reduced neointima formation in $Nf1^{+/-}$ mice when compared with vehicle-treated $Nf1^{+/-}$ mice (Fig. 5B and C). While there was a trend toward reduction of neointima area and I/M ratio in WT mice treated with INCB 3284 when compared with WT mice receiving PBS treatment, statistical significance was not achieved ($P = 0.11$ and 0.5, respectively). Mac-3+ macrophage content was also reduced in $Nf1^{+/-}$ mice treated with INCB 3284 when compared with $Nf1^{+/-}$ mice receiving PBS treatment (16.3 ± 3.2% versus 24.12 ± 3.1% of total cell number, $P < 0.05$; Fig. 5D). Weight gain was similar between INCB 3284 and vehicle treatment groups, and no toxicities were observed on autopsy and inspection of visceral organs. These are the first data to suggest that a competitive CCR2 antagonist may be a viable therapeutic intervention for NF1 patients with evidence of cardiovascular disease.

Discussion

To date, therapeutic interventions for NF1 patients with cardiovascular disease have been limited, and tailored therapies directed at neurofibromin deficiency or its downstream targets are non-existent. Multiple extracellular signaling inputs converge on canonical Ras to maintain normal cell turnover, which limits the long-term use of Ras kinase inhibitors in patients with NF1 cardiovascular disease. Thus, a complete understanding of the pathogenesis of arterial disease in NF1 patients is imperative to inform novel therapeutic approaches leading to disease-specific clinical trials. Along this line of reasoning, emerging evidence suggests that NF1 patients experience chronic inflammation including increased cytokine production and frequency of circulating proinflammatory $CD14^{+}CD16^{+}$ monocytes in their peripheral blood (13). These findings are supported by our recent observation that $Nf1^{+/-}$ mice have increased circulating $Ly6C^{hi}$ monocytes, which closely resemble human proinflammatory intermediate monocytes (16). Increased cell surface expression of CCR2 is characteristic of $Ly6C^{hi}$ monocytes and enables these primitive myeloid cells to emigrate from the bone marrow and home to sites of inflammation where they differentiate into

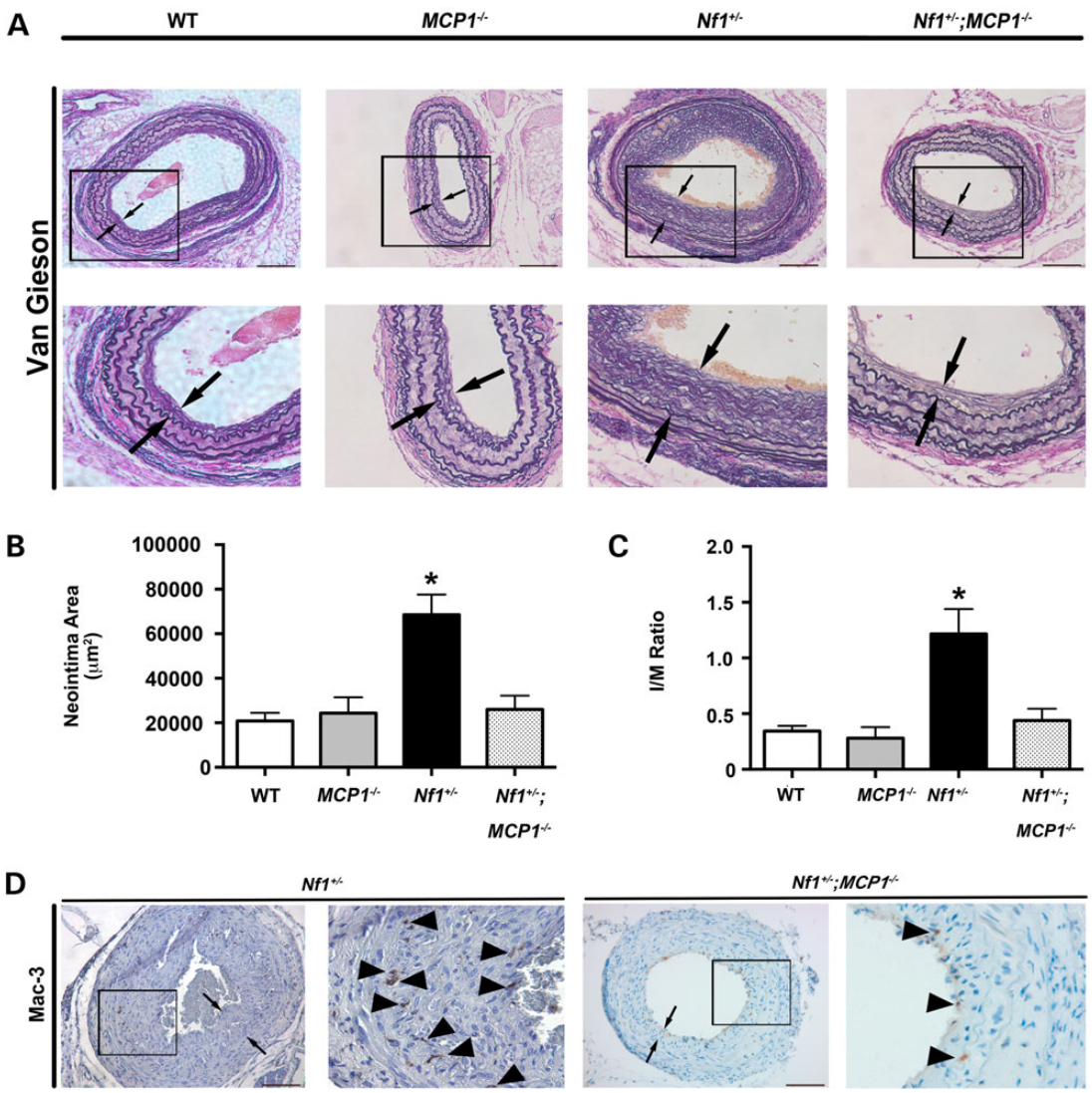

Figure 3. Genetic deletion of MCP-1 inhibits $Nf1^{+/-}$ neointima formation. Representative photomicrographs (**A**) and quantification of neointima area (**B** and **C**) of injured carotid arteries from WT, $MCP1^{-/-}$, $Nf1^{+/-}$ and $Nf1^{+/-}$;$MCP1^{-/-}$ mice. (A) Black arrows indicate neointima boundaries. Black boxes identify area of injured artery that is magnified below. Scale bars: 100 μm. (B and C) Quantification of neointima area (B) and I/M ratio (C) of injured carotid arteries from WT, $MCP1^{-/-}$, $Nf1^{+/-}$ and $Nf1^{+/-}$; $MCP1^{-/-}$ mice. Data represent mean neointima area or I/M ratio ± SEM, $n = 10–12$. *$P < 0.01$ for WT, $MCP1^{-/-}$ and $Nf1^{+/-}$;$MCP1^{-/-}$ mice versus $Nf1^{+/-}$ mice. (**D**) Representative photomicrographs of Mac-3 staining in injured carotid arteries from $Nf1^{+/-}$ and $Nf1^{+/-}$;$MCP1^{-/-}$ mice. Black arrows indicate neointima boundaries. Black box identifies area of injured artery that is magnified in the right column. Black arrowheads represent positive macrophage (anti-Mac3) staining. Scale bars: 100 μm.

macrophages and secrete growth factors, reactive oxygen species and cytokines (35). Neurofibromin appears to play a central role in their derivation and mobilization from the bone marrow. Similar to $Nf1^{+/-}$ mice, mice harboring a lineage-restricted deletion of a single *Nf1* gene copy in myeloid cells have increased Ly6-C^{hi}CCR2+ monocytes in the peripheral blood (15). Interestingly, genetic deletion of both *Nf1* gene copies resulted in a 4-fold increase in circulating Ly6C^{hi}CCR2+ monocyte frequency, which strongly suggests that neurofibromin directly regulates monocyte mobilization and inflammation via a cell autonomous and gene-dosage-dependent mechanism (15).

Not surprisingly, monocytes and macrophages appear to play a central role in the pathogenesis of NF1-related arterial stenosis. Experimental ligation of the common carotid artery in mice harboring a myeloid-specific deletion of *Nf1* results in a robust neointima that is identical to $Nf1^{+/-}$ mice and NF1 patients. Deletion of both *Nf1* alleles in myeloid cells resulted in a near-total occlusion of the carotid artery after injury. Thus, neointima formation in *Nf1*-mutant mice is directly regulated by neurofibromin expression in myeloid cells via a gene-dosage-dependent mechanism. Based on the observation that neointima formation and CCR2+, inflammatory monocyte frequency is directly regulated by myeloid cell-specific mutations in the *Nf1* gene, we utilized MCP-1 and CCR2 knockout mice to specifically interrogate the role of neurofibromin in regulating CCR2-dependent monocyte mobilization and homing during cardiovascular remodeling. Here we show that loss of MCP-1 or CCR2 expression prevents macrophage infiltration into the arterial wall and abolishes neointima formation in $Nf1^{+/-}$ mice. The recruitment of bone marrow monocytes appears to be strongly linked to the presence and activation of CCR2. CCR2-deficient mice have a dramatic reduction in mature monocyte frequency in the peripheral blood, whereas the bone marrow appears to be enriched with primitive and precursor myeloid cells indicating that CCR2 participates in

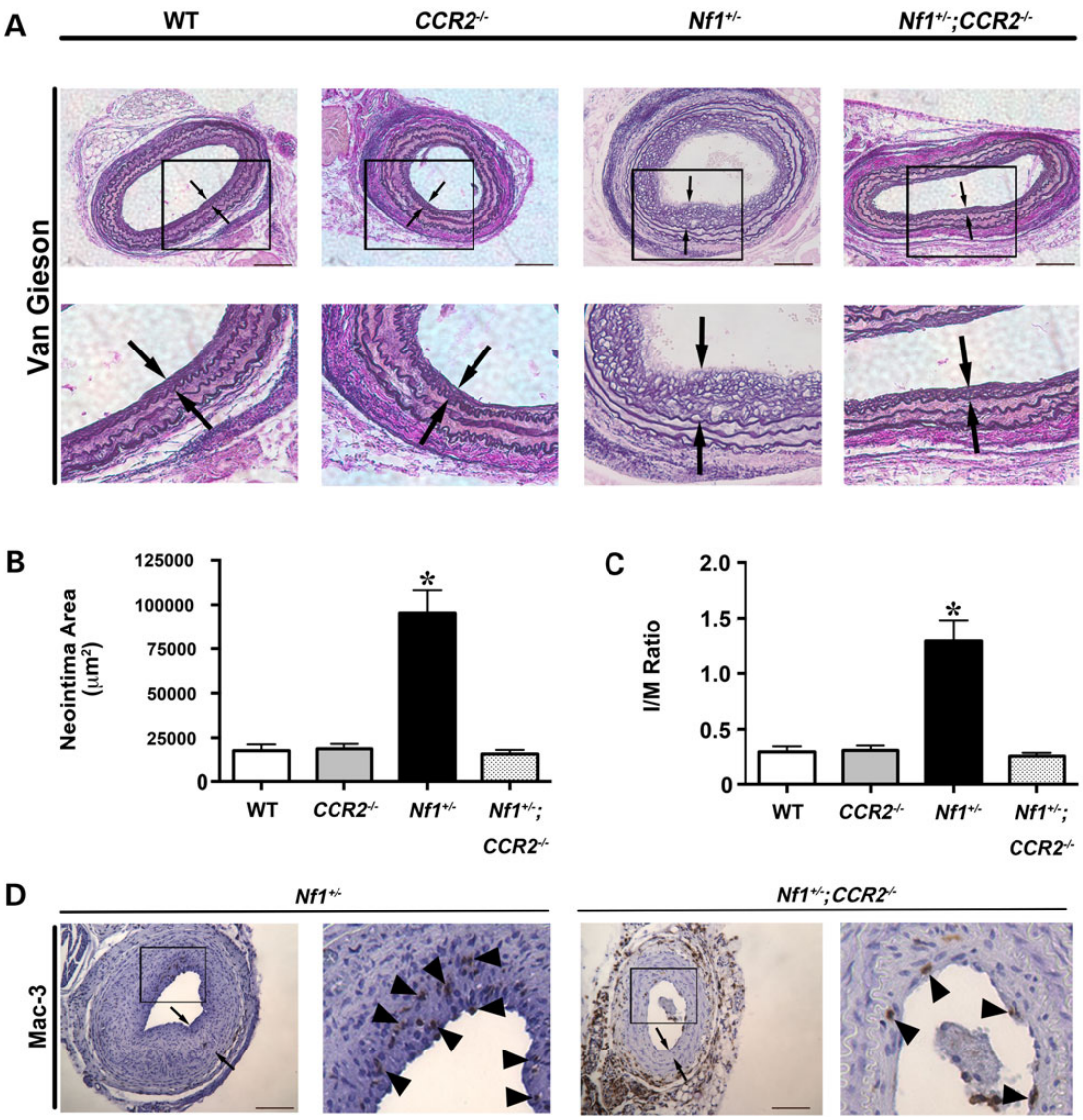

Figure 4. Genetic deletion of *CCR2* inhibits $Nf1^{+/-}$ neointima formation. Representative photomicrographs (**A**) and quantification of neointima area (**B** and **C**) of injured carotid arteries from WT, $CCR2^{-/-}$, $Nf1^{+/-}$ and $Nf1^{+/-}$;$CCR2^{-/-}$ mice. (A) Black arrows indicate neointima boundaries. Black boxes identify area of injured artery that is magnified below. Scale bars: 100 μm. (B and C) Quantification of neointima area (B) and I/M ratio (C) of injured carotid arteries from WT, $CCR2^{-/-}$, $Nf1^{+/-}$ and $Nf1^{+/-}$;$CCR2^{-/-}$ mice. Data represent mean neointima area or I/M ratio ± SEM, $n = 10–12$. *$P < 0.005$ for WT, $CCR2^{-/-}$ and $Nf1^{+/-}$;$CCR2^{-/-}$ mice versus $Nf1^{+/-}$ mice. (**D**) Representative photomicrographs of Mac-3 staining in injured carotid arteries from $Nf1^{+/-}$ and $Nf1^{+/-}$;$CCR2^{-/-}$ mice. Black arrows indicate neointima boundaries. Black box identifies area of injured artery that is magnified in the right column. Black arrowheads represent positive macrophage (anti-Mac3) staining. Scale bars: 100 μm.

the mobilization of monocytes from the bone marrow (25,36,37). Monocyte differentiation in $CCR2^{-/-}$ mice remains intact; however, mature monocytes fail to accumulate in the spleen and respond to inflammatory stimuli (36). Surprisingly, *CCR2* deletion failed to reduce neointima formation in our experimental model system. The demonstrated reduction in neointima formation in CCR2-deficient mice has largely been demonstrated in compound mutant mice (i.e. $CCR2^{-/-}$;$ApoE^{-/-}$) and may rely on a hyperlipidemic background to mediate its effects (38,39). Further, C57Bl/6 mice are highly resistant to arterial remodeling in multiple animal models, which is consistent with our experimental results and previous reports (12,13,15,27,40).

Although MCP-1 is the principal ligand for CCR2, other monocyte chemotactic proteins have affinity for CCR2 and have a role in monocyte function, SMC proliferation and arterial remodeling (25,41,42). Thus, complimentary studies in $Nf1^{+/-}$ mice lacking MCP-1 expression were critical to link the increased sensitivity of neurofibromin-deficient monocytes/macrophages to MCP-1 and the mobilization of CCR2+ proinflammatory monocytes in *Nf1*-mutant mice. The lack of neointima formation in $Nf1^{+/-}$;$MCP1^{-/-}$ mice mirrors our findings in CCR2-deficient $Nf1^{+/-}$ mice and provides strong genetic evidence that this signaling axis is necessary for $Nf1^{+/-}$ neointima formation. The underlying mechanisms of this interaction remain unclear; however, we show that MCP-1 preferentially activates Erk signaling in $Nf1^{+/-}$ SMC and multiple Ras-dependent kinases in $Nf1^{+/-}$ monocytes, including Akt. Interestingly, Erk and Akt, the primary downstream targets of Ras, activate several transcription factors including SP-1, c-Jun and AP-1, which control the expression of MCP-1 and other cytokines (43–46). In turn, expression of chemokines such as MCP-1 largely controls leukocyte and SMC function via RTK-mediated Ras activation. This may contribute to a positive feedback loop where

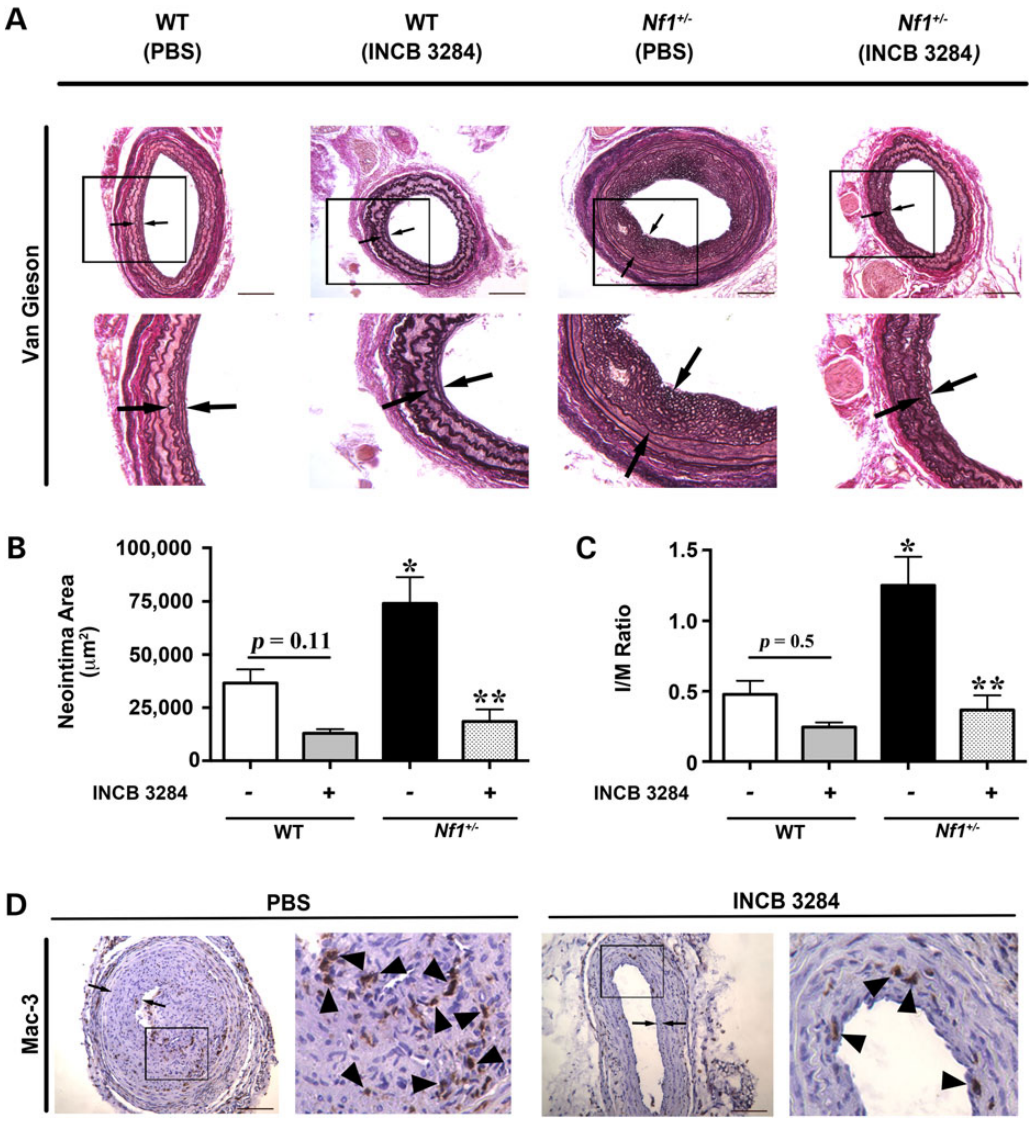

Figure 5. CCR2 antagonist reduces neointima formation in $Nf1^{+/-}$ mice. Representative photomicrographs (**A**) and quantification of neointima area (**B** and **C**) of injured carotid arteries from WT and $Nf1^{+/-}$ mice treated with INCB 3284 (15 mg/kg/day) or PBS. (A) Black arrows indicate neointima boundaries. Black boxes identify area of injured artery that is magnified below. Scale bars: 100 μm. (B and C) Quantification of neointima area (B) and I/M ratio (C) of injured carotid arteries from WT and $Nf1^{+/-}$ mice treated with INCB 3284 or PBS. Data represent mean neointima area or I/M ratio ± SEM, $n = 6–8$. *$P < 0.01$ for WT mice with PBS treatment versus $Nf1^{+/-}$ mice with PBS treatment. **$P < 0.001$ for $Nf1^{+/-}$ mice with PBS treatment versus $Nf1^{+/-}$ mice with INCB 3284 treatment. No statistically significant difference was observed between WT mice with PBS treatment and WT mice with INCB 3284 treatment. Experiments were performed in triplicate. (**D**) Representative photomicrographs of Mac-3 staining in injured carotid arteries from $Nf1^{+/-}$ mice with PBS treatment versus $Nf1^{+/-}$ mice with INCB 3284 treatment. Black arrows indicate neointima boundaries. Black box identifies area of injured artery that is magnified in the right column. Black arrowheads represent positive macrophage (anti-Mac3) staining. Scale bars: 100 μm.

cytokines can propagate their own production, which may be amplified in the setting of Ras deregulation (47–49). Our observation that neurofibromin-deficient macrophages have increased production and secretion of MCP-1, which may potentiate their own function, is congruent with this line of investigation. For example, mTOR signaling is proximally regulated by neurofibromin and loss of neurofibromin increases Akt activity in response to MCP-1 in murine monocytes. Recent studies in human and murine monocytes have revealed that MCP-1 production is directly regulated by mTOR activation and that inhibition of mTOR signaling results in decreased MCP-1 expression and secretion via an NF-κB-dependent mechanism. Interestingly genetic deletion of tuberous sclerosis complex 2 amplifies mTOR signaling and also increases MCP-1 expression, which suggests that this pathway directly regulates MCP-1 production. Therefore, it is plausible that decreased expression of neurofibromin may enhance downstream signaling networks that increase MCP-1 expression to provide a greater local concentration of MCP-1 to activate CCR2 on circulating monocytes/macrophages and vascular wall cells. While long-term use of an mTOR inhibitor for the prevention or treatment of NF1 vasculopathy is unlikely, interrogation of this pathway may provide substantial mechanistic insights into the regulation of monocyte-specific chemokines and their function in the setting of neurofibromin deficiency. Ongoing studies in our laboratory are focused on understanding how Ras signaling controls the transcription and/or activity of MCP-1.

Targeted therapies directed against either MCP-1 have yielded promising results in preclinical animal models, but have largely

proven to lack efficacy in human clinical trials (50–55). Bindarit, an indazolic derivative that binds to the promoter of the MCP-1 gene and limits MCP-1 expression, inhibits human and murine SMC proliferation and de-differentiation as well as neointima formation in several animal models (28,55,56). However, the use of a monoclonal antibody directed against MCP-1 in persons with rheumatoid arthritis did not improve clinical symptoms and demonstrated a dose-responsive increase in serum MCP-1 concentrations, which suggests that clearance of the antibody complex is limited (57). Antibodies directed against MCP-1 in the treatment of cardiovascular disease have not been proposed, though bindarit is presently under investigation for the treatment of diabetic nephropathy. MCP-1 may prove to be a difficult target for the treatment of cardiovascular disease because it is expressed and secreted by multiple cell types, including EC, SMC, leukocytes and perivascular adipocytes, and demonstrates affinity for other receptors including CCR4 (32,33). Further, MCP-1 secretion provides important feedback between perivascular cells (i.e. adipocytes) and remote tissues, including skeletal muscle and hepatocytes (58,59), which makes sequestering MCP-1 activity clinically difficult.

Local inhibition of CCR2, on the other hand, is an attractive therapeutic target for the treatment of NF1 vasculopathy because its expression and ligand-binding affinity is relatively limited. CCR2 antagonists have been studied in multiple clinical trials for the treatment of cardiovascular disease, autoimmunity, chronic inflammation, diabetes and malignancy (60–62). In particular, CCR2 antagonism may prove efficacious in the treatment of multiple manifestations of NF1, because acceleration of Ras activity in myeloid progenitor cells leads to dysfunctional differentiation and increased sensitivity to cytokines and growth factors (1,63–65). Our genetic and pharmacologic data support our hypothesis that MCP-1/CCR2 activation is highly regulated by neurofibromin and may represent a viable therapeutic target for NF1 patients with cardiovascular disease. Further studies directed at understanding how neurofibromin and/or Ras activation control the expression of MCP-1 and facilitate the mobilization of CCR2+ monocytes from the bone marrow are critical for future translational work and human studies of NF1 vasculopathy.

Materials and Methods

Animals

Protocols were approved by Laboratory Animal Services at Augusta University and Indiana University. *Nf1*$^{+/-}$ mice were obtained from Tyler Jacks (Massachusetts Institute of Technology, Cambridge, MA) and backcrossed 13 generations into the C57BL/6J strain. *MCP-1* (4434) and *CCR2* (4999) knockout mice were purchased from The Jackson Laboratory and maintained on C57BL/6 strain. *Nf1*$^{+/-}$ mice were intercrossed with *MCP1* and *CCR2* knockout mice to produce *Nf1*$^{+/-}$;*MCP1*$^{-/-}$ and *Nf1*$^{+/-}$;*CCR2*$^{-/-}$ mice. Male mice (12–15 weeks of age) were used for experiments to limit the confounding effects of circulating hormones.

Carotid artery ligation

Carotid artery injury was induced by ligation of the right common carotid artery as described (15). Briefly, mice were anesthetized by inhalation of an isoflurane (2%)/oxygen (98%) mixture. Under a dissecting scope, the right carotid artery was exposed through a midline neck incision and ligated proximal to the bifurcation using a 6–0 silk suture. The contralateral carotid artery was sham ligated as a control. Mice were administered 15 μg of buprenorphine (ip) following the procedure and recovered for 28 days. In some experiments, *Nf1*$^{+/-}$ and WT mice were administered 15 mg/kg INCB3284 (Caymen Chemical, IC_{50} 3.7 nM and $t_{½}$ 15 h) or vehicle via IP injection immediately after arterial injury and continued once daily for 10 days.

Morphometric analysis

Van Gieson-stained arterial cross sections 400, 800 and 1200 μm proximal to the ligation were analyzed for neointima formation using ImageJ (NIH, Bethesda, MD). Lumen area, area inside the internal elastic lamina (IEL), and area inside the external elastic lamina (EEL) were measured for each cross section. To account for potential thrombus formation, arteries containing significant thrombus (>50% lumen occlusion) at 400 μm proximal to the ligation were excluded from analysis. The number of excluded arteries was not different between experimental groups. Representative photomicrographs for each figure are taken from arterial cross sections between 600 and 1200 μm proximal to the bifurcation. Intima area was calculated by subtracting the lumen area from the IEL area, and the media area was calculated by subtracting the IEL area from the EEL area. I/M ratio was calculated as intima area divided by media area.

Histopathology and immunohistochemistry

For immunohistochemistry, serial sections were blocked for endogenous peroxidase activity with 3% hydrogen peroxide in methanol following antigen retrieval in Antigen Unmasking Solution (Vector Laboratories) at 95°C. Sections were blocked with Protein Block (Dako) for 1 h and were incubated with anti-Mac3 (1:50; BD Biosciences) primary antibodies. Sections were incubated with a biotinylated secondary antibody and visualized by 3,3′-diaminobenidine and counterstained with hematoxylin. Sections were examined, and images of sections were collected using a Zeiss Axioskop microscope (Carl Zeiss) with a 20× or 40× CP-ACHROMAT/0.12NA objective. Images were acquired using a SPOT RT color camera (Diagnostic Instruments). To quantify the number of macrophages within the neointima of each experimental group, Mac-3+ cells and SMCs were counted in three random 40× images by a blinded observer. To correct for a reduction in cell volume within the neointima, a ratio of Mac-3+ cells and SMC was calculated and analyzed for each mouse.

Isolation of bone-marrow-derived macrophages and characterization

Bone-marrow-derived macrophage isolation and characterization was performed as described (13). Proliferation was assessed by incorporation of radioactive thymidine in WT and *Nf1*$^{+/-}$ BM-derived macrophages. Briefly, WT and *Nf1*$^{+/-}$ macrophages (5×10^4 cells) were serum-starved for 12–18 h and placed in a 96-well plate in 200 μl starvation media in either the absence or presence of MCP-1 (10 ng/ml). Cells were cultured for 24 h and subsequently pulsed with 1.0 μCi (0.037 MBq) [^{3}H] thymidine for 6 h. Cells were harvested using a cell harvester and thymidine incorporation was determined as counts per minute (cpm).

For macrophage migration, the bottom of Transwell filters (8-μm pore filter; Costar) were coated with 20 μg/ml fibronectin CH296 peptide for 2 h at 37°C and rinsed twice with PBS containing 2% BSA. WT and *Nf1*$^{+/-}$ macrophages (2.5×10^5 cells) were placed in the upper chamber of the transwell and allowed to migrate toward the bottom of the transwell containing indicated

concentration of MCP-1. After 24 h, non-migrated cells in the upper chamber were removed with a cotton swab and migrated cells that attached to the bottom surface of the membrane were stained with 0.1% crystal violet dissolved in 0.1 M borate, pH 9.0 and 2% ethanol for 5 min at room temperature. The number of migrated cells was determined in five random fields with an inverted microscope using a 20 × objective lens. All experiments were performed in triplicate.

Smooth muscle cell isolation and proliferation

SMC isolation and proliferation assays were performed as described (14). SMCs were obtained by outgrowth from explants of WT, $Nf1^{+/-}$ and $Nf1^{+/-}$;$CCR2^{-/-}$ thoracic aortas. SMCs were cultured in DMEM supplemented with 10% fetal bovine serum and 100 U/ml penicillin/streptomycin in a 37°C, 5% CO_2-humidified incubator. For cell proliferation, SMC (5000 cells/cm^2) were placed in a 96-well plate and deprived of growth factors for 12–18 h. Quiescent SMC were stimulated with MCP-1 (10 ng/ml) for 24 h and pulse-labeled with 1 µCi/ml of [^{3}H] thymidine for 6 h. Beta emission was measured and reported as cpm. In some experiments, SMCs were incubated with indicated concentrations of PD0325901 (Erk inhibitor). All experiments were performed in triplicate.

Statistical analysis

All values are presented as mean or percent ± SEM. Cell proliferation and migration were analyzed by two-way ANOVA with Tukey's post hoc test for multiple comparisons. All experiments were performed in triplicate. MCP-1 concentration was analyzed by Student's *t*-test. Intima area and I/M ratio analysis was assessed by one-way ANOVA with Tukey's post hoc test for multiple comparisons. Murine experiments utilizing INCB 3284 were analyzed using two-way ANOVA with Tukey's post hoc test for multiple comparisons. Percent Mac-3+ cells was analyzed by Student's *t*-test. Analysis was performed using GraphPad Prism version 5.0d. $P < 0.05$ were considered significant.

Conflict of Interest statement. None declared.

Funding

This work is supported by the Department of Defense (NF140031, B.K.S.), the American Heart Association (15SDG2550005, B.K.S.), the Department of Pediatrics at Augusta University (B.K.S.) and the National Institutes of Health (P50 NS052606, D.A.I.).

References

1. Staser, K., Park, S.J., Rhodes, S.D., Zeng, Y., He, Y.Z., Shew, M. A., Gehlhausen, J.R., Cerabona, D., Menon, K., Chen, S. *et al.* (2013) Normal hematopoiesis and neurofibromin-deficient myeloproliferative disease require Erk. *J. Clin. Invest.*, **123**, 329–334.
2. Friedman, J.M., Arbiser, J., Epstein, J.A., Gutmann, D.H., Huot, S.J., Lin, A.E., McManus, B. and Korf, B.R. (2002) Cardiovascular disease in neurofibromatosis 1: report of the NF1 cardiovascular task force. *Genet. Med.*, **4**, 105–111.
3. Oderich, G.S., Sullivan, T.M., Bower, T.C., Gloviczki, P., Miller, D.V., Babovic-Vuksanovic, D., Macedo, T.A. and Stanson, A. (2007) Vascular abnormalities in patients with neurofibromatosis syndrome type I: clinical spectrum, management, and results. *J. Vasc. Surg.*, **46**, 475–484.
4. Rasmussen, S.A., Yang, Q. and Friedman, J.M. (2001) Mortality in neurofibromatosis 1: an analysis using U.S. death certificates. *Am. J. Hum. Genet.*, **68**, 1110–1118.
5. Lin, A.E., Birch, P.H., Korf, B.R., Tenconi, R., Niimura, M., Poyhonen, M., Armfield Uhas, K., Sigorini, M., Virdis, R., Romano, C. *et al.* (2000) Cardiovascular malformations and other cardiovascular abnormalities in neurofibromatosis 1. *Am. J. Med. Genet.*, **95**, 108–117.
6. D'Arco, F., D'Amico, A., Caranci, F., Di Paolo, N., Melis, D. and Brunetti, A. (2014) Cerebrovascular stenosis in neurofibromatosis type 1 and utility of magnetic resonance angiography: our experience and literature review. *Radiol. Med.*, **119**, 415–421.
7. Rea, D., Brandsema, J.F., Armstrong, D., Parkin, P.C., deVeber, G., MacGregor, D., Logan, W.J. and Askalan, R. (2009) Cerebral arteriopathy in children with neurofibromatosis type 1. *Pediatrics*, **124**, e476–e483.
8. Salyer, W.R. and Salyer, D.C. (1974) The vascular lesions of neurofibromatosis. *Angiology*, **25**, 510–519.
9. Kanter, R.J., Graham, M., Fairbrother, D. and Smith, S.V. (2006) Sudden cardiac death in young children with neurofibromatosis type 1. *J. Pediatr.*, **149**, 718–720.
10. Hamilton, S.J. and Friedman, J.M. (2000) Insights into the pathogenesis of neurofibromatosis 1 vasculopathy. *Clin. Genet.*, **58**, 341–344.
11. Lie, J.T. (1998) Vasculopathies of neurofibromatosis type 1 (von Recklinghausen Disease). *Cardiovasc. Pathol.*, **7**, 97–108.
12. Lasater, E.A., Bessler, W.K., Mead, L.E., Horn, W.E., Clapp, D. W., Conway, S.J., Ingram, D.A. and Li, F. (2008) Nf1+/– mice have increased neointima formation via hyperactivation of a Gleevec sensitive molecular pathway. *Hum. Mol. Genet.*, **17**, 2336–2344.
13. Lasater, E.A., Li, F., Bessler, W.K., Estes, M.L., Vemula, S., Hingtgen, C.M., Dinauer, M.C., Kapur, R., Conway, S.J. and Ingram, D.A. Jr. (2010) Genetic and cellular evidence of vascular inflammation in neurofibromin-deficient mice and humans. *J. Clin. Invest.*, **120**, 859–870.
14. Li, F., Munchhof, A.M., White, H.A., Mead, L.E., Krier, T.R., Fenoglio, A., Chen, S., Wu, X., Cai, S., Yang, F.C. *et al.* (2006) Neurofibromin is a novel regulator of RAS-induced signals in primary vascular smooth muscle cells. *Hum. Mol. Genet.*, **15**, 1921–1930.
15. Stansfield, B.K., Bessler, W.K., Mali, R., Mund, J.A., Downing, B., Li, F., Sarchet, K.N., DiStasi, M.R., Conway, S.J., Kapur, R. *et al.* (2013) Heterozygous inactivation of the Nf1 gene in myeloid cells enhances neointima formation via a rosuvastatin-sensitive cellular pathway. *Hum. Mol. Genet.*, **22**, 977–988.
16. Stansfield, B.K. and Ingram, D.A. (2015) Clinical significance of monocyte heterogeneity. *Clin. Transl. Med.*, **4**, 5.
17. Hilgendorf, I., Gerhardt, L.M., Tan, T.C., Winter, C., Holderried, T.A., Chousterman, B.G., Iwamoto, Y., Liao, R., Zirlik, A., Scherer-Crosbie, M. *et al.* (2014) Ly-6C high monocytes depend on Nr4a1 to balance both inflammatory and reparative phases in the infarcted myocardium. *Circ. Res.*, **114**, 1611–1622.
18. Robbins, C.S., Chudnovskiy, A., Rauch, P.J., Figueiredo, J.L., Iwamoto, Y., Gorbatov, R., Etzrodt, M., Weber, G.F., Ueno, T., van Rooijen, N. *et al.* (2012) Extramedullary hematopoiesis generates Ly-6C (high) monocytes that infiltrate atherosclerotic lesions. *Circulation*, **125**, 364–374.
19. Giunti, S., Pinach, S., Arnaldi, L., Viberti, G., Perin, P.C., Camussi, G. and Gruden, G. (2006) The MCP-1/CCR2 system has direct proinflammatory effects in human mesangial cells. *Kidney Int.*, **69**, 856–863.

20. Tieu, B.C., Lee, C., Sun, H., Lejeune, W., Recinos, A. 3rd, Ju, X., Spratt, H., Guo, D.C., Milewicz, D., Tilton, R.G. *et al.* (2009) An adventitial IL-6/MCP1 amplification loop accelerates macrophage-mediated vascular inflammation leading to aortic dissection in mice. *J. Clin. Invest.*, **119**, 3637–3651.
21. Sakai, N., Wada, T., Furuichi, K., Shimizu, K., Kokubo, S., Hara, A., Yamahana, J., Okumura, T., Matsushima, K., Yokoyama, H. *et al.* (2006) MCP-1/CCR2-dependent loop for fibrogenesis in human peripheral CD14-positive monocytes. *J. Leukoc. Biol.*, **79**, 555–563.
22. Lin, Y.M., Hsu, C.J., Liao, Y.Y., Chou, M.C. and Tang, C.H. (2012) The CCL2/CCR2 axis enhances vascular cell adhesion molecule-1 expression in human synovial fibroblasts. *PLoS ONE*, **7**, e49999.
23. Kalderen, C., Forsgren, M., Karlstrom, U., Stefansson, K., Svensson, R., Berglund, M.M., Palm, G., Selander, M., Sundbom, M., Nilsson, J. *et al.* (2012) A truncated analogue of CCL2 mediates anti-fibrotic effects on murine fibroblasts independently of CCR2. *Biochem. Pharmacol.*, **83**, 644–652.
24. Si, Y., Tsou, C.L., Croft, K. and Charo, I.F. (2010) CCR2 mediates hematopoietic stem and progenitor cell trafficking to sites of inflammation in mice. *J. Clin. Invest.*, **120**, 1192–1203.
25. Tsou, C.L., Peters, W., Si, Y., Slaymaker, S., Aslanian, A.M., Weisberg, S.P., Mack, M. and Charo, I.F. (2007) Critical roles for CCR2 and MCP-3 in monocyte mobilization from bone marrow and recruitment to inflammatory sites. *J. Clin. Invest.*, **117**, 902–909.
26. Hartl, D., Krauss-Etschmann, S., Koller, B., Hordijk, P.L., Kuijpers, T.W., Hoffmann, F., Hector, A., Eber, E., Marcos, V., Bittmann, I. *et al.* (2008) Infiltrated neutrophils acquire novel chemokine receptor expression and chemokine responsiveness in chronic inflammatory lung diseases. *J. Immunol.*, **181**, 8053–8067.
27. Stansfield, B.K., Bessler, W.K., Mali, R., Mund, J.A., Downing, B. D., Kapur, R. and Ingram, D.A. Jr. (2014) Ras-mek-erk signaling regulates nf1 heterozygous neointima formation. *Am. J. Pathol.*, **184**, 79–85.
28. Maddaluno, M., Grassia, G., Di Lauro, M.V., Parisi, A., Maione, F., Cicala, C., De Filippis, D., Iuvone, T., Guglielmotti, A., Maffia, P. *et al.* (2012) Bindarit inhibits human coronary artery smooth muscle cell proliferation, migration and phenotypic switching. *PLoS ONE*, **7**, e47464.
29. Porreca, E., Di Febbo, C., Reale, M., Castellani, M.L., Baccante, G., Barbacane, R., Conti, P., Cuccurullo, F. and Poggi, A. (1997) Monocyte chemotactic protein 1 (MCP-1) is a mitogen for cultured rat vascular smooth muscle cells. *J. Vasc. Res.*, **34**, 58–65.
30. Selzman, C.H., Miller, S.A., Zimmerman, M.A., Gamboni-Robertson, F., Harken, A.H. and Banerjee, A. (2002) Monocyte chemotactic protein-1 directly induces human vascular smooth muscle proliferation. *Am J Physiol. Heart Circ. Physiol.*, **283**, H1455–H1461.
31. Viedt, C., Vogel, J., Athanasiou, T., Shen, W., Orth, S.R., Kubler, W. and Kreuzer, J. (2002) Monocyte chemoattractant protein-1 induces proliferation and interleukin-6 production in human smooth muscle cells by differential activation of nuclear factor-kappaB and activator protein-1. *Arterioscler. Thromb. Vasc. Biol.*, **22**, 914–920.
32. Kim, M.S., Magno, C.L., Day, C.J. and Morrison, N.A. (2006) Induction of chemokines and chemokine receptors CCR2b and CCR4 in authentic human osteoclasts differentiated with RANKL and osteoclast like cells differentiated by MCP-1 and RANTES. *J. Cell. Biochem.*, **97**, 512–518.
33. Schecter, A.D., Berman, A.B., Yi, L., Ma, H., Daly, C.M., Soejima, K., Rollins, B.J., Charo, I.F. and Taubman, M.B. (2004) MCP-1-dependent signaling in CCR2(–/–) aortic smooth muscle cells. *J. Leukoc. Biol.*, **75**, 1079–1085.
34. Xue, C.B., Feng, H., Cao, G., Huang, T., Glenn, J., Anand, R., Meloni, D., Zhang, K., Kong, L., Wang, A. *et al.* (2011) Discovery of INCB3284, a potent, selective, and orally bioavailable hCCR2 antagonist. *ACS Med. Chem. Lett.*, **2**, 450–454.
35. Libby, P., Nahrendorf, M. and Swirski, F.K. (2013) Monocyte heterogeneity in cardiovascular disease. *Semin. Immunopathol.*, **35**, 553–562.
36. Serbina, N.V. and Pamer, E.G. (2006) Monocyte emigration from bone marrow during bacterial infection requires signals mediated by chemokine receptor CCR2. *Nat. Immunol.*, **7**, 311–317.
37. Ishibashi, M., Egashira, K., Zhao, Q., Hiasa, K., Ohtani, K., Ihara, Y., Charo, I.F., Kura, S., Tsuzuki, T., Takeshita, A. *et al.* (2004) Bone marrow-derived monocyte chemoattractant protein-1 receptor CCR2 is critical in angiotensin II-induced acceleration of atherosclerosis and aneurysm formation in hypercholesterolemic mice. *Arterioscler. Thromb. Vasc. Biol.*, **24**, e174–e178.
38. Liehn, E.A., Piccinini, A.M., Koenen, R.R., Soehnlein, O., Adage, T., Fatu, R., Curaj, A., Popescu, A., Zernecke, A., Kungl, A.J. *et al.* (2010) A new monocyte chemotactic protein-1/chemokine CC motif ligand-2 competitor limiting neointima formation and myocardial ischemia/reperfusion injury in mice. *J. Am. College Cardiol.*, **56**, 1847–1857.
39. Schober, A., Zernecke, A., Liehn, E.A., von Hundelshausen, P., Knarren, S., Kuziel, W.A. and Weber, C. (2004) Crucial role of the CCL2/CCR2 axis in neointimal hyperplasia after arterial injury in hyperlipidemic mice involves early monocyte recruitment and CCL2 presentation on platelets. *Circ. Res.*, **95**, 1125–1133.
40. Kuhel, D.G., Zhu, B., Witte, D.P. and Hui, D.Y. (2002) Distinction in genetic determinants for injury-induced neointimal hyperplasia and diet-induced atherosclerosis in inbred mice. *Arterioscler. Thromb. Vasc. Biol.*, **22**, 955–960.
41. Gong, X., Gong, W., Kuhns, D.B., Ben-Baruch, A., Howard, O.M. and Wang, J.M. (1997) Monocyte chemotactic protein-2 (MCP-2) uses CCR1 and CCR2B as its functional receptors. *J. Biol. Chem.*, **272**, 11682–11685.
42. Maddaluno, M., Di Lauro, M., Di Pascale, A., Santamaria, R., Guglielmotti, A., Grassia, G. and Ialenti, A. (2011) Monocyte chemotactic protein-3 induces human coronary smooth muscle cell proliferation. *Atherosclerosis*, **217**, 113–119.
43. Li, X. and Tai, H.H. (2013) Activation of thromboxane A2 receptor (TP) increases the expression of monocyte chemoattractant protein -1 (MCP-1)/chemokine (C-C motif) ligand 2 (CCL2) and recruits macrophages to promote invasion of lung cancer cells. *PLoS ONE*, **8**, e54073.
44. Lim, J.H., Um, H.J., Park, J.W., Lee, I.K. and Kwon, T.K. (2009) Interleukin-1beta promotes the expression of monocyte chemoattractant protein-1 in human aorta smooth muscle cells via multiple signaling pathways. *Exp. Mol. Med.*, **41**, 757–764.
45. Shimizu, H., Bolati, D., Higashiyama, Y., Nishijima, F., Shimizu, K. and Niwa, T. (2012) Indoxyl sulfate upregulates renal expression of MCP-1 via production of ROS and activation of NF-kappaB, p53, ERK, and JNK in proximal tubular cells. *Life Sci.*, **90**, 525–530.
46. Shang, F., Wang, J., Liu, X., Li, J., Zheng, Q., Xue, Y. and Zhao, L. (2012) Involvement of reactive oxygen species and JNK in increased expression of MCP-1 and infiltration of inflammatory cells in pressure-overloaded rat hearts. *Mol. Med. Rep.*, **5**, 1491–1496.

47. Jimenez-Sainz, M.C., Fast, B., Mayor, F. Jr and Aragay, A.M. (2003) Signaling pathways for monocyte chemoattractant protein 1-mediated extracellular signal-regulated kinase activation. *Mol. Pharmacol.*, **64**, 773–782.
48. Patial, S., Saini, Y., Parvataneni, S., Appledorn, D.M., Dorn, G. W. 2nd, Lapres, J.J., Amalfitano, A., Senagore, P. and Parameswaran, N. (2011) Myeloid-specific GPCR kinase-2 negatively regulates NF-kappaB1p105-ERK pathway and limits endotoxemic shock in mice. *J. Cell. Physiol.*, **226**, 627–637.
49. Yang, C.Q., Li, W., Li, S.Q., Li, J., Li, Y.W., Kong, S.X., Liu, R.M., Wang, S.M. and Lv, W.M. (2014) MCP-1 stimulates MMP-9 expression via ERK 1/2 and p38 MAPK signaling pathways in human aortic smooth muscle cells. *Cell. Physiol. Biochem.*, **34**, 266–276.
50. Arefieva, T.I., Krasnikova, T.L., Potekhina, A.V., Ruleva, N.U., Nikitin, P.I., Ksenevich, T.I., Gorshkov, B.G., Sidorova, M.V., Bespalova Zh, D., Kukhtina, N.B. *et al.* (2011) Synthetic peptide fragment (65–76) of monocyte chemotactic protein-1 (MCP-1) inhibits MCP-1 binding to heparin and possesses anti-inflammatory activity in stable angina patients after coronary stenting. *Inflamm. Res.*, **60**, 955–964.
51. Egashira, K., Nakano, K., Ohtani, K., Funakoshi, K., Zhao, G., Ihara, Y., Koga, J., Kimura, S., Tominaga, R. and Sunagawa, K. (2007) Local delivery of anti-monocyte chemoattractant protein-1 by gene-eluting stents attenuates in-stent stenosis in rabbits and monkeys. *Arterioscler. Thromb. Vasc. Biol.*, **27**, 2563–2568.
52. Nakano, K., Egashira, K., Ohtani, K., Zhao, G., Funakoshi, K., Ihara, Y. and Sunagawa, K. (2007) Catheter-based adenovirus-mediated anti-monocyte chemoattractant gene therapy attenuates in-stent neointima formation in cynomolgus monkeys. *Atherosclerosis*, **194**, 309–316.
53. Ohtani, K., Usui, M., Nakano, K., Kohjimoto, Y., Kitajima, S., Hirouchi, Y., Li, X.H., Kitamoto, S., Takeshita, A. and Egashira, K. (2004) Antimonocyte chemoattractant protein-1 gene therapy reduces experimental in-stent restenosis in hypercholesterolemic rabbits and monkeys. *Gene Ther.*, **11**, 1273–1282.
54. Zhao, Q. (2010) Dual targeting of CCR2 and CCR5: therapeutic potential for immunologic and cardiovascular diseases. *J. Leukoc. Biol.*, **88**, 41–55.
55. Ialenti, A., Grassia, G., Gordon, P., Maddaluno, M., Di Lauro, M. V., Baker, A.H., Guglielmotti, A., Colombo, A., Biondi, G., Kennedy, S. *et al.* (2011) Inhibition of in-stent stenosis by oral administration of bindarit in porcine coronary arteries. *Arterioscler. Thromb. Vasc. Biol.*, **31**, 2448–2454.
56. Grassia, G., Maddaluno, M., Guglielmotti, A., Mangano, G., Biondi, G., Maffia, P. and Ialenti, A. (2009) The anti-inflammatory agent bindarit inhibits neointima formation in both rats and hyperlipidaemic mice. *Cardiovasc. Res.*, **84**, 485–493.
57. Haringman, J.J., Gerlag, D.M., Smeets, T.J., Baeten, D., van den Bosch, F., Bresnihan, B., Breedveld, F.C., Dinant, H.J., Legay, F., Gram, H. *et al.* (2006) A randomized controlled trial with an anti-CCL2 (anti-monocyte chemotactic protein 1) monoclonal antibody in patients with rheumatoid arthritis. *Arthritis Rheum.*, **54**, 2387–2392.
58. Westerbacka, J., Corner, A., Kolak, M., Makkonen, J., Turpeinen, U., Hamsten, A., Fisher, R.M. and Yki-Jarvinen, H. (2008) Insulin regulation of MCP-1 in human adipose tissue of obese and lean women. *Am. J. Physiol. Endocrinol. Metab.*, **294**, E841–E845.
59. Younce, C. and Kolattukudy, P. (2012) MCP-1 induced protein promotes adipogenesis via oxidative stress, endoplasmic reticulum stress and autophagy. *Cell. Physiol. Biochem.*, **30**, 307–320.
60. Lin, K.L., Sweeney, S., Kang, B.D., Ramsburg, E. and Gunn, M. D. (2011) CCR2-antagonist prophylaxis reduces pulmonary immune pathology and markedly improves survival during influenza infection. *J. Immunol.*, **186**, 508–515.
61. Mildner, A., Mack, M., Schmidt, H., Bruck, W., Djukic, M., Zabel, M.D., Hille, A., Priller, J. and Prinz, M. (2009) CCR2+Ly-6Chi monocytes are crucial for the effector phase of autoimmunity in the central nervous system. *Brain*, **132**, 2487–2500.
62. Sullivan, T.J., Miao, Z., Zhao, B.N., Ertl, L.S., Wang, Y., Krasinski, A., Walters, M.J., Powers, J.P., Dairaghi, D.J., Baumgart, T. *et al.* (2013) Experimental evidence for the use of CCR2 antagonists in the treatment of type 2 diabetes. *Metabolism: Clin. Exp.*, **62**, 1623–1632.
63. Gritsman, K., Yuzugullu, H., Von, T., Yan, H., Clayton, L., Fritsch, C., Maira, S.M., Hollingworth, G., Choi, C., Khandan, T. *et al.* (2014) Hematopoiesis and RAS-driven myeloid leukemia differentially require PI3K isoform p110alpha. *J. Clin. Invest.*, **124**, 1794–1809.
64. Zeng, Y., Broxmeyer, H.E., Staser, K., Chitteti, B.R., Park, S.J., Hahn, S., Cooper, S., Sun, Z., Jiang, L., Yang, X. *et al.* (2015) Pak2 regulates hematopoietic progenitor cell proliferation, survival and differentiation. *Stem Cells*, **33**, 1630–1641.
65. Bollag, G., Clapp, D.W., Shih, S., Adler, F., Zhang, Y.Y., Thompson, P., Lange, B.J., Freedman, M.H., McCormick, F., Jacks, T. *et al.* (1996) Loss of NF1 results in activation of the Ras signaling pathway and leads to aberrant growth in haematopoietic cells. *Nat. Genet.*, **12**, 144–148.

Am J Physiol Heart Circ Physiol 313: H1168–H1179, 2017.
First published September 29, 2017; doi:10.1152/ajpheart.00296.2017.

RESEARCH ARTICLE | *Mining Natural Products for Cardiovascular Benefits*

Role of myeloperoxidase in abdominal aortic aneurysm formation: mitigation by taurine

Ha Won Kim,[1]* Andra L. Blomkalns,[5]* Mourad Ogbi,[1] Manesh Thomas,[7] Daniel Gavrila,[7] Bonnie S. Neltner,[6] Lisa A. Cassis,[10] Robert W. Thompson,[9] Robert M. Weiss,[7] Paul D. Lindower,[7] Victor M. Blanco,[6] Michael L. McCormick,[8] Alan Daugherty,[11] Xiaoming Fu,[12] Stanley L. Hazen,[12] Brian K. Stansfield,[2] Yuqing Huo,[3] David J. Fulton,[4] Tapan Chatterjee,[1†] and Neal L. Weintraub[1]

[1]*Division of Cardiology, Department of Medicine, Medical College of Georgia at Augusta University, Augusta, Georgia;* [2]*Department of Pediatrics, Medical College of Georgia at Augusta University, Augusta, Georgia;* [3]*Department of Cellular Biology and Anatomy, Medical College of Georgia at Augusta University, Augusta, Georgia;* [4]*Department of Pharmacology and Toxicology, Vascular Biology Center, Medical College of Georgia at Augusta University, Augusta, Georgia;* [5]*Department of Emergency Medicine, Medical College of Georgia at Augusta University, Augusta, Georgia;* [6]*Division of Cardiovascular Diseases, Department of Internal Medicine, University of Cincinnati, Cincinnati, Ohio;* [7]*Division of Cardiovascular Medicine, University of Iowa, Iowa City, Iowa;* [8]*Department of Radiation Oncology, University of Iowa, Iowa City, Iowa;* [9]*Department of Surgery, Washington University School of Medicine, St. Louis, Missouri;* [10]*Department of Pharmacology and Nutritional Sciences, University of Kentucky, Lexington, Kentucky;* [11]*Departmentof Physiology and Saha Cardiovascular Research Center, University of Kentucky, Lexington, Kentucky; and* [12]*Department of Cellular and Molecular Medicine, Cleveland Clinic, Cleveland, Ohio*

Submitted 31 May 2017; accepted in final form 28 August 2017

Kim HW, Blomkalns AL, Ogbi M, Thomas M, Gavrila D, Neltner BS, Cassis LA, Thompson RW, Weiss RM, Lindower PD, Blanco VM, McCormick ML, Daugherty A, Fu X, Hazen SL, Stansfield BK, Huo Y, Fulton DJ, Chatterjee T, Weintraub NL. Role of myeloperoxidase in abdominal aortic aneurysm formation: mitigation by taurine. *Am J Physiol Heart Circ Physiol* 313: H1168–H1179, 2017. First published September 29, 2017; doi:10.1152/ajpheart.00296.2017.—Oxidative stress plays a fundamental role in abdominal aortic aneurysm (AAA) formation. Activated polymorphonuclear leukocytes (or neutrophils) are associated with AAA and express myeloperoxidase (MPO), which promotes inflammation, matrix degradation, and other pathological features of AAA, including enhanced oxidative stress through generation of reactive oxygen species. Both plasma and aortic MPO levels are elevated in patients with AAA, but the role of MPO in AAA pathogenesis has, heretofore, never been investigated. Here, we show that MPO gene deletion attenuates AAA formation in two animal models: ANG II infusion in apolipoprotein E-deficient mice and elastase perfusion in C57BL/6 mice. Oral administration of taurine [1% or 4% (wt/vol) in drinking water], an amino acid known to react rapidly with MPO-generated oxidants like hypochlorous acid, also prevented AAA formation in the ANG II and elastase models as well as the $CaCl_2$ application model of AAA formation while reducing aortic peroxidase activity and aortic protein-bound dityrosine levels, an oxidative cross link formed by MPO. Both MPO gene deletion and taurine supplementation blunted aortic macrophage accumulation, elastin fragmentation, and matrix metalloproteinase activation, key features of AAA pathogenesis. Moreover, MPO gene deletion and taurine administration significantly attenuated the induction of serum amyloid A, which promotes ANG II-induced AAAs. These data implicate MPO in AAA pathogenesis and suggest that studies exploring whether taurine can serve as a potential therapeutic for the prevention or treatment of AAA in patients merit consideration.

NEW & NOTEWORTHY Neutrophils are abundant in abdominal aortic aneurysm (AAA), and myeloperoxidase (MPO), prominently expressed in neutrophils, is associated with AAA in humans. This study demonstrates that MPO gene deletion or supplementation with the natural product taurine, which can scavenge MPO-generated oxidants, can prevent AAA formation, suggesting an attractive potential therapeutic strategy for AAA.

abdominal aortic aneurysm; myeloperoxidase; taurine; angiotensin II; elastase; calcium chloride

INTRODUCTION

Abdominal aortic aneurysms (AAA) are a common and life-threatening condition that occurs in up to 9% of elderly individuals >65 yr of age (37). This complex vascular disorder involves loss of smooth muscle cells and damage of structural connective tissue leading to progressive aortic dilation and/or catastrophic rupture and death (18). Surgical and percutaneous repair is associated with significant operative risks and complications (3), and, currently, there is no effective medical treatment for AAA.

Oxidative stress plays an important role in AAA pathogenesis (23, 24). Polymorphonuclear leukocytes (PMNs or neutrophils) are key mediators of oxidative stress and are present abundantly in human AAA tissues and elastase-induced AAA, where they play a crucial role in recruiting inflammatory cells to the aorta (12). Activated PMNs release myeloperoxidase (MPO), an enzyme that produces hypochlorous acid (HOCl) from H_2O_2 and Cl^-; HOCl reacts with a variety of biomolecules, including proteins, the double bonds of cholesterol and fatty acid groups, and nucleic acids, thereby causing oxidative

† 13 May 2015.

* H. Won Kim and A. L. Blomkalns contributed equally to this study.

Address for reprint requests and other correspondence: N. L. Weintraub, Dept. of Medicine, Div. of Cardiology, Vascular Biology Center, Medical College of Georgia at Augusta Univ., 1459 Laney Walker Blvd., Augusta, GA 30912 (e-mail: nweintraub@augusta.edu).

damage (17). MPO-derived HOCl inactivates tissue inhibitor of metalloproteinase-1 and α_1-antiprotease, which may indirectly stimulate proteolytic activity and matrix degradation (4, 41). Moreover, MPO can use H_2O_2 to convert L-tyrosine to tyrosyl radical and dityrosine (diTyr), an indicator of posttranslational oxidative cross link of proteins (11, 15). MPO can also use nitric oxide to promote protein nitration and lipid peroxidation, consistent with a complex and multifaceted role in promoting oxidative stress (10). Together, these studies suggest that MPO-mediated oxidative stress may play an important role in the pathogenesis of AAA.

Serum amyloid A (SAA) is an inducible acute-phase reactant produced by the liver, inflammatory cells, and adipocytes, whose induction has been linked to oxidative stress produced by lipid peroxidation products in mice fed an atherogenic diet (20). Cytokines produced during chronic inflammation also induce SAA, which, in turn, upregulates chemokine expression and activates matrix metalloproteinases (MMPs), key mediators of AAA. SAA expression has been recently reported to be upregulated in ANG II-induced AAA, and genetic deletion of SAA prevented ANG II-induced AAA formation (42), suggesting that SAA upregulation contributes to AAA pathogenesis. However, whether MPO regulates SAA in the context of AAA formation is unknown.

Taurine, a naturally occurring amino acid, has been studied in conditions associated with enhanced oxidative stress, including smoking, rheumatoid arthritis, osteoarthritis, neuronal injury, diabetes, cyclosporine-induced hepatotoxicity, ischemia-reperfusion injury, and diabetes in humans (6, 8, 14, 16, 27, 33). By reacting with HOCl to form taurine-chloramine, taurine can attenuate HOCl-mediated oxidation and tissue damage, reducing inflammation. Taurine also possesses other potential antioxidant effects, including suppression of reactive oxygen species generation and favorably modulating antioxidant enzyme levels (35).

In this study, we investigated the role of MPO in AAA formation and the preventive effects of taurine using three murine models of AAA: *1*) ANG II infusion into hyperlipidemic apolipoprotein E knockout ($ApoE^{-/-}$) mice, *2*) elastase perfusion, and *3*) $CaCl_2$ application in C57BL/6 mice. We also examined the impact of MPO deficiency on AAA formation using MPO knockout ($MPO^{-/-}$) mice. Our results suggest that MPO plays an important role in AAA pathogenesis and that taurine supplementation is effective at mitigating AAA formation.

MATERIALS AND METHODS

Animals. C57BL/6, $ApoE^{-/-}$, and $MPO^{-/-}$ mice were purchased from Jackson Laboratory (Bar Harbor, ME). $MPO^{-/-}$ mice were bred with $ApoE^{-/-}$ mice to obtain heterozygotes in the $ApoE^{-/-}$ background, which were interbred to produce littermates that were wild-type (WT), heterozygous ($^{+/-}$), or homozygous ($^{-/-}$) for MPO. The animal experimental protocols were approved by the Institutional Animal Care and Use Committees at the University of Iowa, University of Cincinnati, and Medical College of Georgia at Augusta University.

ANG II-induced AAA model. Six-month-old male $ApoE^{-/-}$, $ApoE^{-/-}MPO^{+/-}$, and $ApoE^{-/-}MPO^{-/-}$ mice received saline (placebo control) or ANG II (1,000 $ng \cdot kg^{-1} \cdot min^{-1}$, A9525, Sigma, St. Louis, MO) infused via osmotic mini-pumps (model 2004, Alzet, Cupertino, CA) inserted into the subcutaneous space in the interscapular area under parenteral anesthesia, as previously described (7). In separate experiments, $ApoE^{-/-}$ mice received saline or infusion of ANG II in the presence or absence of oral taurine [1% and 4% (wt/vol)]. These taurine concentrations were chosen on the basis of good tolerability and efficacy at reducing oxidative stress in mice and rats (8, 25). Mice were placed on plain or taurine-supplemented drinking water for 5 days before mini-pump implantation and continued for the study duration of 28 days. Aneurysms of the suprarenal aorta occur in ~80% of ANG II-infused mice at this dose and time period. Blood pressure measurements were obtained using a previously validated tail-cuff method (Coda 6, Kent Scientific, Torrington, CT). Mice were conditioned to the instrument and procedure for 5 consecutive days before pump implantation. To ensure a more robust estimation of systolic blood pressure (SBP), we used the interquartile mean of SBP measurements achieved through 30 measurement cycles every other day. Unless otherwise specified, mice were euthanized 4 wk after pump implantation for the assessment of aneurysm formation and other parameters, as described below.

Elastase-induced AAA model. Male C57BL/6 mice at ~3 mo of age were randomly assigned to receive water without or with taurine supplementation [1% or 4% (wt/vol)] for 5 days before elastase induction of AAA. Under parenteral anesthesia with pentobarbital, a laparotomy was performed, and the infrarenal abdominal aorta from beneath the left renal vein to the iliac bifurcation was isolated. The isolated segment was tied off, exsanguinated, and then perfused with porcine pancreatic elastase (PPE) type I (E-1250, Sigma) for 5 min. Heat-inactivated elastase was perfused in control mice. In separate experiments, elastase was perfused in WT and $MPO^{-/-}$ mice. Unless otherwise specified, mice were euthanized 14 days after elastase perfusion for the assessment of aneurysm formation and other parameters, as described below. This protocol was adapted with permission from Thompson et al. (37).

$CaCl_2$-induced AAA model. Twelve-week-old male C57BL/6 mice received water without or with taurine supplementation [1% (wt/vol)] for 5 days before $CaCl_2$ induction of AAA. Mice were anesthetized, and a laparotomy was performed as described above, after which saline (sham control) or 0.5 mol/l $CaCl_2$ (Sigma-Aldrich) was applied to the infrarenal aortic adventitial surface for 15 min followed by a rinse with 0.9% sterile saline and surgical closure. After 21 days, animals were anesthetized, aortic outer diameter was measured, and aortic tissues were removed for further experiments, as described above.

Aortic tissue collection and measurement. Aortic tissue samples were harvested at several time points over the aneurysm induction period (3 and 14 days in the elastase and $CaCl_2$ models and 4, 7, and 28 days in the ANG II model). The chest and abdominal cavities were opened, and blood was drawn from the right ventricle at the time of euthanasia. Aortas were irrigated with cold PBS through the left ventricle. Using a dissection microscope, we collected aortic roots for atherosclerosis quantification, exposed the abdominal aorta, and dissected the periadventitial tissue carefully from the wall of the aorta. Aortic measurements were determined with a stage micrometer and optical eyepiece reticle. For the elastase model, the percent increase in outer diameter was calculated from the difference between the preintervention and final measurements. An AAA was defined as an increase in the baseline outer diameter of 50%. The abdominal aorta, from the last intercostal artery to the ileal bifurcation, was sectioned and weighed, and the aneurysmal areas were fixed in paraformaldehyde [4% (wt/vol)] for immunohistochemistry or homogenized/sonicated for biochemical assays. Representative images of aortic histology were taken at the midpoint of the suprarenal aorta (ANG II model) or infrarenal aorta (elastase model) to maintain consistency. Aortic root sections were analyzed for atherosclerosis, as previously reported (7, 36). Blood samples were assayed for lipid profiles, as previously reported (36).

Gelatin zymography for detection of MMP-2 and MMP-9. Protein was extracted from excised abdominal aortas that had been snap frozen in liquid nitrogen and homogenized in a buffer containing 1 M

NaCl, 2 M urea, 0.2 mM PMSF, 50 mM Tris (pH 7.4), 0.1% EDTA, 0.1% Brij-35, and a 1:100 dilution of protease inhibitor cocktail (P8340, Sigma). Samples were sonicated on ice and centrifuged, and supernatants were used to quantify protein content (Pierce BCA system, Pierce, Rockford, IL). Protein lysate (600 μg) was placed in a nonreducing zymogram buffer (no. 161-0764, Bio-Rad, Hercules, CA) and applied without boiling to a 10% zymogram gel (no. 161-1167, Bio-Rad). Gels were incubated in 2% Triton X-100 at room temperature for 30 min and then rinsed in H_2O for 5 min. Gels were incubated overnight at 37°C with gentle agitation in buffer containing 50 mM Tris·HCl (pH 7.5), 0.15 mM NaCl, 5 mM anhydrous D-glucose, 5 μM $ZnCl_2$, and 30% Brij-35. Proteins were stained with Coomassie brilliant blue R-250 solution (Bio-Rad) and destained with a solution containing 40% methanol, 10% acetic acid, and 50% H_2O.

Peroxidase activity assay. Abdominal aortic tissues were snap frozen in liquid nitrogen and homogenized in 50 mM potassium phosphate buffer containing 0.5% hexadecyltrimethylammonium bromide. Homogenates were then freeze-thawed twice and sonicated on ice. Suspensions were centrifuged at 40,000 *g* for 15 min, and supernatants were harvested and separated using Sephadex G-75 columns. Assays were performed using *o*-dianisidine-based peroxidase activity measurements, as previously described (43). Briefly, 0.1 ml of samples was mixed with 2.9 ml of 50 mM phosphate buffer containing 0.53 mM *o*-dianisidine and 0.15 mM H_2O_2. Absorbance changes at 460 nm were measured in a spectrometer every 15 s for 10 min. Peroxidase activity was calculated from a standard curve prepared using purified human neutrophil-derived MPO. For the elastase and $CaCl_2$ models, we used a commercial detection kit (Fluoro MPO kit, Cell Technology), as previously reported (26), according to the manufacturer's instructions.

Immunohistochemistry. Paraformaldehyde-fixed [4% (wt/vol)] aortic sections were transferred to ethanol before being embedded in paraffin. Cross sections (5 μm) were mounted and stained with hematoxylin-and-eosin (H&E) or Verhoeff van Gieson stain for elastin. Antibodies for MPO (ab45977, Abcam, Cambridge, MA), Mac-3 (553322, BD PharMingen, Franklin Lakes, NJ), and SAA (AF2948, R&D Systems, Minneapolis, MN) were used in conjunction with the HistoMouse-SP kit (95-9541, Invitrogen, Carlsbad, CA) or DAB substrate kit (SK-4100, Vector Laboratories, Burlingame, CA).

Tyrosine modification analysis by LC/MS/MS. Stable isotope dilution LC/MS/MS analyses were performed to quantify the oxidized amino acids in abdominal aortic tissues, as previously reported (1). Briefly, samples were delipidated, isotope-labeled internal standards were added, and samples were then hydrolyzed in methane sulfonic acid under inert atmosphere. Hydrolysates were resolved on an ultra-high-performance, reverse-phase column and introduced into a Shimadzu 8050 triple quadrupole mass spectrometer using a discontinuous gradient. Oxidized amino acids and their precursors were monitored with characteristic parent-daughter ion transitions, as previously described (1).

Western blot analysis. Protein extraction and Western blot analysis were performed as previously described (7). The antibodies used were SAA (AF2948, R&D Systems), transferrin (ab82411, Abcam), MPO (ab9535, Abcam), and GAPDH (Ambion).

Statistical analysis. Results are expressed as means ± SE unless otherwise noted. Differences between two groups were analyzed by Student's *t*-test, and differences between multiple groups were analyzed by one-way ANOVA followed by least significant difference testing for multiple comparisons. Only those mice with elastase-induced aneurysms from the same enzyme lot were compared. A Fisher exact test was used to analyze categorical data. *P* values of <0.05 were considered to be significant.

RESULTS

MPO deficiency protected against AAA formation induced by ANG II in ApoE-deficient mice. To test the hypothesis that MPO contributes to AAA formation, we infused ANG II into MPO/ApoE compound-deficient mice. Reduced MPO protein expression level in these mice was confirmed by Western blot analysis (Fig. 1*A*). Interestingly, deletion of one ($MPO^{+/-}$) or both ($MPO^{-/-}$) alleles markedly protected against ANG II-induced AAA formation, as evidenced by reduced aneurysm incidence and maximal aortic diameter (Fig. 1, *B* and *C*). Histological analyses demonstrated that thrombus formation, macrophage accumulation, and elastase degradation during AAA formation were reduced significantly in MPO/ApoE-deficient mice (Fig. 1, *E–F*). MMP-2 and MMP-9 levels were also significantly diminished in MPO-deficient mice (Fig. 1*H*). Importantly, diffuse immunostaining for MPO was detected in aortic tissues of ApoE-deficient mice, particularly in the adventitia, which was abrogated in MPO/ApoE-deficient mice (Fig. 1*G*).

MPO deficiency reduced SAA expression during AAA formation. SAA expression in the plasma, liver, and aorta during AAA formation was markedly reduced in MPO/ApoE-deficient mice compared with $ApoE^{-/-}$ mice (Fig. 2, *A* and *B*). Reduced SAA accumulation in aortic tissues from MPO/ApoE-deficient mice was also confirmed by immunostaining (Fig. 2*C*). In contrast, MPO gene deletion did not affect blood pressure in response to ANG II infusion (data not shown).

Supplemental taurine attenuated ANG II-induced AAA formation. We next supplemented the drinking water of $ApoE^{-/-}$ mice with taurine [1% or 4% (wt/vol)], both of which significantly reduced ANG II-induced AAA formation, as assessed by maximal aortic diameter (Fig. 3*A*) and weight (data not shown) measured at death. Because both 4% and 1% taurine supplementation produced qualitatively similar results, in subsequent experiments, we used 1% taurine to limit potentially nonspecific effects associated with higher doses. To test the impact of taurine on peroxidase activity, we adopted a biochemical assay designed to exclude myoglobin and hemoglobin contaminants that could be associated with tissue thrombus (43). Using this assay, we detected a significant increase in aortic peroxidase activity induced during ANG II infusion that was strongly blocked by taurine administration (Fig. 3*B*). To quantify the effects of taurine on one aspect of oxidative stress noted to be produced by MPO, we analyzed aortic protein-bound diTyr levels, a posttranslational oxidative cross link of proteins generated by MPO and other tyrosyl radical-generating pathways (15, 19), using LC/MS/MS. We detected a significant increase in diTyr levels in aortas from ANG II-infused mice, which was markedly reduced by taurine treatment (Fig. 3*C*). Histological analyses demonstrated extensive intramural thrombus formation (H&E; Fig. 3*D*), macrophage accumulation (Mac-3; Fig. 3*E*), and localized MPO accumulation (MPO; Fig. 3*F*) in aortas of ANG II-infused mice, all of which were attenuated markedly by taurine. Taurine administration also resulted in a dose-dependent diminution in an AAA pathology score (data not shown), as defined by Manning et al. (22). Mortality from AAA dissection/rupture was 20% in control mice and 0% in taurine-administered mice (data not shown). Although taurine supplementation conferred protection against AAA, it did not reduce known parameters associ-

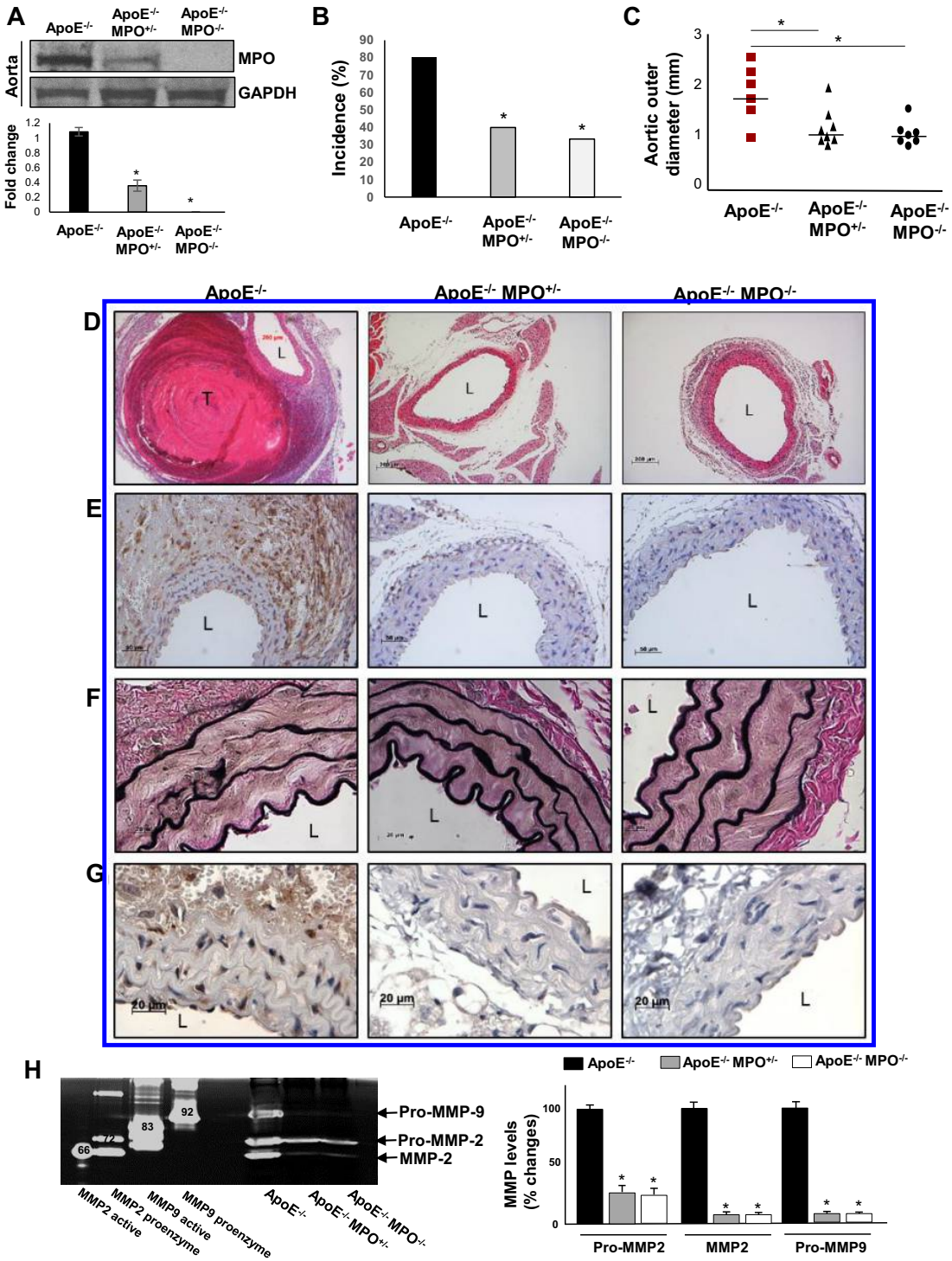

Fig. 1. Characterization of ANG II-induced abdominal aortic aneurysms (AAA) in apolipoprotein E (ApoE)-deficient ($ApoE^{-/-}$) mice versus ApoE/myeloperoxidase (MPO) double-knockout mice. *A*: MPO protein expression levels in $ApoE^{-/-}$, $ApoE^{-/-}MPO^{+/-}$, and $ApoE^{-/-}MPO^{-/-}$ mice, as examined by Western blot analysis. *$P < 0.01$ vs. wild-type (WT) mice ($n = 3$). *B* and *C*: AAA incidence (*B*) and mean aortic outer diameter (*C*) in $ApoE^{-/-}$, $ApoE^{-/-}MPO^{+/-}$, and $ApoE^{-/-}MPO^{-/-}$ mice infused with ANG II. *$P < 0.05$ vs. $ApoE^{-/-}$ control mice ($n = 10$). Representative histology demonstrated thrombus formation (*D*; hematoxylin and eosin staining), macrophage accumulation (*E*; Mac-3 staining), elastin fragmentation (*F*: Verhoeff van Gieson staining), and MPO immunostaining (*G*). L, lumen; T, intramural thrombus. *H*: representative zymogram (*left*) demonstrating aortic pro-matrix metalloproteinase (MMP)-2, MMP-2, and pro-MMP-9 levels and quantified data (*right*). Positive controls are shown in the left four lanes of the zymogram; bands denote molecular weights of the respective enzymes. *$P < 0.05$ vs. $ApoE^{-/-}$ control ($n = 3$).

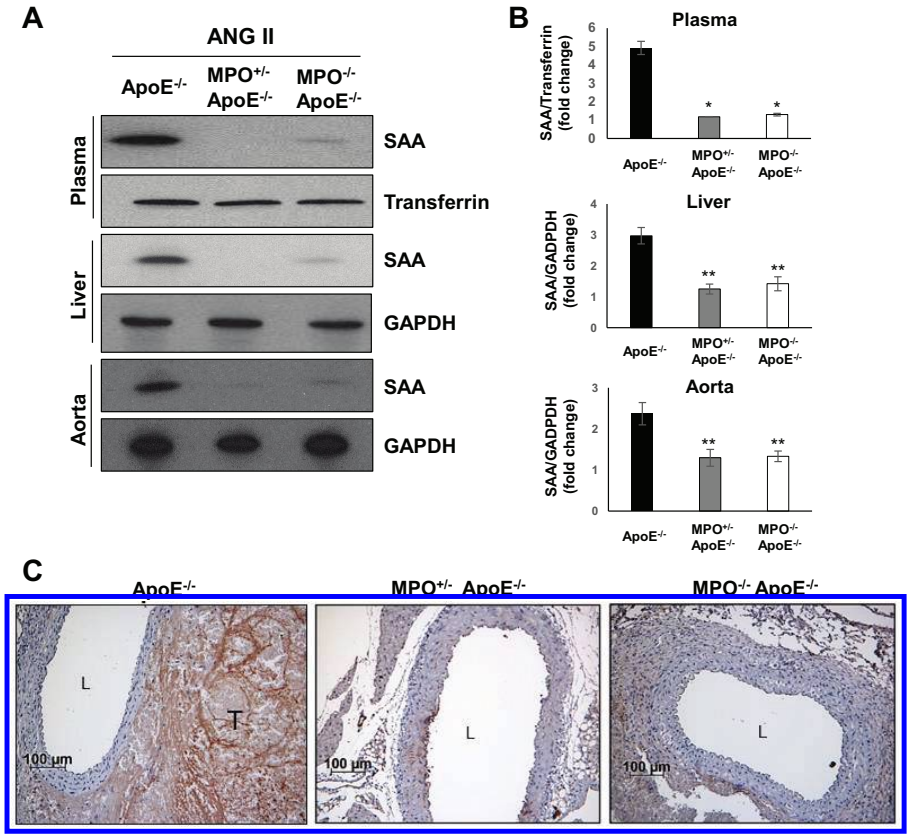

Fig. 2. Serum amyloid A (SAA) expression levels in apolipoprotein E-deficient ($ApoE^{-/-}$) mice versus ApoE/myeloperoxidase (MPO) double-knockout mice infused with ANG II. *A*: representative Western blot showing SAA protein expression in the plasma, liver, and aorta in $ApoE^{-/-}$, $ApoE^{-/-}/MPO^{+/-}$, and $ApoE^{-/-}/MPO^{-/-}$ mice infused with ANG II. Transferrin and GAPDH are shown as loading controls. *B*: densitometric analysis of SAA protein expression. $*P < 0.01$ and $**P < 0.05$ vs. wild-type control mice ($n = 3$). *C*: representative images of aortic SAA immunostaining in $ApoE^{-/-}$, $ApoE^{-/-}/MPO^{+/-}$, and $ApoE^{-/-}/MPO^{-/-}$ mice infused with ANG II. L, lumen; T, intramural thrombus.

ated with aneurysmal growth rate, such as SBP, aortic root atherosclerosis, or lipid levels (data not shown).

Taurine reduced SAA expression induced during AAA formation. Given that MPO gene deletion blocked induction of SAA during AAA formation (Fig. 2) and that taurine reduced peroxidase activity (Fig. 3), we next tested whether taurine supplementation inhibited SAA induction during AAA formation. ANG II infusion into $ApoE^{-/-}$ mice significantly increased SAA levels in the plasma, liver, and aorta, all of which were effectively reduced by taurine supplementation (Fig. 4, *A* and *B*). Immunostaining demonstrated that SAA accumulated primarily in the adventitia in aortas of ANG II-infused mice and was effectively blocked by taurine treatment (Fig. 4*C*).

Taurine and MPO gene deletion protected against elastase-induced AAA formation. We next investigated whether taurine inhibited AAA formation using a distinct model, elastase-induced AAA formation. Elastase infusion produced ~80% increase in aortic diameter compared with control, and taurine supplementation prevented elastase-induced AAA formation (Fig. 5*A*). Peroxidase activity assay showed marked increases in aortas extracted from mice 3 days after elastase infusion compared with aortas from mice infused with heat-inactivated elastase (Fig. 5*B*). This was consistent with previous observations and corresponds to the time point of maximal aortic PMN accumulation in this experimental model (26). Tissue histology showed prominent macrophage accumulation in the adventitia of elastase-infused aortas that was blunted by taurine supplementation (Fig. 5, *C* and *D*). In addition, elastase infusion strongly induced elastin degradation (Fig. 5*D*) and aortic MMP-2/MMP-9 activation (Fig. 5*E*), which were also blocked by taurine supplementation. Similar to our findings with taurine, deletion of *MPO* also strongly protected mice against AAA formation in the elastase model (Fig. 6*A*). MMP-2/MMP-9 activation (Fig. 6*B*) and elastin fragmentation (Fig. 6*C*) were diminished markedly in $MPO^{-/-}$ mice compared with WT control mice.

Taurine protected against $CaCl_2$-induced AAA formation. We further investigated whether taurine treatment could mitigate AAA formation induced by $CaCl_2$ application in C57BL/6 mice, another animal model of AAA, which is associated with PMN infiltration and elastin fragmentation. As shown in Fig. 7, *A* and *B*, taurine treatment significantly reduced aortic diameter and MPO activity induced by $CaCl_2$ application. Prominent elastin fragmentation, macrophage infiltration, and MPO accumulation were observed in $CaCl_2$-induced AAA tissues compared with sham control tissues, which were markedly inhibited by taurine treatment (Fig. 7, *C*–*E*). Furthermore, taurine blocked induction of aortic MMP-2/MMP-9 by $CaCl_2$ application (Fig. 7*F*).

DISCUSSION

Oxidative stress is hypothesized to exert a prominent role in AAA pathogenesis (23). MPO, an enzyme expressed predominantly in PMNs and monocytes, is an important mediator of vascular oxidative stress, and its levels have been positively associated with AAA in humans (12, 19). Here, using three distinct animal models of AAA, we report that deletion of *MPO* or supplementation with taurine, a naturally occurring

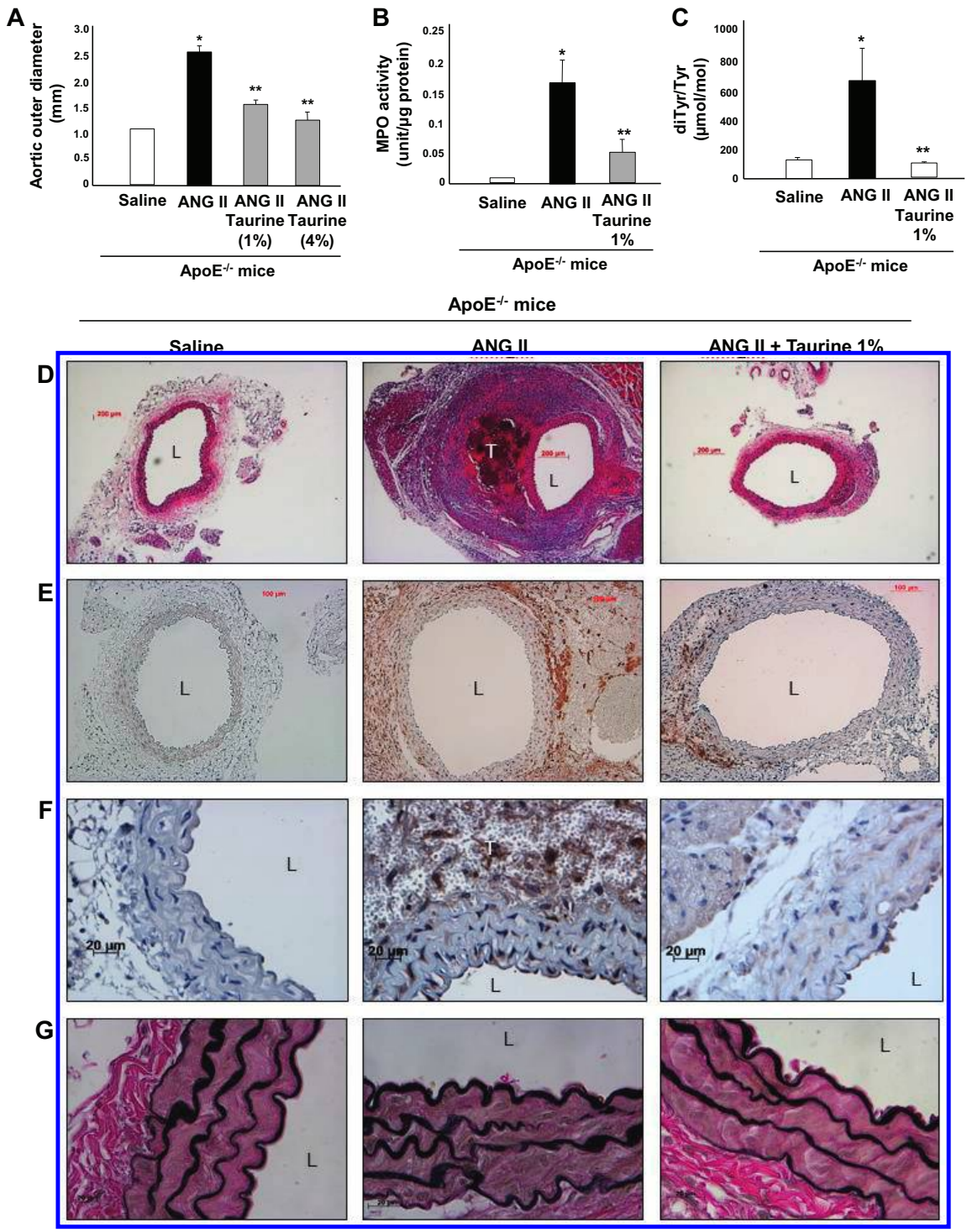

Fig. 3. Effects of taurine supplementation on ANG II-induced abdominal aortic aneurysm formation in apolipoprotein E-deficient ($ApoE^{-/-}$) mice. *A*−*C*: effects of taurine [1% or 4% (wt/vol) in drinking water] on mean outer aortic diameter (*A*), myeloperoxidase (MPO) activity (*B*), and dityrosine (diTyr) levels (*C*). $*P < 0.05$ vs. saline control; $**P < 0.05$ vs. ANG II ($n = 12$). *D*−*G*: representative histology demonstrating thrombus formation (*D*; hematoxylin and eosin staining), macrophage infiltration (*E*; Mac-3 staining), MPO accumulation (*F*), and elastin degradation (*G*; Verhoeff van Gieson staining). L, lumen; T, intramural thrombus.

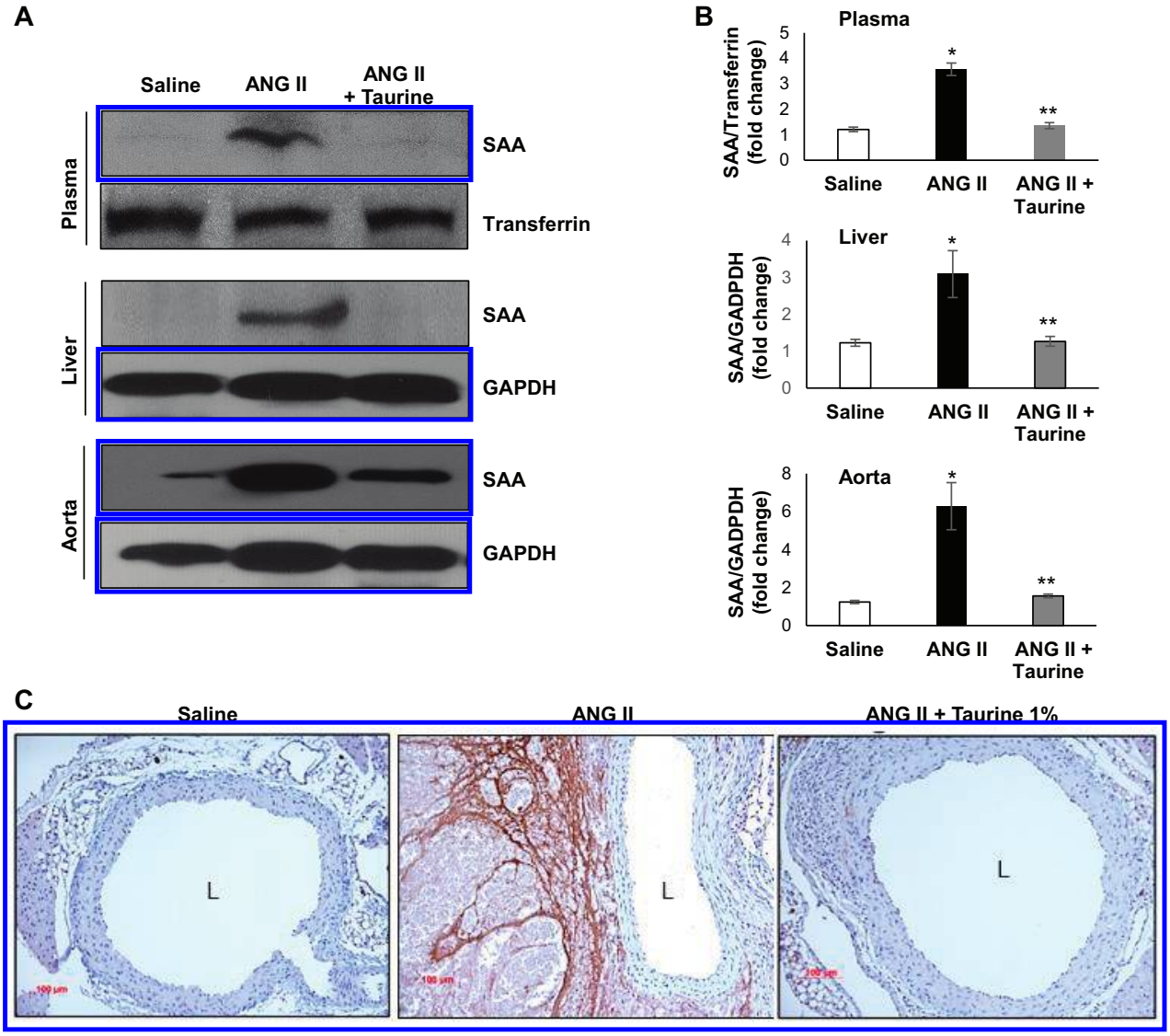

Fig. 4. Serum amyloid A (SAA) expression levels in apolipoprotein E-deficient (ApoE$^{-/-}$) mice treated with or without taurine and infused with ANG II. *A*: representative Western blot demonstrating effects of ANG II with and without taurine supplementation on SAA protein expression in the plasma, liver, and aorta. Transferrin and GAPDH are shown as loading controls. *B*: densitometric analysis of SAA protein expression. *$P < 0.01$ vs. saline; **$P < 0.01$ vs. ANG II ($n = 3$). *C*: representative images of aortic SAA immunostaining in mice treated with or without taurine supplementation. L, lumen.

amino acid that is reported to ameliorate MPO-mediated oxidative stress, mitigates AAA formation. Mechanistically, both *MPO* gene deletion and taurine supplementation blunted aortic macrophage accumulation, elastin fragmentation, and MMP activation, key features of AAA pathogenesis. Moreover, induction of SAA, which amplifies inflammation and activates MMPs and has been implicated in AAA (42), was strongly attenuated by MPO gene deletion and taurine supplementation. These data implicate MPO in the pathogenesis of AAA and raise the possibility that taurine supplementation be evaluated for its therapeutic efficacy in subjects with AAA.

The contribution of MPO to vascular disease was supported by previous studies that identified MPO-oxidized molecular species in human atherosclerotic plaques (2, 9, 13, 46). In the circulation, MPO is bound tightly to and oxidatively modifies high-density lipoprotein (HDL), thereby disrupting its anti-atherogenic effects (13, 47). MPO levels are independently associated with the presence of coronary artery disease, linked to catalytic consumption of nitric oxide and endothelial dysfunction in vivo, and are predictive of future myocardial infarction and major adverse cardiac and peripheral arterial events (2, 39). Interestingly, studies using genetically modified mice to examine a role of MPO in atherosclerosis have produced variable results (38). This discrepancy between murine studies and human data may, in part, reflect species differences in MPO, since murine leukocytes contain ~10-fold less MPO than human leukocytes (28).

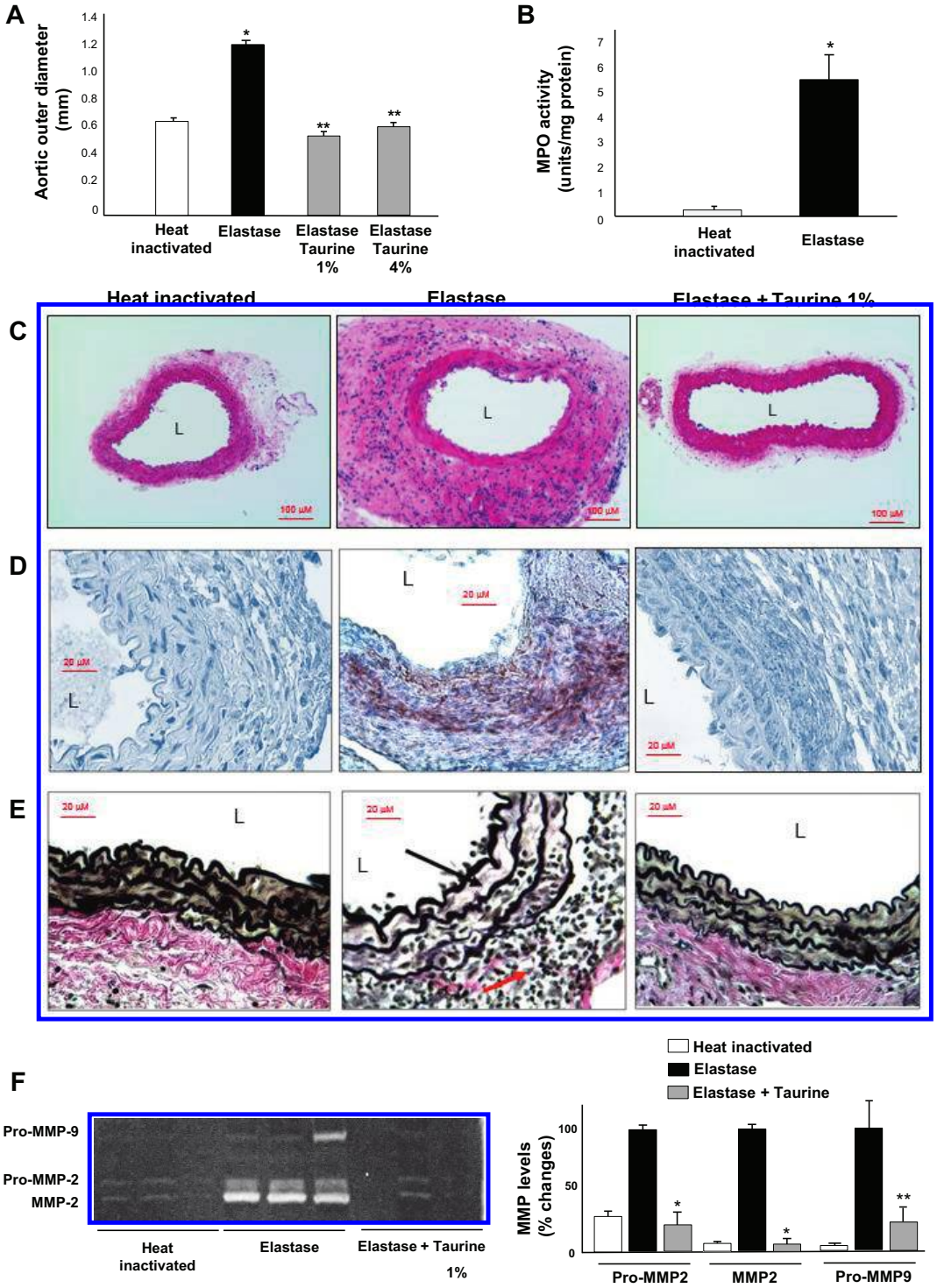

Fig. 5. Effects of taurine supplementation on elastase-induced abdominal aortic aneurysms. *A*: myeloperoxidase (MPO) activity in aortic segments from mice infused with native or heat-inactivated elastase. *B*: mean outer aortic diameters in elastase-induced abdominal aortic aneurysm mice with or without taurine supplementation [1% or 4% (wt/vol)] in drinking water. *$P < 0.05$ vs. heat-inactivated control; **$P < 0.05$ vs. elastase ($n = 8$). *C*: representative hematoxylin and eosin staining in aortic tissues from mice infused native or heat-inactivated elastase or elastase with taurine [1% (wt/vol)] supplementation. *D*: representative Mac-3 macrophage immunostaining in aortic tissues. *E*: representative Verhoeff van Gieson elastin staining in aortic segments. Black arrow indicates elastin; red arrow indicates inflammatory cells. *F*: representative zymogram (*left*) demonstrating aortic pro-matrix metalloproteinase (MMP)-2, MMP-2, and pro-MMP-9 levels and quantified data (*right*). L, lumen. *$P < 0.01$ and **$P < 0.05$ vs. elastase ($n = 3$).

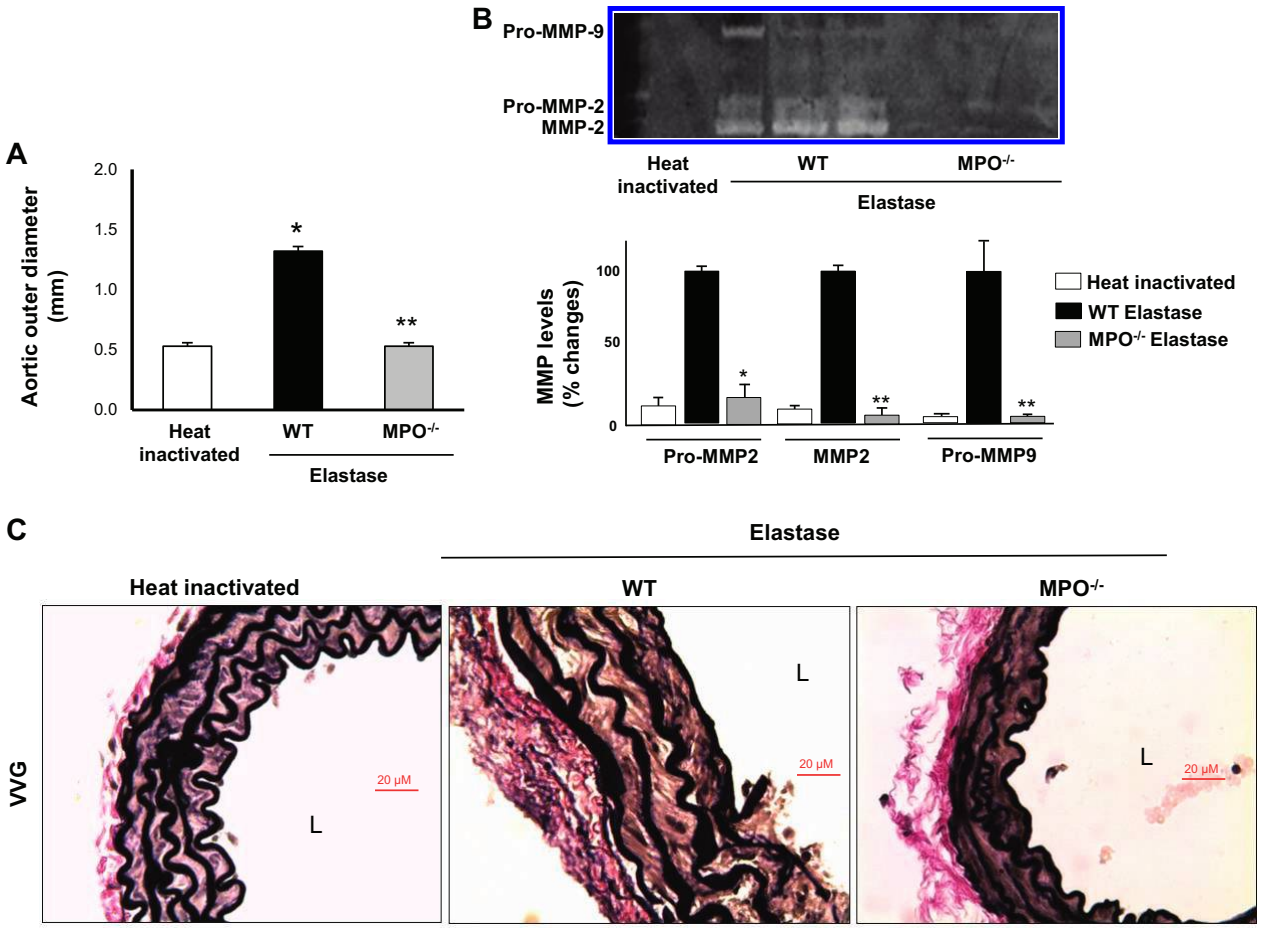

Fig. 6. Characterization of elastase-induced abdominal aortic aneurysms in wild-type (WT) mice versus myeloperoxidase (MPO)$^{-/-}$ mice. *A*: mean outer aortic diameter after elastase infusion in WT mice and MPO$^{-/-}$ mice. *$P < 0.05$ vs. heat-inactivated control; **$P < 0.05$ vs. elastase-infused WT ($n = 8$). *B*: representative zymogram (*top*) of pro-matrix metalloproteinase (MMP)-2, MMP-2, and pro-MMP-9 levels and quantified data (*bottom*). *$P < 0.05$ and **$P < 0.01$ vs. elastase ($n = 3$). *C*: Verhoeff van Gieson (VVG) elastin staining in the aortas from WT mice or MPO$^{-/-}$ mice infused with elastase. L, lumen.

The potential role of MPO in AAA has received little attention despite the compelling evidence linking PMNs to the pathogenesis of AAA in humans. For example, PMNs isolated from patients with AAA are activated, release more MPO, and exhibit higher intracellular H_2O_2 levels compared with controls, suggesting a fundamental state of redox imbalance (12, 29, 30). These PMNs become trapped within the thrombus associated with AAA and release MPO, plasma levels of which are also elevated in patients with AAA (12, 30). Smoking, a major risk factor for AAA, upregulates MPO expression and activity in PMNs, and MPO upregulation was also observed after in vitro exposure of PMNs to nicotine (21). Interestingly, nicotine infusion was demonstrated to promote AAA in mice (40), which further suggests a biological link between smoking, PMNs, MPO, and AAA.

Here, we used three murine models of AAA formation to test the hypothesis that MPO contributes to AAA pathogenesis. In the elastase and $CaCl_2$ models, PMN infiltration is prominent, and aortic MPO accumulation precedes onset of aneurysm formation (5, 26). These findings, coupled with our data showing that MPO gene deletion or taurine supplementation prevented elastin- and $CaCl_2$-induced AAA, provide strong support for our hypothesis. However, unlike the elastase or $CaCl_2$ models, PMN infiltration is not a prominent feature of the ANG II infusion model (32), although PMNs can become trapped within the thrombus that forms in the media. Biochemical and histological analyses demonstrated evidence of increased peroxidase activity and MPO protein, respectively, in aortas from ANG II-infused mice; immunostaining specificity was established using tissues from MPO knockout mice. The diffuse pattern of immunostaining suggests MPO expression by macrophages prevalent in the vascular wall and/or tissue uptake in response to ANG II infusion, a hypothesis that will need to be addressed in future studies.

MPO uses H_2O_2 to convert L-tyrosine to tyrosyl radical. Activated PMNs use this system to oxidize free L-tyrosine to *o*,*o'*-diTyr, and levels of protein-bound diTyr are elevated in atherosclerotic tissues (9, 15, 19). In this study, diTyr levels measured by LC/MS/MS were markedly increased in AAA tissues in conjunction with increased peroxidase activity. Attenuation of ANG II-induced AAA by taurine was associated with diminished peroxidase activity and diTyr levels, consis-

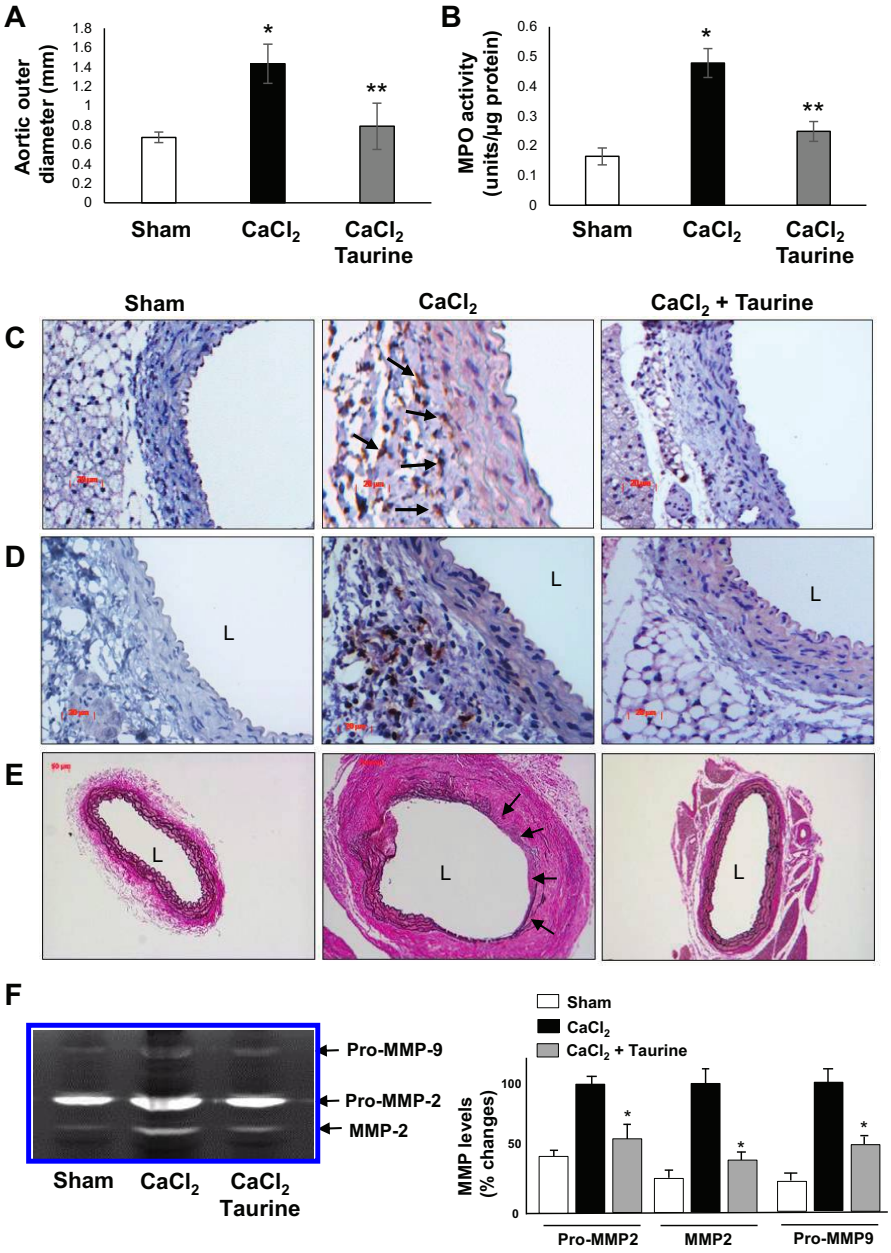

Fig. 7. Effects of taurine on $CaCl_2$-induced abdominal aortic aneurysms in wild-type (WT) mice. *A* and *B*: effects of taurine on mean outer aortic diameter (*A*) and myeloperoxidase (MPO) activity (*B*). $*P < 0.05$ vs. sham control; $**P < 0.05$ vs. $CaCl_2$-treated WT mice (*A*: $n = 10$, *B*: $n = 3$). *C*–*E*: representative histology demonstrating elastin degradation (*C*; Verhoeff van Gieson staining), macrophage infiltration (*D*; Mac-3 staining), and MPO accumulation (*E*). Black arrows indicate macrophages (*C*) and elastin degradation (*E*). L, lumen. *F*: representative zymogram (*left*) of pro-matrix metalloproteinase (MMP)-2, MMP-2, and pro-MMP-9 levels as well as quantified data (*right*). $*P < 0.05$ vs. $CaCl_2$ ($n = 3$).

tent with inhibiting MPO, although taurine possesses other biological actions that could favorably modulate AAA (25).

SAA is a cytokine-inducible, acute-phase reactant, expressed primarily in hepatocytes, inflammatory cells, and adipocytes. Plasma SAA concentrations are elevated in chronic inflammatory diseases, and both SAA and MPO can circulate bound to HDL. Our findings of increased SAA levels in the liver, plasma, and aorta in the ANG II-induced AAA model confirm the findings of Webb et al. (42), who proceeded to demonstrate a key role for SAA in the pathogenesis of AAA using SAA1/2 knockout mice. Here, we show that MPO gene deletion and taurine treatment prevented upregulation of SAA during ANG II infusion, suggesting that MPO may promote AAA, at least in part, through SAA induction. The extent to which local versus hepatic production of SAA contributes to aortic pathology remains to be determined. Interestingly, MPO gene deletion attenuated hepatic inflammation in mice fed a high-fat diet, which may support a role for MPO in regulating SAA expression in liver (31). Moreover, increased plasma levels of circulating inflammatory cytokines such as IL-6 and TNF-α during AAA formation may contribute to liver inflammation and induction of hepatic SAA expression. Indepth studies are required in the future to determine the mechanisms of SAA regulation by MPO.

Taurine supplementation is generally regarded as safe, is thought to function through inhibition of oxidative stress, and

has been provided in doses up to 10 g/day administered for 6–12 mo with minimal adverse effects (34). Oral taurine (3 g/day) ameliorated lipid-induced oxidative stress and insulin resistance in obese, nondiabetic men (44). Moreover, supplementation with 6 g/day taurine reduced oxidative DNA damage in leukocytes measured 24 h after intense aerobic exercise (45). Taurine supplementation also improved parameters of cardiovascular dysfunction in smokers, such as endothelial cell function and viability (6). Our findings suggest that taurine supplementation mitigates AAA formation in three distinct murine models. Given taurine's safety record and low cost, it merits consideration for efficacy testing in patients with AAA.

In conclusion, we report, for the first time, that the neutrophil enzyme MPO, levels of which are elevated in plasma and aneurysm tissues of patients with AAA, plays a pivotal role in AAA formation induced experimentally in mice using pathogenically distinct models of aneurysm formation. Moreover, supplementation with taurine, a naturally occurring amino acid, which is safe and effective at ameliorating MPO-mediated oxidative stress, can mitigate experimental AAA formation. Further studies are indicated to test the effects of taurine supplementation on parameters of MPO-mediated oxidative stress and AAA progression in patients with this disorder.

GRANTS

This study was supported by National Heart, Lung, and Blood Institute Grants HL-076684, HL-62984, HL-105675, and HL-112640 (to N. L. Weintraub) and P01 HL076491 (S. L. Hazen) and by Department of Defense Grant NF-140031 (B. K. Stansfield).

DISCLOSURES

No conflicts of interest, financial or otherwise, are declared by the authors.

AUTHOR CONTRIBUTIONS

H.W.K., A.L.B., and N.L.W. conceived and designed research; H.W.K., A.L.B., M.O., D.G., B.S.N., V.M.B., M.L.M., and X.F. performed experiments; H.W.K., A.L.B., M.O., M.T., D.G., B.S.N., R.W.T., R.M.W., V.M.B., M.L.M., A.D., X.F., S.L.H., B.K.S., D.J.F., T.C., and N.L.W. analyzed data; H.W.K., A.L.B., M.O., M.T., D.G., B.S.N., L.A.C., R.W.T., R.M.W., P.D.L., V.M.B., M.L.M., A.D., S.L.H., B.K.S., Y.H., D.J.F., T.C., and N.L.W. interpreted results of experiments; H.W.K., A.L.B., and M.O. prepared figures; H.W.K., A.L.B., and N.L.W. drafted manuscript; H.W.K., A.L.B., M.T., D.G., L.A.C., R.W.T., R.M.W., P.D.L., V.M.B., M.L.M., A.D., S.L.H., B.K.S., Y.H., D.J.F., T.C., and N.L.W. edited and revised manuscript; H.W.K., A.L.B., M.O., M.T., D.G., B.S.N., L.A.C., R.W.T., R.M.W., P.D.L., V.M.B., M.L.M., A.D., X.F., S.L.H., B.K.S., Y.H., D.J.F., T.C., and N.L.W. approved final version of manuscript.

REFERENCES

1. **Brennan ML, Wu W, Fu X, Shen Z, Song W, Frost H, Vadseth C, Narine L, Lenkiewicz E, Borchers MT, Lusis AJ, Lee JJ, Lee NA, Abu-Soud HM, Ischiropoulos H, Hazen SL.** A tale of two controversies: defining both the role of peroxidases in nitrotyrosine formation in vivo using eosinophil peroxidase and myeloperoxidase-deficient mice, and the nature of peroxidase-generated reactive nitrogen species. *J Biol Chem* 277: 17,415–17,427, 2002. doi:10.1074/jbc.M112400200.
2. **Brennan ML, Penn MS, Van Lente F, Nambi V, Shishehbor MH, Aviles RJ, Goormastic M, Pepoy ML, McErlean ES, Topol EJ, Nissen SE, Hazen SL.** Prognostic value of myeloperoxidase in patients with chest pain. *N Engl J Med* 349: 1595–1604, 2003. doi:10.1056/NEJMoa035003.
3. **Brewster DC, Cronenwett JL, Hallett JW, Jr, Johnston KW, Krupski WC, Matsumura JS; Joint Council of the American Association for Vascular Surgery and Society for Vascular Surgery.** Guidelines for the treatment of abdominal aortic aneurysms. Report of a subcommittee of the joint council of the American Association for Vascular Surgery and Society for Vascular Surgery. *J Vasc Surg* 37: 1106–1117, 2003. doi:10.1067/mva.2003.363.
4. **Carr AC, Hawkins CL, Thomas SR, Stocker R, Frei B.** Relative reactivities of N-chloramines and hypochlorous acid with human plasma constituents. *Free Radic Biol Med* 30: 526–536, 2001. doi:10.1016/S0891-5849(00)00495-0.
5. **Eliason JL, Hannawa KK, Ailawadi G, Sinha I, Ford JW, Deogracias MP, Roelofs KJ, Woodrum DT, Ennis TL, Henke PK, Stanley JC, Thompson RW, Upchurch GR Jr.** Neutrophil depletion inhibits experimental abdominal aortic aneurysm formation. *Circulation* 112: 232–240, 2005. doi:10.1161/CIRCULATIONAHA.104.517391.
6. **Fennessy FM, Moneley DS, Wang JH, Kelly CJ, Bouchier-Hayes DJ.** Taurine and vitamin C modify monocyte and endothelial dysfunction in young smokers. *Circulation* 107: 410–415, 2003. doi:10.1161/01.CIR.0000046447.72402.47.
7. **Gavrila D, Li WG, McCormick ML, Thomas M, Daugherty A, Cassis LA, Miller FJ, Jr, Oberley LW, Dellsperger KC, Weintraub NL.** Vitamin E inhibits abdominal aortic aneurysm formation in angiotensin II-infused apolipoprotein E-deficient mice. *Arterioscler Thromb Vasc Biol* 25: 1671–1677, 2005. doi:10.1161/01.ATV.0000172631.50972.0f.
8. **Hagar HH.** The protective effect of taurine against cyclosporine A-induced oxidative stress and hepatotoxicity in rats. *Toxicol Lett* 151: 335–343, 2004. doi:10.1016/j.toxlet.2004.03.002.
9. **Hazen SL, Heinecke JW.** 3-Chlorotyrosine, a specific marker of myeloperoxidase-catalyzed oxidation, is markedly elevated in low-density lipoprotein isolated from human atherosclerotic intima. *J Clin Invest* 99: 2075–2081, 1997. doi:10.1172/JCI119379.
10. **Hazen SL, Zhang R, Shen Z, Wu W, Podrez EA, MacPherson JC, Schmitt D, Mitra SN, Mukhopadhyay C, Chen Y, Cohen PA, Hoff HF, Abu-Soud HM.** Formation of nitric oxide-derived oxidants by myeloperoxidase in monocytes: pathways for monocyte-mediated protein nitration and lipid peroxidation in vivo. *Circ Res* 85: 950–958, 1999. doi:10.1161/01.RES.85.10.950.
11. **Heinecke JW, Hsu FF, Crowley JR, Hazen SL, Leeuwenburgh C, Mueller DM, Rasmussen JE, Turk J.** Detecting oxidative modification of biomolecules with isotope dilution mass spectrometry: sensitive and quantitative assays for oxidized amino acids in proteins and tissues. *Methods Enzymol* 300: 124–144, 1999. doi:10.1016/S0076-6879(99)00121-4.
12. **Houard X, Touat Z, Ollivier V, Louedec L, Philippe M, Sebbag U, Meilhac O, Rossignol P, Michel JB.** Mediators of neutrophil recruitment in human abdominal aortic aneurysms. *Cardiovasc Res* 82: 532–541, 2009. doi:10.1093/cvr/cvp048.
13. **Huang Y, DiDonato JA, Levison BS, Schmitt D, Li L, Wu Y, Buffa J, Kim T, Gerstenecker GS, Gu X, Kadiyala CS, Wang Z, Culley MK, Hazen JE, Didonato AJ, Fu X, Berisha SZ, Peng D, Nguyen TT, Liang S, Chuang CC, Cho L, Plow EF, Fox PL, Gogonea V, Tang WH, Parks JS, Fisher EA, Smith JD, Hazen SL.** An abundant dysfunctional apolipoprotein A1 in human atheroma. *Nat Med* 20: 193–203, 2014. doi:10.1038/nm.3459.
14. **Iida Y, Xu B, Xuan H, Glover KJ, Tanaka H, Hu X, Fujimura N, Wang W, Schultz JR, Turner CR, Dalman RL.** Peptide inhibitor of CXCL4-CCL5 heterodimer formation, MKEY, inhibits experimental aortic aneurysm initiation and progression. *Arterioscler Thromb Vasc Biol* 33: 718–726, 2013. doi:10.1161/ATVBAHA.112.300329.
15. **Jacob JS, Cistola DP, Hsu FF, Muzaffar S, Mueller DM, Hazen SL, Heinecke JW.** Human phagocytes employ the myeloperoxidase-hydrogen peroxide system to synthesize dityrosine, trityrosine, pulcherosine, and isodityrosine by a tyrosyl radical-dependent pathway. *J Biol Chem* 271: 19950–19956, 1996. doi:10.1074/jbc.271.33.19950.
16. **Johnston WF, Salmon M, Su G, Lu G, Stone ML, Zhao Y, Owens GK, Upchurch GR, Jr, Ailawadi G.** Genetic and pharmacologic disruption of interleukin-1β signaling inhibits experimental aortic aneurysm formation. *Arterioscler Thromb Vasc Biol* 33: 294–304, 2013. doi:10.1161/ATVBAHA.112.300432.
17. **Lau D, Baldus S.** Myeloperoxidase and its contributory role in inflammatory vascular disease. *Pharmacol Ther* 111: 16–26, 2006. doi:10.1016/j.pharmthera.2005.06.023.
18. **Lederle FA, Johnson GR, Wilson SE, Ballard DJ, Jordan WD, Jr, Blebea J, Littooy FN, Freischlag JA, Bandyk D, Rapp JH, Salam AA; Veterans Affairs Cooperative Study #417 Investigators.** Rupture rate of large abdominal aortic aneurysms in patients refusing or unfit for elective repair. *JAMA* 287: 2968–2972, 2002. doi:10.1001/jama.287.22.2968.
19. **Leeuwenburgh C, Rasmussen JE, Hsu FF, Mueller DM, Pennathur S, Heinecke JW.** Mass spectrometric quantification of markers for protein oxidation by tyrosyl radical, copper, and hydroxyl radical in low density

lipoprotein isolated from human atherosclerotic plaques. *J Biol Chem* 272: 3520–3526, 1997. doi:10.1074/jbc.272.6.3520.

20. **Liao F, Andalibi A, Qiao JH, Allayee H, Fogelman AM, Lusis AJ.** Genetic evidence for a common pathway mediating oxidative stress, inflammatory gene induction, and aortic fatty streak formation in mice. *J Clin Invest* 94: 877–884, 1994. doi:10.1172/JCI117409.
21. **Loke WM, Lam KM, Chong WL, Chew SE, Quek AM, Lim EC, Seet RC.** Products of 5-lipoxygenase and myeloperoxidase activities are increased in young male cigarette smokers. *Free Radic Res* 46: 1230–1237, 2012. doi:10.3109/10715762.2012.701291.
22. **Manning MW, Cassis LA, Huang J, Szilvassy SJ, Daugherty A.** Abdominal aortic aneurysms: fresh insights from a novel animal model of the disease. *Vasc Med* 7: 45–54, 2002. doi:10.1191/1358863x02vm413ra.
23. **McCormick ML, Gavrila D, Weintraub NL.** Role of oxidative stress in the pathogenesis of abdominal aortic aneurysms. *Arterioscler Thromb Vasc Biol* 27: 461–469, 2007. doi:10.1161/01.ATV.0000257552.94483.14.
24. **Miller FJ, Jr, Sharp WJ, Fang X, Oberley LW, Oberley TD, Weintraub NL.** Oxidative stress in human abdominal aortic aneurysms: a potential mediator of aneurysmal remodeling. *Arterioscler Thromb Vasc Biol* 22: 560–565, 2002. doi:10.1161/01.ATV.0000013778.72404.30.
25. **Oudit GY, Trivieri MG, Khaper N, Husain T, Wilson GJ, Liu P, Sole MJ, Backx PH.** Taurine supplementation reduces oxidative stress and improves cardiovascular function in an iron-overload murine model. *Circulation* 109: 1877–1885, 2004. doi:10.1161/01.CIR.0000124229.40424.80.
26. **Pagano MB, Bartoli MA, Ennis TL, Mao D, Simmons PM, Thompson RW, Pham CT.** Critical role of dipeptidyl peptidase I in neutrophil recruitment during the development of experimental abdominal aortic aneurysms. *Proc Natl Acad Sci USA* 104: 2855–2860, 2007. doi:10.1073/pnas.0606091104.
27. **Park HS, Choi GH, Hahn S, Yoo YS, Lee JY, Lee T.** Potential role of vascular smooth muscle cell-like progenitor cell therapy in the suppression of experimental abdominal aortic aneurysms. *Biochem Biophys Res Commun* 431: 326–331, 2013. doi:10.1016/j.bbrc.2012.12.099.
28. **Podrez EA, Abu-Soud HM, Hazen SL.** Myeloperoxidase-generated oxidants and atherosclerosis. *Free Radic Biol Med* 28: 1717–1725, 2000. doi:10.1016/S0891-5849(00)00229-X.
29. **Ramos-Mozo P, Madrigal-Matute J, Martinez-Pinna R, Blanco-Colio LM, Lopez JA, Camafeita E, Meilhac O, Michel J-B, Aparicio C, Vega de Ceniga M, Egido J, Martín-Ventura JL.** Proteomic analysis of polymorphonuclear neutrophils identifies catalase as a novel biomarker of abdominal aortic aneurysm: potential implication of oxidative stress in abdominal aortic aneurysm progression. *Arterioscler Thromb Vasc Biol* 31: 3011–3019, 2011. doi:10.1161/ATVBAHA.111.237537.
30. **Ramos-Mozo P, Madrigal-Matute J, Vega de Ceniga M, Blanco-Colio LM, Meilhac O, Feldman L, Michel J-B, Clancy P, Golledge J, Norman PE, Egido J, Martin-Ventura JL.** Increased plasma levels of NGAL, a marker of neutrophil activation, in patients with abdominal aortic aneurysm. *Atherosclerosis* 220: 552–556, 2012. doi:10.1016/j.atherosclerosis.2011.11.023.
31. **Rensen SS, Bieghs V, Xanthoulea S, Arfianti E, Bakker JA, Shiri-Sverdlov R, Hofker MH, Greve JW, Buurman WA.** Neutrophil-derived myeloperoxidase aggravates non-alcoholic steatohepatitis in low-density lipoprotein receptor-deficient mice. *PLoS One* 7: e52411, 2012. doi:10.1371/journal.pone.0052411.
32. **Saraff K, Babamusta F, Cassis LA, Daugherty A.** Aortic dissection precedes formation of aneurysms and atherosclerosis in angiotensin II-infused, apolipoprotein E-deficient mice. *Arterioscler Thromb Vasc Biol* 23: 1621–1626, 2003. doi:10.1161/01.ATV.0000085631.76095.64.
33. **Schaffer SW, Azuma J, Mozaffari M.** Role of antioxidant activity of taurine in diabetes. *Can J Physiol Pharmacol* 87: 91–99, 2009. doi:10.1139/Y08-110.
34. **Shao A, Hathcock JN.** Risk assessment for the amino acids taurine, L-glutamine and L-arginine. *Regul Toxicol Pharmacol* 50: 376–399, 2008. doi:10.1016/j.yrtph.2008.01.004.
35. **Shimada K, Jong CJ, Takahashi K, Schaffer SW.** Role of ROS production and turnover in the antioxidant activity of taurine. *Adv Exp Med Biol* 803: 581–596, 2015. doi:10.1007/978-3-319-15126-7_47.
36. **Thomas M, Gavrila D, McCormick ML, Miller FJ, Jr, Daugherty A, Cassis LA, Dellsperger KC, Weintraub NL.** Deletion of p47^{phox} attenuates angiotensin II-induced abdominal aortic aneurysm formation in apolipoprotein E-deficient mice. *Circulation* 114: 404–413, 2006. doi:10.1161/CIRCULATIONAHA.105.607168.
37. **Thompson RW.** Detection and management of small aortic aneurysms. *N Engl J Med* 346: 1484–1486, 2002. doi:10.1056/NEJM200205093461910.
38. **Tiyerili V, Camara B, Becher MU, Schrickel JW, Lütjohann D, Mollenhauer M, Baldus S, Nickenig G, Andrié RP.** Neutrophil-derived myeloperoxidase promotes atherogenesis and neointima formation in mice. *Int J Cardiol* 204: 29–36, 2016. doi:10.1016/j.ijcard.2015.11.128.
39. **Vita JA, Brennan ML, Gokce N, Mann SA, Goormastic M, Shishehbor MH, Penn MS, Keaney JF, Jr, Hazen SL.** Serum myeloperoxidase levels independently predict endothelial dysfunction in humans. *Circulation* 110: 1134–1139, 2004. doi:10.1161/01.CIR.0000140262.20831.8F.
40. **Wang S, Zhang C, Zhang M, Liang B, Zhu H, Lee J, Viollet B, Xia L, Zhang Y, Zou MH.** Activation of AMP-activated protein kinase α_2 by nicotine instigates formation of abdominal aortic aneurysms in mice in vivo. *Nat Med* 18: 902–910, 2012. doi:10.1038/nm.2711.
41. **Wang Y, Rosen H, Madtes DK, Shao B, Martin TR, Heinecke JW, Fu X.** Myeloperoxidase inactivates TIMP-1 by oxidizing its N-terminal cysteine residue: an oxidative mechanism for regulating proteolysis during inflammation. *J Biol Chem* 282: 31826–31834, 2007. doi:10.1074/jbc.M704894200.
42. **Webb NR, De Beer MC, Wroblewski JM, Ji A, Bailey W, Shridas P, Charnigo RJ, Noffsinger VP, Witta J, Howatt DA, Balakrishnan A, Rateri DL, Daugherty A, De Beer FC.** Deficiency of endogenous acute-phase serum amyloid A protects apoE$^{-/-}$ mice from angiotensin II-induced abdominal aortic aneurysm formation. *Arterioscler Thromb Vasc Biol* 35: 1156–1165, 2015. doi:10.1161/ATVBAHA.114.304776.
43. **Xia Y, Zweier JL.** Measurement of myeloperoxidase in leukocyte-containing tissues. *Anal Biochem* 245: 93–96, 1997. doi:10.1006/abio.1996.9940.
44. **Xiao C, Giacca A, Lewis GF.** Oral taurine but not *N*-acetylcysteine ameliorates NEFA-induced impairment in insulin sensitivity and beta cell function in obese and overweight, non-diabetic men. *Diabetologia* 51: 139–146, 2008. doi:10.1007/s00125-007-0859-x.
45. **Zhang M, Bi LF, Fang JH, Su XL, Da GL, Kuwamori T, Kagamimori S.** Beneficial effects of taurine on serum lipids in overweight or obese non-diabetic subjects. *Amino Acids* 26: 267–271, 2004. doi:10.1007/s00726-003-0059-z.
46. **Zhang R, Brennan ML, Fu X, Aviles RJ, Pearce GL, Penn MS, Topol EJ, Sprecher DL, Hazen SL.** Association between myeloperoxidase levels and risk of coronary artery disease. *JAMA* 286: 2136–2142, 2001. doi:10.1001/jama.286.17.2136.
47. **Zheng L, Nukuna B, Brennan ML, Sun M, Goormastic M, Settle M, Schmitt D, Fu X, Thomson L, Fox PL, Ischiropoulos H, Smith JD, Kinter M, Hazen SL.** Apolipoprotein A-I is a selective target for myeloperoxidase-catalyzed oxidation and functional impairment in subjects with cardiovascular disease. *J Clin Invest* 114: 529–541, 2004. doi:10.1172/JCI200421109.

Hindawi Publishing Corporation
BioMed Research International
Volume 2017, Article ID 7268521, 12 pages
https://doi.org/10.1155/2017/7268521

Review Article

Genetic and Epigenetic Regulation of Aortic Aneurysms

Ha Won Kim[1] and Brian K. Stansfield[1,2]

[1]*Vascular Biology Center, Augusta University, Augusta, GA, USA*
[2]*Department of Pediatrics, Medical College of Georgia, Augusta University, Augusta, GA, USA*

Correspondence should be addressed to Brian K. Stansfield; bstansfield@augusta.edu

Received 1 November 2016; Accepted 15 December 2016; Published 2 January 2017

Academic Editor: Xuwei Hou

Aneurysms are characterized by structural deterioration of the vascular wall leading to progressive dilatation and, potentially, rupture of the aorta. While aortic aneurysms often remain clinically silent, the morbidity and mortality associated with aneurysm expansion and rupture are considerable. Over 13,000 deaths annually in the United States are attributable to aortic aneurysm rupture with less than 1 in 3 persons with aortic aneurysm rupture surviving to surgical intervention. Environmental and epidemiologic risk factors including smoking, male gender, hypertension, older age, dyslipidemia, atherosclerosis, and family history are highly associated with abdominal aortic aneurysms, while heritable genetic mutations are commonly associated with aneurysms of the thoracic aorta. Similar to other forms of cardiovascular disease, family history, genetic variation, and heritable mutations modify the risk of aortic aneurysm formation and provide mechanistic insight into the pathogenesis of human aortic aneurysms. This review will examine the relationship between heritable genetic and epigenetic influences on thoracic and abdominal aortic aneurysm formation and rupture.

1. Introduction

Aortic aneurysm formation is the result of a thinning medial layer and deterioration of the elastic lamina resulting in weakening of the tensile strength of the arterial wall. Aortic aneurysms are commonly identified in the thoracic and infrarenal aorta, with the latter referred to as abdominal aortic aneurysms (AAA). AAA represent the majority of aortic aneurysms and are classically associated with dyslipidemia, male sex, older age, smoking, and hypertension [1, 2]. The expansion of AAA is not a passive process but more closely mimics chronic inflammatory diseases characterized by hematopoietic cell infiltration and degradation of the extracellular matrix and vascular structures. Close association of inflammatory cells with breaks in the elastic lamina and the presence of reactive oxygen species suggests that AAA is an indolent process that eventually reaches a stress point resulting in aneurysm rupture [1, 3].

Thoracic aneurysms, on the other hand, are relatively rare and exhibit a strong heritable pattern. Approximately 20 percent of persons with thoracic aneurysms have a family history of aortic aneurysms. The relationship between thoracic aortic aneurysms and family history is strongest in first-degree relatives with 10-fold increased risk [4]. Syndromes associated with thoracic aortic aneurysms include Marfan syndrome (MFS), Loeys-Dietz syndrome (LDS), Ehlers-Danlos syndrome (EDS), familial thoracic aortic aneurysms and dissections (TAAD), autosomal dominant polycystic kidney disease (ADPKD), bicuspid aortic valve (BAV), and neurofibromatosis type 1 (NF1). Of these, MFS is the most common familial connective tissue disorder associated with thoracic aortic aneurysm, but each of these heritable syndromes shed light on the pathogenesis of aortic aneurysm formation [5]. A comprehensive understanding of heritable gene mutations and epigenetic modifications associated with aortic aneurysms will allow scientists and clinicians to design effective therapies and identify disease-specific biomarkers for tracking progression and risk for aneurysm rupture.

2. Syndromes Associated with Aortic Aneurysms

Marfan syndrome is the result of mutations in the *FBN1* gene on chromosome 15, which encodes fibrillin-1, an extracellular

Table 1: Summary of genetic and epigenetic relationships with TAAD and AAA.

Mutation	Syndrome	TAAD	AAA
FBN1 [5–8]	Marfan	+	
TGFBR1 [9], TGFBR2 [9, 10]	Loeys-Dietz	+	
COL3A1 [11–14]	Ehlers-Danlos	+	+/−
TGFBR2, MYH11 [15, 16], ACTA2 [17, 18] LOX [19], MAT2A [20], SMAD3 [21, 22]	Familial TAAD	+	
PKD1 [23, 24], PKD2 [24]	ADPKD	+	+/−
NF1 [25–27]	NF1	+	+/−
FBLN5 [28–30]		+	
ELN [14]	Williams		+
MMP2 [31], MMP9 [32], MMP12 [33]			+/−
MMP3 [34, 35]			+
TIMP1 [14]			+
LDLR1 [36, 37]			+
APOE E3/E3 [38]			+
PTPN11 [39–41]	Noonan	+	
MTHFR C677T [42–44]			+
ALOX15 [45, 46]			+
CNN2 [47]			+
SERPINB9 [47]			+
ADCY10P1 [47]			+
miR-21 [48], miR-146a [48]			+
miR-29b [49, 50]		+	+

matrix (ECM) protein that forms microfibrils and controls vessel elasticity. Fibrillin-1 plays a vital role in maintaining the vascular architecture via transforming growth factor- (TGF-) β signaling, a cytokine that controls cell proliferation and differentiation [51, 52]. The importance of TGF-β signaling in maintaining vascular integrity was confirmed by the identification of mutations in the TGF-β receptor genes 1 and 2 *(TGFBR1* and *TGFBR2)*, which cause Loeys-Dietz syndrome [53]. Similar to Marfan syndrome, mutations in both *TGFBR1* and *TGFBR2* result in disruption of collagen and elastin fiber biology in the vessel wall and aortic aneurysm formation [9]. Mutations in *TGFBR2* have also been linked to familial thoracic aortic aneurysms and dissections (TAAD), a syndrome associated with aneurysms of the ascending aorta and aortic dissections at relatively early stages of dilatation [54, 55]. TAAD represents a heterogeneous population of inherited disorders with mutations in myosin heavy chain-11 *(MYH11)* and α-smooth muscle actin-2 *(ACTA2)* among several, which are also linked to TAAD [15, 17, 19–21, 56–61].

Autosomal dominant polycystic kidney disease is commonly associated with intracerebral aneurysms but has been linked to thoracic aortic aneurysms and dissection as well [62, 63]. The etiology of this risk increase is thought to be multifactorial, as persons with ADPKD have increased prevalence of hypertension, a risk factor for thoracic aneurysms and AAA, and mutations in the *PKD1* and *PKD2* genes increase vascular smooth muscle cell (VSMC) apoptosis and induce dissecting aneurysms in mice [23, 63, 64]. While reports suggest that persons with APDPKD have an increased risk of AAA, a large cohort study failed to demonstrate an increased AAA prevalence in ADPKD [24]. Likewise, cardiovascular manifestations of neurofibromatosis type 1 occur in up to 10% of patients and tend to occur in adolescents and young adults [25]. Mutations in the *NF1* tumor suppressor gene increase VSMC proliferation and apoptosis, while mice with inactivating mutations in *Nf1* develop more frequent and severe aortic aneurysms than mice without the *Nf1* mutation [26, 27].

3. Candidate Genes Contributing to Aortic Aneurysm

The emergence of gene sequencing technology has greatly enabled the systematic search for candidate mutations and single nucleotide polymorphisms (SNPs) associated with aortic aneurysm formation. Much of this focus has been on identifying genes associated with AAA as the heritability of thoracic aneurysms is more commonly recognized [65], although mutational analysis of nonsyndromic thoracic aneurysms has gained interest. Recently, genome-wide association studies (GWAS) have identified several candidate SNPs related to nonsyndromic thoracic aneurysms and AAA [10, 66–68]. Table 1 summarizes genomic and epigenomic relationships with thoracic and abdominal aortic aneurysms. Many of these candidate genes require additional verification and must demonstrate functional plausibility in the pathogenesis of aortic aneurysms.

3.1. Extracellular Matrix Proteins. Fibrillin-1, coded by the *FBN1* gene, is an extracellular matrix glycoprotein that helps maintain the structural integrity of elastic fibers and other

connective tissues. Mutations in the *FBN1* gene have been identified in 70–93% of persons who meet the diagnostic criteria for Marfan syndrome with more than 1,000 unique *FBN1* mutations observed in this population [6–8, 69]. GWAS studies of patients with sporadic thoracic aneurysms identified five independent SNPs in the *FBN1* coding region on chromosome 15, which may have predictive and diagnostic ability in nonsyndromic thoracic aortic aneurysms [7].

Fibulins (FBLN) are elastin-binding proteins that associate with fibronectin-containing fibers and lamina within the aorta and other large arteries [28]. FBLN5 functions as a bridging peptide to promote the adhesion of vascular endothelial cells. Mutations in the *FBLN5* gene result in cutis laxa and are potentially linked to age-related macular degeneration, a disease characterized by degradation of the elastin support structures [70]. Further, *Fbln5* knockout mice exhibit fragmentation of the elastic lamina and downregulation of FBLN5 is associated with aortic dilation in humans, which supports a role for FBLN5 in the pathogenesis of AAA [29, 71]. However, Badger et al. examined peripheral blood samples from 230 persons with AAA and 278 controls for three common SNPs in the *FBLN5* gene locus [30]. The frequency of each SNP was similar between cases and controls.

Degradation of collagen, a major component of the extracellular matrix (ECM), contributes to aneurysm formation and rupture due to a loss of tensile strength within the aorta. The *COL3A1* gene encodes a type III collagen found in the vascular wall that provides extensibility to the aorta. Mutations in the *COL3A1* gene cause Ehlers-Danlos Syndrome type IV [8] and hemizygous deletions have been linked to familial aortic aneurysm rupture [11]. Similar results were identified in *COL3A1* haploinsufficient mice [12, 13]. However, SNP analysis of AAA and control patients for the T581C variant of *COL3A1* failed to demonstrate a difference in the allele frequency between study populations [14].

Mutations in the *ELN* gene, encoding elastin (ELN), result in Williams Syndrome, a syndrome characterized by supravalvar aortic stenosis, cutis laxa, and other disorders of connective tissue [72]. Elastin is a highly elastic protein found in the lamina of muscular arteries and accommodates arterial dilation and facilitates recoil. *ELN* knockout mice develop severe hypertension and die shortly after birth, while *ELN* heterozygous mice develop muscularized arteries and moderate hypertension [73]. Additionally, decreased elastin expression potentiates VSMC proliferation and increases arterial fragility. Thus, elastin appears to play an important role in maintaining vascular wall integrity under stress. However, a propensity for aortic aneurysm formation has not been demonstrated in *ELN* mutant mice. SNPs in the *ELN* gene have been identified in patients with a strong family history of AAA, but cohort studies of nonrelated AAA and control patients have failed to show a difference in SNP frequency [14].

Matrix metalloproteinases (MMP) are zinc-containing peptidases that are biologically active molecules involved in the degradation of ECM proteins and play an important role in cell proliferation, migration, and apoptosis. Matrix metalloproteinase-2 (MMP2) is highly expressed in VSMC and AAA in both mice and humans, but mutational analysis of AAA and control patients has failed to reveal a predictive SNP in the *MMP2* gene [31, 74–79]. Similarly, MMP9 and MMP12 appear to participate in the pathogenesis of AAA in mouse models, but no association between *MMP9* or *MMP12* gene variants and AAA has been identified [32, 33, 77, 80]. MMP3, on the other hand, is highly expressed in human AAA and a common SNP in the promoter region of the *MMP3* gene was found to correlate positively with AAA formation and coronary aneurysms in humans [34, 35]. Tissue inhibitor of metalloproteinases (TIMPs) inhibits MMP activation and plays a pivotal role in determining the influence of the ECM and cell adhesion molecules on VSMC function within the vascular wall. SNP analysis of the *TIMP1* gene has yielded conflicting data with one study showing an association with AAA patients without a family history of AAA and a larger meta-analysis failing to show an association between *TIMP1* polymorphisms and AAA [14, 81]. No association between AAA and *TIMP2* or *TIMP3* has been identified [14].

3.2. TGF-β Pathway. Transforming growth factor-β (TGF-β) is a cytokine that regulates a variety of cellular functions, including differentiation, transformation, and proliferation. Dysregulated TGF-β signaling has been implicated in the pathogenesis of both thoracic aneurysms and AAA. The TGF-β superfamily members can bind to fibrillin; therefore, fibrillin-1 deficiency impairs matrix sequestration of latent TGF-β, leading to uncontrolled secretion of TGF-β and upregulated TGF-β signaling [82, 83]. More recently, noncanonical TGF-β signaling through SMAD proteins has been shown to induce thoracic aortic aneurysm formation via the mitogen-activated protein kinase (MAPK) pathway [84–86]. These later observations are particularly interesting as SMAD mediated MAPK activation overlaps with other syndromes with a predisposition for thoracic aneurysm formation.

Likewise, TGF-β signaling has been implicated in the inflammatory AAA animal models and human AAA. However, TGF-β appears to play a protective role in AAA. TGF-β and TGFBR2 are poorly expressed in human AAA tissue samples compared to controls and disruption of TGF-β signaling prevents AAA formation in the elastase and angiotensin (AngII) animal models of AAA [87–90]. Interestingly, AngII increases the expression and activation of all TGF-β isoforms and TGFBR1 and TGFBR2 within both the thoracic and abdominal murine aorta [91–93]. Analysis of the *TGFB1* and *TGFBR1* genes failed to reveal an association with human AAA [14, 81], but two SNPs in *TGFBR2* (rs1036095 and rs4522809) were associated with AAA [10]. Additionally, mutations in the *SMAD3* gene have been linked with aneurysm-osteoarthritis syndrome, which further demonstrates the critical role of noncanonical TGF-β in aortic aneurysm formation [22].

3.3. Smooth Muscle-Related Proteins. Smooth muscle cells, along with the elastic lamina and ECM, provide the structural integrity of the vascular wall. Thus, mutations affecting VSMC function and/or their ability to maintain the ECM could render the aorta vulnerable to dilation and/or rupture. Mutations in smooth muscle myosin *(MYH11)*, coding for

smooth muscle myosin heavy chain, have been linked to isolated familial thoracic aortic aneurysm [16]. Ascending aortic aneurysms in patients with *MYH11* mutations are accompanied by a high rate of patent ductus arteriosus (PDA), but disruption of this locus is responsible for only a small fraction of sporadic PDA [16, 94]. Similarly, mutations in α-smooth muscle actin *(ACTA2)* are associated with several manifestations of cardiovascular disease including thoracic and cerebral aneurysms, myocardial infarction, and neurovascular malformations [18]. Given that ACTA2 is a component of smooth muscle cells and also a transcriptional target of TGF-β signaling, mutations in this gene likely affect VSMC functions and impair vascular contraction.

3.4. Lipid Metabolism. Apolipoprotein E (APOE) binds to the low-density lipoprotein receptor (LDLR) to clear lipoprotein particles from the blood and is critical for lipid and lipoprotein metabolism. Mutations in the *LDLR* gene are linked to familial hypercholesterolemia and type III hyperlipidemia, which significantly increase the susceptibility to premature and severe atherosclerosis [95]. GWAS have identified mutations in the *LDLR*, located on chromosome 19p13.2, and the low-density lipoprotein receptor-related protein 1 (LRP1), located on chromosome 12q13.3, which are associated with genetic susceptibility to AAA [36, 37, 96]. Additionally, several *APOE* polymorphisms modify the risk for atherosclerosis and AAA. Multiple studies have examined APOE$*$2, -$*$3, and $*$4 alleles in patients with AAAs, and individuals with the E3/E4 genotype showed a markedly lower AAA expansion rate than those with the E3/E3 genotype [38]. Interestingly the E4 genotype is associated with shorter lifespan in several cross-sectional epidemiologic studies [97–99].

3.5. RAS-Related Pathway. Neurofibromin is encoded by the *NF1* tumor suppressor gene and functions as a negative regulator of $p21^{Ras}$ (Ras) activity in circulating hematopoietic and vascular wall cells [26, 100–103]. Mutations in the *NF1* gene are associated with neurofibromatosis type I and Watson syndrome, a variant of NF1 [104]. The incidence of cardiovascular disease and aneurysm formation in persons with NF1 approaches 10% [105–109]. Most aortic aneurysms in NF1 are located in the thoracic descending aorta, but animal models of *Nf1* mutant animals demonstrate a strong predisposition for infra-renal AAA as well [27]. Broader epidemiologic studies of NF1 patients and aneurysm risk have yet to be performed.

PTPN11 (SH2 domain-containing protein tyrosine phosphatase-2) is encoded by the *PTPN11* gene and regulates a variety of cell functions, including mitogenic activation and gene transcription. Mutations in the *PTPN11* gene cause Noonan syndrome, a relatively rare inherited disorder characterized by accelerated Ras-MAPK signaling transduction. Persons with Noonan syndrome are at increased risk for dilation of the aortic root and aneurysm formation in the ascending aorta [39–41]. It is mechanistically plausible that other inherited mutations in the Ras pathway may modify the risk of thoracic aneurysm formation, but animal studies and/or human data supporting this hypothesis are limited.

4. Epigenetic Risk Factors

Epigenetics refers to heritable and acquired modifications to the genome that alter gene expression without changing the DNA sequence. In some instances, epigenetic modifications are stable and passed on to future generations, but many modifications are relatively dynamic and responsive to environmental cues. Epigenetic modifications include DNA methylation, histone modifications, and noncoding RNA, which can directly interact with the primary nucleotide sequence and regulate gene expression. Methyltransferases are enzymes that methylate DNA and the supporting elements including histones to alter gene activity and chromatin structure. DNA methylation occurs naturally as a result of aging and cell differentiation but is also recognized as an important modifier of disease risk.

Similarly, posttranslational histone modification by the addition or removal of methyl or acetyl groups, phosphorylation, ubiquitylation, and sumoylation results in suppression or activation of gene transcription by altering the chromatin structure or recruiting additional histone modifiers. Modifications that increase chromatin condensation restrict access of transcription factors to the gene target, while modifications that decrease chromatin condensation lead to a more open chromatin structure and increase gene expression. Histone modifying enzymes, such as histone deacetylases (HDACs), histone methyltransferases (HMT), and histone acetyltransferases (HAT), have been implicated in cardiovascular disease, cancer initiation and propagation, and Alzheimer's disease. Presently, epigenetic effects on the frequency, severity, and progression of thoracic aneurysms and AAA are limited with most of the data on AAA being inferred from studies of atherosclerosis and other inflammatory conditions. However, atherosclerosis and AAA are distinct clinical entities with overlapping risk factors and disease mechanisms. Thus, interpretation of study results from related cardiovascular diseases must be viewed with some caution.

4.1. Epigenetic Modification in Matrix Degradation. MMP expression and activation are a hallmark feature of AAA. In particular, MMP-2 and MMP-9 are highly expressed in human and murine AAA and likely have some role in thoracic aortic aneurysms [75, 77, 110–112]. Increased expression of active MMPs predicts severity of other chronic inflammatory diseases such as rheumatoid arthritis, chronic kidney disease, and degenerative inflammatory disorder [113–115]. Demethylation of the *MMP2* gene promoter increases MMP-2 expression in noninvasive breast cancer cell lines and cells treated with trichostatin A, an HDAC inhibitor, demonstrated increased histone acetylation and reduced *MMP2* mRNA expression [116, 117]. Likewise, methylation and acetylation of *MMP9* result in downregulation of MMP-9 expression and inhibit MMP-9 binding to the CREB transcription factor via Class II major histocompatibility complex transactivator, respectively [118, 119]. Interestingly, HDAC2 binding to the *MMP9* promoter region suppresses MMP-9 expression and suggests that epigenetic modification of MMPs is tightly regulated [120]. While MMP expression is highly associated with human and murine aortic aneurysms,

the regulation of MMP expression in cardiovascular tissues or primary cells remains poorly understood.

Classes I and II HDACs contain a conserved HDAC domain but differ in their expression patterns with broad expression of Class I HDACs and more limited expression of Class II HDACs. In human AAA, Galán et al. recently reported increased expression of HDACs 1, 2 (Class I), 4, and 7 (Class II) in human AAA compared to aortic tissue samples from healthy organ donors [121]. Further, the use of HDAC inhibitors significantly reduced AngII-induced AAA in *APOE* knockout mice via downregulation of MMP-2 and MMP-9 in the vascular wall [122]. Administration of Class I or Class II HDAC inhibitors were efficacious in reducing the frequency and severity of AAA in mice, which further supports the hypothesis that epigenetic modifications are critical to the pathogenesis of aortic aneurysms and HDAC inhibitors represent a promising therapeutic strategy [121].

Epidemiologic data suggests that carriers of the *MTHFR* C677T allele are at increased risk for AAA [42–44]. Persons with this polymorphism express a heat-labile MTHFR enzyme with reduced activity and increased plasma homocysteine levels, which is a known risk factor for AAA and growth rate [123–125]. Homocysteine is considered a potent inhibitor of methyltransferases by increasing the intracellular accumulation of s-adenosyl homocysteine and sequestering methyl donor groups [126, 127]. In support of this hypothesis, *MTHFR* knockout mice exhibit global DNA hypomethylation and enhanced atherosclerosis, although an increased susceptibility to AAA in animal models has not been demonstrated [128]. The role of methyltransferases in AAA is an emerging area of interest.

4.2. Epigenetic Modification in Smoking. Smoking is a strong risk factor for AAA; however, the underlying mechanisms for this risk association are poorly understood. Exposure to prolonged smoking alters the epigenome, particularly in high-turnover cell lines such as bone marrow-derived leukocytes. Current smoking status and prenatal exposure to cigarette smoke strongly influence the methylation signature of DNA [129–132]. In one of the most insightful studies of cigarette exposure and the epigenome, Stephanie London and colleagues conducted a meta-analysis of 15,907 individuals to identify the methylation footprint of smokers and nonsmokers across the epigenome [133]. They showed that 1/3 (>7,000) of currently recognized human genes have smoking-associated methylation patterns. Interestingly, CpGs (cytosine-rich methylation sites) that are causally related to cardiovascular diseases showed the strongest correlations for both current and former smokers as compared to persons who have never smoked [133]. Former smokers appear to have a methylation signature that more closely mimics nonsmokers; however, smoking cessation does not appear to fully reverse these changes [133–135].

Examination of specific gene promoters has identified similar changes in DNA methylation for candidate genes associated with AAA formation including protease-activated receptor-4 (PAR4 or F2RL3) and 15-lipoxygenase (ALOX15). Breitling et al. examined the methylation status of 27,000 CpGs to show that methylation of the *F2RL3* gene was reduced by 12% in smokers when compared with nonsmokers [130]. Further, CpG methylation correlated negatively with the quantity of cigarettes smoked and positively with duration of smoking abstinence. Broader examination of intergenic CpG methylation has identified similar relationships between smoking and altered DNA methylation [136, 137]. Methylation status of the *Alox15* promoter directly affects gene expression with heavy smokers showing a substantial increase in 15-lipoxygenase levels compared to nonsmokers [138, 139]. 15-Lipoxygenase has been implicated in the pathogenesis of AAA and pharmacologic or genetic inhibition of 5-lipoxygenase signaling has demonstrated efficacy in preventing AAA in animal models [45, 46]. However, further epigenomic studies of human AAA are needed to demonstrate the precise mechanisms relating smoking to AAA formation.

4.3. Epigenetic Modification in Aging. Older age is associated with higher risk for AAA and aging-related epigenetic changes have been proposed as a potential mechanism for this increased risk. After methylation patterns have been established during human development, progressive, time-dependent, global hypomethylation occurs [140–142]. Most of these observations have been made in primary cell lines or animal models of cancer and other age-related diseases with few observations in older adults with AAA. Studies of atheroma in humans and atherogenic mice exhibit a global loss of genomic 5-methyl-Cytosine content, a common occurrence in neoplastic cells [143–145]. 5-Methyl-C is produced by transfer of a methyl group from S-adenosylmethionine, a process that is inhibited by decreased MTHFR activity and elevated homocysteine levels associated with aging [146–148]. One investigator proposes that DNA methylation measures the cumulative effect of the epigenetic maintenance system and may predict many age-related diseases [149]. These observations are likely relevant to aging and increased risk for AA formation.

4.4. Epigenetic Modification in Inflammatory Responses. Chronic inflammation characterizes AAA, wherein inflammatory leukocytes and cytokines as well as reactive oxygen species are found within the vascular wall in human AAA and animal models of AAA. Inflammation also influences the epigenome of circulating leukocytes and vascular wall cells. Ryer et al. examined the genome-wide DNA methylation profiles of mononuclear cells isolated from 20 humans with AAA and 21 controls. Four genes with differential CpG methylation were identified: kelch-like family member 35 (*KLHL35*), calponin 2 (*CNN2*), serpin peptidase inhibitor clade B (ovalbumin) member 9 (*SERPINB9*), and adenylate cyclase 10 pseudogene 1 *(ADCY10P1)* [47]. For three of these genes (*CNN2*, *SERPINB9*, and *ADCY10P1*), methylation more closely correlated with the presence of AAA than with either age or smoking status and suggests that the methylation status of these genes may represent an independent and additive risk factor for AAA.

Changes in DNA methylation within the promoter region of immunomodulatory cytokines may also affect risk for AAA. Treatment of cultured human lymphocytes with interleukin-6 increases global methylation in these cells [114].

Promoter methylation regulates the expression and activity of other inflammatory cytokines implicated in AAA formation including TNF-α, IL-1β, and monocyte chemotactic protein-1 (MCP-1 or CCL2) [150–154]. Likewise, reactive oxygen species (ROS) can increase histone acetylation via modulation of HAT activity to promote inflammation in several cell lines [155–157]. Hydrogen peroxide induces gene acetylation by increasing HAT activity and suppressing HDAC activity [158]. Thus, blunting oxidative stress may be a promising strategy to suppress inflammatory conditions such as AAA.

4.5. Noncoding RNAs in AAA. Noncoding RNAs (ncRNA) are functional RNA transcribed from DNA but fail to be translated into proteins. ncRNA, including transfer RNA (tRNA), ribosomal RNA (rRNA), microRNA (miRNA), and long noncoding RNA (lncRNA), are abundant, biologically active molecules that modify gene expression. MicroRNA are short (21–25 nucleotides), single-stranded RNA molecules that mimic small interfering RNA and function in RNA silencing and posttranscriptional regulation of gene expression.

A significant number of miRNAs are differentially expressed in AAA and normal aortic tissue samples; however, most studies fail to identify similar miRNA trends, which is likely due to the heterogeneity of AAA tissue [159]. Pahl et al. showed that AAA have increased expression of miR-181a, -146a, and -21 and lower expression of miR-133b, -331-3p, -133a, -30c, and -204 when compared with control biopsies [160]. Other miRNA with differential expression in AAA and control tissue include miR-126, -20a, -27a, -155 -221, -222, -223, -124a, -29b, and let-7 [161]. Of these, miR-21 and -146a expressions are consistently elevated in AAA compared to healthy aorta, and miR-21 has been shown to inhibit VSMC apoptosis and protect against AAA formation in *APOE* knockout mice [48]. Several other miRNA, including miR-146a, promote VSMC survival and participate in the pathogenesis of AAA [49, 162, 163]. Interestingly, miR-29b has been implicated in both AAA and thoracic aneurysms associated with Marfan syndrome [49, 50].

Analysis of circulating miRNAs in peripheral blood has also yielded useful insight into AAA. Zhang et al. identified increased expression of miR-191-3p, -455-3p, and -1281 in the whole blood of AAA patients compared to controls, while a separate study showed decreased expression of miR-126, -124a, -146a, -155, -223, -29b, -15a, and -15b in AAA [164, 165]. Stather et al. reported reduced expression of let-7e, miR-15a, and -196b in the peripheral blood of AAA patients and increased expression of miR-411 as compared to controls [165]. The increased expression of some miRNA in AAA tissue and decreased expression in peripheral blood (i.e., miR-146a and miR-29b) demonstrate the complex nature of using miRNA as biomarkers of disease progression. Larger studies comparing miRNA expression in peripheral blood and primary tissue would shed considerable light on the role of miRNA in AAA formation.

Recently, an intense interest in the role of noncoding RNAs has broadened our understanding of the influence of the epigenome on aortic aneurysm formation. After showing that miR-29b is significantly downregulated in two animal models of AAA, Maegdefessel et al. showed that administration of an anti-miR to further diminish miR-29b expression in the aortic wall reduced aorta dilation and AAA formation [49]. Conversely, administration of a pre-miR-29b to increase miR-29b expression within the aorta exacerbated AAA formation and aneurysm rupture (63% versus 33%). In both animal models and human AAA tissue samples, miR-29b appears to target genes that encode extracellular matrix proteins including Col1a1, Col3a1, Col5a1, and ELN as well as matrix metalloproteinases (i.e., MMP9). This same group identified a role for miR-29b in thoracic aortic aneurysms in a murine model of Marfan syndrome. Contrary to AAA, aortas from *Fbn1* mutant mice (Marfan) expressed higher quantities of miR-29b, which corresponded with enhanced apoptosis, increased MMP expression, and suppression of nuclear factor kappa-light-chain-enhancer of activated B cells (NF-κB) activity, a repressor of miR-29b [50]. Boon et al. examined the aortas of young and old mice as well as tissue samples of human thoracic aneurysms to identify patterns of microRNA expression. The miR-29 family was highly expressed in aortas from older mice and was associated with downregulation of ECM protein expression [166]. Similar to the mice, human tissue samples of thoracic aortic aneurysm expressed high levels of miR-29b when compared to human controls.

While the data for a pathological role for miR-29b in AAA is compelling, other miRNAs have been implicated in AAA as well. miR-21 controls VSMC proliferation and apoptosis during AAA formation and upregulation of miR-21 has been demonstrated in AAA biopsy samples [48]. Nicotine enhances both miR-21 expression and AAA size in mice and AAA biopsy samples isolated from frequent smokers showed a twofold increase in miR-21 expression when compared with AAA from nonsmokers [48]. In both mice and humans, the increase in miR-21 expression was associated with reduced expression of phosphatase and tensin homolog (PTEN) and increased activation of protein kinase B (Akt).

Murine AAA exhibited increased expression of miR-24 with genetic deletion of miR-24 further enhancing murine AAA size and severity [167]. Chitinase 3-like 1 gene (Chi3l1), which promotes cytokine synthesis in leukocytes and VSMC migration, appears to be a potential target of miR-24 [167]. Additionally, miR-712 and its human homolog miR-205 suppress metalloprotease inhibitor activity in response to AngII to stimulate MMP activity in aortic VSMC and facilitate AAA formation [168]. Although miRNA influence aortic aneurysm formation and severity, it remains to be seen if targeting specific miRNA is a viable therapeutic approach for the prevention or treatment of human aortic aneurysms.

5. Conclusions

In this review, we provide a comprehensive assessment of the genetic and epigenetic landscape of aortic aneurysms. We have long appreciated the influence of inherited syndromes on aortic aneurysm formation and aneurysm rupture and the multiple environmental and familial risk factors associated with AAA, but more and more, we are gaining insight into the complexities of gene regulation and protein function in the pathogenesis of aortic aneurysms. Of these recent advances,

miRNAs and epigenetic modifiers are particularly intriguing and may represent viable therapeutic targets for patients with aortic aneurysms as seen in other patient populations. Future work must include comparisons between findings in human tissue and animal models of aortic aneurysm to draw clinically relevant conclusions about the role of miRNAs or other epigenome modifiers in aortic aneurysm formation.

Competing Interests

The authors declare that no conflict of interests exists regarding the publication of this paper.

References

[1] N. L. Weintraub, "Understanding abdominal aortic aneurysm," *The New England Journal of Medicine*, vol. 361, no. 11, pp. 1114–1116, 2009.

[2] J. A. Cowan Jr., J. B. Dimick, P. K. Henke, J. Rectenwald, J. C. Stanley, and G. R. Upchurch Jr., "Epidemiology of aortic aneurysm repair in the United States from 1993 to 2003," *Annals of the New York Academy of Sciences*, vol. 1085, pp. 1–10, 2006.

[3] A. Wanhainen, K. Mani, and J. Golledge, "Surrogate markers of abdominal aortic aneurysm progression," *Arteriosclerosis, Thrombosis, and Vascular Biology*, vol. 36, no. 2, pp. 236–244, 2016.

[4] G. Albornoz, M. A. Coady, M. Roberts et al., "Familial thoracic aortic aneurysms and dissections-incidence, modes of inheritance, and phenotypic patterns," *Annals of Thoracic Surgery*, vol. 82, no. 4, pp. 1400–1405, 2006.

[5] H. C. Dietz, C. R. Cutting, R. E. Pyeritz et al., "Marfan syndrome caused by a recurrent de novo missense mutation in the fibrillin gene," *Nature*, vol. 352, no. 6333, pp. 337–339, 1991.

[6] L. Faivre, A. Masurel-Paulet, G. Collod-Beroud et al., "Clinical and molecular study of 320 children with marfan syndrome and related type I fibrillinopathies in a series of 1009 probands with pathogenic FBN1 mutations," *Pediatrics*, vol. 123, no. 1, pp. 391–398, 2009.

[7] S. A. LeMaire, M.-L. N. McDonald, D.-C. Guo et al., "Genome-wide association study identifies a susceptibility locus for thoracic aortic aneurysms and aortic dissections spanning FBN1 at 15q21.1," *Nature Genetics*, vol. 43, no. 10, pp. 996–1000, 2011.

[8] G. Collod-Béroud, S. Le Bourdelles, L. Ades et al., "Update of the UMD-FBN1 mutation database and creation of an FBN1 polymorphism database," *Human Mutation*, vol. 22, no. 3, pp. 199–208, 2003.

[9] B. L. Loeys, J. Chen, E. R. Neptune et al., "A syndrome of altered cardiovascular, craniofacial, neurocognitive and skeletal development caused by mutations in TGFBR1 or TGFBR2," *Nature Genetics*, vol. 37, no. 3, pp. 275–281, 2005.

[10] A. F. Baas, J. Medic, R. van 't Slot et al., "Association of the TGF-β receptor genes with abdominal aortic aneurysm," *European Journal of Human Genetics*, vol. 18, no. 2, pp. 240–244, 2010.

[11] S. Kontusaari, G. Tromp, H. Kuivaniemi, R. L. Ladda, and D. J. Prockop, "Inheritance of an RNA splicing mutation (G+ 1 IVS20) in the type III procollagen gene (COL3A1) in a family having aortic aneurysms and easy bruisability: phenotypic overlap between familial arterial aneurysms and Ehlers-Danlos syndrome type IV," *American Journal of Human Genetics*, vol. 47, no. 1, pp. 112–120, 1990.

[12] L. B. Smith, P. W. F. Hadoke, E. Dyer et al., "Haploinsufficiency of the murine Col3a1 locus causes aortic dissection: a novel model of the vascular type of EhlersDanlos syndrome," *Cardiovascular Research*, vol. 90, no. 1, pp. 182–190, 2011.

[13] J. Faugeroux, H. Nematalla, W. Li et al., "Angiotensin II promotes thoracic aortic dissections and ruptures in Col3a1 haploinsufficient mice," *Hypertension*, vol. 62, no. 1, pp. 203–208, 2013.

[14] T. Ogata, H. Shibamura, G. Tromp et al., "Genetic analysis of polymorphisms in biologically relevant candidate genes in patients with abdominal aortic aneurysms," *Journal of Vascular Surgery*, vol. 41, no. 6, pp. 1036–1042, 2005.

[15] H. Pannu, V. Tran-Fadulu, C. L. Papke et al., "MYH11 mutations result in a distinct vascular pathology driven by insulin-like growth factor 1 and angiotensin II," *Human Molecular Genetics*, vol. 16, no. 20, pp. 2453–2462, 2007.

[16] L. Zhu, R. Vranckx, P. K. Van Kien et al., "Mutations in myosin heavy chain 11 cause a syndrome associating thoracic aortic aneurysm/aortic dissection and patent ductus arteriosus," *Nature Genetics*, vol. 38, no. 3, pp. 343–349, 2006.

[17] D.-C. Guo, H. Pannu, V. Tran-Fadulu et al., "Mutations in smooth muscle α-actin (ACTA2) lead to thoracic aortic aneurysms and dissections," *Nature Genetics*, vol. 39, no. 12, pp. 1488–1493, 2007.

[18] D.-C. Guo, C. L. Papke, V. Tran-Fadulu et al., "Mutations in smooth muscle alpha-actin (ACTA2) cause coronary artery disease, stroke, and Moyamoya disease, along with thoracic aortic disease," *The American Journal of Human Genetics*, vol. 84, no. 5, pp. 617–627, 2009.

[19] D.-C. Guo, E. S. Regalado, L. Gong et al., "LOX mutations predispose to thoracic aortic aneurysms and dissections," *Circulation Research*, vol. 118, no. 6, pp. 928–934, 2016.

[20] D.-C. Guo, L. Gong, E. S. Regalado et al., "MAT2A mutations predispose individuals to thoracic aortic aneurysms," *American Journal of Human Genetics*, vol. 96, no. 1, pp. 170–177, 2015.

[21] E. S. Regalado, D.-C. Guo, C. Villamizar et al., "Exome sequencing identifies SMAD3 mutations as a cause of familial thoracic aortic aneurysm and dissection with intracranial and other arterial aneurysms," *Circulation Research*, vol. 109, no. 6, pp. 680–686, 2011.

[22] I. M. B. H. Van De Laar, R. A. Oldenburg, G. Pals et al., "Mutations in SMAD3 cause a syndromic form of aortic aneurysms and dissections with early-onset osteoarthritis," *Nature Genetics*, vol. 43, no. 2, pp. 121–126, 2011.

[23] I. S. Lantinga-van Leeuwen, J. G. Dauwerse, H. J. Baelde et al., "Lowering of Pkd1 expression is sufficient to cause polycystic kidney disease," *Human Molecular Genetics*, vol. 13, no. 24, pp. 3069–3077, 2004.

[24] R. Torra, C. Nicolau, C. Badenas et al., "Abdominal aortic aneurysms and autosomal dominant polycystic kidney disease," *Journal of the American Society of Nephrology*, vol. 7, no. 11, pp. 2483–2486, 1996.

[25] J. M. Friedman, J. Arbiter, J. A. Epstein et al., "Cardiovascular disease in neurofibromatosis 1: report of the NF1 Cardiovascular Task Force," *Genetics in Medicine*, vol. 4, no. 3, pp. 105–111, 2002.

[26] B. K. Stansfield, W. K. Bessler, R. Mali et al., "Ras-mek-erk signaling regulates Nf1 heterozygous neointima formation," *American Journal of Pathology*, vol. 184, no. 1, pp. 79–85, 2014.

[27] F. Li, B. D. Downing, L. C. Smiley et al., "Neurofibromin-deficient myeloid cells are critical mediators of aneurysm formation in vivo," *Circulation*, vol. 129, no. 11, pp. 1213–1224, 2014.

[28] H. Yanagisawa, E. C. Davist, B. C. Starcher et al., "Fibulin-5 is an elastin-binding protein essential for elastic fibre development in vivo," *Nature*, vol. 415, no. 6868, pp. 168–171, 2002.

[29] M. Orriols, S. Varona, I. Martí-Pàmies et al., "Down-regulation of Fibulin-5 is associated with aortic dilation: role of inflammation and epigenetics," *Cardiovascular Research*, vol. 110, no. 3, pp. 431–442, 2016.

[30] S. A. Badger, C. V. Soong, M. E. O'Donnell, M. A. Sharif, R. R. Makar, and A. E. Hughes, "Common polymorphisms of Fibulin-5 and the risk of abdominal aortic aneurysm development," *Vascular Medicine*, vol. 15, no. 2, pp. 113–117, 2010.

[31] I. Hinterseher, H. Bergert, E. Kuhlisch et al., "Matrix metalloproteinase 2 polymorphisms in a caucasian population with abdominal aortic aneurysm," *Journal of Surgical Research*, vol. 133, no. 2, pp. 121–128, 2006.

[32] L. Smallwood, R. Allcock, F. Van Bockxmeer et al., "Polymorphisms of the matrix metalloproteinase 9 gene and abdominal aortic aneurysm," *British Journal of Surgery*, vol. 95, no. 10, pp. 1239–1244, 2008.

[33] G. M. Longo, S. J. Buda, N. Fiotta et al., "MMP-12 has a role in abdominal aortic aneurysms in mice," *Surgery*, vol. 137, no. 4, pp. 457–562, 2005.

[34] J. Deguara, K. G. Burnand, J. Berg et al., "An increased frequency of the 5A allele in the promoter region of the MMP3 gene is associated with abdominal aortic aneurysms," *Human Molecular Genetics*, vol. 16, no. 24, pp. 3002–3007, 2007.

[35] N. Lamblin, C. Bauters, X. Hermant, J.-M. Lablanche, N. Helbecque, and P. Amouyel, "Polymorphisms in the promoter regions of MMP-2, MMP-3, MMP-9 and MMP-12 genes as determinants of aneurysmal coronary artery disease," *Journal of the American College of Cardiology*, vol. 40, no. 1, pp. 43–48, 2002.

[36] M. J. Bown, G. T. Jones, S. C. Harrison et al., "Abdominal aortic aneurysm is associated with a variant in low-density lipoprotein receptor-related protein 1," *The American Journal of Human Genetics*, vol. 89, no. 5, pp. 619–627, 2011.

[37] D. T. Bradley, A. E. Hughes, S. A. Badger et al., "A variant in LDLR is associated with abdominal aortic aneurysm," *Circulation: Cardiovascular Genetics*, vol. 6, no. 5, pp. 498–504, 2013.

[38] L. U. Gerdes, J. S. Lindholt, S. Vammen, E. W. Henneberg, and H. Fasting, "Apolipoprotein E genotype is associated with differential expansion rates of small abdominal aortic aneurysms," *British Journal of Surgery*, vol. 87, no. 6, pp. 760–765, 2000.

[39] J. W. Cornwall, R. S. Green, J. C. Nielsen, and B. D. Gelb, "Frequency of aortic dilation in Noonan syndrome," *The American Journal of Cardiology*, vol. 113, no. 2, pp. 368–371, 2014.

[40] M. E. Lindsay and H. C. Dietz, "Lessons on the pathogenesis of aneurysm from heritable conditions," *Nature*, vol. 473, no. 7347, pp. 308–316, 2011.

[41] R. Purnell, I. Williams, U. Von Oppell, and A. Wood, "Giant aneurysms of the sinuses of Valsalva and aortic regurgitation in a patient with Noonan's syndrome," *European Journal of Cardio-Thoracic Surgery*, vol. 28, no. 2, pp. 346–348, 2005.

[42] H. Cao, X. Hu, Q. Zhang et al., "Hyperhomocysteinaemia, low folate concentrations and MTHFR C677T mutation in abdominal aortic aneurysm," *Vasa—European Journal of Vascular Medicine*, vol. 43, no. 3, pp. 181–188, 2014.

[43] J. Liu, X. Jia, H. Li et al., "Association between MTHFR C677T polymorphism and abdominal aortic aneurysm risk," *Medicine*, vol. 95, no. 36, Article ID e4793, 2016.

[44] F. Ferrara, S. Novo, S. Grimaudo et al., "Methylenetetrahydrofolate reductase mutation in subjects with abdominal aortic aneurysm subdivided for age," *Clinical Hemorheology and Microcirculation*, vol. 34, no. 3, pp. 421–426, 2006.

[45] C. M. Bhamidipati, C. A. Whatling, G. S. Mehta et al., "5-Lipoxygenase pathway in experimental abdominal aortic aneurysms," *Arteriosclerosis, Thrombosis, and Vascular Biology*, vol. 34, no. 12, pp. 2669–2678, 2014.

[46] L. Zhao, M. P. W. Moos, R. Gräbner et al., "The 5-lipoxygenase pathway promotes pathogenesis of hyperlipidemia-dependent aortic aneurysm," *Nature Medicine*, vol. 10, no. 9, pp. 966–973, 2004.

[47] E. J. Ryer, K. E. Ronning, R. Erdman et al., "The potential role of DNA methylation in abdominal aortic aneurysms," *International Journal of Molecular Sciences*, vol. 16, no. 5, pp. 11259–11275, 2015.

[48] L. Maegdefessel, J. Azuma, R. Toh et al., "MicroRNA-21 blocks abdominal aortic aneurysm development and nicotine-augmented expansion," *Science Translational Medicine*, vol. 4, no. 122, Article ID 122ra22, 2012.

[49] L. Maegdefessel, J. Azuma, R. Toh et al., "Inhibition of microRNA-29b reduces murine abdominal aortic aneurysm development," *The Journal of Clinical Investigation*, vol. 122, no. 2, pp. 497–506, 2012.

[50] D. R. Merk, J. T. Chin, B. A. Dake et al., "miR-29b participates in early aneurysm development in Marfan syndrome," *Circulation Research*, vol. 110, no. 2, pp. 312–324, 2012.

[51] S. S. Chaudhry, S. A. Cain, A. Morgan, S. L. Dallas, C. A. Shuttleworth, and C. M. Kielty, "Fibrillin-1 regulates the bioavailability of TGFβ1," *The Journal of Cell Biology*, vol. 176, no. 3, pp. 355–367, 2007.

[52] F. Ramirez, L. Y. Sakai, D. B. Rifkin, and H. C. Dietz, "Extracellular microfibrils in development and disease," *Cellular and Molecular Life Sciences*, vol. 64, no. 18, pp. 2437–2446, 2007.

[53] B. L. Loeys, U. Schwarze, T. Holm et al., "Aneurysm syndromes caused by mutations in the TGF-β receptor," *New England Journal of Medicine*, vol. 355, no. 8, pp. 788–798, 2006.

[54] H. Pannu, V. Tran-Fadulu, and D. M. Milewicz, "Genetic basis of thoracic aortic aneurysms and aortic dissections," *American Journal of Medical Genetics Part C: Seminars in Medical Genetics*, vol. 139, no. 1, pp. 10–16, 2005.

[55] H. Pannu, V. T. Fadulu, J. Chang et al., "Mutations in transforming growth factor-β receptor type II cause familial thoracic aortic aneurysms and dissections," *Circulation*, vol. 112, no. 4, pp. 513–520, 2005.

[56] D.-C. Guo, E. Regalado, D. E. Casteel et al., "Recurrent gain-of-function mutation in PRKG1 causes thoracic aortic aneurysms and acute aortic dissections," *American Journal of Human Genetics*, vol. 93, no. 2, pp. 398–404, 2013.

[57] D.-C. Guo, E. S. Regalado, C. Minn et al., "Familial thoracic aortic aneurysms and dissections identification of a novel locus for stable aneurysms with a low risk for progression to aortic dissection," *Circulation: Cardiovascular Genetics*, vol. 4, no. 1, pp. 36–42, 2011.

[58] S.-Q. Kuang, O. Medina-Martinez, D.-C. Guo et al., "FOXE3 mutations predispose to thoracic aortic aneurysms and dissections," *The Journal of Clinical Investigation*, vol. 126, no. 3, pp. 948–961, 2016.

[59] E. Regalado, S. Medrek, V. Tran-Fadulu et al., "Autosomal dominant inheritance of a predisposition to thoracic aortic aneurysms and dissections and intracranial saccular

aneurysms," *American Journal of Medical Genetics A*, vol. 155, no. 9, pp. 2125–2130, 2011.

[60] D. M. Milewicz and E. Regalado, "Thoracic aortic aneurysms and aortic dissections," in *GeneReviews®*, R. A. Pagon, M. P. Adam, H. H. Ardinger et al., Eds., University of Washington, Seattle, Wash, USA, 1993.

[61] D. M. Milewicz and E. S. Regalado, "Use of genetics for personalized management of heritable thoracic aortic disease: how do we get there?" *The Journal of Thoracic and Cardiovascular Surgery*, vol. 149, no. 2, pp. S3–S5, 2015.

[62] A. B. Chapman, D. Rubinstein, R. Hughes et al., "Intracranial aneurysms in autosomal dominant polycystic kidney disease," *The New England Journal of Medicine*, vol. 327, no. 13, pp. 916–920, 1992.

[63] T. Ecder and R. W. Schrier, "Cardiovascular abnormalities in autosomal-dominant polycystic kidney disease," *Nature Reviews Nephrology*, vol. 5, no. 4, pp. 221–228, 2009.

[64] S. Hassane, N. Claij, I. S. Lantinga-van Leeuwen et al., "Pathogenic sequence for dissecting aneurysm formation in a hypomorphic polycystic kidney disease 1 mouse model," *Arteriosclerosis, Thrombosis, and Vascular Biology*, vol. 27, no. 10, pp. 2177–2183, 2007.

[65] I. Hinterseher, G. Tromp, and H. Kuivaniemi, "Genes and abdominal aortic aneurysm," *Annals of Vascular Surgery*, vol. 25, no. 3, pp. 388–412, 2011.

[66] A. F. Baas, J. Medic, R. van't Slot et al., "Association study of single nucleotide polymorphisms on chromosome 19q13 with abdominal aortic aneurysm," *Angiology*, vol. 61, no. 3, pp. 243–247, 2010.

[67] J. R. Elmore, M. A. Obmann, H. Kuivaniemi et al., "Identification of a genetic variant associated with abdominal aortic aneurysms on chromosome 3p12.3 by genome wide association," *Journal of Vascular Surgery*, vol. 49, no. 6, pp. 1525–1531, 2009.

[68] S. Gretarsdottir, A. F. Baas, G. Thorleifsson et al., "Genome-wide association study identifies a sequence variant within the DAB2IP gene conferring susceptibility to abdominal aortic aneurysm," *Nature Genetics*, vol. 42, no. 8, pp. 692–697, 2010.

[69] L. Faivre, G. Collod-Beroud, B. Callewaert et al., "Pathogenic FBN1 mutations in 146 adults not meeting clinical diagnostic criteria for marfan syndrome: further delineation of type 1 fibrillinopathies and focus on patients with an isolated major criterion," *American Journal of Medical Genetics, Part A*, vol. 149, no. 5, pp. 854–860, 2009.

[70] B. Loeys, L. Van Maldergem, G. Mortier et al., "Homozygosity for a missense mutation in fibulin-5 (FBLN5) results in a severe form of cutis laxa," *Human Molecular Genetics*, vol. 11, no. 18, pp. 2113–2118, 2002.

[71] C. L. Papke and H. Yanagisawa, "Fibulin-4 and fibulin-5 in elastogenesis and beyond: insights from mouse and human studies," *Matrix Biology*, vol. 37, pp. 142–149, 2014.

[72] A. K. Ewart, C. A. Morris, D. Atkinson et al., "Hemizygosity at the elastin locus in a developmental disorder, Williams syndrome," *Nature Genetics*, vol. 5, no. 1, pp. 11–16, 1993.

[73] J. E. Wagenseil, C. H. Ciliberto, R. H. Knutsen, M. A. Levy, A. Kovacs, and R. P. Mecham, "The importance of elastin to aortic development in mice," *American Journal of Physiology—Heart and Circulatory Physiology*, vol. 299, no. 2, pp. H257–H264, 2010.

[74] W.-H. Fan and M. J. Karnovsky, "Increased MMP-2 expression in connective tissue growth factor over-expression vascular smooth muscle cells," *The Journal of Biological Chemistry*, vol. 277, no. 12, pp. 9800–9805, 2002.

[75] G. M. Longo, W. Xiong, T. C. Greiner, Y. Zhao, N. Fiotti, and B. T. Baxter, "Matrix metalloproteinases 2 and 9 work in concert to produce aortic aneurysms," *The Journal of Clinical Investigation*, vol. 110, no. 5, pp. 625–632, 2002.

[76] J. S. Matsumura and W. H. Pearce, "Infrarenal aortic aneurysms," *The New England Journal of Medicine*, vol. 336, no. 24, pp. 1756–1758, 1997.

[77] N. Sakalihasan, P. Delvenne, B. V. Nusgens, R. Limet, and C. M. Lapiere, "Activated forms of MMP2 and MMP9 in abdominal aortic aneurysms," *Journal of Vascular Surgery*, vol. 24, no. 1, pp. 127–133, 1996.

[78] U. Schönbeck, F. Mach, G. K. Sukhova et al., "Regulation of matrix metalloproteinase expression in human vascular smooth muscle cells by T lymphocytes: a role for CD40 signaling in plaque rupture?" *Circulation Research*, vol. 81, no. 3, pp. 448–454, 1997.

[79] N. A. Tamarina, W. D. McMillan, V. P. Shively, and W. H. Pearce, "Expression of matrix metalloproteinases and their inhibitors in aneurysms and normal aorta," *Surgery*, vol. 122, no. 2, pp. 264–272, 1997.

[80] M. Folkesson, M. Kazi, C. Zhu et al., "Presence of NGAL/MMP-9 complexes in human abdominal aortic aneurysms," *Thrombosis and Haemostasis*, vol. 98, no. 2, pp. 427–433, 2007.

[81] A. R. Thompson, F. Drenos, H. Hafez, and S. E. Humphries, "Candidate gene association studies in abdominal aortic aneurysm disease: a review and meta-analysis," *European Journal of Vascular and Endovascular Surgery*, vol. 35, no. 1, pp. 19–30, 2008.

[82] E. R. Neptune, P. A. Frischmeyer, D. E. Arking et al., "Dysregulation of TGF-β activation contributes to pathogenesis in Marfan syndrome," *Nature Genetics*, vol. 33, no. 3, pp. 407–411, 2003.

[83] E. Gillis, L. Van Laer, and B. L. Loeys, "Genetics of thoracic aortic aneurysm: at the crossroad of transforming growth factor-β signaling and vascular smooth muscle cell contractility," *Circulation Research*, vol. 113, no. 3, pp. 327–340, 2013.

[84] J. P. Habashi, D. P. Judge, T. M. Holm et al., "Losartan, an AT1 antagonist, prevents aortic aneurysm in a mouse model of Marfan syndrome," *Science*, vol. 312, no. 5770, pp. 117–121, 2006.

[85] J. P. Habashi, J. J. Doyle, T. M. Holm et al., "Angiotensin II type 2 receptor signaling attenuates aortic aneurysm in mice through ERK antagonism," *Science*, vol. 332, no. 6027, pp. 361–365, 2011.

[86] T. M. Holm, J. P. Habashi, J. J. Doyle et al., "Noncanonical TGFβ signaling contributes to aortic aneurysm progression in marfan syndrome mice," *Science*, vol. 332, no. 6027, pp. 358–361, 2011.

[87] Y. Wang, S. Krishna, P. J. Walker, P. Norman, and J. Golledge, "Transforming growth factor-β and abdominal aortic aneurysms," *Cardiovascular Pathology*, vol. 22, no. 2, pp. 126–132, 2013.

[88] Y. Wang, H. Ait-Oufella, O. Herbin et al., "TGF-β activity protects against inflammatory aortic aneurysm progression and complications in angiotensin II-infused mice," *The Journal of Clinical Investigation*, vol. 120, no. 2, pp. 422–432, 2010.

[89] F. Gao, P. Chambon, S. Offermanns et al., "Disruption of TGF-β signaling in smooth muscle cell prevents elastase-induced abdominal aortic aneurysm," *Biochemical and Biophysical Research Communications*, vol. 454, no. 1, pp. 137–143, 2014.

[90] H. Ait-Oufella, Y. Wang, O. Herbin, A. Tedgui, and Z. Mallat, "Role of TGFβ in a model of abdominal aortic aneurysm in mice," *Médecine Science*, vol. 26, no. 10, pp. 795–797, 2010.

[91] L. Lucarini, E. Sticchi, F. Sofi et al., "ACE and TGFBR1 genes interact in influencing the susceptibility to abdominal aortic aneurysm," *Atherosclerosis*, vol. 202, no. 1, pp. 205–210, 2009.

[92] A. Siegert, E. Ritz, S. Orth, and J. Wagner, "Differential regulation of transforming growth factor receptors by angiotensin II and transforming growth factor-β1 in vascular smooth muscle," *Journal of Molecular Medicine*, vol. 77, no. 5, pp. 437–445, 1999.

[93] N. Fukuda, W.-Y. Hu, A. Kubo et al., "Angiotensin II upregulates transforming growth factor-β type I receptor on rat vascular smooth muscle cells," *American Journal of Hypertension*, vol. 13, no. 2, pp. 191–198, 2000.

[94] L. Zhu, D. Bonnet, M. Boussion, B. Vedie, D. Sidi, and X. Jeunemaitre, "Investigation of the MYH11 gene in sporadic patients with an isolated persistently patent arterial duct," *Cardiology in the Young*, vol. 17, no. 6, pp. 666–672, 2007.

[95] A. K. Soutar and R. P. Naoumova, "Mechanisms of disease: genetic causes of familial hypercholesterolemia," *Nature Clinical Practice Cardiovascular Medicine*, vol. 4, no. 4, pp. 214–225, 2007.

[96] M. J. Bown, "Genomic insights into abdominal aortic aneurysms," *Annals of the Royal College of Surgeons of England*, vol. 96, no. 6, pp. 405–414, 2014.

[97] D. C. Ewbank, "The APOE gene and differences in life expectancy in Europe," *The Journals of Gerontology—Series A Biological Sciences and Medical Sciences*, vol. 59, no. 1, pp. 16–20, 2004.

[98] L. U. Gerdes, B. Jeune, K. A. Ranberg, H. Nybo, and J. W. Vaupel, "Estimation of apolipoprotein E genotype-specific relative mortality risks from the distribution of genotypes in centenarians and middle-aged men: apolipoprotein E gene is a 'frailty gene,' not a 'longevity gene'," *Genetic Epidemiology*, vol. 19, no. 3, pp. 202–210, 2000.

[99] R. Jacobsen, T. Martinussen, L. Christiansen et al., "Increased effect of the ApoE gene on survival at advanced age in healthy and long-lived Danes: two nationwide cohort studies," *Aging Cell*, vol. 9, no. 6, pp. 1004–1009, 2010.

[100] D. Viskochil, A. M. Buchberg, G. Xu et al., "Deletions and a translocation interrupt a cloned gene at the neurofibromatosis type 1 locus," *Cell*, vol. 62, no. 1, pp. 187–192, 1990.

[101] W. K. Bessler, F. Z. Hudson, H. Zhang et al., "Neurofibromin is a novel regulator of Ras-induced reactive oxygen species production in mice and humans," *Free Radical Biology & Medicine*, vol. 97, pp. 212–222, 2016.

[102] W. K. Bessler, G. Kim, F. Z. Hudson et al., "*Nf1* $^{+/-}$ monocytes/macrophages induce neointima formation via CCR2 activation," *Human Molecular Genetics*, vol. 25, no. 6, pp. 1129–1139, 2016.

[103] B. K. Stansfield, W. K. Bessler, R. Mali et al., "Heterozygous inactivation of the NF1 gene in myeloid cells enhances neointima formation via a rosuvastatin-sensitive cellular pathway," *Human Molecular Genetics*, vol. 22, no. 5, pp. 977–988, 2013.

[104] J. E. Allanson, M. Upadhyaya, G. H. Watson et al., "Watson syndrome: is it a subtype of type 1 neurofibromatosis?" *Journal of Medical Genetics*, vol. 28, no. 11, pp. 752–756, 1991.

[105] G. S. Oderich, T. M. Sullivan, T. C. Bower et al., "Vascular abnormalities in patients with neurofibromatosis syndrome type I: clinical spectrum, management, and results," *Journal of Vascular Surgery*, vol. 46, no. 3, pp. 475–484, 2007.

[106] D. Rea, J. F. Brandsema, D. Armstrong et al., "Cerebral arteriopathy in children with neurofibromatosis type 1," *Pediatrics*, vol. 124, no. 3, pp. e476–e483, 2009.

[107] E. Fossali, E. Signorini, R. C. Intermite et al., "Renovascular disease and hypertension in children with neurofibromatosis," *Pediatric Nephrology*, vol. 14, no. 8-9, pp. 806–810, 2000.

[108] M. Henkemeyer, D. J. Rossi, D. P. Holmyard et al., "Vascular system defects and neuronal apoptosis in mice lacking Ras GTPase-activating protein," *Nature*, vol. 377, no. 6551, pp. 695–701, 1995.

[109] T. L. Rosser, G. Vezina, and R. J. Packer, "Cerebrovascular abnormalities in a population of children with neurofibromatosis type 1," *Neurology*, vol. 64, no. 3, pp. 553–555, 2005.

[110] S. A. Lemaire, X. Wang, J. A. Wilks et al., "Matrix metalloproteinases in ascending aortic aneurysms: bicuspid versus trileaflet aortic valves," *Journal of Surgical Research*, vol. 123, no. 1, pp. 40–48, 2005.

[111] W. D. McMillan, N. A. Tamarina, M. Cipollone, D. A. Johnson, M. A. Parker, and W. H. Pearce, "Size matters: the relationship between MMP-9 expression and aortic diameter," *Circulation*, vol. 96, no. 7, pp. 2228–2232, 1997.

[112] M. Shen, J. Lee, R. Basu et al., "Divergent roles of matrix metalloproteinase 2 in pathogenesis of thoracic aortic aneurysm," *Arteriosclerosis, Thrombosis, and Vascular Biology*, vol. 35, no. 4, pp. 888–898, 2015.

[113] S. Zhang, B. Zhong, M. Chen et al., "Epigenetic reprogramming reverses the malignant epigenotype of the MMP/TIMP axis genes in tumor cells," *International Journal of Cancer*, vol. 134, no. 7, pp. 1583–1594, 2014.

[114] P. Stenvinkel, M. Karimi, S. Johansson et al., "Impact of inflammation on epigenetic DNA methylation—a novel risk factor for cardiovascular disease?" *Journal of Internal Medicine*, vol. 261, no. 5, pp. 488–499, 2007.

[115] N. R. Fuggle, F. A. Howe, R. Allen, and N. Sofat, "New insights into the impact of neuro-inflammation in rheumatoid arthritis," *Frontiers in Neuroscience*, vol. 8, article 357, 2014.

[116] I. T. Pereira, E. A. S. Ramos, E. T. Costa et al., "Fibronectin affects transient MMP2 gene expression through DNA demethylation changes in non-invasive breast cancer cell lines," *PLoS ONE*, vol. 9, no. 9, Article ID e105806, 2014.

[117] M. Ailenberg and M. Silverman, "Trichostatin A—histone deacetylase inhibitor with clinical therapeutic potential—is also a selective and potent inhibitor of gelatinase A expression," *Biochemical and Biophysical Research Communications*, vol. 298, no. 1, pp. 110–115, 2002.

[118] C. Yuan, L. Zhang, Y. Gao, D. Peng, J. Liu, and Y. Cai, "DNA demethylation at the promoter region enhances the expression of MMP-9 in ectopic endometrial stromal cells of endometriosis," *Chinese Journal of Cellular and Molecular Immunology*, vol. 30, no. 12, pp. 1258–1261, 2014.

[119] S. Nozell, Z. Ma, C. Wilson, R. Shah, and E. N. Benveniste, "Class II major histocompatibility complex transactivator (CIITA) inhibits matrix metalloproteinase-9 gene expression," *The Journal of Biological Chemistry*, vol. 279, no. 37, pp. 38577–38589, 2004.

[120] C. Yan, H. Wang, Y. Toh, and D. D. Boyd, "Repression of 92-kDa type IV collagenase expression by MTA1 is mediated through direct interactions with the promoter via a mechanism, which is both dependent on and independent of histone deacetylation," *The Journal of Biological Chemistry*, vol. 278, no. 4, pp. 2309–2316, 2003.

[121] M. Galán, S. Varona, M. Orriols et al., "Induction of histone deacetylases (HDACs) in human abdominal aortic aneurysm: therapeutic potential of HDAC inhibitors," *Disease Models and Mechanisms*, vol. 9, no. 5, pp. 541–552, 2016.

[122] A. Vinh, T. A. Gaspari, H. B. Liu, L. F. Dousha, R. E. Widdop, and A. E. Dear, "A novel histone deacetylase inhibitor reduces abdominal aortic aneurysm formation in angiotensin II-infused apolipoprotein E-deficient mice," *Journal of Vascular Research*, vol. 45, no. 2, pp. 143–152, 2008.

[123] T. Brunelli, D. Prisco, S. Fedi et al., "High prevalence of mild hyperhomocysteinemia in patients with abdominal aortic aneurysm," *Journal of Vascular Surgery*, vol. 32, no. 3, pp. 531–536, 2000.

[124] J. Liu, S. W. Zuo, Y. Li et al., "Hyperhomocysteinaemia is an independent risk factor of abdominal aortic aneurysm in a Chinese Han population," *Scientific Reports*, vol. 6, Article ID 17966, 2016.

[125] K. J. Halazun, K. A. Bofkin, S. Asthana, C. Evans, M. Henderson, and J. I. Spark, "Hyperhomocysteinaemia is associated with the rate of abdominal aortic aneurysm expansion," *European Journal of Vascular and Endovascular Surgery*, vol. 33, no. 4, pp. 391–394, 2007.

[126] S. M. Krishna, A. Dear, J. M. Craig, P. E. Norman, and J. Golledge, "The potential role of homocysteine mediated DNA methylation and associated epigenetic changes in abdominal aortic aneurysm formation," *Atherosclerosis*, vol. 228, no. 2, pp. 295–305, 2013.

[127] B. J. Toghill, A. Saratzis, S. C. Harrison, A. R. Verissimo, E. B. Mallon, and M. J. Bown, "The potential role of DNA methylation in the pathogenesis of abdominal aortic aneurysm," *Atherosclerosis*, vol. 241, no. 1, pp. 121–129, 2015.

[128] Z. Chen, A. C. Karaplis, S. L. Ackerman et al., "Mice deficient in methylenetetrahydrofolate reductase exhibit hyperhomocysteinemia and decreased methylation capacity, with neuropathology and aortic lipid deposition," *Human Molecular Genetics*, vol. 10, no. 5, pp. 433–443, 2001.

[129] K. W. K. Lee and Z. Pausova, "Cigarette smoking and DNA methylation," *Frontiers in Genetics*, vol. 4, article no. 132, 2013.

[130] L. P. Breitling, R. Yang, B. Korn, B. Burwinkel, and H. Brenner, "Tobacco-smoking-related differential DNA methylation: 27K discovery and replication," *American Journal of Human Genetics*, vol. 88, no. 4, pp. 450–457, 2011.

[131] B. A. Mercer, A. M. Wallace, C. E. Brinckerhoff, and J. M. D'Armiento, "Identification of a cigarette smoke-responsive region in the distal MMP-1 promoter," *American Journal of Respiratory Cell and Molecular Biology*, vol. 40, no. 1, pp. 4–12, 2009.

[132] R. Satta, E. Maloku, A. Zhubi et al., "Nicotine decreases DNA methyltransferase 1 expression and glutamic acid decarboxylase 67 promoter methylation in GABAergic interneurons," *Proceedings of the National Academy of Sciences of the United States of America*, vol. 105, no. 42, pp. 16356–16361, 2008.

[133] R. Joehanes, A. C. Just, R. E. Marioni et al., "Epigenetic signatures of cigarette smoking," *Circulation: Cardiovascular Genetics*, vol. 9, no. 5, pp. 436–447, 2016.

[134] L. G. Tsaprouni, T.-P. Yang, J. Bell et al., "Cigarette smoking reduces DNA methylation levels at multiple genomic loci but the effect is partially reversible upon cessation," *Epigenetics*, vol. 9, no. 10, pp. 1382–1396, 2014.

[135] S. Ambatipudi, C. Cuenin, H. Hernandez-Vargas et al., "Tobacco smoking-associated genome-wide DNA methylation changes in the EPIC study," *Epigenomics*, vol. 8, no. 5, pp. 599–618, 2016.

[136] M. M. Monick, S. R. H. Beach, J. Plume et al., "Coordinated changes in AHRR methylation in lymphoblasts and pulmonary macrophages from smokers," *American Journal of Medical Genetics, Part B: Neuropsychiatric Genetics*, vol. 159, no. 2, pp. 141–151, 2012.

[137] J. Sandoval, H. A. Heyn, S. Moran et al., "Validation of a DNA methylation microarray for 450,000 CpG sites in the human genome," *Epigenetics*, vol. 6, no. 6, pp. 692–702, 2011.

[138] U. P. Kelavkar, N. S. Harya, J. Hutzley et al., "DNA methylation paradigm shift: 15-lipoxygenase-1 upregulation in prostatic intraepithelial neoplasia and prostate cancer by atypical promoter hypermethylation," *Prostaglandins and Other Lipid Mediators*, vol. 82, no. 1–4, pp. 185–197, 2007.

[139] H. Takagi and T. Umemoto, "Smoking promotes pathogenesis of aortic aneurysm through the 5-lipoxygenase pathway," *Medical Hypotheses*, vol. 64, no. 6, pp. 1117–1119, 2005.

[140] P. A. Jones, S. M. Taylor, and V. L. Wilson, "Inhibition of DNA methylation by 5-azacytidine," *Recent Results in Cancer Research*, vol. 84, pp. 202–211, 1983.

[141] V. L. Wilson and P. A. Jones, "DNA methylation decreases in aging but not in immortal cells," *Science*, vol. 220, no. 4601, pp. 1055–1057, 1983.

[142] M. Jung and G. P. Pfeifer, "Aging and DNA methylation," *BMC Biology*, vol. 13, article 7, 2015.

[143] M. O. Hiltunen, M. P. Turunen, T. P. Häkkinen et al., "DNA hypomethylation and methyltransferase expression in atherosclerotic lesions," *Vascular Medicine*, vol. 7, no. 1, pp. 5–11, 2002.

[144] X. Lin, W. Zhang, Q. Lu et al., "Effect of MTHFR gene polymorphism impact on atherosclerosis via genome-wide methylation," *Medical Science Monitor*, vol. 22, pp. 341–345, 2016.

[145] S. B. Baylin, J. G. Herman, J. R. Graff, P. M. Vertino, and J. P. Issa, "Alterations in DNA methylation: a fundamental aspect of neoplasia," *Advances in Cancer Research*, vol. 72, pp. 141–169, 1998.

[146] M. El-Sammak, M. Kandil, S. El-Hifni, R. Hosni, and M. Ragab, "Elevated plasma homocysteine is positively associated with age independent of C677T mutation of the methylenetetrahydrofolate reductase gene in selected Egyptian subjects," *International Journal of Medical Sciences*, vol. 1, no. 3, pp. 181–192, 2004.

[147] L. D. Spotila, P. F. Jacques, P. B. Berger, K. V. Ballman, R. C. Ellison, and R. Rozen, "Age Dependence of the Influence of Methylenetetrahydrofolate Reductase Genotype on Plasma Homocysteine Level," *American Journal of Epidemiology*, vol. 158, no. 9, pp. 871–877, 2003.

[148] A. Straßburg, C. Krems, P. M. Lührmann, B. Hartmann, and M. Neuhäuser-Berthold, "Effect of age on plasma homocysteine concentrations in young and elderly subjects considering serum vitamin concentrations and different lifestyle factors," *International Journal for Vitamin and Nutrition Research*, vol. 74, no. 2, pp. 129–136, 2004.

[149] S. Horvath, "DNA methylation age of human tissues and cell types," *Genome Biology*, vol. 14, no. 10, article R115, 2013.

[150] S. Kochanek, A. Radbruch, H. Tesch, D. Renz, and W. Doerfler, "DNA methylation profiles in the human genes for tumor necrosis factors α and β in subpopulations of leukocytes and in leukemias," *Proceedings of the National Academy of Sciences of the United States of America*, vol. 88, no. 13, pp. 5759–5763, 1991.

[151] Z. H. Liu, L. L. Chen, X. L. Deng et al., "Methylation status of CpG sites in the MCP-1 promoter is correlated to serum MCP-1 in type 2 diabetes," *Journal of Endocrinological Investigation*, vol. 35, no. 6, pp. 585–589, 2012.

[152] K. E. Sullivan, A. B. M. Reddy, K. Dietzmann et al., "Epigenetic regulation of tumor necrosis factor alpha," *Molecular and Cellular Biology*, vol. 27, no. 14, pp. 5147–5160, 2007.

[153] J. Wang, Y. Jiang, A. Yang et al., "Hyperhomocysteinemia-induced monocyte chemoattractant protein-1 promoter DNA methylation by nuclear factor-κB/DNA methyltransferase 1 in apolipoprotein E–deficient mice," *BioResearch Open Access*, vol. 2, no. 2, pp. 118–127, 2013.

[154] I. Wessels, D. Fleischer, L. Rink, and P. Uciechowski, "Changes in chromatin structure and methylation of the human interleukin-1β gene during monopoiesis," *Immunology*, vol. 130, no. 3, pp. 410–417, 2010.

[155] J. Makino, R. Ogasawara, T. Kamiya et al., "Royal Jelly constituents increase the expression of extracellular superoxide dismutase through histone acetylation in monocytic THP-1 cells," *Journal of Natural Products*, vol. 79, no. 4, pp. 1137–1143, 2016.

[156] N. N. Soe, M. Sowden, P. Baskaran et al., "Acetylation of cyclophilin A is required for its secretion and vascular cell activation," *Cardiovascular Research*, vol. 101, no. 3, pp. 444–453, 2014.

[157] F. M. Moodie, J. A. Marwick, C. S. Anderson et al., "Oxidative stress and cigarette smoke alter chromatin remodeling but differentially regulate NF-κB activation and proinflammatory cytokine release in alveolar epithelial cells," *The FASEB Journal*, vol. 18, no. 15, pp. 1897–1899, 2004.

[158] D. Pons, F. R. de Vries, P. J. van den Elsen, B. T. Heijmans, P. H. A. Quax, and J. W. Jukema, "Epigenetic histone acetylation modifiers in vascular remodelling: new targets for therapy in cardiovascular disease," *European Heart Journal*, vol. 30, no. 3, pp. 266–277, 2009.

[159] I. Hinterseher, R. Erdman, J. R. Elmore et al., "Novel pathways in the pathobiology of human abdominal aortic aneurysms," *Pathobiology*, vol. 80, no. 1, pp. 1–10, 2013.

[160] M. C. Pahl, K. Derr, G. Gäbel et al., "MicroRNA expression signature in human abdominal aortic aneurysms," *BMC Medical Genomics*, vol. 5, article 25, 2012.

[161] K. Kin, S. Miyagawa, S. Fukushima et al., "Tissue- and plasma-specific MicroRNA signatures for atherosclerotic abdominal aortic aneurysm," *Journal of the American Heart Association*, vol. 1, no. 5, Article ID e000745, 2012.

[162] S.-G. Sun, B. Zheng, M. Han et al., "MiR-146a and Krüppel-like factor 4 form a feedback loop to participate in vascular smooth muscle cell proliferation," *EMBO Reports*, vol. 12, no. 1, pp. 56–62, 2011.

[163] M. Adam, U. Raaz, J. M. Spin, and P. S. Tsao, "MicroRNAs in abdominal aortic aneurysm," *Current Vascular Pharmacology*, vol. 13, no. 3, pp. 280–290, 2015.

[164] W. Zhang, T. Shang, C. Huang et al., "Plasma microRNAs serve as potential biomarkers for abdominal aortic aneurysm," *Clinical Biochemistry*, vol. 48, no. 15, pp. 988–992, 2015.

[165] P. W. Stather, N. Sylvius, D. A. Sidloff et al., "Identification of microRNAs associated with abdominal aortic aneurysms and peripheral arterial disease," *British Journal of Surgery*, vol. 102, no. 7, pp. 755–766, 2015.

[166] R. A. Boon, T. Seeger, S. Heydt et al., "MicroRNA-29 in aortic dilation: implications for aneurysm formation," *Circulation Research*, vol. 109, no. 10, pp. 1115–1119, 2011.

[167] L. Maegdefessel, J. M. Spin, U. Raaz et al., "miR-24 limits aortic vascular inflammation and murine abdominal aneurysm development," *Nature Communications*, vol. 5, p. 5214, 2014.

[168] C. W. Kim, S. Kumar, D. J. Son, I.-H. Jang, K. K. Griendling, and H. Jo, "Prevention of abdominal aortic aneurysm by anti-microRNA-712 or anti-microRNA-205 in angiotensin II-infused mice," *Arteriosclerosis, Thrombosis, and Vascular Biology*, vol. 34, no. 7, pp. 1412–1421, 2014.

THE JOURNAL OF BIOLOGICAL CHEMISTRY VOL. 292, NO. 15, pp. 6312–6324, April 14, 2017

A novel role for the Wnt inhibitor APCDD1 in adipocyte differentiation: Implications for diet-induced obesity

Received for publication, September 9, 2016, and in revised form, February 15, 2017 Published, JBC Papers in Press, February 27, 2017, DOI 10.1074/jbc.M116.758078

Nicole K. H. Yiew[‡§1], Tapan K. Chatterjee[†§¶1], Yao Liang Tang[§¶], Rod Pellenberg[‖], Brian K. Stansfield[§‖], Zsolt Bagi[§¶], David J. Fulton[‡§], David W. Stepp[§], Weiqin Chen[**], Vijay Patel[‡‡], Vinayak M. Kamath[‡‡], Sheldon E. Litwin[§§], David Y. Hui[¶¶], Steven M. Rudich[‖‖], Ha Won Kim[§¶1,2], and Neal L. Weintraub[§¶3]**

*From the Departments of [‡]Pharmacology and Toxicology, [¶]Medicine, Division of Cardiology, [‖]Pediatrics, **Physiology, [‡‡]Cardiothoracic and Vascular Surgery, and [§]Vascular Biology Center, Medical College of Georgia at Augusta University, Augusta, Georgia 30912, the [§§]Department of Medicine, Division of Cardiology, Medical University of South Carolina, Charleston, South Carolina 29425, the [¶¶]Department of Pathology and Lab Medicine, University of Cincinnati, Cincinnati, Ohio 45219, and [‖‖]Gift of Life Michigan, Ann Arbor, Michigan 48108*

Edited by Dennis R. Voelker

Impaired adipogenic differentiation during diet-induced obesity (DIO) promotes adipocyte hypertrophy and inflammation, thereby contributing to metabolic disease. Adenomatosis polyposis coli down-regulated 1 (APCDD1) has recently been identified as an inhibitor of Wnt signaling, a key regulator of adipogenic differentiation. Here we report a novel role for APCDD1 in adipogenic differentiation via repression of Wnt signaling and an epigenetic linkage between miR-130 and APCDD1 in DIO. APCDD1 expression was significantly up-regulated in mature adipocytes compared with undifferentiated preadipocytes in both human and mouse subcutaneous adipose tissues. siRNA-based silencing of APCDD1 in 3T3-L1 preadipocytes markedly increased the expression of Wnt signaling proteins (Wnt3a, Wnt5a, Wnt10b, LRP5, and β-catenin) and inhibited the expression of adipocyte differentiation markers (CCAAT/enhancer-binding protein α (C/EBPα) and peroxisome proliferator-activated receptor γ (PPARγ)) and lipid droplet accumulation, whereas adenovirus-mediated overexpression of APCDD1 enhanced adipogenic differentiation. Notably, DIO mice exhibited reduced APCDD1 expression and increased Wnt expression in both subcutaneous and visceral adipose tissues and impaired adipogenic differentiation *in vitro*. Mechanistically, we found that miR-130, whose expression is up-regulated in adipose tissues of DIO mice, could directly target the 3′-untranslated region of the APCDD1 gene. Furthermore, transfection of an miR-130 inhibitor in preadipocytes enhanced, whereas an miR-130 mimic blunted, adipogenic differentiation, suggesting that miR-130 contributes to impaired adipogenic differentiation during DIO by repressing APCDD1 expression. Finally, human subcutaneous adipose tissues isolated from obese individuals exhibited reduced expression of APCDD1, C/EBPα, and PPARγ compared with those from non-obese subjects. Taken together, these novel findings suggest that APCDD1 positively regulates adipogenic differentiation and that its down-regulation by miR-130 during DIO may contribute to impaired adipogenic differentiation and obesity-related metabolic disease.

Adipose tissue is the major energy reserve in higher eukaryotes and is remarkably flexible at storing and releasing triacylglycerols during periods of caloric excess and deprivation. Adipose tissue can expand by increasing the volume of pre-existing adipocytes (hypertrophy) and/or by increasing the number of new adipocytes (hyperplasia) via adipogenic differentiation of partially committed stem cells, termed preadipocytes (1). Adipogenic differentiation of preadipocytes is a normal physiological function required for adipose tissue development and remodeling. However, in obesity, adipogenic differentiation is typically insufficient to meet metabolic demand, and the excess calories are primarily stored in pre-existing adipocytes, which become overloaded with lipid. The resulting mechanical stress leads to adipose tissue inflammation, glucose intolerance, insulin resistance, and ectopic lipid accumulation (2, 3). Studies in humans suggest that adipocyte cell size is an independent predictor of the development of obesity-related metabolic disease (4). Thus, understanding the mechanisms that regulate adipogenic differentiation during obesity may provide important insights into the pathogenesis and treatment of metabolic disease.

The Wnt signaling pathway is a fundamental regulator of cell proliferation, polarization, and differentiation (5, 6). Wnt-family proteins exert their effects on cellular processes through canonical and non-canonical pathways (7, 8). The canonical

This work was supported by National Institutes of Health Grants HL126949 and HL112640 (to N. L. W.) and HL134354 and AR070029 (to Y. L. T. and N. L. W.) and Department of Defense Grant NF140031 (to B. K. S.). The authors declare that they have no conflicts of interest with the contents of this article. The content is solely the responsibility of the authors and does not necessarily represent the official views of the National Institutes of Health.

This work is dedicated to the late Dr. Tapan K. Chatterjee at the Vascular Biology Center, Medical College of Georgia at Augusta University.

This article contains supplemental Figs. S1–S5.

[†] Deceased, May 13, 2015.

[1] These authors contributed equally to this work.

[2] To whom correspondence may be addressed: Dept. of Medicine, Division of Cardiology, Vascular Biology Center, Medical College of Georgia at Augusta University, 1459 Laney Walker Blvd., Augusta, GA 30912. Tel.: 706-721-1715; Fax: 706-721-9799; E-mail: hkim3@augusta.edu.

[3] To whom correspondence may be addressed: Dept. of Medicine, Division of Cardiology, Vascular Biology Center, Medical College of Georgia at Augusta University, 1459 Laney Walker Blvd., Augusta, GA 30912. Tel.: 706-721-1715; Fax: 706-721-9799; E-mail: nweintraub@augusta.edu.

Wnt/β-catenin pathway is activated by binding of Wnt ligands to Frizzled (Fz)[4] receptors and co-receptors, low-density lipoprotein-related protein (LRP)5/6, leading to β-catenin stabilization and subsequent translocation into the nucleus, where it affects the transcription of Wnt target genes (9–11). Wnt signaling has been reported to negatively regulate adipogenic differentiation through several mechanisms; for example, Wnt6, Wnt10a, and Wnt10b inhibit adipogenic differentiation through a β-catenin dependent mechanism (12), and Wnt3a suppresses C/EBPβ/δ-induced adipogenesis of 3T3-L1 cells by inhibiting PPARγ induction (13). Thus, regulation of Wnt signaling in obesity may impact the development and/or progression of metabolic disease.

Recently, adenomatosis polyposis coli down-regulated 1 (APCDD1), a membrane-bound protein expressed during tissue development, has been identified as a novel Wnt inhibitor (14). Mechanistically, APCDD1 was reported to physically interact with the canonical Wnt3a ligand and LRP5 receptor at the cell surface, thereby repressing the biological effects of Wnt signaling and contributing to neural development in chicks and in *Xenopus* embryos. APCDD1 is widely expressed in adult human tissues, including the heart, pancreas, prostate, hair follicles, liver, kidney, and adipose tissues (14–16), but the biological functions of APCDD1 are poorly understood. Previously, using an unbiased genome-wide microarray approach, we observed that APCDD1 expression was significantly higher in well differentiated subcutaneous adipocytes compared with poorly differentiated visceral (perivascular) adipocytes isolated from the same human subjects (17), suggesting the possibility that APCDD1 could play a role in adipogenic differentiation, perhaps through its ability to inhibit Wnt signaling.

In this study, we investigated the role of APCDD1 in regulating the differentiation of human and mouse preadipocytes. We provide evidence that down-regulation of endogenous APCDD1 expression increases the Wnt/β-catenin signaling pathway, leading to the inhibition of key adipogenic transcription factors (C/EBPα and PPARγ) and impaired adipogenic differentiation. Conversely, overexpression of APCDD1 promotes adipogenic differentiation. We also report that APCDD1 expression in adipose tissue is decreased under obese conditions in both mouse and human subjects compared with non-obese controls. Furthermore, miR-130 was identified as a posttranscriptional regulator of APCDD1 gene expression during DIO. These findings may have important implications for the role of APCDD1 in the pathogenesis of obesity-related metabolic disease.

Results

Increased APCDD1 expression in conjunction with decreased Wnt signaling during adipogenic differentiation

Wnt expression was reported to be down-regulated during differentiation of murine preadipocytes (18). To confirm that Wnt expression is down-regulated during *in vitro* adipogenic differentiation of human preadipocytes, we assayed the mRNA expression of Wnt1, Wnt3a, and Wnt10b. All three genes were significantly down-regulated 6 days after induction of differentiation compared with undifferentiated cells (Fig. 1*A*). Next, to examine whether APCDD1 is differentially expressed in mature adipocytes *versus* undifferentiated preadipocytes (PA), we fractionated human subcutaneous adipose tissues to obtain floating mature adipocytes and the stromal vascular fraction, which is enriched in preadipocytes. Interestingly, APCDD1 mRNA levels were markedly higher in mature human adipocytes compared with the stromal vascular fraction (Fig. 1*B*). In addition, APCDD1 mRNA expression was significantly increased during *in vitro* differentiation of human subcutaneous preadipocytes (Fig. 1*C*). Time course experiments in mouse 3T3-L1 preadipocytes demonstrated that APCDD1 mRNA expression is rapidly induced following the onset of adipogenic differentiation, with levels peaking by day 3 and sustained for up to 12 days (Fig. 1*D*). Furthermore, APCDD1 protein expression was markedly up-regulated during adipogenic differentiation in isolated murine adipocytes (Fig. 1*E*) and in 3T3-L1 preadipocytes (Fig. 1*F* and supplemental Fig. S1) compared with undifferentiated cells. Thus, Wnt expression is down-regulated during adipogenic differentiation in conjunction with increased APCDD1 expression in both humans and mice.

APCDD1 gene silencing attenuates adipogenic differentiation in conjunction with increased Wnt signaling

To investigate whether APCDD1 expression participates in adipogenic differentiation, we silenced *APCDD1* in 3T3-L1 preadipocytes by transfection with siRNA specific for *APCDD1* or a scrambled control. Knockdown of *APCDD1* blunted adipogenic differentiation, as demonstrated by reduced lipid droplet accumulation (Fig. 2*A*) and adipogenic marker (C/EBPα and PPARγ) expression (Fig. 2, *B* and *C*). Furthermore, APCDD1 gene silencing increased the expression of proteins associated with the Wnt/β-catenin signaling pathway, including Wnt3a, Wnt5a, Wnt10b, LRP5, and β-catenin, in 3T3-L1 preadipocytes (Fig. 2, *B* and *C*). These data indicate that knockdown of APCDD1 blocks adipogenic differentiation while up-regulating Wnt signaling.

Overexpression of APCDD1 enhances adipogenic differentiation and inhibits Wnt signaling

To establish APCDD1 as a positive regulator of adipogenic differentiation, 3T3-L1 preadipocytes were transduced with adenovirus overexpressing APCDD1 or GFP control. At 7 days of adipogenic differentiation, APCDD1-overexpressing cells exhibited increased lipid droplet accumulation (Fig. 3*A*) and adipogenic marker (adiponectin, FABP4, C/EBPα, and PPARγ) expression (Fig. 3, *B* and *C*) compared with GFP control-transduced cells. Moreover, the expression of Wnt signaling proteins, including Wnt3a, Wnt5a, LRP5, and β-catenin, was attenuated in APCDD1-overexpressing cells compared with the control. These findings suggest that APCDD1 positively regulates adipogenic differentiation while suppressing the Wnt signaling pathway.

Reduced APCDD1 expression in parallel with impaired adipocyte differentiation in obese mice

To investigate the potential role of APCDD1 in DIO *in vivo*, we quantified APCDD1 expression in the subcutaneous adi-

[4] The abbreviations used are: Fz, Frizzled; PA, preadipocyte; CD, chow diet; HFD, high-fat diet; SQ, subcutaneous; SV, stromal vascular; qPCR, quantitative PCR; C/EBPα, CCAAT/enhancer-binding protein α; PPARγ, peroxisome proliferator-activated receptor γ; BMI, body mass index.

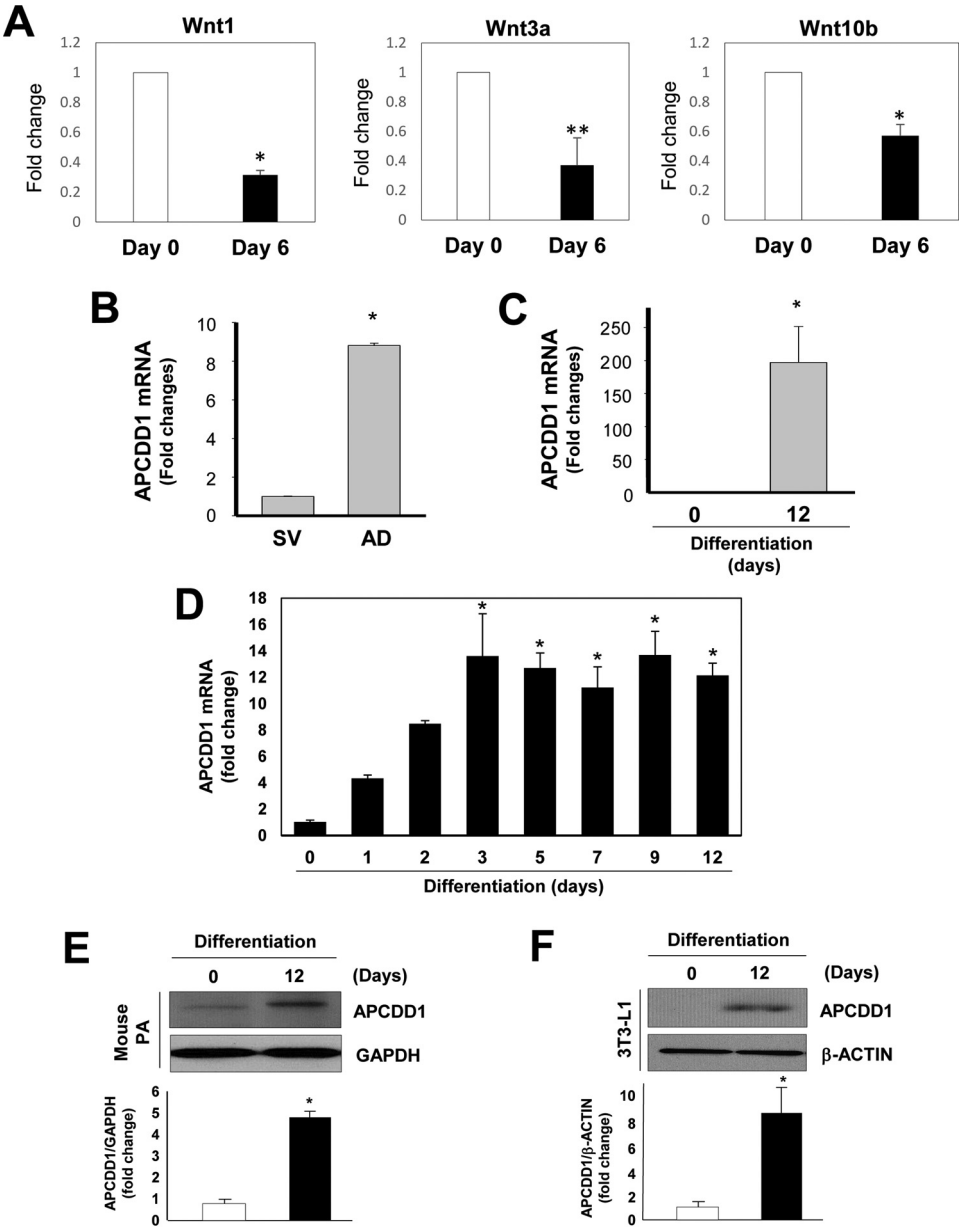

Figure 1. Wnt and APCDD1 expression in relation to adipogenic differentiation. *A*, expression of Wnt1, Wnt3a, and Wnt10b mRNAs was down-regulated during adipogenic differentiation (6 days) of human subcutaneous preadipocytes ($n = 3$). *, $p < 0.01$; **, $p < 0.05$ *versus* control (*Day 0*). *B*, the APCDD1 mRNA level was up-regulated in mature human adipocytes (*AD*) compared with PAs within the SV fraction ($n = 3$). *, $p < 0.01$ *versus* control (SV). *C*, APCDD1 mRNA expression was increased during *in vitro* adipogenic differentiation (12 days) of primary cultured human preadipocytes ($n = 3$). *, $p < 0.01$ *versus* control (*Day 0*). *D*, time course expression of APCDD1 mRNA during adipogenic differentiation of 3T3-L1 preadipocytes ($n = 3$). *, $p < 0.05$ *versus* control (*Day 0*). *E* and *F*, APCDD1 protein expression was increased during *in vitro* adipogenic differentiation (12 days) of 3T3-L1 preadipocytes and primary cultured mouse preadipocytes ($n = 3$). *, $p < 0.05$ *versus* control (*Day 0*). Levels of mRNA and protein expressions were determined by qPCR and Western blotting, respectively.

pose tissues of lean chow diet (CD)-fed mice and obese high-fat diet (HFD) mice. Body weight was significantly increased by HFD feeding (60% calories from lard fat) in WT (C57Bl/6) mice (Fig. 4*A*). Intriguingly, after 18 weeks of HFD feeding, APCDD1 mRNA and protein expression were reduced in subcutaneous (SQ) adipose tissues compared with CD mice (Fig. 4, *B* and *C*). Similarly, APCDD1 protein expression was also significantly decreased in HFD mouse-derived visceral adipose tissues (Fig. 4*D*). On the other hand, Wnt3a protein expression was increased in adipose tissues isolated from HFD mice. Importantly, as we reported previously (19), preadipocytes isolated from subcutaneous adipose tissue of HFD male mice demonstrated impaired *in vitro* differentiation compared with that from CD mice, as evidenced by diminished lipid droplet accumulation (Fig. 4*E*). These results indicate that impaired adipogenic differentiation during HFD is associated with reduced APCDD1 expression.

miR-130 overexpression induced by HFD directly targets APCDD1 gene expression

Next, we investigated the potential mechanisms whereby APCDD1 expression is down-regulated during DIO. We

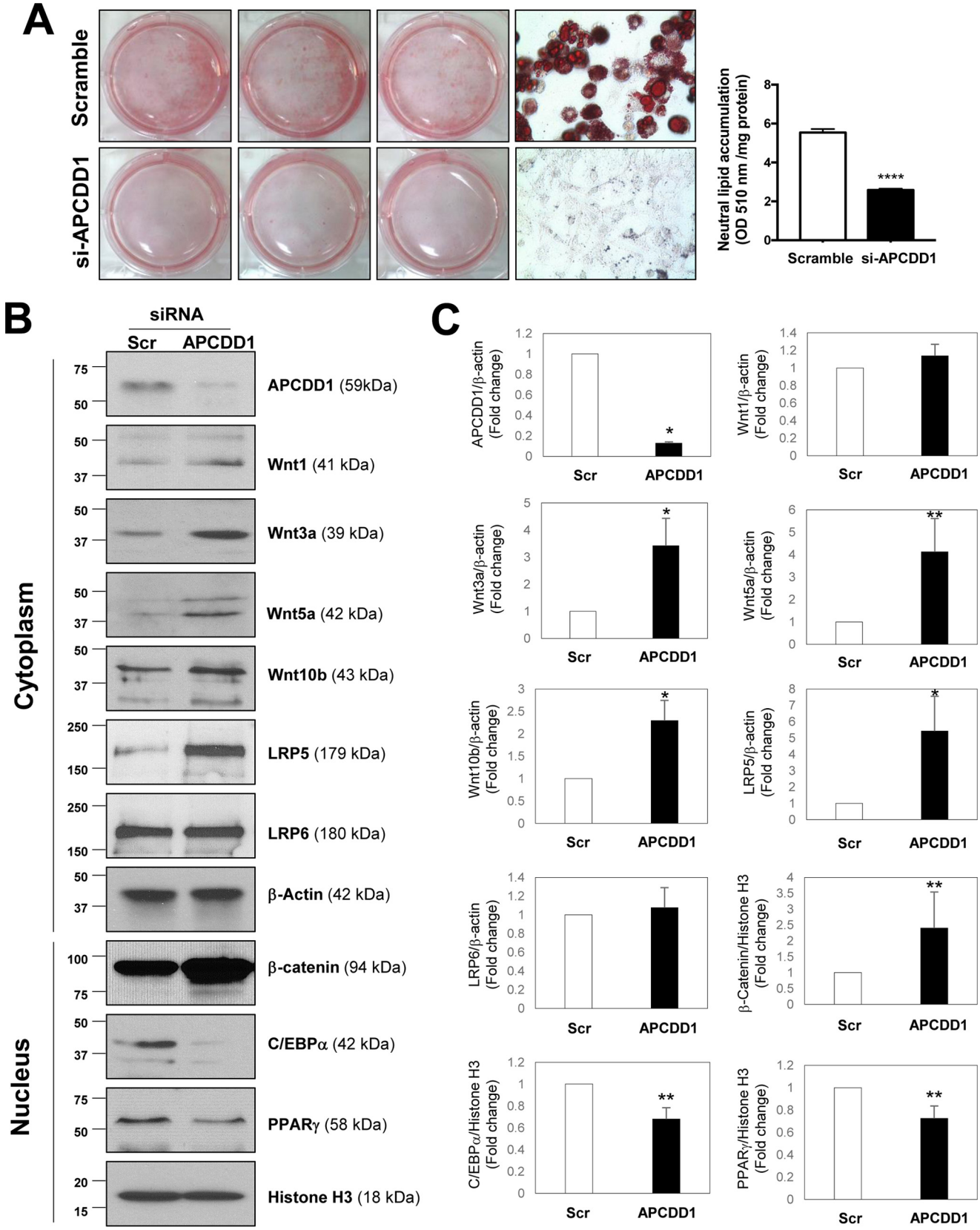

Figure 2. APCDD1 gene silencing suppresses adipogenic differentiation in conjunction with up-regulated expression of Wnt signaling proteins in 3T3-L1 preadipocytes. *A*, adipogenic differentiation was impaired in 3T3-L1 preadipocytes transfected with APCDD1 siRNA compared with the scrambled control, as indicated by reduced cytoplasmic lipid droplet accumulation (Oil red O). ****, $p < 0.0001$ *versus* control (*Scramble*). *B* and *C*, transfection of 3T3-L1 preadipocytes with APCDD1 siRNA increased expression of Wnt signaling proteins (Wnt3a, Wnt5a, Wnt10b, LRP5, and β-catenin) and decreased expression of adipogenic markers (C/EBPα and PPARγ) ($n = 3$). β-catenin, C/EBPα, and PPARγ expression levels were examined in the nuclear fraction. *, $p < 0.01$; **, $p < 0.05$ *versus* control. Protein expressions were determined by Western blotting and densitometry analysis. *Scr*, scrambled.

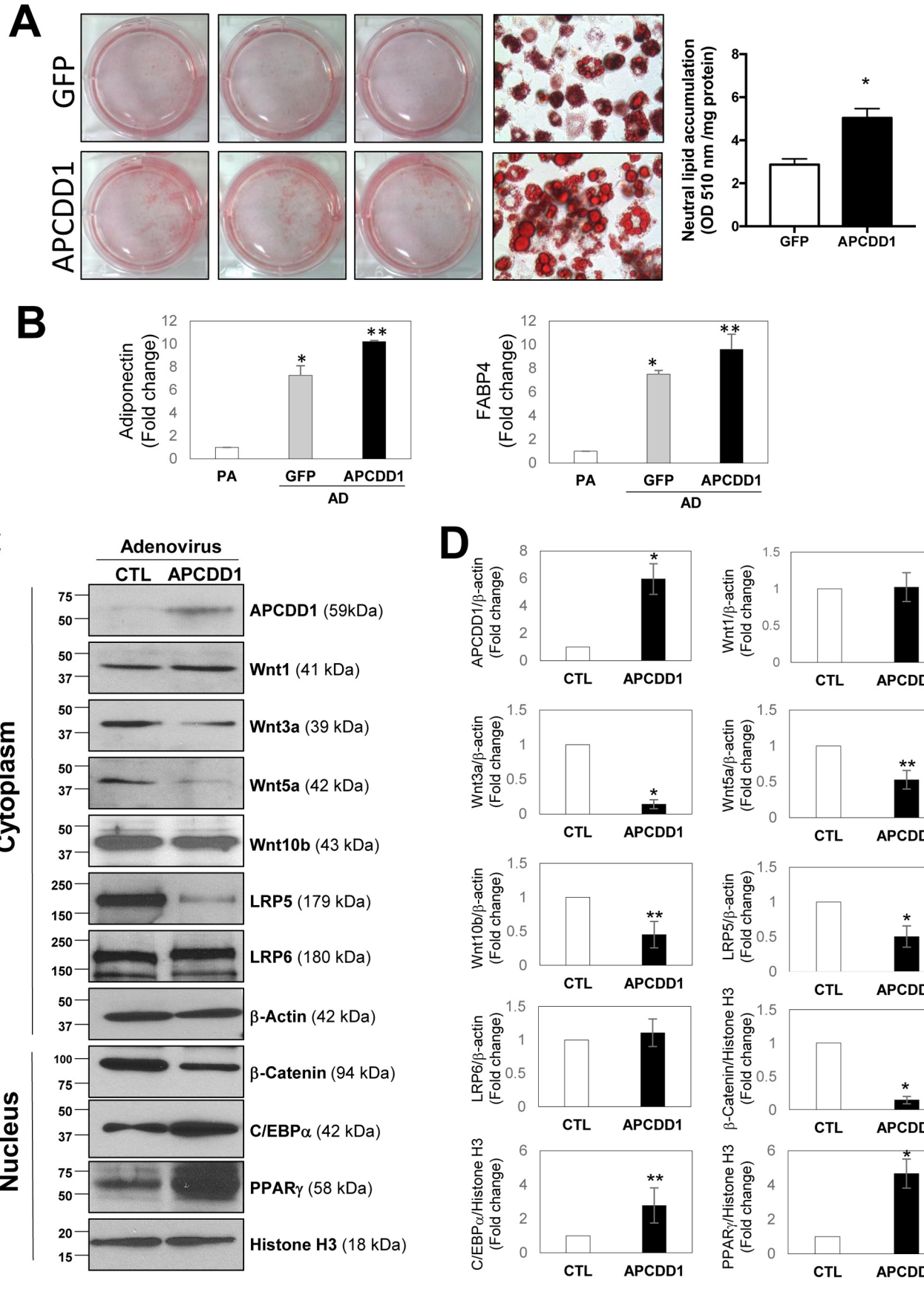

hypothesized that a specific set of miRNAs may be induced by HFD to regulate APCDD1 expression in preadipocytes. To test this hypothesis, we first examined databases (Targetscan, miRWalk, and PicTar) to search for miRNAs potentially targeting *APCDD1*, which predicted that miRNA 130a-3p and miRNA 130b-3p directly bind to the 3′ UTR of APCDD1 mRNA (Fig. 5*A*). We quantified the expression of miR-130a-3p and miR-130b-3p in 3T3-L1 cells and observed that both of these miRNAs were down-regulated within 1 day after induction of differentiation and remained repressed for up to 12 days (Fig. 5*B* and supplemental Fig. S2). To experimentally validate that APCDD1 is a target gene of miR-130, expression of miR-130a-3p and miR-130b-3p was knocked down by specific antisense inhibitors. Transfection of 3T3-L1 preadipocytes with anti-miR-130a-3p or anti-miR-130b-3p significantly augmented APCDD1 protein expression (Fig. 5*C*), indicating that APCDD1 is a direct target of miR-130. To investigate whether miR-130 is induced by HFD, we examined the expression levels of miR-130 in subcutaneous and visceral adipose tissues. Interestingly, expression of miR-130a-3p and miR-130b-3p was markedly increased in both subcutaneous and visceral adipose tissues from HFD mice compared with control mice (Fig. 5*D*). Furthermore, transfection of 3T3-L1 preadipocytes with miR-130a-3p inhibitor enhanced, whereas overexpression of miR-130a-3p blunted, adipogenic differentiation, as evaluated by cytoplasmic lipid droplet measurement (Fig. 5, *D–F*).

MiR-130 could potentially inhibit adipogenic differentiation by targeting genes other than APCDD1. Thus, we tested the effects of forced overexpression of APCDD1 in 3T3-L1 preadipocytes transfected with an miR-130a-3p mimic. As shown in supplemental Fig. S3, the miR-130a-3p mimic failed to inhibit adipogenic differentiation in APCDD-1-overexpressing cells. These findings support a mechanistic link between miR-130 and APCDD1 in the inhibition of adipogenic differentiation. Moreover, our results are consistent with the notion that HFD-induced miR-130 targets APCDD1 in DIO mice to impair adipogenic differentiation.

APCDD1 expression is down-regulated in obese individuals in conjunction with reduced adipogenic gene expression

To investigate the functional relevance of APCDD1 in human obesity, we examined APCDD1 expression in subcutaneous adipose tissues isolated from obese (BMI $>$ 30) and non-obese (BMI $<$ 30) human subjects. Interestingly, APCDD1 protein expression was significantly down-regulated in obese compared with non-obese subjects. Furthermore, adipogenic markers (C/EBPα and PPARγ) protein expression was markedly reduced in obese subjects (Fig. 6, *A* and *B*). There was also a strong trend toward decreased adiponectin gene expression with increasing BMI in our patient population (supplemental Fig. S4). Notably, expression of Wnt3a, one of the targets of APCDD1, tended to be up-regulated in adipose tissues isolated from obese subjects ($p = 0.06$ *versus* non-obese control). miR-130 expression in human subcutaneous adipose tissues exhibited considerable variability but showed a trend toward an increase in obese individuals (supplemental Fig. S5). These findings in human adipose tissues support our data obtained from mice as well as *in vitro* cell culture experiments in that impaired adipogenic differentiation during DIO could potentially be linked to reduced APCDD1 expression.

Discussion

The Wnt signaling pathway negatively regulates adipogenic differentiation and may play an important role in promoting metabolic dysfunction in obesity. Here we report that APCDD1 is a positive regulator of adipogenic differentiation through its repression of Wnt signaling. APCDD1 is weakly expressed in subcutaneous adipose tissues isolated from obese mice and humans, consistent with reports of impaired adipocyte differentiation in DIO. Moreover, overexpression of APCDD1 in 3T3-LI cells enhances adipogenic differentiation and inhibits expression of proteins in the Wnt signaling pathway, whereas siRNA-mediated APCDD1 gene silencing blunts adipogenic differentiation and up-regulates Wnt protein expression. Mechanistically, we demonstrated that APCDD1 is directly targeted by miR-130, which is overexpressed in adipose tissues of obese mice. Taken together, these findings uncover a novel role for APCDD1 in adipogenic differentiation and raise the possibility that suppression of APCDD1 expression by miR-130 in adipose tissues contributes to obesity-related metabolic disease.

Wnt signaling has been reported to repress adipogenic differentiation by blocking the induction of key adipogenic transcription factors, PPARγ and C/EBPα (18, 20). Wnts are secreted, cysteine-rich glycoproteins that act as autocrine or paracrine factors, regulating a variety of developmental processes, including cell proliferation and differentiation (5, 21). Wnt signaling encompasses both canonical and non-canonical pathways, with the former being better characterized in adipogenic differentiation. Pioneering studies demonstrated that overexpression of Wnt1 or a GSK3β phosphorylation-defective β-catenin mutant inhibited adipogenic differentiation in 3T3-L1 preadipocytes (18). Overexpression of canonical Wnt10b ligand stabilized β-catenin and blocked adipogenic differentiation in 3T3-L1 preadipocytes (18). Also, transgenic mice overexpressing Wnt10b under the control of the adipose-specific FABP4 promoter exhibited a 50% reduction in total body adiposity and resistance to HFD-induced white adipose tissue expansion (22). Although the canonical Wnt pathway has been consistently implicated in

Figure 3. APCDD1 overexpression accelerates adipogenic differentiation and down-regulates the expression of Wnt signaling proteins in 3T3-L1 preadipocytes. *A*, adipogenic differentiation, as indicated by lipid droplet accumulation (Oil red O), was increased in 3T3-L1 preadipocytes transfected with adenoviral APCDD1 compared with the control. *, $p < 0.01$ *versus* control (Adeno-GFP). *B*, mRNA expression of adipogenic markers (adiponectin and FABP4) was up-regulated in adenoviral APCDD1-transduced 3T3-L1 preadipocytes during differentiation (7 days) ($n = 4$). *, $p < 0.01$ *versus* control (PA); **, $p < 0.05$ *versus* GFP. *AD*, adipocyte. *C* and *D*, transduction of 3T3-L1 preadipocytes with adenoviral APCDD1 down-regulated Wnt-associated protein expression (Wnt3a, Wnt5a, Wnt10b, LRP5, and β-catenin) and up-regulated adipogenic marker (C/EBPα and PPARγ) protein expression during differentiation ($n = 3$). *, $p < 0.01$; **, $p < 0.05$ *versus* control (*CTL*). Levels of mRNA and protein expressions were determined by qPCR and Western blotting, respectively. Representative blots are shown in *C* and densitometry in *D*.

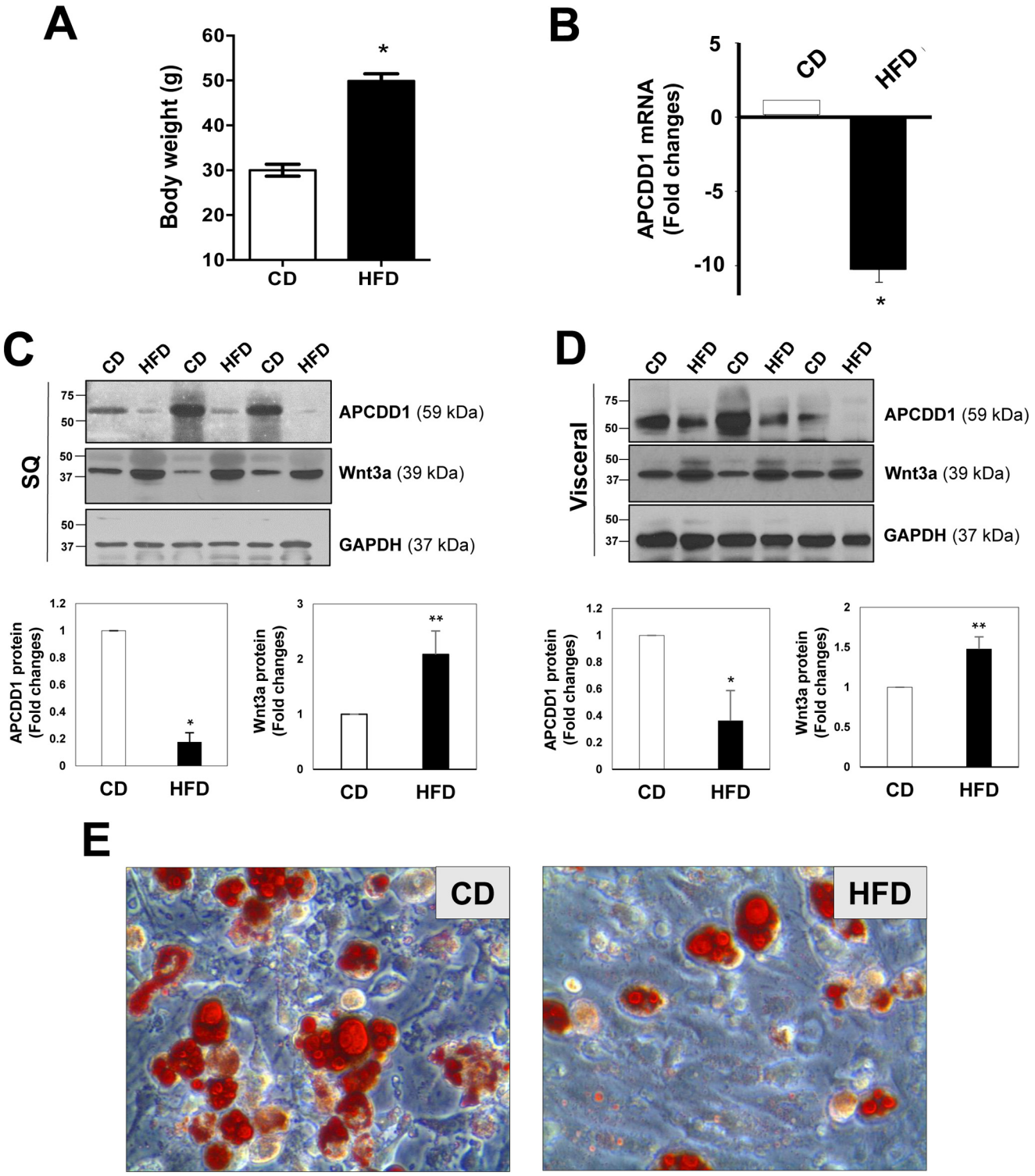

Figure 4. Reduced APCDD1 expression is associated with up-regulated Wnt3a and blunted adipogenic differentiation in DIO mice. *A*, 18 weeks of HFD feeding, compared with CD feeding, significantly increased body weight in mice ($n = 3$). *B—D*, APCDD1 mRNA (*B*) and protein (*C*) levels were down-regulated, whereas Wnt3a was up-regulated, in extracts of SQ (*C*) and visceral (*D*) adipose tissues isolated from HFD-fed DIO mice compared with lean controls ($n = 3$). Relative mRNA and protein expression were quantified by qPCR and Western blotting, respectively. *, $p < 0.01$; **, $p < 0.05$ *versus* control (*CD*). *E*, adipogenic differentiation (7 days) was impaired in preadipocytes isolated from subcutaneous adipose tissues of DIO mice. Light microscopy of neutral cytoplasmic lipid droplet accumulation was assessed by Oil red O staining.

inhibition of adipogenic differentiation *in vitro* and *in vivo*, non-canonical Wnt pathways (independent of β-catenin) are poorly understood and may exert opposing effects on adipogenesis. For instance, Wnt5b, a non-canonical ligand, is transiently induced during adipogenic differentiation and partially inhibits the canonical Wnt/β-catenin pathway to facilitate differentiation (23). Thus, the canonical and non-canonical Wnt pathways are interconnected and cross-talk

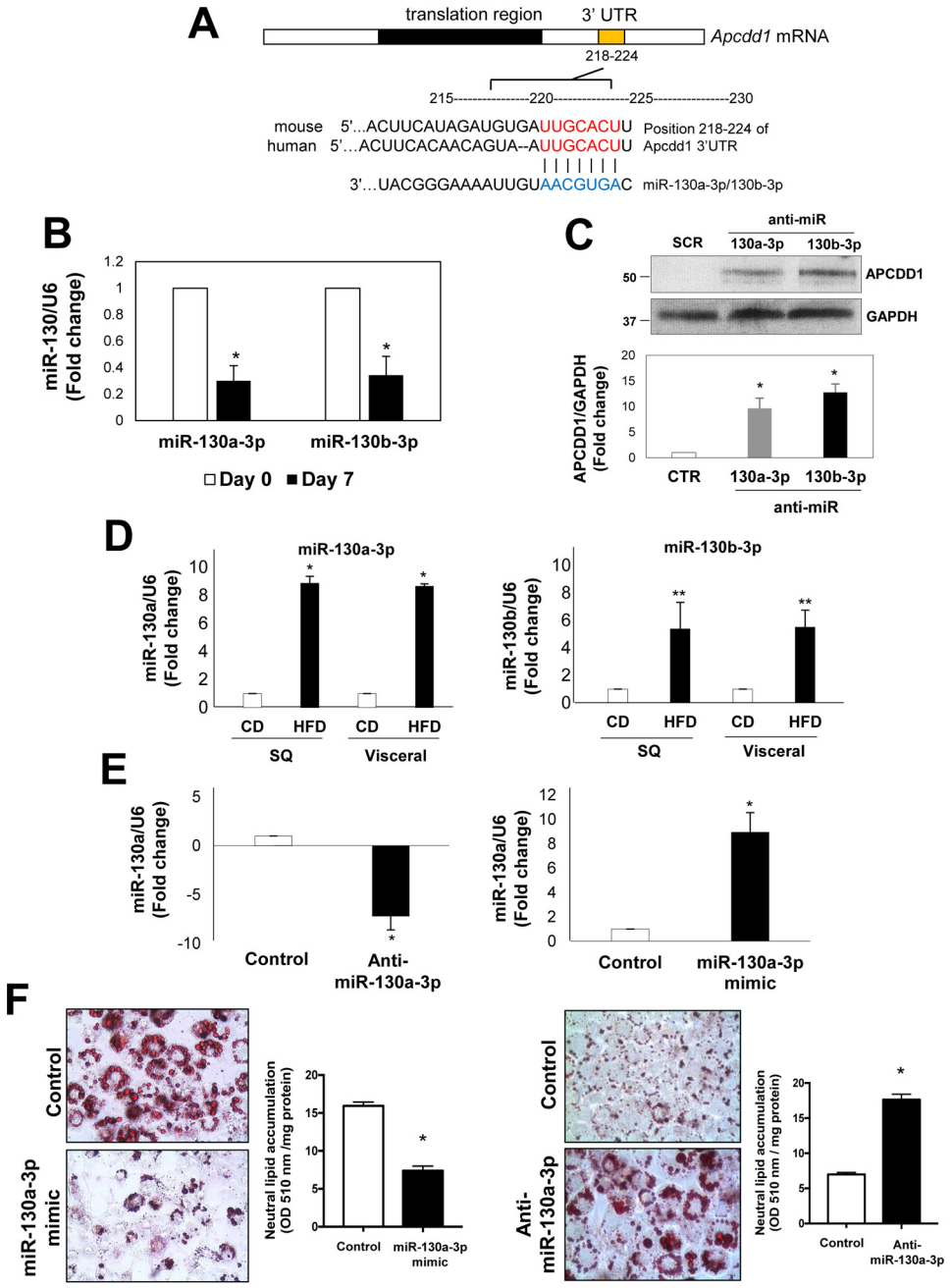

Figure 5. HFD-induced miR-130 targets *APCDD1* and inhibits adipogenic differentiation. *A*, computational analysis predicted that miR-130a-3p and miR-130b-3p can directly bind the 3′ UTR of APCDD1. *B*, miR-130a-3p and miR103b-3p levels were down-regulated during adipogenic differentiation in 3T3-L1 preadipocytes. *, $p < 0.05$ *versus* control (*Day 0*). *C*, APCDD1 protein expression was increased by transfection of miR-130 inhibitor in 3T3-L1 preadipocytes ($n = 3$). *, $p < 0.05$ *versus* control (*CTR*). *SCR*, scramble. *D*, miR-130a-3p and miR-130b-3p levels were increased in the SQ and visceral adipose depots of HFD-fed DIO mice ($n = 5$). *, $p < 0.01$; **, $p < 0.05$ *versus* control (*CD*). *E*, miR-130a-3p expression was significantly reduced or increased by transfection of miR-130a-3p inhibitor or mimic, respectively, in 3T3-L1 preadipocytes ($n = 3$). *, $p < 0.01$ *versus* control. *F*, adipogenic differentiation of 3T3-L1 preadipocytes was enhanced by transfection of miR-130a-3p inhibitor and reduced by transfection of miR-130a-3p mimic. *, $p < 0.0001$ *versus* control. Light microscopy of neutral cytoplasmic lipid droplets accumulation was evaluated by Oil red O staining and optical density measurement by spectrophotometer.

with one another to regulate adipogenic differentiation in a complex manner.

The components of Wnt signaling pathways are modulated by a number of endogenous activators and inhibitors, among them APCDD1 (24). APCDD1 is an evolutionarily conserved plasma membrane glycoprotein that has only been recently identified as a Wnt inhibitor (14). The APCDD1 gene is located on chromosome 18 in mice and humans and was first identified in colon cancer tissues (14, 16, 25). It encodes an ~58-kDa transmembrane protein whose transcription is regulated by the β-catenin·Tcf complex (14, 16). APCDD1 expression was found to be elevated in 18 of 27 primary colon cancer tissues compared with corresponding noncancerous mucosa, and its exogenous expression was shown to promote cancer cell growth (16). In humans, APCDD1 is expressed during tissue development and in numerous adult tissue types (14–16), sug-

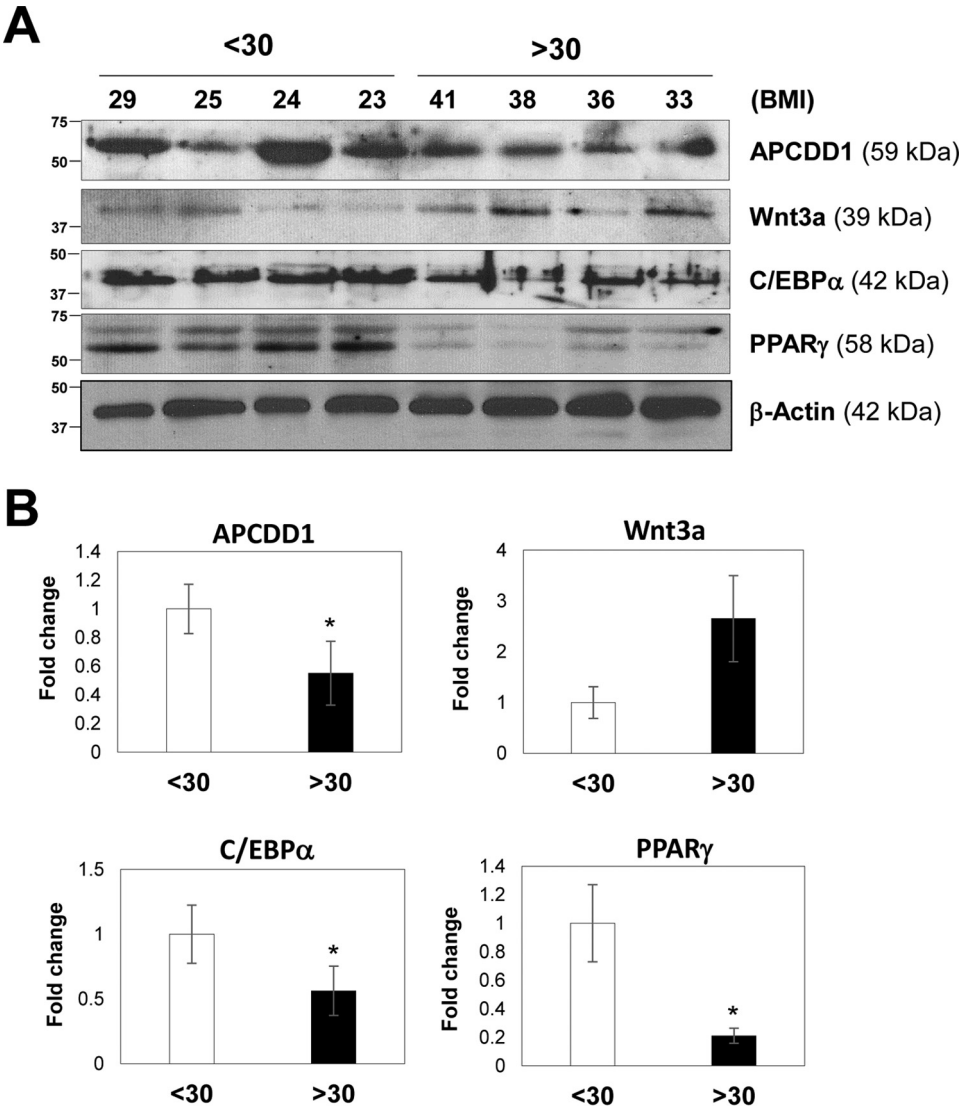

Figure 6. Down-regulated expression of APCDD1 in adipose tissues from obese humans is associated with reduced adipogenic gene expression. *A* and *B*, protein expression of APCDD1, in conjunction with C/EBPα, PPARγ, was down-regulated, whereas Wnt3a levels tended to be up-regulated ($p = 0.06$), in subcutaneous adipose tissues isolated from obese (BMI > 30) compared with non-obese subjects (BMI < 30). *, $p < 0.05$ *versus* non-obese control. Protein expressions were analyzed by Western blotting (*A*, representative data) and densitometry (*B*, $n = 8$).

gesting a diverse role for APCDD1 in biological processes associated with Wnt signaling. Indeed, recent studies have documented that APCDD1 is involved in gliogenesis, tooth morphogenesis, oligodendrocyte differentiation, osteogenic differentiation of human dental follicle cells, and diseases such as hereditary hypotrichosis simplex (14, 26–29). Although most studies support an inhibitory role for APCDD1 in Wnt/β-catenin signaling, Morsczeck and co-workers (28) reported that APCDD1 sustained the expression and activation of β-catenin during osteogenic differentiation of human dental follicle cells. Moreover, microarray results indicated that APCDD1 expression is >300-fold higher in dental follicle cells than in mesenchymal stem cells (30). This suggests that the level of APCDD1 expression and its impact on Wnt/β-catenin signaling may vary considerably in individual cells and tissues.

Although a role for APCDD1 in mammalian adipose development and adipocyte differentiation is heretofore unreported, Ullah *et al.* (15) recently identified APCDD1 as a potential human adipocyte-specific marker gene using GeneChips analysis and bioinformatics. Our study is the first to directly examine the functional significance of APCDD1 in adipogenic differentiation of human and murine preadipocytes *in vitro*. We demonstrate that APCDD1 gene expression is rapidly induced during adipogenic differentiation and propose a functional link between APCDD1 and the adipogenic program through a Wnt signaling-dependent mechanism. APCDD1 was demonstrated to physically interact with Wnt3a and Fz co-receptor LRP5 proteins, thereby preventing the formation of Wnt receptor complexes (14). Here we show that APCDD1 inhibits the expression of Wnt pathway-related proteins, including Wnt3a, LRP5, and β-catenin, in 3T3-L1 preadipocytes, revealing a mechanism by which APCDD1 could disrupt canonical Wnt signaling. In addition to canonical Wnt signaling, we found that APCDD1 may also regulate the expression of non-canonical Wnt5a. The precise mechanisms whereby APCDD1 inhibits Wnt pathways

in the context of adipogenic differentiation thus appear to be complex. It is also possible that APCDD1 regulates adipocyte differentiation via Wnt-independent mechanisms. Future studies will be required to investigate these possibilities.

Although adipose tissue contains a large number of preadipocytes that are potentially able to differentiate into fully mature, lipid-storing adipocytes, it nevertheless primarily expands by enlargement of pre-existing adipocytes in obesity (31, 32), thus promoting insulin resistance and hepatic steatosis, key aspects of metabolic syndrome (3, 33). This suggests that the level of adipogenic differentiation is insufficient to match the metabolic demand in obesity. The rate of preadipocyte replication is actually *increased* in adipose tissues of obese mice (34), suggesting that the insufficient level of adipocyte differentiation in obesity is not caused by reduced adipogenic precursor cell abundance. Interestingly, we have reported previously that HFD impairs adipogenic differentiation, promoting accumulation of inefficiently differentiated adipocytes that exhibit diminished expression of adipogenic differentiation-specific genes (35). This impairment in adipogenic differentiation in HFD-induced obesity therefore may be related to the inability of preadipocytes to efficiently undergo differentiation and/or maintain the differentiated state.

Mounting evidence indicates that Wnt signaling may be dysregulated in obesity and thus could potentially contribute to the impaired adipogenic differentiation. Two independent groups have reported increased circulating Wnt5a in obese patients compared with lean control subjects (36, 37). Expression of Wnt5a mRNA in visceral adipose tissues was also found to be increased, whereas secreted Fz-related protein 5 (SFRP5), an adipokine that represses Wnt signaling by binding and sequestering Wnt ligands, was reduced in obese patients (37). In line with these findings, we showed that obese subjects (BMI $>$ 30) tended to display increased Wnt3a expression in their subcutaneous adipose tissues compared with non-obese subjects (BMI $<$ 30). The mechanisms responsible for up-regulated Wnt ligand expression in obesity are unknown. Interestingly, we observed decreased APCDD1 protein expression in both obese human and mouse adipose tissues compared with their corresponding controls. Based on our findings, we postulate that reduced APCDD1 expression in obese adipose tissues may potentiate Wnt signaling, thereby contributing to impaired adipogenic differentiation *in vivo*. Future studies directly targeting APCDD1 in animal models of obesity will be required to test this hypothesis.

Identifying the mechanisms whereby APCDD1 expression is down-regulated in obese adipose tissues may provide insights into the pathogenesis of metabolic syndrome and new approaches for treatment. Here we focused on epigenetic mechanisms of gene regulation, which play a prominent role in the pathogenesis of obesity-related diabetes (38). In particular miRNAs, through their potent effects on posttranscriptional regulation, are functionally important in adipogenic differentiation. For instance, miR-143 stimulates adipogenic differentiation through inhibition of ERK5 (39), whereas miR-210 enhances adipogenesis by inhibiting TCF7L2, a key transcription factor in Wnt signaling (40). Moreover, miR-124 and miR-17–92 promote adipogenic differentiation by repressing Dlx5 and retinoblastoma (RB)-family Rb2/p130, respectively (41, 42). On the other hand, several miRNAs have been reported to negatively regulate adipogenesis. TNF-α-induced up-regulation of miR-155 inhibits adipogenic differentiation by down-regulating cAMP-response element-binding protein (CREB) and C/EBPβ (43), and let-7 was reported to inhibit adipogenesis by regulating the expression of high mobility group AT-hook2 (HMGA-2) (44). Notably, the miR-130 family has been shown to impair human preadipocyte differentiation by repressing PPARγ biosynthesis, and TNF-α-induced miR-130 was reported to promote adipocyte dysfunction during obesity (45, 46). Here we confirmed a previous report that miR-130 expression is up-regulated in adipose tissues of HFD-fed obese mice (46). Computational analysis of the 3′ UTR of the APCDD1 gene predicted a binding site for miR-130a and miR-130b, which share the same seed sequence but are encoded by two independent loci (miRBase Database). Knockdown of miR-130 in preadipocytes increased APCDD1 expression, suggesting that it may directly target APCDD1. Indeed, transfection of an miR-130a-3p inhibitor in preadipocytes enhanced, whereas an miR-130a-3p mimic blunted, adipogenic differentiation. Based on these findings, we hypothesize that elevated miR-130 in obese adipose tissues may contribute to impaired adipogenic differentiation via its inhibitory effect on APCDD1 expression (Fig. 7). Although this study focused on the role of miRNA, the importance of other epigenetic mechanisms, including DNA methylation and histone modifications, in regulating APCDD1 gene expression in obesity remains to be determined. Finally, what role, if any, adipocyte enlargement in obesity plays in down-regulating APCDD1 expression also remains to be determined.

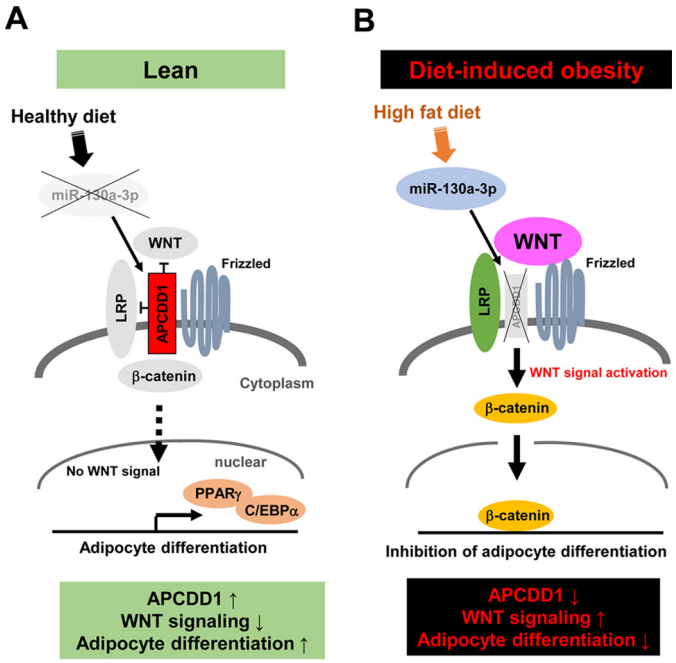

Figure 7. Schematic depicting the potential mechanisms of APCDD1-mediated adipogenic differentiation in the lean state *versus* DIO. Under normal physiological conditions, APCDD1 inhibits the expression of Wnt signaling proteins, leading to the induction of key adipogenic transcription factors (C/EBPα and PPARγ) and adipogenic differentiation. In DIO, HFD-induced miR-130 in adipose tissues blocks APCDD1 gene expression, thereby augmenting Wnt signaling and repressing adipogenic differentiation.

In conclusion, we provide novel evidence that APCDD1, an endogenous inhibitor of Wnt signaling, is an essential component of the adipogenic differentiation program. Based on our findings, we propose a working model (Fig. 7, *A* and *B*) to suggest that, under normal physiological conditions, APCDD1 inhibits the expression of Wnt signaling proteins, leading to the induction of key adipogenic transcription factors (C/EBPα and PPARγ) and induction of adipogenic differentiation. In DIO, up-regulated expression of miR-130 in adipose tissues blocks APCDD1 gene expression, thereby augmenting Wnt signaling and repressing adipogenic differentiation. These findings may have important implications for the pathogenesis of obesity-related metabolic disease.

Experimental procedures

Preparation of mouse adipose tissues

Male C57BL/6J mice were maintained on chow diet after weaning. At 6 weeks of age, these mice were either maintained on CD (Harlan Teklad, LM-485) or switched to an HFD (Research Diet, D12492, 60% calories from lard fat) for 18 weeks. Mice were euthanized, blood was collected via cardiocentesis, and subcutaneous and visceral adipose tissues were collected following tissue perfusion with saline. All animal studies were conducted using a protocol approved by the Institutional Animal Care and Use Committee of the University of Cincinnati College of Medicine and Medical College of Georgia at Augusta University.

Preparation of human adipose tissues

Human adipose tissues were collected from obese (BMI $>$ 30) and non-obese (BMI $<$ 30) patients undergoing abdominal surgeries. The study protocol was approved by the Institutional Review Boards of the University of Cincinnati and Medical College of Georgia at Augusta University.

Isolation of adipocytes, preadipocytes, and in vitro adipogenic differentiation

To isolate adipocytes and preadipocytes from adipose tissues, mouse or human adipose tissues were thoroughly minced, digested with collagenase (Worthington), filtered, and centrifuged to separate mature floating adipocytes from the pelleted stromal vascular (SV) fraction cells (preadipocyte-enriched) as described previously (47). Then, SV pellets were resuspended, plated, and grown in preadipocyte growth medium (Cell Applications) as described previously (47). The cells were expanded for two to four passages in culture and differentiated in the presence of adipocyte differentiation medium (Cell Applications), which was replaced with fresh medium every 2 days. 3T3-L1 preadipocytes were cultured in 3T3-L1 preadipocytes medium and differentiated in 3T3-L1 differentiation medium (ZenBio). These commercial media include a standard combination of adipogenic differentiation factors, including FBS (5–10%), insulin (100–1700 nM), dexamethasone (250–1000 nM), 3-isobutyl-1-methylxanthine (100–500 nM), indomethacin, biotin, pantothenate, etc. and induce adipogenic differentiation with high efficiency. For molecular studies, adipose tissues were flash-frozen in liquid nitrogen immediately after collection for subsequent analysis of RNA or protein expression. 3T3-L1 preadipocytes, obtained from the ATCC, were grown in preadipocyte medium (ZenBio) and differentiated in the presence of adipocyte differentiation medium (ZenBio) according to the instructions of the manufacturer.

Cytoplasmic lipid droplet measurement by Oil red O

0.4% of Oil red O (Sigma) in isopropanol (stock solution) was diluted at 3:2 (Oil red O:ddH_2O) ratio to form Oil red O working solution. Cells were washed with PBS and fixed with 4% paraformaldehyde for 1 h. Cells were then washed with ddH_2O followed by 60% isopropanol. Oil red O working solution was then added to the fixed cells and incubated for 10 min at room temperature. After incubation, cells were washed with ddH_2O and imaged using light microscopy. Oil red O quantification was carried out by measuring the optical density (510 nm) with a spectrophotometer.

siRNA transfection of 3T3-L1 preadipocytes

3T3-L1 preadipocytes were transfected with APCDD1-specific siRNA (Santa Cruz Biotechnology; final concentration, 20 nM) or scramble control by using Lipofectamine 2000^{TM} (Invitrogen) according to the instructions of the manufacturer, and then the cells were differentiated in the presence of adipocyte differentiation medium. After 72 h of differentiation, the cells were retransfected with APCDD1 siRNA or scramble control in the same manner to boost the transfection efficiency. At 7 days of differentiation, cells were stained with Oil red O to evaluate lipid accumulation (an index of adipocyte differentiation) or harvested for molecular studies.

Adenovirus transduction of 3T3-L1 preadipocytes

The human APCDD1 adenovirus (Applied Biological Materials) was amplified by transducing HEK 293 cells, and the medium supernatant containing the adenovirus was collected and titrated according to the instructions of the manufacturer. 3T3-L1 preadipocytes were transduced with adenoviruses carrying APCDD1 or a control gene at a multiplicity of infection of 500 with 0.5 μg/ml poly-L-lysine in preadipocyte medium for 6 h and then differentiated in the presence of adipocyte differentiation medium. At 7 days of differentiation, cells were stained with Oil red O or harvested for molecular studies.

Quantitative PCR

Total RNA was extracted from tissues or cells with QIAzol lysis reagent and purified with the RNeasy lipid tissue mini kit (Qiagen) according to the instructions of the manufacturer. Real-time quantification of mRNA levels of the genes of interest was performed using Brilliant II SYBR Green QPCR Master Mix (Agilent Technologies) according to the instructions of the manufacturer. Normalized Ct values were subjected to statistical analysis, and the -fold difference was calculated by the $\Delta\Delta$ Ct method as described previously (48).

Western blotting

Proteins were extracted from tissues or cells by radioimmune precipitation (RIPA) assay lysis buffer, separated on SDS-PAGE gel, transferred to nitrocellulose membranes, and probed with

the appropriate antibodies, and subsequently blots were developed using ECL system (Thermo Scientific). For detection of nuclear proteins (β-catenin, C/EBPα, and PPARγ), nuclear fractionation was performed using an NE-PER nuclear and cytoplasmic extraction reagents kit (Thermo Scientific) according to the protocol of the manufacturer. The specific antibodies used in this study were as follows: APCDD1, C/EBPα, Wnt1, Wnt3a, Wnt10b, LRP5, LRP6, and β-actin (Santa Cruz Biotechnology); Wnt5a (Abcam); GAPDH (Ambion); PPARγ (Novus Biologicals); histone H3 (Cell Signaling Technology); and β-catenin (Upstate).

miRNA target prediction

Computational miRNA target prediction analysis was performed using three databases (TargetScan, PicTar, and miRWalk algorithms) to predict potential binding between 3′ UTR of target genes and selective miRNAs.

miRNA isolation and detection

Total RNA, including miRNA, was extracted using the *mir*Vana™ miRNA isolation kit (Ambion), and miR-130a-3p and miR-130b-3p were detected using All-in-One first-strand cDNA synthesis kits and All-in-One miRNA quantitative RT-PCR reagent kits (GeneCopoeia). Specific miR-130 primers for quantitative RT-PCR were as follows: miRNA universal reverse, 5′-CCAGTGCAGGGTCCGAGGTA; miR-130a-3p RT, 5′-CTCAACTGGTGTCGTGGAGTCGGCAATTCAGTTGAGATGCCCTT; miR-130a-3p forward, 5′-ACACTCCAGCTGGGCAGTGCAATGTTAAAA; miR-130b-3p RT, 5′-CTCAACTGGTGTCGTGGAGTCGGCAATTCAGTTGAGATGCCCTT; and miR-130a-3p forward, 5′-ACACTCCAGCTGGGCAGTGCAATGATGAAA.

Transfection of 3T3-L1 preadipocytes with miRNA inhibitor or mimic

miR-130 mimic (miRIDIAN miRNA mimic) and anti-miR-130 (hairpin inhibitor) were synthesized by Dharmacon. 3T3-L1 preadipocytes were transfected with 50 nM miRNA anti-miR or mimic using Lipofectamine 2000 (Invitrogen) according to the instructions of the manufacturer, and then the cells were differentiated in the presence of adipocyte differentiation medium. After 48 h of differentiation, the cells were retransfected in the same manner to boost transfection efficiency. At 5 days of differentiation, cells were stained with Oil red O. In some experiments, 3T3-L1 preadipocytes were co-transfected with the APCDD1 plasmid and miR-130a-3p mimic by adenovirus and Lipofectamine 2000, respectively, in preadipocyte medium for 6 h and then differentiated in the presence of adipocyte differentiation medium.

Statistical analysis

Data are expressed as mean ± S.E. Comparison between two mean values was evaluated by an unpaired Student's two-tailed *t* test and between three or more groups by one-way analysis of variance followed by Bonferroni post hoc analysis. The statistical relationship between two continuous variables was evaluated by linear repression analysis. $p < 0.05$ was considered statistically significant.

Author contributions— N. K. H. Y., T. K. C., H. W. K., and N. L. W. were involved in study conception and design, data acquisition, analysis, interpretation, and manuscript writing. R. P. performed the experiments and analyzed the results. Z. B., V. P., V. M. K., and S. M. R. provided human tissue samples and reviewed the manuscript. Y. L. T., B. K. S., D. J. F., D. W. S., W. C., S. E. L., and D. Y. H. contributed to interpretation of data and manuscript review.

References

1. MacDougald, O. A., and Mandrup, S. (2002) Adipogenesis: forces that tip the scales. *Trends Endocrinol. Metab.* **13,** 5–11
2. Klöting, N., and Blüher, M. (2014) Adipocyte dysfunction, inflammation and metabolic syndrome. *Rev. Endocr. Metab. Disord.* **15,** 277–287
3. Kim, J. I., Huh, J. Y., Sohn, J. H., Choe, S. S., Lee, Y. S., Lim, C. Y., Jo, A., Park, S. B., Han, W., and Kim, J. B. (2015) Lipid-overloaded enlarged adipocytes provoke insulin resistance independent of inflammation. *Mol. Cell. Biol.* **35,** 1686–1699
4. Lönn, M., Mehlig, K., Bengtsson, C., and Lissner, L. (2010) Adipocyte size predicts incidence of type 2 diabetes in women. *FASEB J.* **24,** 326–331
5. Kahn, M. (2014) Can we safely target the WNT pathway? *Nat. Rev. Drug Discov.* **13,** 513–532
6. Teo, J. L., and Kahn, M. (2010) The Wnt signaling pathway in cellular proliferation and differentiation: a tale of two coactivators. *Adv. Drug Delivery Rev.* **62,** 1149–1155
7. Veeman, M. T., Axelrod, J. D., and Moon, R. T. (2003) A second canon: functions and mechanisms of β-catenin-independent Wnt signaling. *Dev. Cell* **5,** 367–377
8. Grumolato, L., Liu, G., Mong, P., Mudbhary, R., Biswas, R., Arroyave, R., Vijayakumar, S., Economides, A. N., and Aaronson, S. A. (2010) Canonical and noncanonical Wnts use a common mechanism to activate completely unrelated coreceptors. *Genes Dev.* **24,** 2517–2530
9. MacDonald, B. T., Tamai, K., and He, X. (2009) Wnt/β-catenin signaling: components, mechanisms, and diseases. *Dev. Cell* **17,** 9–26
10. Miller, J. R., Hocking, A. M., Brown, J. D., and Moon, R. T. (1999) Mechanism and function of signal transduction by the Wnt/β-catenin and Wnt/Ca^{2+} pathways. *Oncogene* **18,** 7860–7872
11. Eastman, Q., and Grosschedl, R. (1999) Regulation of LEF-1/TCF transcription factors by Wnt and other signals. *Curr. Opin. Cell Biol.* **11,** 233–240
12. Cawthorn, W. P., Bree, A. J., Yao, Y., Du, B., Hemati, N., Martinez-Santibañez, G., and MacDougald, O. A. (2012) Wnt6, Wnt10a and Wnt10b inhibit adipogenesis and stimulate osteoblastogenesis through a β-catenin-dependent mechanism. *Bone* **50,** 477–489
13. Li, H. X., Luo, X., Liu, R. X., Yang, Y. J., and Yang, G. S. (2008) Roles of Wnt/β-catenin signaling in adipogenic differentiation potential of adipose-derived mesenchymal stem cells. *Mol. Cell. Endocrinol.* **291,** 116–124
14. Shimomura, Y., Agalliu, D., Vonica, A., Luria, V., Wajid, M., Baumer, A., Belli, S., Petukhova, L., Schinzel, A., Brivanlou, A. H., Barres, B. A., and Christiano, A. M. (2010) APCDD1 is a novel Wnt inhibitor mutated in hereditary hypotrichosis simplex. *Nature* **464,** 1043–1047
15. Ullah, M., Stich, S., Häupl, T., Eucker, J., Sittinger, M., and Ringe, J. (2013) Reverse differentiation as a gene filtering tool in genome expression profiling of adipogenesis for fat marker gene selection and their analysis. *PLoS ONE* **8,** e69754
16. Takahashi, M., Fujita, M., Furukawa, Y., Hamamoto, R., Shimokawa, T., Miwa, N., Ogawa, M., and Nakamura, Y. (2002) Isolation of a novel human gene, APCDD1, as a direct target of the β-Catenin/T-cell factor 4 complex with probable involvement in colorectal carcinogenesis. *Cancer Res.* **62,** 5651–5656
17. Chatterjee, T. K., Aronow, B. J., Tong, W. S., Manka, D., Tang, Y., Bogdanov, V. Y., Unruh, D., Blomkalns, A. L., Piegore, M. G., Jr., Weintraub, D. S., Rudich, S. M., Kuhel, D. G., Hui, D. Y., and Weintraub, N. L. (2013) Human coronary artery perivascular adipocytes overexpress genes re-

sponsible for regulating vascular morphology, inflammation, and hemostasis. *Physiol. Genomics* **45,** 697–709
18. Ross, S. E., Hemati, N., Longo, K. A., Bennett, C. N., Lucas, P. C., Erickson, R. L., and MacDougald, O. A. (2000) Inhibition of adipogenesis by Wnt signaling. *Science* **289,** 950–953
19. Chatterjee, T. K., Basford, J. E., Yiew, K. H., Stepp, D. W., Hui, D. Y., and Weintraub, N. L. (2014) Role of histone deacetylase 9 in regulating adipogenic differentiation and high fat diet-induced metabolic disease. *Adipocyte* **3,** 333–338
20. Kennell, J. A., and MacDougald, O. A. (2005) Wnt signaling inhibits adipogenesis through β-catenin-dependent and -independent mechanisms. *J. Biol. Chem.* **280,** 24004–24010
21. Sethi, J. K., and Vidal-Puig, A. (2010) Wnt signalling and the control of cellular metabolism. *Biochem. J.* **427,** 1–17
22. Longo, K. A., Wright, W. S., Kang, S., Gerin, I., Chiang, S. H., Lucas, P. C., Opp, M. R., and MacDougald, O. A. (2004) Wnt10b inhibits development of white and brown adipose tissues. *J. Biol. Chem.* **279,** 35503–35509
23. Kanazawa, A., Tsukada, S., Kamiyama, M., Yanagimoto, T., Nakajima, M., and Maeda, S. (2005) Wnt5b partially inhibits canonical Wnt/β-catenin signaling pathway and promotes adipogenesis in 3T3-L1 preadipocytes. *Biochem. Biophys. Res. Commun.* **330,** 505–510
24. Cruciat, C. M., and Niehrs, C. (2013) Secreted and transmembrane Wnt inhibitors and activators. *Cold Spring Harb. Perspect. Biol.* **5,** a015081
25. Lee, K. T., Park, E. W., Moon, S., Park, H. S., Kim, H. Y., Jang, G. W., Choi, B. H., Chung, H. Y., Lee, J. W., Cheong, I. C., Oh, S. J., Kim, H., Suh, D. S., and Kim, T. H. (2006) Genomic sequence analysis of a potential QTL region for fat trait on pig chromosome 6. *Genomics* **87,** 218–224
26. Kang, P., Lee, H. K., Glasgow, S. M., Finley, M., Donti, T., Gaber, Z. B., Graham, B. H., Foster, A. E., Novitch, B. G., Gronostajski, R. M., and Deneen, B. (2012) Sox9 and NFIA coordinate a transcriptional regulatory cascade during the initiation of gliogenesis. *Neuron* **74,** 79–94
27. Neupane, S., Sohn, W. J., Gwon, G. J., Kim, K. R., Lee, S., An, C. H., Suh, J. Y., Shin, H. I., Yamamoto, H., Cho, S. W., Lee, Y., and Kim, J. Y. (2015) The role of APCDD1 in epithelial rearrangement in tooth morphogenesis. *Histochem. Cell Biol.* **144,** 377–387
28. Viale-Bouroncle, S., Klingelhöffer, C., Ettl, T., and Morsczeck, C. (2015) The WNT inhibitor APCDD1 sustains the expression of β-catenin during the osteogenic differentiation of human dental follicle cells. *Biochem. Biophys. Res. Commun.* **457,** 314–317
29. Lee, H. K., Laug, D., Zhu, W., Patel, J. M., Ung, K., Arenkiel, B. R., Fancy, S. P., Mohila, C., and Deneen, B. (2015) Apcdd1 stimulates oligodendrocyte differentiation after white matter injury. *Glia* **63,** 1840–1849
30. Aonuma, H., Ogura, N., Takahashi, K., Fujimoto, Y., Iwai, S., Hashimoto, H., Ito, K., Kamino, Y., and Kondoh, T. (2012) Characteristics and osteogenic differentiation of stem/progenitor cells in the human dental follicle analyzed by gene expression profiling. *Cell Tissue Res.* **350,** 317–331
31. Gustafson, B., Hammarstedt, A., Hedjazifar, S., and Smith, U. (2013) Restricted adipogenesis in hypertrophic obesity: the role of WISP2, WNT, and BMP4. *Diabetes* **62,** 2997–3004
32. Joe, A. W., Yi, L., Even, Y., Vogl, A. W., and Rossi, F. M. (2009) Depot-specific differences in adipogenic progenitor abundance and proliferative response to high-fat diet. *Stem Cells* **27,** 2563–2570
33. Duval, C., Thissen, U., Keshtkar, S., Accart, B., Stienstra, R., Boekschoten, M. V., Roskams, T., Kersten, S., and Müller, M. (2010) Adipose tissue dysfunction signals progression of hepatic steatosis towards nonalcoholic steatohepatitis in C57BL/6 mice. *Diabetes* **59,** 3181–3191
34. Rigamonti, A., Brennand, K., Lau, F., and Cowan, C. A. (2011) Rapid cellular turnover in adipose tissue. *PLoS ONE* **6,** e17637
35. Chatterjee, T. K., Basford, J. E., Knoll, E., Tong, W. S., Blanco, V., Blomkalns, A. L., Rudich, S., Lentsch, A. B., Hui, D. Y., and Weintraub, N. L. (2014) HDAC9 knockout mice are protected from adipose tissue dysfunction and systemic metabolic disease during high-fat feeding. *Diabetes* **63,** 176–187
36. Schulte, D. M., Müller, N., Neumann, K., Oberhäuser, F., Faust, M., Güdelhöfer, H., Brandt, B., Krone, W., and Laudes, M. (2012) Pro-inflammatory wnt5a and anti-inflammatory sFRP5 are differentially regulated by nutritional factors in obese human subjects. *PLoS ONE* **7,** e32437
37. Catalán, V., Gómez-Ambrosi, J., Rodríguez, A., Pérez-Hernández, A. I., Gurbindo, J., Ramírez, B., Méndez-Giménez, L., Rotellar, F., Valentí, V., Moncada, R., Martí, P., Sola, I., Silva, C., Salvador, J., and Frühbeck, G. (2014) Activation of noncanonical Wnt signaling through WNT5A in visceral adipose tissue of obese subjects is related to inflammation. *J. Clin. Endocrinol. Metab.* **99,** E1407–E1417
38. Villeneuve, L. M., Reddy, M. A., and Natarajan, R. (2011) Epigenetics: deciphering its role in diabetes and its chronic complications. *Clin. Exp. Pharmacol. Physiol.* **38,** 451–459
39. Chen, L., Hou, J., Ye, L., Chen, Y., Cui, J., Tian, W., Li, C., and Liu, L. (2014) MicroRNA-143 regulates adipogenesis by modulating the MAP2K5-ERK5 signaling. *Sci. Rep.* **4,** 3819
40. Qin, L., Chen, Y., Niu, Y., Chen, W., Wang, Q., Xiao, S., Li, A., Xie, Y., Li, J., Zhao, X., He, Z., and Mo, D. (2010) A deep investigation into the adipogenesis mechanism: profile of microRNAs regulating adipogenesis by modulating the canonical Wnt/β-catenin signaling pathway. *BMC Genomics* **11,** 320
41. Qadir, A. S., Woo, K. M., Ryoo, H. M., and Baek, J. H. (2013) Insulin suppresses distal-less homeobox 5 expression through the up-regulation of microRNA-124 in 3T3-L1 cells. *Exp. Cell Res.* **319,** 2125–2134
42. Wang, Q., Li, Y. C., Wang, J., Kong, J., Qi, Y., Quigg, R. J., and Li, X. (2008) miR-17–92 cluster accelerates adipocyte differentiation by negatively regulating tumor-suppressor Rb2/p130. *Proc. Natl. Acad. Sci. U.S.A.* **105,** 2889–2894
43. Liu, S., Yang, Y., and Wu, J. (2011) TNFα-induced up-regulation of miR-155 inhibits adipogenesis by down-regulating early adipogenic transcription factors. *Biochem. Biophys. Res. Commun.* **414,** 618–624
44. Wei, J., Li, H., Wang, S., Li, T., Fan, J., Liang, X., Li, J., Han, Q., Zhu, L., Fan, L., and Zhao, R. C. (2014) let-7 enhances osteogenesis and bone formation while repressing adipogenesis of human stromal/mesenchymal stem cells by regulating HMGA2. *Stem Cells Dev.* **23,** 1452–1463
45. Lee, E. K., Lee, M. J., Abdelmohsen, K., Kim, W., Kim, M. M., Srikantan, S., Martindale, J. L., Hutchison, E. R., Kim, H. H., Marasa, B. S., Selimyan, R., Egan, J. M., Smith, S. R., Fried, S. K., and Gorospe, M. (2011) miR-130 suppresses adipogenesis by inhibiting peroxisome proliferator-activated receptor γ expression. *Mol. Cell. Biol.* **31,** 626–638
46. Kim, C., Lee, H., Cho, Y. M., Kwon, O. J., Kim, W., and Lee, E. K. (2013) TNFα-induced miR-130 resulted in adipocyte dysfunction during obesity-related inflammation. *FEBS Lett.* **587,** 3853–3858
47. Chatterjee, T. K., Idelman, G., Blanco, V., Blomkalns, A. L., Piegore, M. G., Jr., Weintraub, D. S., Kumar, S., Rajsheker, S., Manka, D., Rudich, S. M., Tang, Y., Hui, D. Y., Bassel-Duby, R., Olson, E. N., Lingrel, J. B., *et al.* (2011) Histone deacetylase 9 is a negative regulator of adipogenic differentiation. *J. Biol. Chem.* **286,** 27836–27847
48. Chatterjee, T. K., Stoll, L. L., Denning, G. M., Harrelson, A., Blomkalns, A. L., Idelman, G., Rothenberg, F. G., Neltner, B., Romig-Martin, S. A., Dickson, E. W., Rudich, S., and Weintraub, N. L. (2009) Proinflammatory phenotype of perivascular adipocytes: influence of high-fat feeding. *Circ. Res.* **104,** 541–549

A novel role for the Wnt inhibitor APCDD1 in adipocyte differentiation: Implications for diet-induced obesity

Nicole K. H. Yiew, Tapan K. Chatterjee, Yao Liang Tang, Rod Pellenberg, Brian K. Stansfield, Zsolt Bagi, David J. Fulton, David W. Stepp, Weiqin Chen, Vijay Patel, Vinayak M. Kamath, Sheldon E. Litwin, David Y. Hui, Steven M. Rudich, Ha Won Kim and Neal L. Weintraub

J. Biol. Chem. 2017, 292:6312-6324.
doi: 10.1074/jbc.M116.758078 originally published online February 27, 2017

Cardiovascular Drugs and Therapy
https://doi.org/10.1007/s10557-018-6821-y

ORIGINAL ARTICLE

Remote Effects of Transplanted Perivascular Adipose Tissue on Endothelial Function and Atherosclerosis

Tetsuo Horimatsu[1] · Aaron S. Patel[1] · Rosaria Prasad[1] · Lauren E. Reid[1] · Tyler W. Benson[1] · Abdalrahman Zarzour[1] · Mourad Ogbi[1] · Thiago Bruder do Nascimento[1] · Eric Belin de Chantemele[1] · Brian K. Stansfield[2] · Xin-Yun Lu[3] · Ha Won Kim[1] · Neal L. Weintraub[1]

Abstract

Purpose Perivascular adipose tissue (PVAT) surrounds the arterial adventitia and plays an important role in vascular homeostasis. PVAT expands in obesity, and inflamed PVAT can locally promote endothelial dysfunction and atherosclerosis. Here, using adipose tissue transplantation, we tested the hypothesis that expansion of PVAT can also remotely exacerbate vascular disease.

Methods Fifty milligrams of abdominal aortic PVAT was isolated from high-fat diet (HFD)-fed wild-type mice and transplanted onto the abdominal aorta of lean LDL receptor knockout mice. Subcutaneous and visceral adipose tissues were used as controls. After HFD feeding for 10 weeks, body weight, glucose/insulin sensitivity, and lipid levels were measured. Adipocytokine gene expression was assessed in the transplanted adipose tissues, and the thoracic aorta was harvested to quantify atherosclerotic lesions by Oil-Red O staining and to assess vasorelaxation by wire myography.

Results PVAT transplantation did not influence body weight, fat composition, lipid levels, or glucose/insulin sensitivity. However, as compared with controls, transplantation of PVAT onto the abdominal aorta increased thoracic aortic atherosclerosis. Furthermore, PVAT transplantation onto the abdominal aorta inhibited endothelium-dependent relaxation in the thoracic aorta. MCP-1 and TNF-α expression was elevated, while adiponectin expression was reduced, in the transplanted PVAT tissue, suggesting augmented inflammation as a potential mechanism for the remote vascular effects of transplanted PVAT.

Conclusions These data suggest that PVAT expansion and inflammation in obesity can remotely induce endothelial dysfunction and augment atherosclerosis. Identifying the underlying mechanisms may lead to novel approaches for risk assessment and treatment of obesity-related vascular disease.

Keywords Perivascular adipose tissue · Fat transplantation · Endothelial dysfunction · Atherosclerosis · Inflammation

Introduction

Perivascular adipose tissue (PVAT) surrounds most large vessels except the cerebral vasculature and had traditionally been thought to simply provide structural support for blood vessels. Over the past two decades, however, PVAT has become recognized as a physiologically and metabolically active endocrine tissue with important effects on vascular function and disease states [1, 2]. Under physiological conditions, PVAT may exert a protective role against neointimal formation through release of NO and anti-inflammatory adiponectin [3]. However, mounting evidence suggests that in disease states, PVAT contributes to endothelial dysfunction,

Electronic supplementary material The online version of this article (https://doi.org/10.1007/s10557-018-6821-y) contains supplementary material, which is available to authorized users.

✉ Neal L. Weintraub
nweintraub@augusta.edu

[1] Department of Medicine, Cardiology Division, Vascular Biology Center, Medical College of Georgia at Augusta University, 1460 Laney Walker Blvd, Augusta, GA 30912, USA

[2] Pediatrics and Vascular Biology Center, Medical College of Georgia at Augusta University, Augusta, GA, USA

[3] Department of Neuroscience and Regenerative Medicine, Medical College of Georgia at Augusta University, Augusta, GA, USA

Published online: 10 August 2018

neointimal formation, atherosclerosis, and other cardiovascular diseases, including abdominal aortic aneurysms, aortic stiffness, and vasculitis [4–12]. Mechanistically, these effects have been linked to local inflammation, oxidative stress, and decreased nitric oxide (NO) release from endothelium along with uncoupling of endothelial NO synthase (eNOS) in PVAT [13, 14].

In rodent models of obesity, PVAT acquires a pro-inflammatory phenotype with macrophage and leukocyte accumulation and production of pro-inflammatory adipocytokines which contribute to migration of vascular smooth muscle cells and myofibroblasts into the neointima [15]. Recent studies suggest that dysfunctional and inflamed PVAT is also associated with metabolic disease, hallmarked by insulin resistance and glucose intolerance. Indeed, in humans, fat surrounding the heart and great vessels expands in obesity, correlating with increased visceral fat mass and insulin resistance [16]. Moreover, under basal conditions, human perivascular adipocytes secrete much higher levels of pro-inflammatory cytokines such as interleukin (IL)-6, IL-8, and monocyte chemoattractant protein (MCP)-1 compared with other visceral (perirenal) adipocytes [17]. Together, these findings raise the possibility that expansion of PVAT in obesity could also promote vascular disease at distant sites, beyond its well-described function as a local paracrine mediator.

In order to investigate remote effects of PVAT on vascular disease, we adopted an adipose tissue transplantation model. Transplantation of adipose tissues onto arteries is a useful approach to investigate the local impact of PVAT on vascular diseases [5, 18, 19]. Our laboratory previously established a PVAT transplantation model to investigate the role of PVAT in neointimal formation in conjunction with wire injury of the carotid artery [20]. Adapting a similar PVAT transplantation model to the abdominal aorta, this study investigated the systemic and remote effects of PVAT on metabolic disease and atherosclerosis. We found that transplanting just 50 mg of PVAT harvested from obese mice onto the abdominal aorta of recipient hyperlipidemic mice was sufficient to induce endothelial dysfunction and augment atherosclerosis in the remote thoracic aorta. These systemic vascular effects of PVAT were independent of changes in body weight, fat composition, insulin and glucose sensitivity, or plasma lipid levels. Although the precise mechanisms remain to be determined, this study provides the first evidence showing a systemic effect of PVAT on vascular disease.

Methods

Adipose Tissue Transplantation

Using a dissecting microscope, 15 or 50 mg of white PVAT was isolated from abdominal aortas of donor of C57Bl/6J mice fed a HFD (60% kcal fat, D12492, Research Diets, New Brunswick, NJ, USA) for more than 10 weeks. Subcutaneous adipose tissue (SAT), and in some experiments visceral adipose tissue (VAT), was isolated from the HFD-fed mice for use as controls. The isolated adipose tissues were transplanted onto the infrarenal abdominal aortas of 8-week-old male LDL receptor knockout ($LDLR^{-/-}$, C57Bl/6J background) mice. In brief, after a midline abdominal incision, the abdominal aorta between the left renal vein to the iliac bifurcation was carefully mobilized from the retroperitoneum using microsurgery forceps. Then, after removing the surrounding connecting tissue, adipose tissue was transplanted onto the abdominal aorta and affixed using a synthetic absorbable surgical tissue adhesive (Tissuemend II, Veterinary Products Laboratories, Phoenix, AZ, USA). To account for the impact of surgical manipulation, adipose tissue transplanted mice were compared against sham-operated (non-transplanted) mice otherwise treated identically. After recovering from surgery, the mice were maintained on a HFD for up to 12 weeks, and body weight was monitored weekly. The mice were sacrificed 10–12 weeks after transplantation, and aortas and transplanted adipose tissues were collected for further studies. Endogenous visceral (epididymal) and subcutaneous adipose tissues were carefully dissected and weighed as previously described [21]. Blood was also withdrawn via ventricular puncture and assayed for lipid profiling. Mice were housed at thermoneutrality (30 °C) throughout the study with a 12-h light/dark cycle. All animal studies were registered and approved by the Institutional Animal Care and Use Committee of the Medical College of Georgia at Augusta University.

Nuclear Magnetic Resonance

Fat composition was measured by quantitative nuclear magnetic resonance (NMR) as previously described [21].

Total Cholesterol and Triglyceride Measurement

Total cholesterol and triglyceride were quantified using commercial assays (Wako Pure Chemical Industries, Osaka, Japan) as previously described [22].

Insulin and Glucose Tolerance

Insulin and glucose tolerance tests (ITT, GTT) were performed using glucose strips as previously described [21]. Briefly, at 10 weeks after adipose tissue transplantation, glucose levels were measured in blood obtained from tail veins immediately before and every 10 min after intraperitoneal injection of 0.75 U/kg body weight of human

insulin (Humulin R®, Lilly) in mice fasted for 6 h. One week later, glucose levels were also assessed before and every 10 min after intraperitoneal injection of 2 g/kg body weight of glucose in mice fasted for 24 h.

Atherosclerosis Lesion Analysis in Thoracic Aorta

LDLR$^{-/-}$ mice were fed a HFD for 10 weeks after adipose tissue transplantation. After euthanizing mice, the thoracic aorta (from the aortic root to the diaphragm) was isolated and fixed in 4% paraformaldehyde for 24 h, and atherosclerotic lesions were stained with Oil-red O. Images were captured using a microscope digital camera (MU500, AmScope, USA). Quantitative analysis of atherosclerotic lesions was performed using Image-Pro Plus software (Media Cybernetics).

Wire Myography

Thoracic aortas were carefully isolated and cleaned of surrounding tissue, dissected into 2–3 mm of four rings, and mounted on a wire myography as described previously [23]. In brief, two tungsten wires were inserted into the lumen of the arteries and fixed to a force transducer and a micrometer. Arteries were bathed in a physiological salt solution and equilibrated for 60 min. Arterial viability was determined twice with a potassium (KCl)-rich solution (60 mmol/L). Then, dose-dependent constriction curve response to KCl (10 mmol/L to 60 mmol/L) was performed. Endothelium-dependent and -independent relaxation curves were respectively tested with acetylcholine (ACh, 0.1 nmol/L to 100 μmol/L) and sodium nitroprusside (SNP, 0.01 nmol/L to 10 μmol/L). Vessels were preconstricted to 50 to 80% of their maximal 60 mM KCl constriction with serotonin before assessing relaxation responses. Constriction responses to KCl are presented in grams of tension, while relaxation responses to acetylcholine and sodium nitroprusside are expressed as a percentage of constriction induced by serotonin. The relaxation curves were fitted by nonlinear regression analysis, and maximum responses (Emax) were compared amongst the groups.

RNA Extraction and Quantitative RT-PCR

RNA was isolated with a commercially available kit (RNeasy® mini kit, Qiagen), and quantitative analysis of mRNA expression was performed using an MX3000p thermal cycler system and Brilliant II SYBR Green qPCR Master Mix kit (Agilent Technologies). mRNA expression was normalized to the housekeeping gene Arbp and analyzed according to the $2^{-\Delta\Delta Ct}$ method. Primer sequences are listed in the Supplementary Table 1.

Histology

Abdominal aortas with surrounding adipose tissues were fixed in 10% formaldehyde and embedded in paraffin. Paraffin sections were stained with hematoxylin-eosin (H&E).

Statistical Analysis

Data were expressed as mean ± standard error of the mean. Differences between two groups were analyzed by Student's t test. Multiple group datasets were evaluated for normality, and differences were analyzed by one-way ANOVA followed by Bonferroni post-hoc testing. A p value < 0.05 was considered statistically significant. All statistical analyses were performed using GraphPad Prism version 7.0 for Mac OS X (GraphPad Software, La Jolla California, USA).

Results

Adipose Tissues Transplantation in Abdominal Aorta

Representative images of donor SAT or PVAT transplanted to abdominal (infrarenal) aorta of recipient LDLR$^{-/-}$ mice are shown in Fig. 1a. Histological analysis confirmed that both SAT and PVAT were well engrafted into the adventitia of recipient aorta at 9 weeks after transplantation (Fig. 1b). The transplanted PVAT exhibited typical histological appearance of white adipose tissue (Fig. 1b).

Adipose Tissue Transplantation Did Not Alter Body Weight, Fat Composition or Lipid Levels in Recipient LDLR$^{-/-}$ Mice

All mice progressively gained weight on the HFD following adipose tissue transplantation, and no significant differences in weight (assessed either by absolute grams or percentage change) were observed amongst the various groups of mice (Fig. 2a, b). Likewise, body composition (fat versus lean mass) measured by nuclear magnetic resonance (Fig. 2c) and endogenous subcutaneous and visceral adipose tissues masses were not significantly influenced by adipose tissue transplantation (Fig. 2d). Lipid analysis at 12 weeks after adipose tissue transplantation demonstrated that levels of total cholesterol and triglycerides in serum were similar amongst the various groups (Fig. 2e, f). These results suggest that neither SAT nor PVAT transplantation affected systemic parameters such as body weight, fat composition, or lipid profile in recipient LDLR$^{-/-}$ mice.

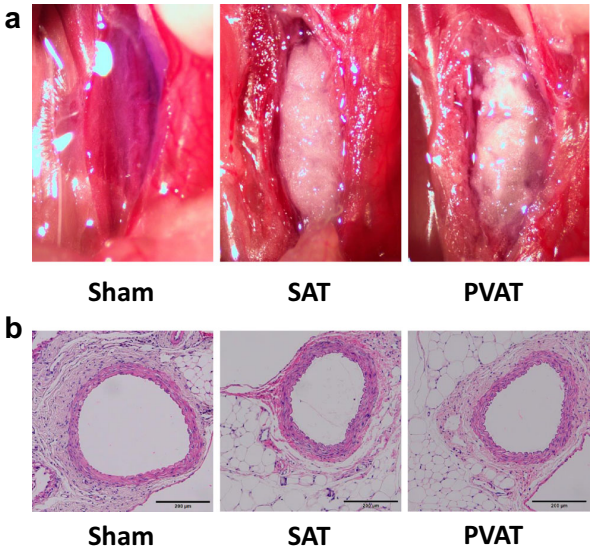

Fig. 1 Representative images and H&E staining of donor SAT and PVAT transplanted to infrarenal abdominal aorta. **a** Adipose tissue transplantation was performed onto infrarenal abdominal aorta, and images taken at the conclusion of the procedure are shown here. **b** H&E staining of transplanted adipose tissues on abdominal aorta at 10 weeks after transplantation

Adipose Tissue Transplantation Did Not Affect Insulin Sensitivity or Glucose Tolerance

Blood glucose levels prior to intraperitoneal administration of either insulin or glucose were comparable amongst the groups (Fig. 3a, b). ITT demonstrated that the hypoglycemic response to insulin was similar at each time point amongst all groups (Fig. 3a). Hyperglycemic responses to glucose, examined by GTT, were likewise similar amongst all groups (Fig. 3b), suggesting that adipose tissue transplantation did not affect total body insulin sensitivity or glucose tolerance.

Abdominal Transplantation of PVAT, but Not SAT or VAT, Augmented Atherosclerosis in Thoracic Aorta

Quantitative analysis indicated that the extent of atherosclerotic lesions in aortic arch and thoracic aorta was significantly higher in the PVAT transplantation group compared with the other groups (Sham; 1.67 ± 0.21, SAT; 2.33 ± 0.45, VAT; 2.43 ± 0.56, PVAT; 4.5 ± 0.68, $p = 0.011$, Fig. 4a, b). Given that PVAT transplantation

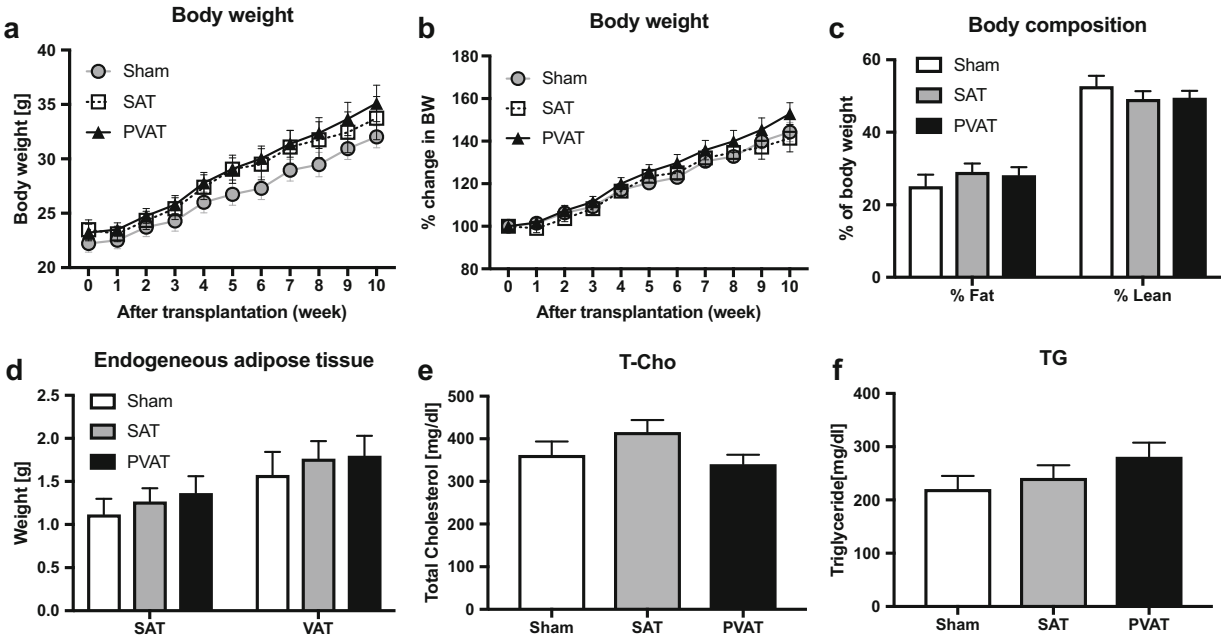

Fig. 2 Body weight, fat composition, endogenous adipose tissue weights, and serum lipid levels after adipose tissue transplantation. **a**, **b** Body weight gain during 60% HFD feeding for 10 weeks after transplantation in the Sham (circle), SAT (square), and PVAT (triangle) groups ($n = 14$). Absolute weight is shown in (**a**), and % change in body weight is shown in (**b**). **c** Fat and lean mass measured by nuclear magnetic resonance spectroscopy ($n = 14$). **d** Endogenous SAT and VAT were harvested and weighed at 12 weeks after transplantation ($n = 10$). **e** Plasma total cholesterol (T-Cho) and **f** triglyceride (TG) levels in mice fed HFD for 10–12 weeks after transplantation ($n = 14$). **c**–**f** Sham (open columns), SAT (gray columns), PVAT (black columns)

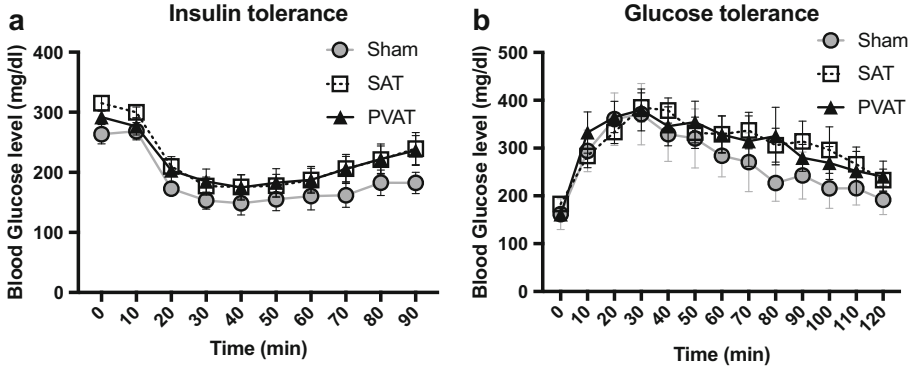

Fig. 3 Effects of adipose tissue transplantation on insulin sensitivity and glucose tolerance. Hypoglycemic responses to insulin at 10 weeks after transplantation (**a**), and hyperglycemic responses to glucose at 11 weeks after transplantation, in the Sham (circle), SAT (square), and PVAT (triangle) groups ($n = 14$)

did not significantly affect systemic metabolic or lipid parameters, this finding suggested that increased abdominal aortic PVAT might augment thoracic aortic atherosclerosis by promoting inflammation. Interestingly, expression of the inflammatory genes MCP-1 and TNF-α was elevated in transplanted PVAT, while expression of adiponectin, an anti-inflammatory adipokine, was markedly reduced (Fig. 4c–e).

PVAT Transplanted in Abdominal Aorta Promoted Endothelial Dysfunction in Thoracic Aorta

Dose-dependent constriction responses to KCl in thoracic aorta were comparable amongst the groups (Fig. 5a, b). Interestingly, following sub-maximal preconstruction by phenylephrine, Ach-induced relaxation (10 μmol/L and 100 μmol/L) was significantly lower in the PVAT transplanted

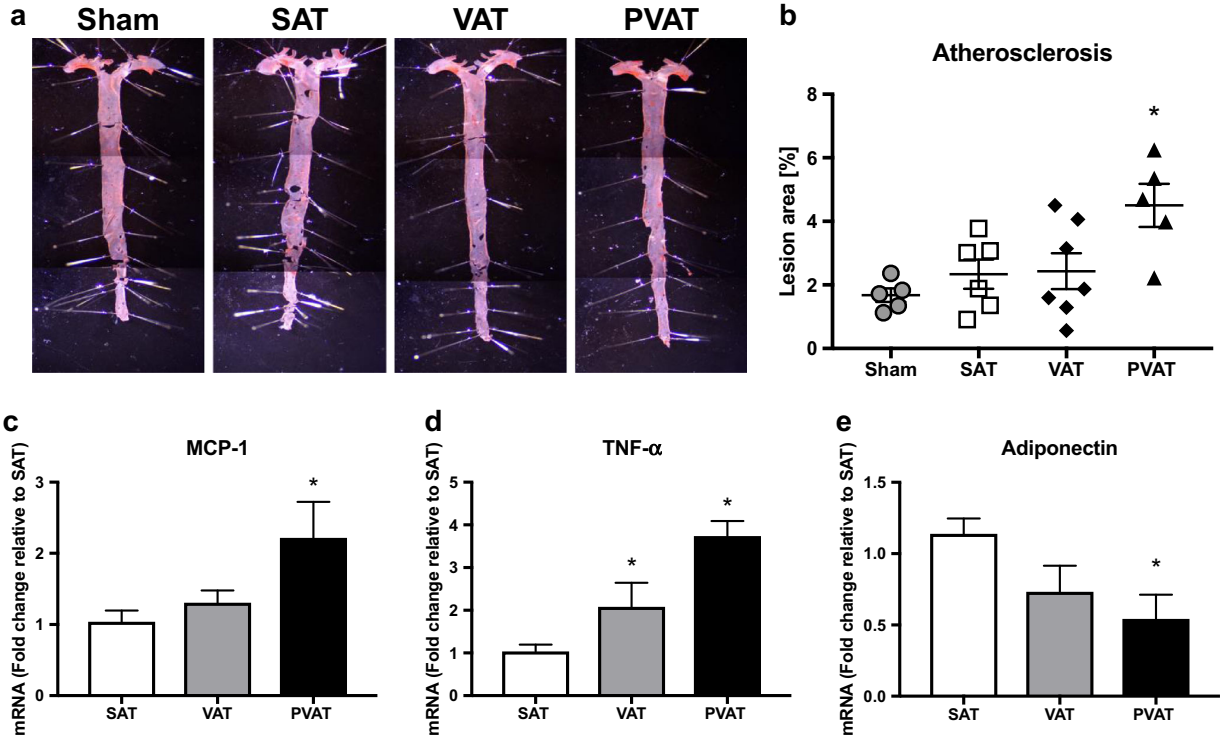

Fig. 4 Quantification of atherosclerosis in thoracic aorta, and inflammation in the transplanted abdominal aortic adipose tissues. **a**)After sham procedure or adipose tissue transplantation to the abdominal aortas, thoracic aortas were harvested following 10 weeks of HFD feeding, and atherosclerotic lesions were stained by Oil-red O. Representative whole mount images are shown. **b** Quantitative analysis of atherosclerotic lesions (*$p < 0.05$ vs Sham, SAT, and VAT, $n = 5–6$). **c**, **d**, **e** mRNA expression of adipocytokines in transplanted adipose tissues after 10 weeks of HFD feeding following transplantation (*$p < 0.05$ vs SAT, $n = 5–6$)

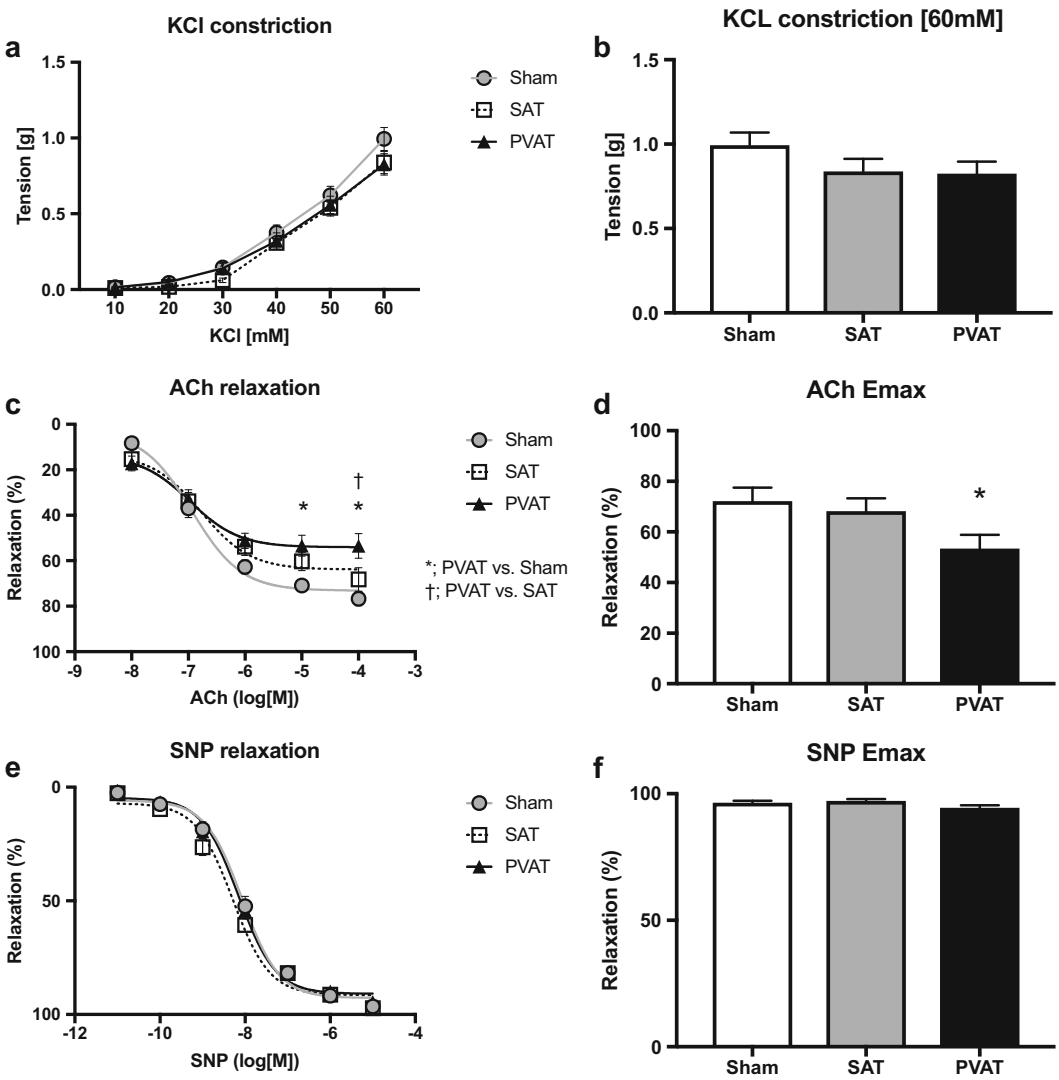

Fig. 5 Effects of adipose tissue transplantation to the abdominal aorta on vascular function in the thoracic aorta. **a** Dose-dependent constriction responses to KCl in the Sham (circle), SAT (square), and PVAT (triangle) groups ($n = 9$). **b** Quantitative analysis of vasoconstriction responses to 60 mM KCl. **c** Endothelium-dependent relaxation responses to acetylcholine (ACh) ($n = 9$, $^*p < 0.05$ vs SAT, $\dagger p < 0.05$ vs VAT). **d** Maximum relaxation (Emax) responses to 100 μmol/L of ACh ($^*p < 0.05$ vs SAT). **e** Endothelium-independent relaxation responses to sodium nitroprusside (SNP) ($n = 9$). **f**)Emax response to 10 μmol/L of SNP

group compared with the sham or SAT transplanted groups (Fig. 5c, d). In contrast, endothelium-independent relaxation induced by sodium nitroprusside was unaffected by PVAT transplantation (Fig. 5e, f), suggesting that increased abdominal aortic PVAT can remotely impair endothelial function.

Discussion

PVAT has been recognized as a unique adipose tissue depot, and mounting evidence indicates that both pro- and anti-inflammatory adipocytokines secreted from PVAT regulate vascular homeostasis through paracrine mechanisms. The quantity and pro-inflammatory state of PVAT surrounding atherosclerosis-prone vessels increases in obesity, suggesting that dysfunctional PVAT may contribute locally to atherosclerosis. Here, we demonstrate that transplantation of just 50 mg of PVAT to the abdominal aortas of $LDLR^{-/-}$ mice augments atherosclerosis and promotes endothelial dysfunction at a remote site (the thoracic aorta). These effects were independent of changes in body weight, fat/adipose tissue mass, insulin and glucose sensitivity, and plasma lipid levels. Expression of MCP-1 and TNF-α was significantly increased in the transplanted PVAT, raising the possibility that inflammatory

mediators produced by dysfunctional PVAT in obesity could augment systemic vascular disease.

Endothelial dysfunction, characterized by impaired endothelium-dependent vasodilation and a pro-inflammatory state, is a key event in the development of atherosclerosis. Diminished nitric oxide (NO) availability and an imbalance between endothelium-derived relaxing and contracting factors are well established mechanisms leading to endothelial dysfunction. Previous studies have suggested a contributory role of PVAT to endothelial dysfunction. Lee et al. reported that in obesity, PVAT reduces NO production through increased expression of caveolin-1, which negatively regulates endothelial NO synthase (eNOS) [24]. PVAT also may induce endothelial dysfunction via protein kinase C-β dependent phosphorylation and inactivation of eNOS [25]. Inflamed PVAT mediated by a HFD feeding induces eNOS uncoupling both in endothelium and PVAT, which reduces NO production contributing to impaired endothelial dysfunction [13]. However, the aforementioned mechanisms have been linked to local rather than systemic perturbations in endothelial function. Using an adipose tissue transplantation approach, our study demonstrated that PVAT, but not SAT or VAT, can also promote endothelial dysfunction in remote blood vessels. To the best of our knowledge, this is the first evidence demonstrating that dysfunctional PVAT can remotely perturb endothelial function, though the underlying mechanisms remain to be determined.

We have reported that human perivascular adipocytes exhibit a pro-atherogenic phenotype, releasing substantially more pro-inflammatory cytokines as compared with adipocytes derived from other depots (e.g., SAT, omental or perirenal) [17]. MCP-1 is a key regulator of macrophage infiltration into adipose tissue, and MCP-1 expressed in transplanted PVAT promotes neointimal hyperplasia in wire-injured carotid artery [20]. In this study, MCP-1 expression was significantly higher in transplanted PVAT as compared with SAT or VAT, but whether this small amount of transplanted PVAT was sufficient to increase circulating levels of MCP-1, or other inflammatory mediators, is unclear. On the other hand, adiponectin also plays an important role in modulating inflammation, and decreased levels of circulating adiponectin contribute to atherosclerosis and insulin resistance. Previous studies showed that adiponectin released from PVAT plays an important local role in vasorelaxation through paracrine properties [26]. Adiponectin may oppose vascular constriction through phosphorylation of eNOS at Ser^{1177} to stimulate endothelial NO production [27]. Interestingly, transplantation of PVAT isolated from adiponectin$^{-/-}$ mice onto carotid arteries of apolipoprotein $E^{-/-}$ mice led to accelerated plaque formation [8]. Our data also showed that adiponectin expression in transplanted PVAT was markedly lower than in SAT or VAT at 10 weeks after transplantation, suggesting a potential mechanism of amplification of inflammation in the transplanted PVAT. These results and previous data suggest that an imbalance in pro- and anti-inflammatory mediators in dysfunctional PVAT potentially could remotely promote atherosclerosis as well as endothelial dysfunction, although this hypothesis will require further testing that is beyond the scope of the present study.

In addition, our findings raise a number of important questions. First, the PVAT used for transplantation experiments was harvested from obese mice fed a 60% HFD and maintained under thermoneutral conditions. PVAT in rodents exhibits features of both white and brown adipose tissue depending on the anatomic location, and brown-like function of PVAT has beneficial metabolic effects associated with thermogenesis and fatty acid combustion to ameliorate atherosclerosis [28]. PVAT releases both pro-inflammatory and anti-inflammatory adipocytokines, but when challenged by HFD, this balance is strongly shifted towards inflammation. Indeed, dysfunctional PVAT mediated by HFD plays an important role in atherosclerosis and hypertension [12, 29]. It is entirely possible that transplanting PVAT from mice fed a chow diet, or a HFD with lower fat content, might have produced different (perhaps even protective) effects on endothelial function or atherosclerosis. Likewise, maintaining the mice under ambient temperature conditions might have fostered "browning" of the PVAT to offset the phenotypic changes of the HFD [30]. Such findings would be in keeping with the notion that PVAT has pleiotropic effects on vascular function and may only become pro-atherogenic under certain conditions. Second, the absolute amount of transplanted PVAT required to elicit systemic vascular effects is unknown. In preliminary studies, 15 mg of PVAT was transplanted onto abdominal aorta, and no significant differences were seen in vascular function or atherosclerosis of the aortic arch and thoracic aorta (data not shown), suggesting that a critical amount of PVAT is required. Importantly, researchers should take these findings into account when designing experiments to test the local (paracrine) effects of PVAT on the vasculature. Finally, it remains to be determined whether the systemic effects of the transplanted PVAT were dependent upon a physical association with the vasculature. Additional experiments in which PVAT is transplanted to different locations (vascular vs. non-vascular) will be required to address this question.

In conclusion, this study suggests that HFD-induced inflamed PVAT could contribute to endothelial dysfunction and atherosclerosis in a remote manner, possibly through production of PVAT-derived pro-inflammatory cytokines. These findings support the notion that PVAT is a unique adipose tissue depot that has the potential to profoundly perturb the vasculature under certain conditions, and that targeting PVAT may be a promising therapeutic strategy for treating and preventing obesity-related vascular disease.

Funding This study was funded by grants HL124097, HL126949, HL134354, and AR070029 from the National Institutes of Health (N.L.W).

Compliance with Ethical Standards

Conflict of Interest The authors declare that they have no conflict of interest.

Ethical Approval All applicable international, national, and/or institutional guidelines for the care and use of animals were followed. This article does not contain any studies with human participants.

References

1. Verhagen SN, Visseren FL. Perivascular adipose tissue as a cause of atherosclerosis. Atherosclerosis. 2011;214(1):3–10.
2. Fitzgibbons TP, Czech MP. Epicardial and perivascular adipose tissues and their influence on cardiovascular disease: basic mechanisms and clinical associations. J Am Heart Assoc. 2014;3(2): e000582.
3. Cai XJ, Li CJ, Chen L, Rong YY, Zhang Y, Zhang M. A hypothesis: adiponectin mediates anti-atherosclerosis via adventitia-AMPK-iNOS pathway. Med Hypotheses. 2008;70(5):1044–7.
4. Aghamohammadzadeh R, Unwin RD, Greenstein AS, Heagerty AM. Effects of obesity on perivascular adipose tissue vasorelaxant function: nitric oxide, inflammation and elevated systemic blood pressure. J Vasc Res. 2015;52(5):299–305.
5. Takaoka M, Nagata D, Kihara S, Shimomura I, Kimura Y, Tabata Y, et al. Periadventitial adipose tissue plays a critical role in vascular remodeling. Circ Res. 2009;105(9):906–11.
6. Tanaka K, Komuro I, Sata M. Vascular cells originating from perivascular adipose tissue contribute to vasa vasorum neovascularization in atherosclerosis. Circulation. 2015;132(Suppl_3):A14910.
7. Police SB, Thatcher SE, Charnigo R, Daugherty A, Cassis LA. Obesity promotes inflammation in periaortic adipose tissue and angiotensin II-induced abdominal aortic aneurysm formation. Arterioscler Thromb Vasc Biol. 2009;29(10):1458–64.
8. Li C, Wang Z, Wang C, Ma Q, Zhao Y. Perivascular adipose tissue-derived adiponectin inhibits collar-induced carotid atherosclerosis by promoting macrophage autophagy. PLoS One. 2015;10(5): e0124031.
9. Sakaue T, Suzuki J, Hamaguchi M, Suehiro C, Tanino A, Nagao T et al. Perivascular adipose tissue angiotensin II type 1 receptor promotes vascular inflammation and aneurysm formation. Hypertension. 2017;70(4):780–789.
10. Fleenor BS, Eng JS, Sindler AL, Pham BT, Kloor JD, Seals DR. Superoxide signaling in perivascular adipose tissue promotes age-related artery stiffness. Aging Cell. 2014;13(3):576–8.
11. Hollan I, Prayson R, Saatvedt K, Almdahl SM, Nossent HC, Mikkelsen K, et al. Inflammatory cell infiltrates in vessels with different susceptibility to atherosclerosis in rheumatic and non-rheumatic patients. Circ J. 2008;72(12):1986–92.
12. Öhman M, Luo W, Wang H, Guo C, Abdallah W, Russo H, et al. Perivascular visceral adipose tissue induces atherosclerosis in apolipoprotein E deficient mice. Atherosclerosis. 2011;219(1):33–9.
13. Xia N, Horke S, Habermeier A, Closs EI, Reifenberg G, Gericke A, et al. Uncoupling of endothelial nitric oxide synthase in perivascular adipose tissue of diet-induced obese mice. Arterioscler Thromb Vasc Biol. 2016;36(1):78–85.
14. Xia N, Förstermann U, Li H. Effects of resveratrol on eNOS in the endothelium and the perivascular adipose tissue. Ann N Y Acad Sci. 2017;1403:132–41.
15. Wang P, Xu T-Y, Guan Y-F, Su D-F, Fan G-R, Miao C-Y. Perivascular adipose tissue-derived visfatin is a vascular smooth muscle cell growth factor: role of nicotinamide mononucleotide. Cardiovasc Res. 2009;81(2):370–80.
16. Iacobellis G, Ribaudo MC, Assael F, Vecci E, Tiberti C, Zappaterreno A, et al. Echocardiographic epicardial adipose tissue is related to anthropometric and clinical parameters of metabolic syndrome: a new indicator of cardiovascular risk. J Clin Endocrinol Metab. 2003;88(11):5163–8.
17. Chatterjee TK, Stoll LL, Denning GM, Harrelson A, Blomkalns AL, Idelman G, et al. Proinflammatory phenotype of perivascular adipocytes: influence of high-fat feeding. Circ Res. 2009;104(4):541–9.
18. Matsuda M, Shimomura I, Sata M, Arita Y, Nishida M, Maeda N, et al. Role of adiponectin in preventing vascular stenosis: the missing link of adipo-vascular axis. J Biol Chem. 2002;277(40):37487–91.
19. Tian Z, Miyata K, Tazume H, Sakaguchi H, Kadomatsu T, Horio E, et al. Perivascular adipose tissue-secreted angiopoietin-like protein 2 (Angptl2) accelerates neointimal hyperplasia after endovascular injury. J Mol Cell Cardiol. 2013;57:1–12.
20. Manka D, Chatterjee TK, Stoll LL, Basford JE, Konaniah ES, Srinivasan R, et al. Transplanted perivascular adipose tissue accelerates injury-induced neointimal hyperplasia: role of monocyte chemoattractant protein-1. Arterioscler Thromb Vasc Biol. 2014;34(8):1723–30.
21. Benson TW, Weintraub DS, Crowe M, Yiew NKH, Popoola O, Pillai A, et al. Deletion of the Duffy antigen receptor for chemokines (DARC) promotes insulin resistance and adipose tissue inflammation during high fat feeding. Mol Cell Endocrinol. 2018;473:79–88.
22. Qiang S, Nakatsu Y, Seno Y, Fujishiro M, Sakoda H, Kushiyama A, et al. Treatment with the SGLT2 inhibitor luseogliflozin improves nonalcoholic steatohepatitis in a rodent model with diabetes mellitus. Diabetol Metab Syndr. 2015;7:104.
23. Bruder-Nascimento T, Kennard S, Antonova G, Mintz JD, Bence KK, Belin de Chantemele EJ. Ptp1b deletion in pro-opiomelanocortin neurons increases energy expenditure and impairs endothelial function via TNF-alpha dependent mechanisms. Clin Sci (Lond). 2016;130(11):881–93.
24. Lee MH, Chen SJ, Tsao CM, Wu CC. Perivascular adipose tissue inhibits endothelial function of rat aortas via caveolin-1. PLoS One. 2014;9(6):e99947.
25. Payne GA, Bohlen HG, Dincer UD, Borbouse L, Tune JD. Periadventitial adipose tissue impairs coronary endothelial function via PKC-beta-dependent phosphorylation of nitric oxide synthase. Am J Physiol Heart Circ Physiol. 2009;297(1):H460–5.
26. Ketonen J, Shi J, Martonen E, Mervaala E. Periadventitial adipose tissue promotes endothelial dysfunction via oxidative stress in diet-induced obese C57Bl/6 mice. Circ J. 2010;74(7):1479–87.
27. Cheng KK, Lam KS, Wang Y, Huang Y, Carling D, Wu D, et al. Adiponectin-induced endothelial nitric oxide synthase activation and nitric oxide production are mediated by APPL1 in endothelial cells. Diabetes. 2007;56(5):1387–94.
28. Brown NK, Zhou Z, Zhang J, Zeng R, Wu J, Eitzman DT, et al. Perivascular adipose tissue in vascular function and disease: a review of current research and animal models. Arterioscler Thromb Vasc Biol. 2014;34(8):1621–30.
29. Chang L, Milton H, Eitzman DT, Chen YE. Paradoxical roles of perivascular adipose tissue in atherosclerosis and hypertension. Circ J. 2013;77(1):11–8.
30. Chang L, Villacorta L, Li R, Hamblin M, Xu W, Dou C, et al. Loss of perivascular adipose tissue on peroxisome proliferator-activated receptor-gamma deletion in smooth muscle cells impairs intravascular thermoregulation and enhances atherosclerosis. Circulation. 2012;126(9):1067–78.

Fouda et al. *Cell Death and Disease* (2018)9:1001
DOI 10.1038/s41419-018-1051-6

Cell Death & Disease

ARTICLE Open Access

Arginase 1 promotes retinal neurovascular protection from ischemia through suppression of macrophage inflammatory responses

Abdelrahman Y. Fouda[1,2,3], Zhimin Xu[1,2,3], Esraa Shosha[1,2,3], Tahira Lemtalsi[1,2,3], Jijun Chen[4], Haroldo A. Toque[4,2], Rebekah Tritz[2], Xuezhi Cui[3,5], Brian K. Stansfield[2,6], Yuqing Huo[2,5], Paulo C. Rodriguez[7], Sylvia B. Smith[3,5,8], R. William Caldwell[4,3], S. Priya Narayanan[1,2,3,9] and Ruth B. Caldwell[1,2,3,5,8]

Abstract

The lack of effective therapies to limit neurovascular injury in ischemic retinopathy is a major clinical problem. This study aimed to examine the role of ureohydrolase enzyme, arginase 1 (A1), in retinal ischemia-reperfusion (IR) injury. A1 competes with nitric oxide synthase (NOS) for their common substrate L-arginine. A1-mediated L-arginine depletion reduces nitric oxide (NO) formation by NOS leading to vascular dysfunction when endothelial NOS is involved but prevents inflammatory injury when inducible NOS is involved. Studies were performed using wild-type (WT) mice, global $A1^{+/-}$ knockout (KO), endothelial-specific A1 KO, and myeloid-specific A1 KO mice subjected to retinal IR injury. Global as well as myeloid-specific A1 KO mice showed worsened IR-induced neuronal loss and retinal thinning. Deletion of A1 in endothelial cells had no effect, while treatment with PEGylated (PEG) A1 improved neuronal survival in WT mice. In addition, $A1^{+/-}$ KO mice showed worsened vascular injury manifested by increased acellular capillaries. Western blotting analysis of retinal tissue showed increased inflammatory and necroptotic markers with A1 deletion. In vitro experiments showed that macrophages lacking A1 exhibit increased inflammatory response upon LPS stimulation. PEG-A1 treatment dampened this inflammatory response and decreased the LPS-induced metabolic reprogramming. Moreover, intravitreal injection of A1 KO macrophages or systemic macrophage depletion with clodronate liposomes increased neuronal loss after IR injury. These results demonstrate that A1 reduces IR injury-induced retinal neurovascular degeneration via dampening macrophage inflammatory responses. Increasing A1 offers a novel strategy for limiting neurovascular injury and promoting macrophage-mediated repair.

Introduction

Ischemia-induced retinal neurovascular injury is a primary contributor in blinding diseases that affect neonates (retinopathy of prematurity), working age adults (diabetic retinopathy), and the elderly (branch vein occlusion). The retinal ischemia-reperfusion (IR) injury model has been widely used to study the mechanisms of neurovascular injury in these and other diseases of the central nervous system (CNS) such as stroke[1–5]. Therefore, it provides an excellent model to study the neurovascular damage characteristic of many CNS disorders. The lack of understanding of the mechanisms of IR injury-induced neuronal and vascular injury is a critical barrier for developing clinically effective treatments for these conditions.

Correspondence: Ruth B. Caldwell (rcaldwel@augusta.edu)
[1]Charlie Norwood VA Medical Center, Augusta, GA, USA
[2]Vascular Biology Center, Augusta University, Augusta, GA, USA
Full list of author information is available at the end of the article.
Edited by S. Lavandero

SPRINGER NATURE CDDpress

Arginase has two isoforms, arginase 1 (A1) and arginase 2 (A2)[6]. A1, the cytosolic isoform, is strongly expressed in the liver, where it is the central player in the urea cycle[7]. The mitochondrial isoform, A2, is expressed in extra-hepatic tissues, especially the kidney[8]. Both isoforms are expressed in the retina and brain[9], and have been linked to CNS diseases[10]. A1 is expressed in retinal glia[10]. After experimental stroke, A1 has been reported to be strongest in myeloid cells with less expression in astrocytes[11,12]. A1 and nitric oxide synthase (NOS) enzyme compete for their common substrate the semi-essential amino acid L-arginine[13]. A1 upregulation can lead to suppression of nitric oxide (NO) formation by endothelial NOS (eNOS) resulting in superoxide production, endothelial dysfunction, platelet aggregation, and leukocyte activation and attachment to the vessel wall[14]. However, A1 expression in "M2-like" anti-inflammatory myeloid cells is thought to reduce NO production by iNOS, and thus can dampen oxidative stress and inflammation[15,16]. Interestingly, the number of $A1^+$, $Iba1^+$ macrophages/microglia is correlated with post-stroke neuron survival and recovery in mice[11]. Recent studies have shown that A1 is expressed exclusively by infiltrating myeloid cells and not by microglia after CNS injury[17,18].

We have previously shown that A2 plays a deleterious role in retinal IR injury[19]. Moreover, retinal IR injury is associated with increased expression of A2 and iNOS, and decreased A1[19]. While A1 is a marker for M2 macrophages and is known to improve tissue repair, its role in macrophage polarization and neurovascular damage after CNS IR injury has not been studied[10]. Here we examined for the first time the role of A1 in retinal IR injury using mice with global and cell-specific A1 deletion. We also tested the therapeutic potential of PEGylated A1 (PEG-A1, a drug form of A1 that is currently under investigation as cancer therapy[20–24]) in retinal IR injury.

Results

A1 deletion worsens IR-induced neurovascular degeneration in vivo

We have previously shown that retinal IR injury is associated with decreased A1 mRNA at 3 h[19]. In line with this, we found a sustained decrease in retinal arginase activity starting at 3 h after IR injury and up to 48 h (Fig. S1). To study the role of A1 in retinal IR injury, we used heterozygous ($A1^{+/-}$) global KO mice, since homozygous deletion of A1 is postnatal lethal[25]. WT or $A1^{+/-}$ KO mice were subjected to 40 min of ischemia on the right eye followed by reperfusion as explained in the methods[26]. The left eye served as sham control. The retinal IR injury model is associated with both neuronal and microvascular degeneration that are manifested by neuronal loss and acellular capillary formation[19]. To evaluate neurodegeneration after IR injury, we labeled WT and $A1^{+/-}$ KO retinas with the neuronal marker, NeuN and imaged the surviving neurons in the retinal ganglion cell layer by confocal microscopy[19,26]. IR injury reduced NeuN-positive cells in WT mice at 7 days, which was further worsened in $A1^{+/-}$ mice (Fig. 1a, b). We next examined microvascular degeneration by preparing retina vascular digests and counting the number of acellular capillaries[19,27]. WT IR injured retinas showed a large number of acellular capillaries (≈150/mm^2 empty basement membrane sleeves, red arrows, Fig. 1c, d) at 14 days after IR injury and this was further increased by ≈50% in $A1^{+/-}$ mice.

A1 deletion exacerbates retinal thinning and distortion after IR injury

The IR injury model has been shown to affect the inner retinal layers (ganglion cell layer (GCL), inner plexiform layer (IPL), and inner nuclear layer (INL)) to a greater extent than the outer retina leading to reduced inner retina thickness[26,28,29]. In accordance with this, morphometric analysis on hematoxylin and eosin (H&E)-stained WT IR injured retina sections at 7 days showed reduced thickness of the inner retinal layers compared to sham controls. $A1^{+/-}$ retinas showed further thinning and distortion compared to WT after IR injury (Fig. 2a, b). This was confirmed by optical coherence tomography (OCT) that showed worsened retinal detachment in $A1^{+/-}$ retinas (Fig. 2c).

A1 deletion exacerbates retinal inflammation and necroptosis after IR injury

Next, we examined the underlying mechanism of increased retinal cell death in $A1^{+/-}$ mice after IR injury. Various mechanisms of retinal cell death have been described in the retina IR injury model with studies from our lab and others emphasizing a prominent role of programmed cell death by necroptosis (a caspase-independent programmed form of cell death)[19,30–35]. Necroptosis is associated with an early increase in cell membrane permeability. We evaluated this through propidium iodide (PI) uptake, which is plasma membrane impermeable and only labels the DNA of dying cells. We observed PI-positive cells in GCL and INL of WT retinas within 6 h following IR injury with more cells in $A1^{+/-}$ retinas (Fig. S2).

Unlike apoptosis, necroptosis is associated with release of cellular contents and subsequent inflammatory response. Therefore, we examined the necroptosis marker receptor interacting protein 3 kinase (RIP3) together with other inflammatory markers via western blotting. Western blot analyses showed increases in the stress marker phospho-p38 MAPK in $A1^{+/-}$ retinas at 3 h after IR injury as compared to WT retinas. There was also a trend towards an increase in the mitochondrial fission marker, dynamin-related protein (Drp1) but the difference was not statistically significant (Fig. 3a–c). Furthermore, IR injury induced increases in the inflammatory cytokine,

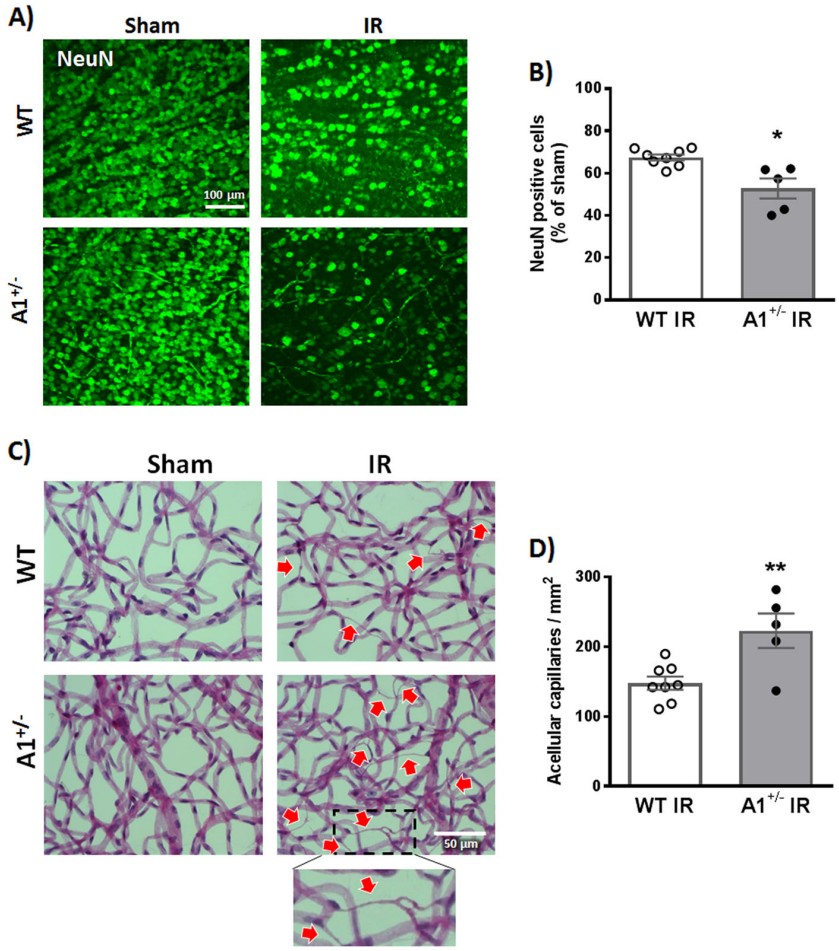

Fig. 1 A1 deletion worsens neuronal and microvascular degeneration after IR injury. a WT and $A1^{+/-}$ mice were subjected to retinal IR injury and sacrificed at 7 days. Flat-mount NeuN staining showed neuronal cell loss in WT retinas after IR injury compared to shams, which was further aggravated in $A1^{+/-}$ mice. Scale bar = 100 µm. **b** Quantification of NeuN-positive cells, $n = 5$ for WT IR and 8 for $A1^{+/-}$ IR, $^{*}p < 0.05$. **c** Vascular digests at 14 days showed increased numbers of acellular capillaries (red arrows) in WT IR injured retinas and this microvascular degeneration was further augmented in $A1^{+/-}$ IR injured retinas. Scale bar = 50 µm. **d** Quantification of acellular capillaries (empty basement membrane sleeves—enlarged in inset), $n = 5$ for WT IR and 8 for $A1^{+/-}$ IR, $^{**}p < 0.01$

tumor necrosis factor alpha (TNF-α), and RIP3 in $A1^{+/-}$ retinas at 6 h (Fig. 3d–g). The increase in inflammation was associated with increases in oxidative stress. This was shown by increased nitrotyrosine formation (a measure of protein tyrosine nitration via peroxynitrite, which is formed by the reaction of NO with superoxide anion). Albumin extravasation (measure of vascular permeability) was also increased in $A1^{+/-}$ as compared to WT mice at 48 h after IR injury (Fig. 3h–j).

Effect of cell-specific A1 deletion on neuronal survival and retinal tissue thinning after IR injury

It has been shown that retinal IR injury induces macrophage/microglia recruitment and proliferation within 24 h with a peak in cell number at 3–5 days[36]. In accordance, we have seen an increase in Iba1-positive cells in the retina after IR injury (Fig. S3A). Interestingly, we detected Iba1-positive cells in the vitreous at 48 h after IR injury, suggesting infiltration of systemic monocyte-derived macrophages (Fig. S3B). Building on this and since global A1 deletion showed a worsened retinal IR injury outcome, we next examined the cell-specific role of A1. For this, A1 floxed (loxP) mice were crossed to $LysM^{cre}$ and $Cdh5^{cre}$ transgenic mice to generate mice lacking A1 in myeloid ($LysM^{cre}$;$A1^{f/f}$) or endothelial ($Cdh5^{cre}$;$A1^{f/f}$) cells, respectively. Mice with myeloid but not endothelial A1 deletion showed exacerbated neuronal loss at 7 days after IR injury compared to littermate floxed

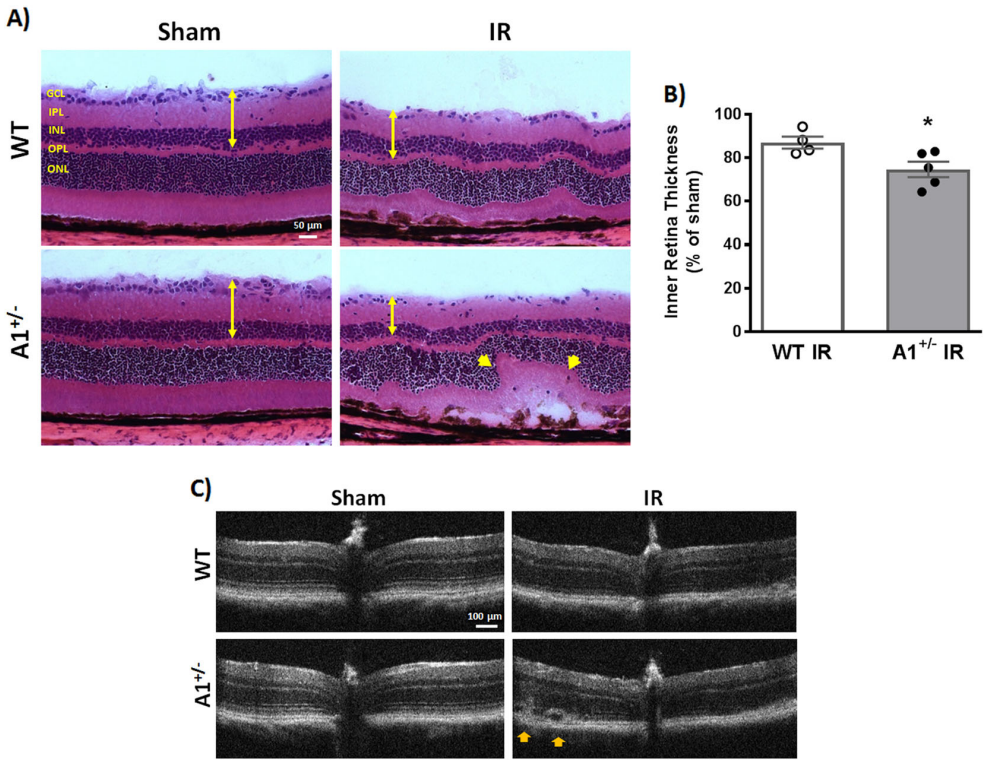

Fig. 2 A1 deletion worsens retinal thinning and distortion after IR injury. a Hematoxylin and eosin (H&E) staining of retinal frozen sections showed less retinal ganglion cells, distorted morphology, and retinal thinning 7 days after IR injury which was further worsened in $A1^{+/-}$ retinas (yellow arrow heads). Scale bar = 50 µm. GCL ganglion cell layer, IPL inner plexiform layer, INL inner nuclear layer, OPL outer plexiform layer, ONL outer nuclear layer. **b** Quantification of inner retina thickness (GCL + IPL + INL, denoted by yellow arrows in panel (**a**)), $n = 4$ for WT IR and 5 for $A1^{+/-}$ IR, $^*p < 0.05$. **c** Optical coherence tomography (OCT) in live mice at 7 days corroborated the H&E results with yellow arrow heads pointing at retinal distortion/detachment, $n = 3$ per group (different cohort of mice than the one used for H&E)

control (Fig. 4a, b). Moreover, myeloid A1 KO retinas showed more thinning and distortion after IR injury (Fig. 4c, d). Western blotting on retinal lysates from endothelial-specific A1 KO mice showed no difference in albumin extravasation at 48 h after IR injury as compared to floxed controls (Fig. S5). Collectively, these data suggest a major protective role of myeloid A1 and a minimal role of endothelial A1 in retinal IR injury. In line with a reparative role of infiltrating macrophages in the retinal IR injury model, systemic macrophage depletion using clodronate liposomes led to worsened neurodegeneration and retinal hemorrhage after IR injury in WT mice (Fig. S7).

PEGylated A1 treatment protected retinal neurons and increased microglia/macrophages after IR injury

To study the effect of increasing A1 levels on neurodegeneration, we used PEG-A1, which is an investigational drug with good safety, pharmacodynamic, and pharmacokinetic profiles in patients[20]. WT mice received intravitreal injection of PEG-A1 (1.7 ng in 1 µl), 3 h before or after IR injury. Either pre- or post-treatment with PEG-A1 improved neuronal survival at 7 days after IR injury. Interestingly, the PEG-A1-mediated neuronal preservation was associated with more retinal macrophages/microglia with elongated morphology as evident by Iba1 staining of retina flat-mounts (Fig. 5a–c).

A1 deletion augments macrophage inflammatory response in vitro and PEGylated A1 treatment mitigates it

To further confirm our in vivo data, we tested the role of A1 expression in macrophage inflammatory response in vitro. Peritoneal macrophages isolated from myeloid A1 KO and floxed littermate controls were treated with interleukin-4 (IL-4, 20 ng/ml) or lipopolysaccharide (LPS, 100 ng/ml) for 24 h to generate anti-inflammatory (M-2 like) or proinflammatory (M-1 like) responses, respectively. As expected, IL-4 treatment increased A1 expression in macrophages isolated from control mice.

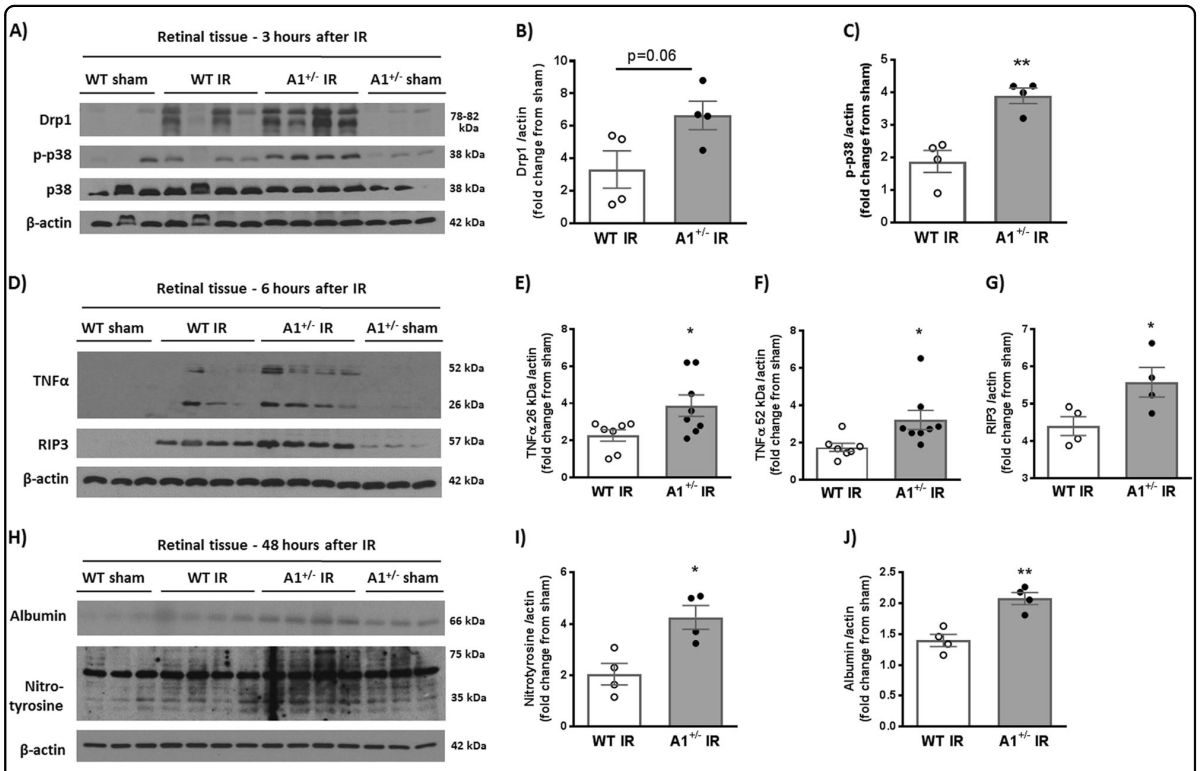

Fig. 3 A1 deletion increases inflammation, oxidative stress, and necroptosis markers after IR injury. a Western blotting on retinal tissues collected at 3 h after IR showed higher levels of the stress marker p-p38 in $A1^{+/-}$ mice compared to WT after IR injury. There was also a trend towards higher levels of the mitochondrial fission protein, Drp1. **b**, **c** show quantification of Drp1 and p-p38 respectively. **d** Analysis at 6 h after IR injury showed a similar trend with increased TNF-α (26 kDa, membrane bound and 52 kDa, homotrimeric form), and RIP3 in $A1^{+/-}$ retinas as compared to WT. **e**–**g** show quantification of TNF-α bands and RIP3 respectively. **h** $A1^{+/-}$ mice showed increased nitrotyrosine (marker for peroxynitrite-mediated oxidative stress via protein nitration) and albumin extravasation (measure of permeability) at 48 h after IR injury. **i**, **j** show quantification of nitrotyrosine and albumin western blotting respectively. *$p < 0.05$, **$p < 0.01$

Upon LPS stimulation, macrophages lacking A1 showed more iNOS expression, TNF-α and inflammasome pathway activation (NLRP3, NFkB, and pro-IL1β) compared to controls. Furthermore, they showed increased NO production in cell supernatant compared to controls as measured by NO analyzer. Collectively, A1 KO macrophages exhibited a more pronounced inflammatory response to LPS stimulation. Cotreatment with PEG-A1 (1 μg/ml) dampened the LPS-induced inflammatory response and reduced NO production in both control and A1 KO macrophages (Fig. 6).

PEGylated A1 rescues LPS-induced mitochondrial dysfunction in macrophages

Next, we examined macrophage metabolic reprogramming, which has been implicated in macrophage polarization and inflammatory response. Seahorse XFe96 analyzer was used to evaluate mitochondrial function by measuring the oxygen consumption rate (OCR). As previously described, LPS stimulation (100 ng/ml) shifted WT bone marrow-derived macrophages (BMDMs) to a more glycolytic phenotype (as measured by increased extracellular acidification rate, ECAR) and decreased mitochondrial respiration parameters (OCR)[37]. PEG-A1 (1 μg/ml) significantly inhibited the LPS-induced alterations in mitochondrial function parameters in WT BMDMs (Fig. 7a–g). In addition, staining live BMDMs with the mitochondrial membrane potential sensitive dye, Rhodamine 123[38], showed mitochondrial fragmentation in response to LPS stimulation which was partially reversed with PEG-A1 cotreatment (Fig. 7i, j). Seahorse analysis of LPS-stimulated A1 KO macrophages showed impaired mitochondrial function as compared to loxP controls (Fig. S8). PEG-A1 treatment of A1 KO macrophages blunted the LPS-induced impaired mitochondrial function (Fig. S9).

NO has been shown to decrease mitochondrial reserve capacity in endothelial cells[39]. We aimed to further examine the link between A1 and mitochondrial respiration in endothelial cells. Bovine retinal

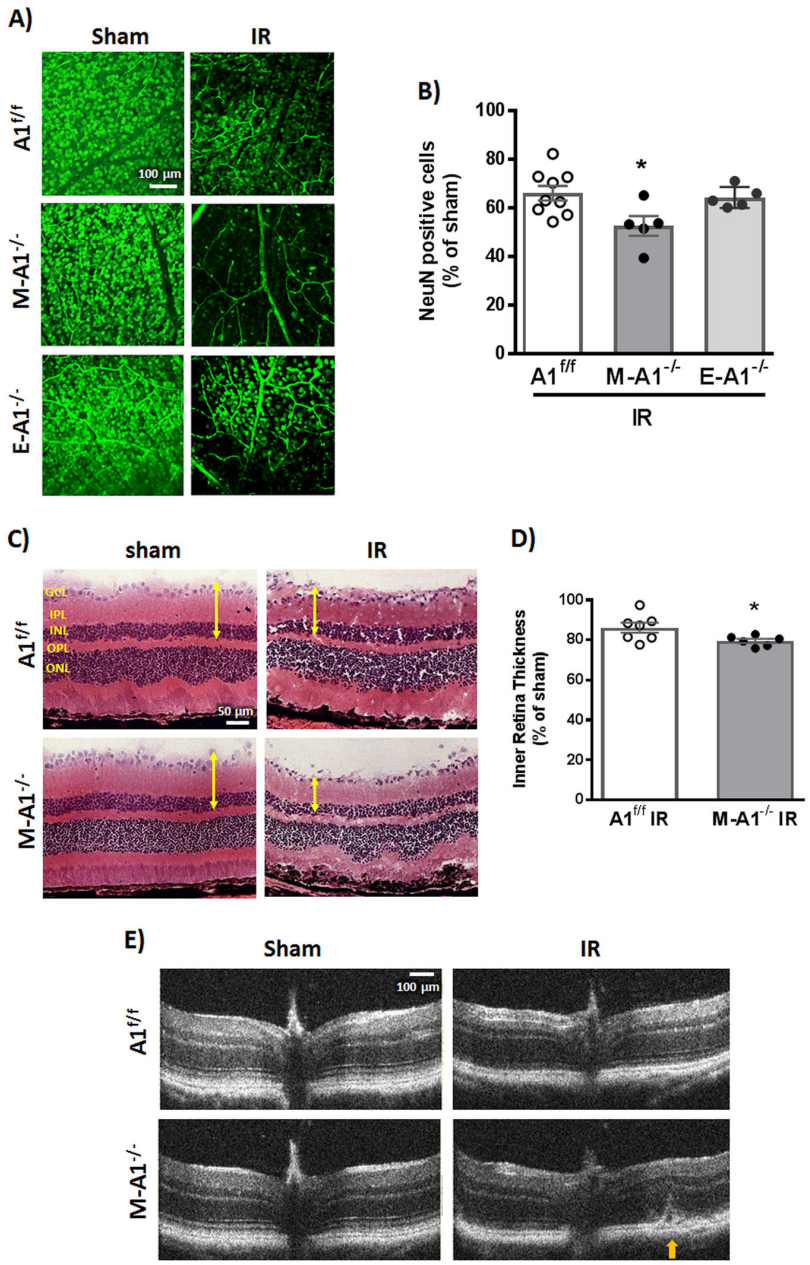

Fig. 4 Myeloid A1 deletion worsens neuronal loss and retinal thinning after IR injury. a Retinas of mice with myeloid but not endothelial-specific A1 deletion showed worsened neuron loss compared to floxed control at 7 days after IR injury. Scale bar = 100 µm. **b** Quantification of NeuN-positive cells, $n = 9$ for $A1^{f/f}$ IR and 5 for M-$A1^{-/-}$ and E-$A1^{-/-}$ IR, $^*p < 0.05$ vs. $A1^{f/f}$. **c** H&E staining at 7 days showed worsened inner retina thinning in M-$A1^{-/-}$ mice compared to control ($A1^{f/f}$). Scale bar = 50 µm. **d** Quantification of inner retina thickness, $n = 7$ for $A1^{f/f}$ IR and 6 for M-$A1^{-/-}$ IR, $^*p < 0.05$. **e** Optical coherence tomography (OCT) corroborated the H&E results with yellow arrow pointing at retinal detachment

endothelial cells were subjected to oxygen-glucose deprivation (OGD) for 5 h followed by 1 h reoxygenation (R). OGD/R impaired mitochondrial respiration parameters and PEG-A1 treatment (1 µg/ml) improved maximal respiration and spare respiratory capacity (difference between maximal respiration and basal respiration) after OGD/R (Fig. S10). Collectively, PEG-A1 treatment rescued the LPS- and OGD/R-induced

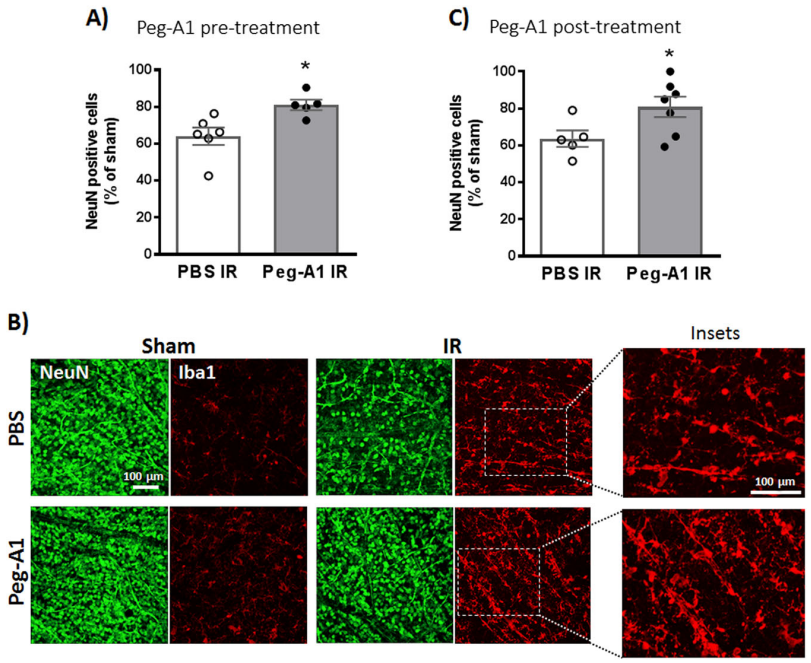

Fig. 5 A1 treatment protects retinal neurons, and increases microglia/ macrophages after IR injury. a Mice received intravitreal injection of PEG-A1 (1.7 ng/µl) 3 h before induction of IR injury and were sacrificed at day 7. PEG-A1 treatment preserved retinal neurons (NeuN-positive cells), $n = 6$ for PBS and 5 for PEG-A1, $^*p < 0.05$. **b** PEG-A1-treated retinas showed increased microglia/macrophage infiltration as evident by Iba1 staining on retina flat-mounts. **c** Treatment with PEG-A1 (1.7 ng/µl) 3 h after IR injury achieved similar neuronal preservation to the pretreatment, thus showing post-injury protective effect, $n = 5$ for PBS and 7 for PEG-A1, $^*p < 0.05$

mitochondrial dysfunction in macrophages and endothelial cells respectively.

Intravitreal injection of A1 KO BMDMs is associated with worsened neurodegeneration after IR injury

Finally, we employed intravitreal injections of BMDMs to further examine the role of A1 in the macrophage reparative/damaging functions. Mice were subjected to IR injury and intravitreal macrophage injection was conducted at day 3. Retinas were collected for NeuN staining at day 7. Indeed, A1 KO macrophage injection was associated with worsened neurodegeneration after IR injury compared to loxP control macrophages (Fig. 8).

Discussion

In this study, we present evidence on the important role of A1 in macrophage polarization toward a reparative phenotype leading to neurovascular recovery after retinal IR injury. We show that global as well as myeloid-specific A1 deletion worsens retinal IR injury outcomes and macrophages lacking A1 exhibit enhanced inflammatory response. Additionally, PEG-A1 treatment reduces retinal IR injury and dampens the macrophage inflammatory response.

Although retinopathies are diagnosed primarily based on vascular abnormalities, studies have demonstrated that inflammation[40–42] and neurodegeneration[43,44] occur before appearance of typical vascular pathology. Our present study in a retinal IR injury mouse model shows that A1 protects against neuronal and vascular injury. This was evident by the worsened neurodegeneration, acellular capillary formation, retinal thinning, and necroptosis in $A1^{+/-}$ mice compared to WT. By contrast, our recent study in $A2^{-/-}$ mice suggests a deleterious role of A2 in retinal IR injury. This could be explained by the differential expression and subcellular localization patterns of the two arginase isoforms. Both of our studies have employed different endpoints to confirm the role of A1 and A2 in retinal IR injury. Other studies have also shown opposing roles of A1 vs. A2 under different disease conditions. In fact, these two isoforms are transcribed from two different genes and appear to function independently in different tissues[10,14]. However, the possible reciprocal regulation and interaction between A1 and A2 remains to be elucidated.

Necroptosis is initiated in response to a death receptor signaling and upon failure of apoptosis induction. TNF-α binding to its receptor can induce necroptosis with RIP3

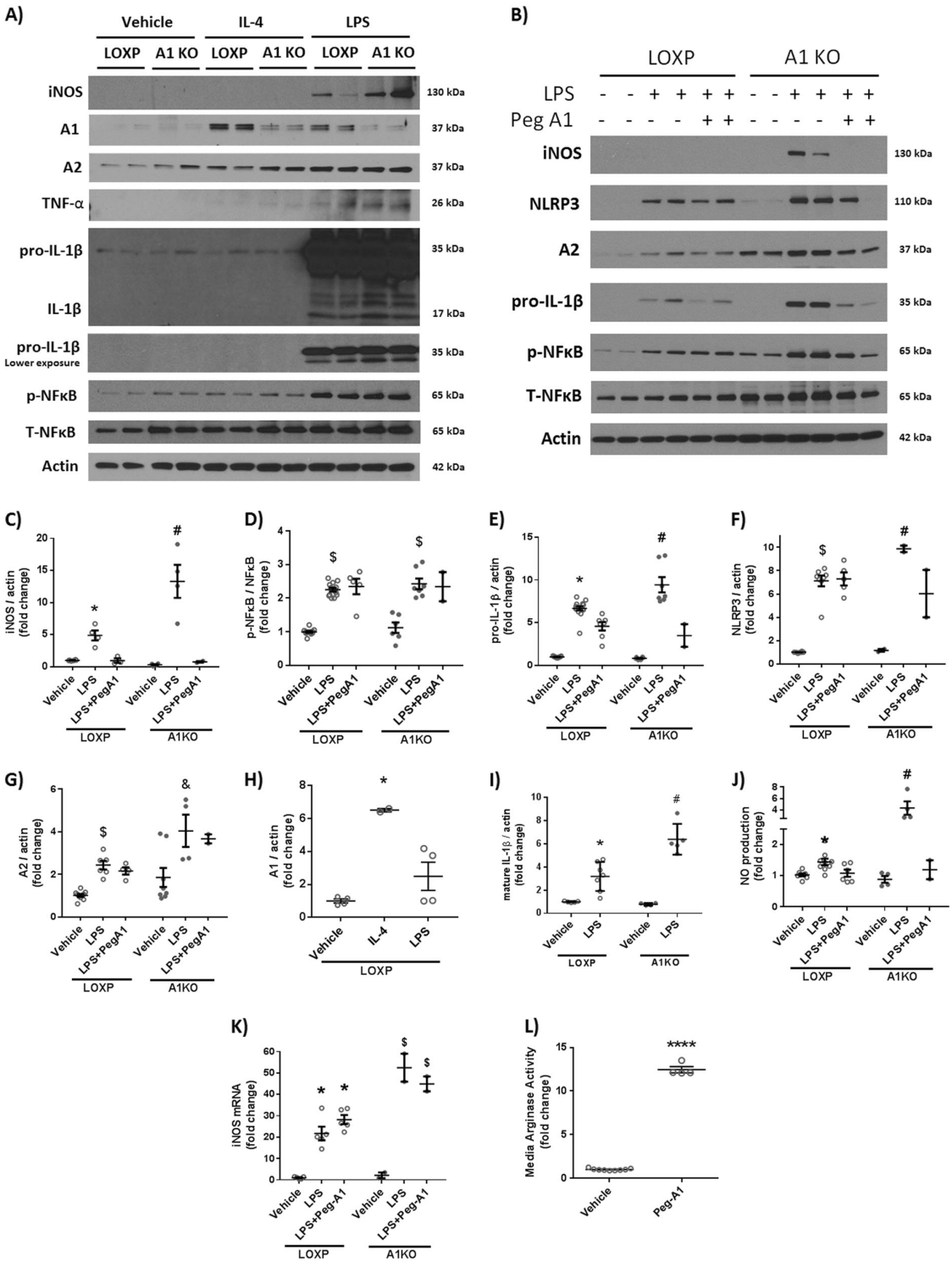

Fig. 6 (See legend on next page.)

(see figure on previous page)

Fig. 6 Macrophages lacking A1 show a more pronounced inflammatory response to LPS stimulation in vitro and PEG-A1 treatment mitigates it. a Western blotting of peritoneal macrophage cell lysates showed increased iNOS expression, TNF-α, and pro-IL-1β upon LPS stimulation which was further augmented in A1 KO macrophages. **b** PEG-A1 treatment (1 μg/ml) reduced this inflammatory response. **c**–**i** Quantification of western blot bands. $^{*}p < 0.05$ vs. loxP vehicle and loxP LPS + PEG-A1, $^{\#}p < 0.05$ vs. loxP LPS, A1KO vehicle and A1KO LPS + PEG-A1, $^{\$}p < 0.05$ vs. respective vehicle. $^{\&}p < 0.05$ vs. loxP LPS. **j** A1 KO macrophages showed more nitric oxide (NO) release into the media in response to LPS, as measured using NO analyzer and this was ameliorated by PEG-A1, $^{*}p < 0.05$ vs. vehicle loxP, $^{\#}p < 0.05$ vs. loxP LPS, A1KO vehicle, A1KO LPS + PEG-A1. **k** RT-PCR on BMDMs showed increased iNOS mRNA expression with LPS that was further increased in A1 KO macrophages. PEG-A1 treatment did not affect iNOS mRNA expression $^{*}p < 0.05$ vs. loxP vehicle, $^{\$}p < 0.05$ vs. respective loxP group. **l** Media from wells treated with PEG-A1 show marked elevation of arginase activity (12-fold increase compared to control) at the end of a 24 h incubation, $^{****}p < 0.0001$

being the main executioner. Necroptosis leads to membrane permeability and release of cell components, which causes an inflammatory response. RIP3 can also directly activate the NLRP3 inflammasome pathway. We and others have shown activation of the necroptosis pathway within hours of the IR injury which can induce inflammation and myeloid cell recruitment. Our previous publication[19], and current data show that while A2 deletion reduces IR injury-induced necroptosis in the retina, A1 deletion can augment it.

Our molecular analyses show that A1 deletion is associated with upregulation of iNOS, peroxynitrite, TNF-α, and RIP3. A1 competes with NOS enzymes for their common substrate L-arginine leading to less NO production[13]. A1 upregulation can decrease NO production by iNOS in myeloid cells, thus reducing oxidative stress and inflammation[15,16]. However, chronic A1 upregulation in endothelial cells can lead to uncoupling of endothelial NOS (eNOS), via reduction of L-arginine, resulting in endothelial dysfunction[14]. In our acute model of retinal IR injury, we did not detect any A1-mediated adverse vascular outcomes. In fact, $A1^{+/-}$ mice showed more microvascular degeneration and greater vascular permeability which was not affected by endothelial-specific deletion of A1. Furthermore, PEG-A1 treatment rescued the OGD/R-induced mitochondrial dysfunction in endothelial cells. Collectively, this suggests a vascular protective role of A1 in our acute injury model in young and otherwise healthy mice. Possible adverse vascular effects of A1 treatment in mouse models of endothelial dysfunction will be addressed in future studies.

A1 has been long used as a marker for anti-inflammatory M2-like macrophages; however, its direct functional role has not been examined in CNS diseases. Using myeloid-specific A1 KO mice as well as in vitro macrophage experiments, we show here that this protective role of A1 in IR injury is mediated through myeloid cells. NO induces TNF-α expression in myeloid cells and potentiates its neurotoxicity[45–54]. Our results suggest that A1 decreases iNOS-mediated NO production and oxidative stress in myeloid cells leading to decreased TNF-α production and subsequent necroptosis and tissue damage. Moreover, NO has been linked to macrophage metabolic reprogramming to a more glycolytic phenotype and less mitochondrial oxidative phosphorylation through nitrosylation of the electron transport chain complexes[55]. In line with this, our data show that PEG-A1 effectively rescues LPS-induced suppression of mitochondrial metabolism. Interestingly, NFkB activation in response to LPS stimulation was not changed by A1 deletion or PEG-A1 treatment suggesting that A1 regulates iNOS and inflammatory cytokines transcription at a level downstream of NFkB phosphorylation. One possibility is that A1 suppresses inflammatory gene transcription in macrophages through epigenetic modification. A recent report has shown that, putrescine, a downstream product of arginase can suppress M1 inflammatory gene transcription through histone modification and altered euchromatin formation[56]. Further studies are needed to elucidate the mechanisms by which A1 promote a less inflammatory macrophage phenotype.

Monocyte-derived macrophages infiltrate the CNS after injury and recent reports have examined their role in CNS injury outcome. Two independent studies have shown that brain-infiltrating macrophages after ischemic stroke acquire an M2-like reparative phenotype[57,58]. Monocyte-derived macrophages have been shown to prevent hemorrhagic transformation and mediate long-term functional recovery after stroke in mice[59,60]. Moreover, brain-infiltrating macrophages reduce lesion volume and neurological deficit in an intracerebral hemorrhage (ICH) mouse model through M2 polarization[61]. Interestingly, macrophages have been shown to promote vascular repair after traumatic brain injury in mice[62], and directly repair cerebrovascular ruptures in zebrafish[63]. On the other hand, one report showed that macrophage depletion reduced myelin damage and promoted neurological recovery in a mouse stroke model[64]. Our current data show that macrophages play a protective role in retinal IR injury and their depletion further worsens neurodegeneration and hemorrhage. Moreover, we show that A1 is a central player in this protective effect. While our in vitro studies focused on A1-mediated dampening of the macrophage inflammatory response, the in vivo studies

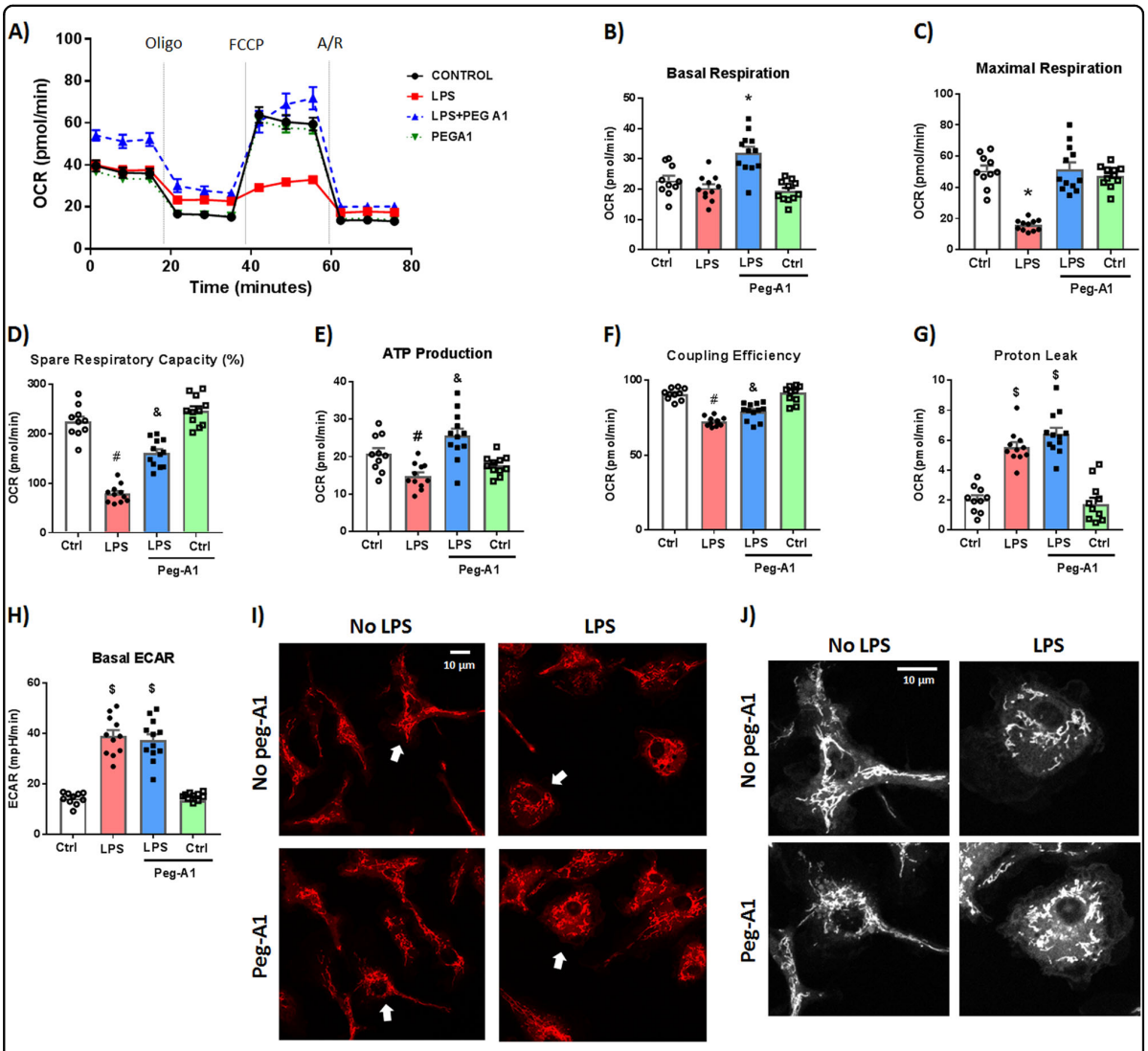

Fig. 7 PEG-A1 treatment protects against LPS-induced mitochondrial dysfunction in WT bone marrow-derived macrophages (BMDMs). WT BMDMs were stimulated with LPS (100 ng/ml) for 24 h ± PEG-A1 (1 µg/ml). Seahorse XFe96 analyzer was used to evaluate mitochondrial function by measuring the oxygen consumption rate (OCR). **a** Change in OCR with time in response to Mito Stress test inhibitors (oligomycin, FCCP, and rotenone/antimycin A). **b**–**g** Mitochondrial respiration parameters were decreased with LPS treatment. PEG-A1 significantly rescued this decrease. $^{*}p < 0.01$ vs. other three groups, $^{\$}p < 0.01$ vs. controls, $^{\&}p < 0.01$ vs. respective control, LPS, $^{\#}p < 0.01$ vs. respective control, and LPS + PEG-A1, $n = 12$ per group. Representative run from two independent experiments that showed the same results. **h** Extracellular acidification rate (ECAR), a measure of glycolysis, was increased with LPS stimulation but was not affected by PEG-A1 cotreatment, $^{\$}p < 0.01$ vs. controls, $n = 12$ per group. **i** WT macrophages under control condition or PEG-A1 treatment alone exhibited an elongated and interconnected mitochondria (stained with Rhodamine 123). LPS-induced mitochondrial fragmentation and localization around the nucleus consistent with a round activated macrophage morphology. PEG-A1 cotreatment of LPS-stimulated macrophages partially reversed the LPS effect. **j** Magnification of cells denoted by arrows in panel (**i**). Images were converted to black and white for clarity. Scale bar = 10 µm

suggest that A1 can promote a reparative macrophage phenotype as well. The proposed protective role of macrophages in our model could be mediated through clearing of dying cells via phagocytosis and promoting vascular repair. Further studies are warranted to examine these mechanisms.

In conclusion, our study shows that A1 ameliorates the IR injury-induced retinal injury via dampening the macrophage inflammatory response. Enhancing myeloid A1 can be a potential therapeutic approach for treatment of CNS ischemic conditions, especially ischemic retinopathies.

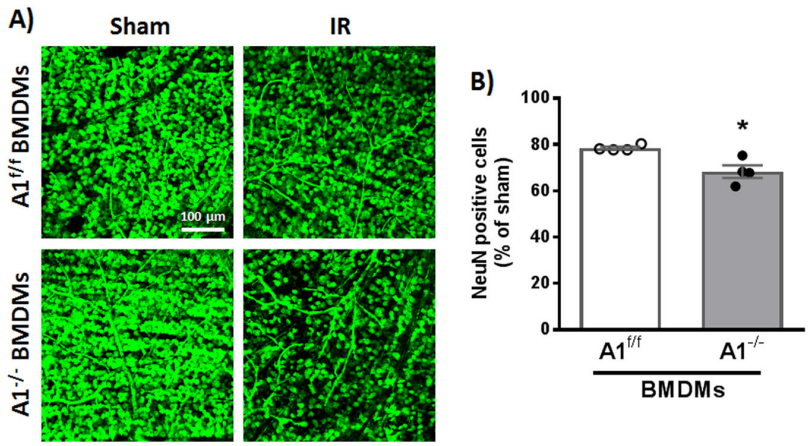

Fig. 8 Macrophages lacking A1 worsen neurodegeneration after IR injury. a NeuN staining showing increased neurodegeneration in WT retinas treated with A1 KO BMDMs (2×10^5 cells, injected intravitreally on day 3 after IR injury), **b** Quantification of NeuN-positive cells, $n = 4$ per group, $^*p < 0.05$. Scale bar = 100 µm

Materials and methods

Mouse retinal IR injury model

All animal procedures were performed in accordance with the Association for Research in Vision and Ophthalmology (ARVO) Statement and adhered to the Public Health Service Policy on Humane Care and Use of Laboratory Animals (revised July 2017). Procedures were approved by the institutional animal care and use committee (Animal Welfare Assurance no. A3307–01). Male mice (10−12 weeks old) were anaesthetized with ketamine/xylazine mixture and the right eye was subjected to IR injury while the left eye served as sham control. IR injury was induced by inserting a needle connected to an elevated saline reservoir into the anterior chamber to raise the intraocular pressure to 110 mmHg for 40 min as previously described[19,26]. The mice were sacrificed at various times after IR injury to examine different endpoints based on the literature and our previous publications[19,26].

Experimental groups

To determine the role of A1 in neurovascular degeneration after IR injury, we used mice with global and conditional A1 deletion: heterozygous $A1^{+/-}$ knockout (KO), endothelial-specific ($Cdh5^{Cre}$;$A1^{f/f}$ or E-$A1^{-/-}$) KO, and myeloid-specific ($LysM^{Cre}$; $A1^{f/f}$ or M-$A1^{-/-}$) A1 KO. $A1^{+/-}$ mice on C57BL6J background were used since $A1^{-/-}$ is postnatal lethal due to hyperamonemia[25,65–67]. Experiments were conducted on littermate control and KO mice to ensure proper comparison. IR injury was conducted on all mice within a litter during the same day. Mice were selected for surgery in a random order irrespective of the genotype. Cell-specific A1 KO mice were generated by crossing C57BL-6 A1 floxed mice ($A1^{f/f}$) with Cre-expressing transgenic mice under control of the VE-Cadherin promoter ($Cdh5^{Cre}$) or lysozyme 2 promoter ($LysM^{Cre}$) to generate endothelial-specific (E-$A1^{-/-}$) or myeloid-specific (M-$A1^{-/-}$) mice respectively. We have recently characterized and confirmed the E-$A1^{-/-}$ mice[68]. Myeloid A1 deletion has been confirmed by tissue immunostaining and western blotting on isolated cells (Fig. S4). Further details are provided in the supplementary data.

Five sets of in vivo experiments were conducted:

Experiment 1: $A1^{+/-}$ KO mice and C57BL6J WT controls were used to examine the effect of whole body deletion of one copy of A1 on IR injury outcome.

Experiment 2: Endothelial-specific (E-$A1^{-/-}$) and myeloid-specific M-$A1^{-/-}$ mice were used and compared to floxed controls ($A1^{f/f}$) to examine the cell-specific role of A1.

Experiment 3: WT mice were treated with clodronate liposomes to deplete systemic monocytes/macrophages or control liposomes to examine the role of these cells in retinal IR injury.

Experiment 4: WT mice were treated with intravitreal injection of PEG-A1 (1.7 ng in 1 µl, dose was selected based on preliminary studies) to examine the effect of increasing intraocular arginase on retinal IR injury outcome.

Experiment 5: WT mice received intravitreal injection of $A1^{-/-}$ or $A1^{f/f}$ macrophages to examine the impact of A1 expression in macrophages on IR injury outcome.

Monocyte/macrophage depletion

Two hundred microliters of clodronate or red fluorescent control liposomes (Encapsula Nanosciences) were

injected intraperitoneally 1 day before and at day 3 after IR injury. This achieved ≈80% systemic monocyte/macrophage depletion at day 7 after IR injury (Fig. S6). Clodronate induces apoptosis when the liposomes are engulfed by macrophages while control liposomes were used to control for the induction of macrophage phagocytic activity. Cages were changed every 2_3 days to maintain a clean environment and mice were closely monitored for any signs of infections.

PEGylated arginase 1 (PEG-A1) treatment

PEG-A1 (1.7 ng/μl) or phosphate-buffered saline (PBS) was administered under anesthesia via intravitreal injection (in 1 μl volume) using a Hamilton syringe 3 h before or after induction of retinal IR injury.

Intravitreal macrophage injection

Cultured BMDMs were suspended in PBS and injected intravitreal (2×10^5 per 1 μl) on day 3 after IR injury.

Evaluation of neurodegeneration

Neuronal degeneration was assessed at 7 days after IR injury as previously described[19,26]. Eyeballs were collected and fixed overnight in 4% paraformaldehyde at 4 °C, then retinas were dissected into flat-mounts and stained for the neuronal marker, NeuN (Millipore, Cat. # MAB377, Billerica, MA). Four images were taken in the retina midperiphery using a confocal microscope (LSM 510; Carl Zeiss, Thornwood, NY) and NeuN-positive cells were counted using ImageJ software. Results are presented as a percent of NeuN-positive cell numbers in the GCL of the IR injured eyes compared to the sham eyes.

Retinal vasculature isolation and measurement of acellular capillaries

Vasculature was isolated at 14 days after IR injury via trypsin digestion of retinas that were dissected from overnight fixed eyeballs as previously described[19,69]. The isolated retinal vasculature was air-dried on silane-coated slides and stained with periodic acid-Schiff and hematoxylin. Acellular capillaries were counted in ten random fields of the mid-retina. The number of acellular capillaries was divided by the field area to get number of acellular capillaries per 1 millimeter square (mm^2) of retina.

Histology and morphometric analysis

Retinal structure was assessed at 7 days on anesthetized mice using OCT (the Bioptigen Spectral Domain Ophthalmic Imaging System, SDOIS; Bioptigen Envisu R2200, NC) as previously described[72]. Retinal thickness was determined by morphometric analysis on H&E-stained retinal frozen cross sections as previously described[19,26,70]. Inner retina (INL + IPL + GCL) thickness was measured on H&E images at three different distances from optic nerve head using ImageJ software. Averaged retinal thickness was presented as percentage compared to the contralateral sham eyes.

Western blot analysis

For in vivo experiments, retinas were collected from the mice, snap-frozen in dry ice, and stored at −80 °C. For analysis of albumin leakage across the blood-retinal barrier, mice were transcardially perfused with PBS to clear blood out of the retina vessels before collection and retinas were processed for western blotting. Retinas were homogenized using a hand homogenizer in RIPA lysis buffer and centrifuged at 20,000 × *g* to prepare the protein extracts. Protein concentration was measured using Pierce BCA protein assay kit (Thermo Scientific). For in vitro experiments, media were collected and cells were washed with ice-cold PBS then collected in RIPA buffer to prepare the cell lysates. Retinas or cell lysates were run on SDS-PAGE then transferred to nitrocellulose membranes (Millipore, Billerica, MA). The membranes were probed with following primary antibodies prepared in 2% BSA: A1 (Santa Cruz Biotechnology Cat. # Sc-20150, 1:500 dilution), phospho p38 (Cell Signaling Technology Cat. # 4511, 1:500), total p38 (Cell Signaling, Cat. # 9212, 1:500), Drp1 (Santa Cruz Biotechnology, Cat. # SC-271583, 1:500), TNF-α (Abcam, Cat. # ab1793), albumin (Bethyl Laboratories, 1:5000), RIP3 (Santa Cruz Biotechnology, Cat. # SC-135170, 1:500), β-actin (Sigma-Aldrich Cat. # A1978, 1:5000), anti-nitrotyrosine antibody (Millipore, Cat. # 05-233, 1:5000), iNOS (Cell Signaling, Cat. # 13120), A2 (Santa Cruz Biotechnology, Cat. # Sc-20151, 1:500 dilution), IL-1β (R&D, Cat. # AF-401-NA), p-NFkB (Cell Signaling, Cat. # 3033, 1:500), T-NFkB (Cell Signaling, Cat. # 4764, 1:500), NLRP3 (Cell Signaling, Cat. # 15101). Secondary antibodies (GE Healthcare) were prepared in 5% milk in 1:2000 dilution. Bands were quantified using ImageJ and normalized to β-actin loading control. For the nitrotyrosine blot, all bands in each lane were quantified except for the thick albumin band (~66 kDa) that appears due to the reaction of the secondary anti-mouse antibody with mouse albumin in the tissue extracts.

Isolation and culture of primary macrophages

Peritoneal macrophages

Mice were injected intraperitoneally with 5 ml of 3% Brewer's thioglycollate medium (Sigma) as described previously[71]. Mice were sacrificed 3_5 days later and peritoneal macrophages were collected in PBS through peritoneal lavage. Cells were centrifuged and then plated in six-well plates (1 million per well) in DMEM containing penicillin/streptomycin (P/S), and 10% fetal bovine serum (FBS). Medium was changed after 2 h to remove

nonadherent nonmacrophage cells. Experiments were done on day 2 in DMEM containing 1% PS and 2% FBS.

Bone marrow-derived macrophages

Bone marrow cells were isolated and differentiated in vitro into macrophages based on a published protocol[72]. Briefly, both femurs and tibias were harvested and flushed with 20−25 ml sterile PBS using a 27-gauge needle. Flushed cells in PBS were spun down and re-suspended in differentiation medium (DMEM high glucose containing 20% FBS, 20% L929 conditioned media, and 1% P/S). Cells were subsequently plated on 100 mm dishes (uncoated, for easier cell detachment). Media was replaced with fresh differentiation media on day 4. On day 7, media was removed and cells were rinsed with sterile PBS twice. Cells were subsequently gently scraped and collected in PBS, spun down, re-suspended in normal growth media (DMEM high glucose containing 20% FBS, and 1% P/S), and then plated in 12-well plates for in vitro polarization or used for in vivo treatment.

Macrophage polarization Cells were stimulated with LPS (100 ng/ml) or interleukin 4 (IL-4, 20 ng/ml) for 24 h to achieve proinflammatory (M1) or anti-inflammatory (M2) phenotype respectively. In some experiments, macrophages were cotreated with LPS and PEG-A1 (1 μg/ml) to examine the effect of PEG-A1 on the LPS-induced macrophage inflammatory response.

Arginase activity assay

Arginase activity assay was conducted as previously described[9]. Briefly, the enzyme was activated by heating the lysate or supernatant at 56 °C in 25 mM Tris buffer (pH 7.4) containing 5 mM $MnCl_2$. L-Arginine hydrolysis was then conducted by incubating 50 μl of the activated samples with 50 μl of 0.5 M L-arginine (pH 9.7) at 37 °C for 60 min. The reaction was stopped by adding 400 μl of acid solution mixture (H_2SO_4:H_3PO_4:H_2O, 1:3:7). The concentration of urea, which is the end product of L-arginine hydrolysis by arginase, was determined after adding 25 μl of 9% α-isonitrosopropiophenone and heating the mixture at 100 °C for 45 min. Urea standards and 200 μl of each sample were transferred to a 96-well plate and read at 540−550 nm in a BioTek microplate reader. Protein concentration in the lysates was determined by a BCA assay (Pierce Biotechnology). Arginase activity was calculated as mmol urea/mg protein and as percent of control.

Nitric oxide (NO) measurement

We measured nitrite (NO_2^-), the stable breakdown product of NO in cell-conditioned medium to reflect NO production by macrophages. The conditioned media were collected at the end of experiments and injected in glacial acetic acid containing sodium iodide. NO_2 is quantitatively reduced to NO under these conditions, which can be quantified by a chemiluminescence detector after reaction with ozone in an NO analyzer (Sievers, Boulder, CO)[68].

Quantitative RT-PCR

Total RNA was extracted from macrophages using TRIzol reagent (Invitrogen, CA, USA). RNA was converted to cDNA using M-MLV reverse transcriptase (Invitrogen, CA, USA). Quantitative PCR for iNOS gene expression was performed using an ABI StepOne Plus Thermocycler (Applied Biosystems, CA, USA) with SYBR Green dye. Forward primer 5′-GTT CTC AGC CCA ACA ATA CAA GA-3′, reverse primer 5′-GTG GAC GGG TCG ATG TCA C3′. Data were normalized to HPRT and the fold change between levels of different transcripts was calculated by the ΔΔCT method.

Seahorse XFe96 Mito stress test

Mito Stress test (Agilent, Cat. # 103015-100, Santa Clara, CA) and Seahorse XFe96 (Agilent, Santa Clara, CA) were used to evaluate mitochondrial function as previously described[37]. Briefly, Seahorse 96-well cell culture plates were used for growing the cells. At day 7, BMDMs were seeded at cell density of 40 K/well in the Seahorse cell culture plate in all the wells except A1, A12, H1 and H12 wells which were used as background wells. The plate was left under the hood for 1 h to ensure even distribution of cells, and then cells were checked under microscope and put in the incubator. Cells were maintained to grow in normal complete media (DMEM, 20% FBS, 1% P/S) for 3−5 h. Then, cells were treated with LPS overnight in DMEM media supplemented with 10% FBS. The Seahorse media was prepared according to manufacturer's instructions and supplemented with 4 mM glutamine (Gemini, West Sacramento, CA), 1 mM pyruvate (Gemini, West Sacramento, CA), and 25 mM glucose (Sigma, St. Louis, MO). On the day of the assay, the pH of the media was adjusted to 7.4 ± 0.1, and the Mito stress test was conducted according to the manufacturer's instructions. The concentrations of the injection compounds used were as follows: oligomycin (1 μM), FCCP (1 μM) and rotenone/antimycin A (0.5 μM). The data were collected and analyzed using the Wave software (Agilent).

Mitochondrial staining

Vectacell^{TM} Rhodamine 123 (Vector Laboratories) was used to label mitochondria in live cells according to the manufacturer's instructions. Briefly, cells were washed three times with modified PBS containing 1 mM $CaCl_2$ and 0.5 mM $MgCl_2$ (PBS^+) (Thermo Fisher). The cells were incubated with the Rhodamine 123 staining solution

in 37 °C for 15 min. Then, the cells were rinsed three times with PBS^{+}. Zeiss LSM 780 Inverted Confocal microscopy (Carl Zeiss AG, Oberkochen, Germany) was used to image the live cells using a ×63 lens. Several images were taken randomly to cover the whole field.

Statistical analysis

Statistical analysis was conducted using GraphPad Prism 7 software. Values were tested to assess whether they followed a normal distribution by the same software. One-way or two-way ANOVA with post-hoc Tukey multiple comparisons was used to analyze the statistical significance of experimental results in studies of three or more groups. The significance of differences between two groups was determined by Student's *t*-test. $p < 0.05$ was considered significant. Sample size for each experiment was decided based on our previously published work. Outliers were checked by GraphPad online outlier calculator. For in vitro studies, each experiment was performed in triplicates and repeated with at least three different batches of isolated primary cells. Graphs were prepared using GraphPad Prism 7 software, and results were expressed as means ± standard errors of the mean (SEM).

Disclaimer

The contents do not represent the views of the Department of Veterans Affairs or the United States Government. The funders had no role in study design, data collection and analysis, decision to publish, or preparation of the manuscript.

Acknowledgements

This work was supported by grants from The National Institute of Health (NIH grant R01-EY11766) to R.B.C., the Department of Veterans Affairs, Veterans Health Administration, Office of Research and Development, Biomedical Laboratory Research and Development (BX001233) to R.B.C., the Culver Vision Discovery Institute at Augusta University, and American Heart Association (AHA) postdoctoral fellowship (18POST34060036) to A.Y.F. R.B.C. is the recipient of a Research Career Scientist Award from the Department of Veterans Affairs. The contents do not represent the views of the Department of Veterans Affairs or the United States Government. The funders had no role in study design, data collection and analysis, decision to publish, or preparation of the manuscript. PEGylated arginase 1 was provided as a kind gift from Dr. Paulo Rodriguez (Moffitt Cancer Center, FL).

Author details

[1]Charlie Norwood VA Medical Center, Augusta, GA, USA. [2]Vascular Biology Center, Augusta University, Augusta, GA, USA. [3]James and Jean Culver Vision Discovery Institute, Augusta University, Augusta, GA, USA. [4]Department of Pharmacology and Toxicology, Augusta University, Augusta, GA, USA. [5]Department of Cell Biology and Anatomy, Augusta University, Augusta, GA, USA. [6]Department of Pediatrics, Augusta University, Augusta, GA, USA. [7]Moffitt Cancer Center, Tampa, FL, USA. [8]Department of Ophthalmology, Augusta University, Augusta, GA, USA. [9]Program in Clinical and Experimental Therapeutics, College of Pharmacy, University of Georgia, Augusta, GA, USA

Conflict of interest

The authors declare that they have no conflict of interest.

Supplementary Information accompanies this paper at (https://doi.org/10.1038/s41419-018-1051-6).

Received: 15 June 2018 Revised: 24 July 2018 Accepted: 6 September 2018
Published online: 25 September 2018

References

1. Osborne, N. N. et al. Retinal ischemia: mechanisms of damage and potential therapeutic strategies. *Prog. Retin. Eye Res.* **23**, 91–147 (2004).
2. D'Onofrio, P. M. & Koeberle, P. D. What can we learn about stroke from retinal ischemia models? *Acta Pharmacol. Sin.* **34**, 91–103 (2013).
3. Hartsock, M. J. et al. A mouse model of retinal ischemia-reperfusion injury through elevation of intraocular pressure. *JoVE* **113**, e54065 (2016).
4. Binet, F. et al. Neuronal ER stress impedes myeloid-cell-induced vascular regeneration through IRE1α degradation of netrin-1. *Cell Metab.* **17**, 353–371 (2013).
5. London, A., Benhar, I. & Schwartz, M. The retina as a window to the brain-from eye research to CNS disorders. *Nat. Rev. Neurol.* **9**, 44–53 (2013).
6. Ash, D. E., Cox, J. D. & Christianson, D. W. Arginase: a binuclear manganese metalloenzyme. *Met. Ions. Biol. Syst.* **37**, 407–428 (2000).
7. Morris, S. M. Jr. Regulation of enzymes of the urea cycle and arginine metabolism. *Annu Rev. Nutr.* **22**, 87–105 (2002).
8. Miyanaka, K. et al. Immunohistochemical localization of arginase II and other enzymes of arginine metabolism in rat kidney and liver. *Histochem. J.* **30**, 741–751 (1998).
9. Patel, C. et al. Arginase as a mediator of diabetic retinopathy. *Front. Immunol.* **4**, 173 (2013).
10. Caldwell, R. B., Toque, H. A., Narayanan, S. P. & Caldwell, R. W. Arginase: an old enzyme with new tricks. *Trends Pharmacol. Sci.* **36**, 395–405 (2015).
11. Hamzei Taj, S., Kho, W., Riou, A., Wiedermann, D. & Hoehn, M. MiRNA-124 induces neuroprotection and functional improvement after focal cerebral ischemia. *Biomaterials* **91**, 151–165 (2016).
12. Quirie, A. et al. Effect of stroke on arginase expression and localization in the rat brain. *Eur. J. Neurosci.* **37**, 1193–1202 (2013).
13. Wu, G. & Morris, S. M. Jr. Arginine metabolism: nitric oxide and beyond. *Biochem J.* **336**(Pt 1), 1–17 (1998).
14. Caldwell, R. W., Rodriguez, P. C., Toque, H. A., Narayanan, S. P. & Caldwell, R. B. Arginase: a multifaceted enzyme important in health and disease. *Physiol. Rev.* **98**, 641–665 (2018).
15. Munder, M. et al. Th1/th2-regulated expression of arginase isoforms in murine macrophages and dendritic cells. *J. Immunol.* **163**, 3771–3777 (1999).
16. Rath, M., Muller, I., Kropf, P., Closs, E. I. & Munder, M. Metabolism via arginase or nitric oxide synthase: two competing arginine pathways in macrophages. *Front. Immunol.* **5**, 532 (2014).
17. Greenhalgh, A. D. et al. Arginase-1 is expressed exclusively by infiltrating myeloid cells in CNS injury and disease. *Brain Behav. Immun.* **56**, 61–67 (2016).
18. Zarruk, J. G., Greenhalgh, A. D. & David, S. Microglia and macrophages differ in their inflammatory profile after permanent brain ischemia. *Exp. Neurol.* **301**(Pt B), 120–132 (2018).
19. Shosha, E. et al. Arginase 2 promotes neurovascular degeneration during ischemia/reperfusion injury. *Cell Death Dis.* **7**, e2483 (2016).
20. Yau, T. et al. Preliminary efficacy, safety, pharmacokinetics, pharmacodynamics and quality of life study of pegylated recombinant human arginase 1 in patients with advanced hepatocellular carcinoma. *Invest. New Drugs* **33**, 496–504 (2015).
21. Morrow, K. et al. Anti-leukemic mechanisms of pegylated arginase I in acute lymphoblastic t-cell leukemia. *Leukemia* **27**, 569–577 (2013).
22. Mussai, F. et al. Arginine dependence of acute myeloid leukemia blast proliferation: a novel therapeutic target. *Blood* **125**, 2386–2396 (2015).
23. Fletcher, M. et al. L-arginine depletion blunts antitumor T-cell responses by inducing myeloid-derived suppressor cells. *Cancer Res.* **75**, 275–283 (2015).
24. Feun, L. G., Kuo, M. T. & Savaraj, N. Arginine deprivation in cancer therapy. *Curr. Opin. Clin. Nutr. Metab. Care* **18**, 78–82 (2015).
25. Iyer, R. K. et al. Mouse model for human arginase deficiency. *Mol. Cell Biol.* **22**, 4491–4498 (2002).

26. Yokota, H. et al. Neuroprotection from retinal ischemia/reperfusion injury by NOX2 NADPH oxidase deletion. *Invest. Ophthalmol. Vis. Sci.* **52**, 8123–8131 (2011).
27. Zheng, L., Gong, B., Hatala, D. A. & Kern, T. S. Retinal ischemia and reperfusion causes capillary degeneration: similarities to diabetes. *Invest. Ophthalmol. Vis. Sci.* **48**, 361–367 (2007).
28. Rosenbaum, D. M. et al. The role of the p53 protein in the selective vulnerability of the inner retina to transient ischemia. *Invest. Ophthalmol. Vis. Sci.* **39**, 2132–2139 (1998).
29. Schmid, H., Renner, M., Dick, H. B. & Joachim, S. C. Loss of inner retinal neurons after retinal ischemia in rats. *Invest. Ophthalmol. Vis. Sci.* **55**, 2777–2787 (2014).
30. Kim, C. R., Kim, J. H., Park, H. L. & Park, C. K. Ischemia reperfusion injury triggers TNFα induced-necroptosis in rat retina. *Curr. Eye Res.* **42**, 771–779 (2017).
31. Gao, S., Andreeva, K. & Cooper, N. G. Ischemia-reperfusion injury of the retina is linked to necroptosis via the ERK1/2-RIP3 pathway. *Mol. Vis.* **20**, 1374–1387 (2014).
32. Dvoriantchikova, G., Degterev, A. & Ivanov, D. Retinal ganglion cell (RGC) programmed necrosis contributes to ischemia-reperfusion-induced retinal damage. *Exp. Eye Res.* **123**, 1–7 (2014).
33. Rosenbaum, D. M. et al. Necroptosis, a novel form of caspase-independent cell death, contributes to neuronal damage in a retinal ischemia-reperfusion injury model. *J. Neurosci. Res.* **88**, 1569–1576 (2010).
34. Park, S. W. et al. A selective inhibitor of DRP1, Mdivi-1, increases retinal ganglion cell survival in acute ischemic mouse retina. *Invest. Ophthalmol. Vis. Sci.* **52**, 2837–2843 (2011).
35. Viringipurampeer, I. A. et al. NLRP3 inflammasome activation drives bystander cone photoreceptor cell death in a P23H rhodopsin model of retinal degeneration. *Hum. Mol. Genet.* **25**, 1501–1516 (2016).
36. Ahmed, A. et al. Minocycline modulates microglia polarization in ischemia-reperfusion model of retinal degeneration and induces neuroprotection. *Sci. Rep.* **7**, 14065 (2017).
37. Van den Bossche, J., Baardman, J. & de Winther, M. P. Metabolic characterization of polarized M1 and M2 bone marrow-derived macrophages using real-time extracellular flux analysis. *JoVE* **105**, e53424 (2015).
38. Scaduto, R. C. Jr & Grotyohann, L. W. Measurement of mitochondrial membrane potential using fluorescent rhodamine derivatives. *Biophys. J.* **76**(1 Pt 1), 469–477 (1999).
39. Dranka, B. P., Hill, B. G. & Darley-Usmar, V. M. Mitochondrial reserve capacity in endothelial cells: the impact of nitric oxide and reactive oxygen species. *Free Radic. Biol. Med.* **48**, 905–914 (2010).
40. Esser, P., Bresgen, M., Fischbach, R., Heimann, K. & Wiedemann, P. Intercellular adhesion molecule-1 levels in plasma and vitreous from patients with vitreoretinal disorders. *Ger. J. Ophthalmol.* **4**, 269–274 (1995).
41. Joussen, A. M. et al. A central role for inflammation in the pathogenesis of diabetic retinopathy. *Faseb J.* **18**, 1450–1452 (2004).
42. Nagai, N. et al. Suppression of diabetes-induced retinal inflammation by blocking the angiotensin II type 1 receptor or its downstream nuclear factor-kappaB pathway. *Invest. Ophthalmol. Vis. Sci.* **48**, 4342–4350 (2007).
43. Barber, A. J. et al. Neural apoptosis in the retina during experimental and human diabetes. Early onset and effect of insulin. *J. Clin. Invest.* **102**, 783–791 (1998).
44. Villarroel, M., Ciudin, A., Hernandez, C. & Simo, R. Neurodegeneration: an early event of diabetic retinopathy. *World J. Diabetes* **1**, 57–64 (2010).
45. Gonzalez-Leon, M. C. et al. Nitric oxide induces SOCS-1 expression in human monocytes in a TNF-alpha-dependent manner. *J. Endotoxin Res.* **12**, 296–306 (2006).
46. Kuo, H. P. et al. Nitric oxide modulates interleukin-1beta and tumor necrosis factor-alpha synthesis by alveolar macrophages in pulmonary tuberculosis. *Am. J. Respir. Crit. Care Med.* **161**, 192–199 (2000).
47. Yan, L., Wang, S., Rafferty, S. P., Wesley, R. A. & Danner, R. L. Endogenously produced nitric oxide increases tumor necrosis factor-alpha production in transfected human U937 cells. *Blood* **90**, 1160–1167 (1997).
48. Van Dervort, A. L. et al. Nitric oxide regulates endotoxin-induced tnf-alpha production by human neutrophils. *J. Immunol.* **152**, 4102–4109 (1994).
49. Eigler, A., Sinha, B. & Endres, S. Nitric oxide-releasing agents enhance cytokine-induced tumor necrosis factor synthesis in human mononuclear cells. *Biochem. Biophys. Res. Commun.* **196**, 494–501 (1993).
50. Wang, S., Yan, L., Wesley, R. A. & Danner, R. L. Nitric oxide increases tumor necrosis factor production in differentiated U937 cells by decreasing cyclic AMP. *J. Biol. Chem.* **272**, 5959–5965 (1997).
51. del Fresno, C. et al. Nitric oxide activates the expression of IRAK-M via the release of TNF-alpha in human monocytes. *Nitric Oxide* **10**, 213–220 (2004).
52. Deakin, A. M., Payne, A. N., Whittle, B. J. & Moncada, S. The modulation of IL-6 and TNF-alpha release by nitric oxide following stimulation of J774 cells with LPS and IFN-gamma. *Cytokine* **7**, 408–416 (1995).
53. Kalra, D. et al. Nitric oxide provokes tumor necrosis factor-alpha expression in adult feline myocardium through a cGMP-dependent pathway. *Circulation* **102**, 1302–1307 (2000).
54. Nakaizumi, A. et al. Nitric oxide potentiates TNF-α-induced neurotoxicity through suppression of NF-κB. *Cell. Mol. Neurobiol.* **32**, 95–106 (2012).
55. Kelly, B. & O'Neill, L. A. Metabolic reprogramming in macrophages and dendritic cells in innate immunity. *Cell Res.* **25**, 771–784 (2015).
56. Hardbower, D. M. et al. Ornithine decarboxylase regulates M1 macrophage activation and mucosal inflammation via histone modifications. *Proc. Natl. Acad. Sci. USA* **114**, E751–e760 (2017).
57. Kronenberg, G. et al. Distinguishing features of microglia- and monocyte-derived macrophages after stroke. *Acta Neuropathol.* **135**, 551–568 (2018).
58. Miro-Mur, F. et al. Immature monocytes recruited to the ischemic mouse brain differentiate into macrophages with features of alternative activation. *Brain Behav. Immun.* **53**, 18–33 (2016).
59. Gliem, M. et al. Macrophages prevent hemorrhagic infarct transformation in murine stroke models. *Ann. Neurol.* **71**, 743–752 (2012).
60. Wattananit, S. et al. Monocyte-derived macrophages contribute to spontaneous long-term functional recovery after stroke in mice. *J. Neurosci.* **36**, 4182–4195 (2016).
61. Min, H., Jang, Y. H., Cho, I. H., Yu, S. W. & Lee, S. J. Alternatively activated brain-infiltrating macrophages facilitate recovery from collagenase-induced intracerebral hemorrhage. *Mol. Brain* **9**, 42 (2016).
62. Russo, M. V., Latour, L. L. & McGavern, D. B. Distinct myeloid cell subsets promote meningeal remodeling and vascular repair after mild traumatic brain injury. *Nat. Immunol.* **19**, 442–452 (2018).
63. Liu, C. et al. Macrophages mediate the repair of brain vascular rupture through direct physical adhesion and mechanical traction. *Immunity* **44**, 1162–1176 (2016).
64. Dejda, A. et al. Neuropilin-1-expressing microglia are associated with nascent retinal vasculature yet dispensable for developmental angiogenesis. *Invest. Ophthalmol. Vis. Sci.* **57**, 1530–1536 (2016).
65. Shi, O. et al. Generation of a mouse model for arginase II deficiency by targeted disruption of the arginase II gene. *Mol. Cell. Biol.* **21**, 811–813 (2001).
66. Narayanan, S. P. et al. Arginase 2 deletion reduces neuro-glial injury and improves retinal function in a model of retinopathy of prematurity. *PLoS ONE* **6**, e22460 (2011).
67. Suwanpradid, J., Rojas, M., Behzadian, M. A., Caldwell, R. W. & Caldwell, R. B. Arginase 2 deficiency prevents oxidative stress and limits hyperoxia-induced retinal vascular degeneration. *PLoS ONE* **9**, e110604 (2014).
68. Bhatta, A. et al. Obesity-induced vascular dysfunction and arterial stiffening requires endothelial cell arginase 1. *Cardiovasc. Res.* **113**, 1664–1676 (2017).
69. Chou, J. C., Rollins, S. D. & Fawzi, A. A. Trypsin digest protocol to analyze the retinal vasculature of a mouse model. *JoVE* **76**, e50489 (2013).
70. Wang, J., Saul, A., Cui, X., Roon, P. & Smith, S. B. Absence of sigma 1 receptor accelerates photoreceptor cell death in a murine model of retinitis pigmentosa. *Invest. Ophthalmol. Vis. Sci.* **58**, 4545–4558 (2017).
71. Layoun, A., Samba, M. & Santos, M. M. Isolation of murine peritoneal macrophages to carry out gene expression analysis upon toll-like receptors stimulation. *JoVE* **98**, e52749 (2015).
72. Ying, W., Cheruku, P. S., Bazer, F. W., Safe, S. H. & Zhou, B. Investigation of macrophage polarization using bone marrow derived macrophages. *JoVE* **76**, e50323 (2013).

Neurofibromin Deficiency Induces Endothelial Cell Proliferation and Retinal Neovascularization

Hanfang Zhang,[1,2] Farlyn Z. Hudson,[1,2] Zhimin Xu,[2] Rebekah Tritz,[1,2] Modesto Rojas,[2,3] Chintan Patel,[2] Stephen B. Haigh,[2] Zsuzsanna Bordán,[2] David A. Ingram,[4,5] David J. Fulton,[2,3] Neal L. Weintraub,[2,6] Ruth B. Caldwell,[2,7–9] and Brian K. Stansfield[1,2,7]

[1]Department of Pediatrics and Neonatal-Perinatal Medicine, Augusta University, Augusta, Georgia, United States
[2]Vascular Biology Center, Augusta University, Augusta, Georgia, United States
[3]Department of Pharmacology and Toxicology, Augusta University, Augusta, Georgia, United States
[4]Herman B. Wells Center for Pediatric Research, Indiana University School of Medicine, Indianapolis, Indiana, United States
[5]Department of Neonatal-Perinatal Medicine, Indiana University School of Medicine, Indianapolis, Indiana, United States
[6]Department of Cardiology, Augusta University, Augusta, Georgia, United States
[7]Vision Discovery Institute, Augusta University, Augusta, Georgia, United States
[8]Department of Cellular Biology and Anatomy, Augusta University, Augusta, Georgia, United States
[9]Charlie Norwood VA Medical Center, Augusta, Georgia, United States

Correspondence: Brian K. Stansfield, Division of Neonatal/Perinatal Medicine, Department of Pediatrics, Augusta University, 1120 15th Street, BIW6033, Augusta, GA 30912, USA; bstansfield@augusta.edu.

Submitted: July 10, 2017
Accepted: April 14, 2018

Citation: Zhang H, Hudson FZ, Xu Z, et al. Neurofibromin deficiency induces endothelial cell proliferation and retinal neovascularization. *Invest Ophthalmol Vis Sci*. 2018;59:XXX–XXX. https://doi.org/10.1167/iovs.17-22588

Purpose. Neurofibromatosis type 1 (NF1) is the result of inherited mutations in the *NF1* tumor suppressor gene, which encodes the protein neurofibromin. Eye manifestations are common in NF1 with recent reports describing a vascular dysplasia in the retina and choroid. Common features of NF1 retinopathy include tortuous and dilated feeder vessels that terminate in capillary tufts, increased endothelial permeability, and neovascularization. Given the retinal vascular phenotype observed in persons with NF1, we hypothesize that preserving neurofibromin may be a novel strategy to control pathologic retinal neovascularization.

Methods. *Nf1* expression in human endothelial cells (EC) was reduced using small hairpin (sh) RNA and EC proliferation, migration, and capacity to form vessel-like networks were assessed in response to VEGF and hypoxia. Wild-type (WT), *Nf1* heterozygous ($Nf1^{+/-}$), and $Nf1^{flox/+}$;Tie2cre pups were subjected to hyperoxia/hypoxia using the oxygen-induced retinopathy model. Retinas were analyzed quantitatively for extent of retinal vessel dropout, neovascularization, and capillary branching.

Results. Neurofibromin expression was suppressed in response to VEGF, which corresponded with activation of Mek-Erk and PI3-K-Akt signaling. Neurofibromin-deficient EC exhibited enhanced proliferation and network formation in response to VEGF and hypoxia via an Akt-dependent mechanism. In response to hyperoxia/hypoxia, $Nf1^{+/-}$ retinas exhibited increased vessel dropout and neovascularization when compared with WT retinas. Neovascularization was similar between $Nf1^{+/-}$ and $Nf1^{flox/+}$;Tie2cre retinas, but capillary drop out in $Nf1^{flox/+}$;Tie2cre retinas was significantly reduced when compared with $Nf1^{+/-}$ retinas.

Conclusions. These data suggest that neurofibromin expression is essential for controlling endothelial cell proliferation and retinal neovascularization and therapies targeting neurofibromin-deficient EC may be beneficial.

Keywords: neurofibromatosis, endothelial cell, VEGF, retinopathy of prematurity, Ras

Neurofibromatosis type 1 (NF1) is the most common autosomal dominant tumor predisposition syndrome and affects 1 in 2500 persons worldwide.[1] Inactivating mutations in the *NF1* tumor suppressor gene cause NF1. Neurofibromin, the product of *NF1*, functions as a GTP-ase activating protein (GAP) for $p21^{Ras}$ (Ras) and suppresses RAS activity by enhancing the slow intrinsic hydrolysis of active GTP-Ras. Thus, neurofibromin-deficient cells exhibit enhanced activity of the Ras-dependent kinases, Erk and Akt, leading to a prosurvival phenotype.

Eye manifestations are diagnostic of NF1.[2] Lisch nodules (iris hamartomas) present in early childhood and optic pathway gliomas (OPG) affect 15% of NF1 patients.[3,4] More recently, abnormalities in the retinal and choroidal vasculature have been appreciated with an estimated prevalence between 60% and 100% of persons with NF1.[5–11] Retinal capillaries and feeder vessels appear tortuous and disorganized and are often found in close proximity to choroidal abnormalities. Similarly, Shields et al.[12,13] have identified an association between retinal vasoproliferative tumors (RVPT) and NF1, which is often associated with visual disturbances. Vascular features of RVPT in NF1 include dilated feeder vessels (100%), edema (100%), exudation (100%), vitreoretinal hemorrhage (50%), and retinal neovascularization (30%). Interestingly, the median age of clinical presentation was 12 years (9–36), which is considerably younger than the median age of presentation in non-NF1 patients (45 years).[14]

Investigative Ophthalmology & Visual Science

Based on the clinical rationale that persons with NF1 are predisposed to pathologic retinal neovascularization and other vascular abnormalities, the present study aims to identify neurofibromin's function in VEGF-induced endothelial cell proliferation, migration, and vessel-like network formation and characterize retinal neovascularization in neurofibromin-deficient mice in response to hyperoxia/hypoxia. Our findings suggest that neurofibromin expression is critical for limiting VEGF and hypoxia-induced EC proliferation and vessel-like network formation via Ras-Akt activation. Using the murine oxygen-induced retinopathy model, we demonstrate that *Nf1* heterozygosity ($Nf1^{+/-}$) enhances retinal neovascularization and impairs vascular regrowth. Further, *Nf1* heterozygosity in Tie2+ EC is sufficient to reproduce the enhanced neovascularization observed in $Nf1^{+/-}$ retinas, but also promotes vascular regrowth following hyperoxia-induced vaso-obliteration.

Methods

Human Endothelial Cell Culture

Pooled human endothelial colony forming cells (ECFC, endothelial outgrowth cells) were purchased from the Angio BioCore at Indiana University (Principal Investigator: Karen Pollock, ~~Ph.D.~~).[15] Human microvascular endothelial cells (HMVEC) were purchased from Lonza (city, state, country). ECFC and HMVEC were maintained in Endothelial Basal Medium-2 (EBM2; Lonza) with additives (bullet kit) provided by the manufacturer. The media was supplemented with 10% FBS (Hyclone, city, state, country) and 2% penicillin/streptomycin. All cells were maintained 37°C, 5% CO_2 at normoxia unless otherwise stated.

NF1 Gene Silencing

Lentiviral vectors expressing *NF1* small hairpin (sh) RNA and shCtr were purchased from Sigma (CAT# TRCN0000023878, TRCN0000039713, and SHC202; city, state, country). To generate lentiviral supernatant, 293 FT packaging cells were plated onto tissue culture plates and transfected the following day using Lipotectamine 3000 (Invitrogen, city, state, country) according to manufacturer's instructions. The transfected cells were incubated in Dulbecco's modified Eagle's Medium (DMEM; manufacturer, city, state, country) supplemented with 10% FBS. Viral stocks were harvested 24 hours after transfection, with collection at 48 and 72 hours, clarified by centrifugation, filtered through a 0.45-μm filter and stored at –80C. Human ECFC were seeded onto tissue culture plates coated with collagen and transduced with lentiviral stock diluted at 1:3 to 1:5 with EOC culture medium in the presence of 8 μg/mL polybrene (manufacturer, city, state, country) for 8 hours. Fresh medium was replaced. At 48 hours posttransduction fresh medium with 0.5 μg/mL puromycin (manufacturer, city, state, country) was replaced for 3 days. Selected cells were subcultured and *NF1* knockdown was confirmed by Western blot.

Reagents

The following antibodies were used: anti-neurofibromin (#A300; Bethyl Laboratories, city, state, country); anti-phospho-Akt XP (#4060), anti-Akt (#2938S), anti-phospho-Erk XP (#4370), anti-Erk (#4695S; Cell Signaling, city, state, country); anti-phospho-endothelial nitric oxide synthase (eNOS) (612392) and FITC-anti-CD31 (BD Laboratories, city, state, country); and anti-GAPDH (Novus, city, state, country). Recombinant human and murine VEGF were purchased from Peprotech (city, state, country). Wortmannin was purchased from Cayman Chemicals (city, state, country).

BrdU Incorporation

BrdU incorporation into ECFC was performed according to the manufacturer's instructions (Millipore, city, state, country). Briefly, ECFC were progressively serum starved (5% FBS for 24 hours, 1% FBS for 7 hours, 0.125% for experiments) prior to the addition of VEGF (25 ng/mL). Two hours after the addition of VEGF, media was supplemented with BrdU and cells were fixed 24 or 48 hours following VEGF stimulation. Fixed cells were labeled with anti-BrdU monoclonal antibody followed by a goat anti-mouse IgG Peroxidase Conjugate. Signal intensity was measured using a spectrophotometer at 450/550 nm (manufacturer, city, state, country). In some experiments, ECFC were cultured in sealed chamber with an environmental oxygen concentration of 1% (ProOx 110; BioSpherix, city, state, country).

Vessel-Like Network Formation

The formation of closed vessel-like networks was assessed in *NF1*KD and Scr ECFC in response to VEGF as previously described.[16] Briefly, 96-well plates were coated with 30 μL Matrigel (Corning, city, state, country) and ECFC were seeded at a density of 10,000 cells per well. Cells were observed every 4 hours using an inverted microscope (manufacturer, city, state, country). and three uniform ×40 high-power images were captured for each well. The number of intact vessel-like networks were counted and averaged per ×20 high-power field.

Animals

All experiments were approved by the Institutional Committee for Animal Use in Research and Education and conformed to the ARVO Statement for the Use of Animals in Ophthalmic and Vision Research. $Nf1^{+/-}$ mice were obtained from Tyler Jacks (Massachusetts Institute of Technology, Cambridge, MA, USA) and backcrossed 13 generations into the C57BL/6J strain. $Nf1^{flox/flox}$ mice were obtained from Luis Parada (University of Texas Southwestern Medical Center, Dallas, TX, USA) and maintained on C57BL/6J background. Tie2cre (4128) and VE-cadherin cre (VEcre, 6137) mice were purchased from The Jackson Laboratory (city, state, country) and maintained on C57BL/6J background. $Nf1^{flox/flox}$ mice were crossed with Tie2cre or VEcre mice to generate $Nf^{flox/+}$;Tie2cre or $Nf^{flox/+}$;VE-cre and $Nf1^{flox/+}$ (control) mice. *Cre*-mediated recombination was confirmed by PCR as previously described.[17]

Matrigel Plug Assay

Matrigel plugs were incubated with VEGF in the presence or absence of wortmannin and inserted into wild-type (WT) and $Nf1^{+/-}$ mice as previously described.[18] Concentrated Matrigel (Corning) was diluted and mixed with VEGF (100 ng/mL)$^{+/-}$ wortmannin (25 nM) on ice. WT and $Nf1^{+/-}$ mice were anesthetized via inhalation of isoflurane (2%)/oxygen (98%) mixture. An equal volume of Matrigel was then injected slowly into the subcutaneous layer on the abdomen of WT and $Nf1^{+/-}$ mice. Ten days after Matrigel insertion, animals were killed and Matrigel plugs were harvested for analysis. Matrigel plugs were photographed using a digital camera (manufacturer, city, state, country), fixed in paraformaldehyde, and labeled with FITC anti-CD31 antibody. Digital images were obtained using a Zeiss Axioplan 2 Imaging System (city, state, country). Six mice per condition were used.

Investigative Ophthalmology & Visual Science

Endothelial Cell Outgrowth From Aortic Rings

Thoracic aortas were isolated from WT and $Nf1^{+/-}$ mice, removed of periadventicial fat, and cut into 1-mm rings. Three aortic rings from each animal were transferred to 24-well collagen-coated plate and maintained in optimized HMVEC growth media. Culture media was supplemented with 100 ng/mL of VEGF (Sigma) and endothelial cell outgrowth was monitored every other day for 12 days. Aortic rings were photographed using an inverted microscope with non–phase contrast optics at day 12 and the number of cells per image was quantified by a blinded observer and averaged for each animal. For some experiments, wortmannin (25 nM) was added to the aortic rings. Aortic rings from three animals per condition were used.

Oxygen-Induced Retinopathy

Retinopathy was induced in newborn C57Bl/6 mice as previously described by Smith et al.[19] On postnatal day 7 (P7), dams and pups were placed in a sealed chamber in which the oxygen concentration was maintained at 75% oxygen. At P12, animals were transferred back to cages maintained in normoxia (21%). Room temperature was maintained on a 12-hour light/dark cycle. Newborn pups and dams were provided standard chow and water ad libitum. Six to seven pups per litter were used for all experiments.

Analysis of Vessel Dropout and Neovascularization

Animals were killed on P17 and eyeballs were removed and fixed in 4% paraformaldehyde for analysis. Following fixation, retinas were isolated, washed in PBS, and retinal flatmounts prepared. Retinal tissue was permeablized in 10% Triton X-100 (Sigma) and incubated with isolectin GS-$1B_4$ Alexa Fluor 594 (Fisher, city, state, country) in the dark overnight at 4°C. Retinas were placed on glass slides, incubated in Vectashield mounting media (Vector Labs, city, state, country)) and digital images were acquired using a Zeiss Axioplan 2 Imaging System. Digital images were assembled using Photoshop (Adobe Systems, Inc., San Jose, CA, USA) for further analysis. Central vessel dropout area was quantified from the digital images using the ImageJ software (http://imagej.nih.gov/ij/; provided in the public domain by the National Institutes of Health, Bethesda, MD, USA) and neovascular area was determined using the Swift_NV macro for ImageJ.[20] Branching was also determined by counting terminal cells proximal to the central vessel dropout zone.

?9

Statistical Analysis

The results of cell culture experiments are presented as mean ± SEM. Vessel dropout, neovascular area, and branching are presented as mean ± SD. Endothelial cell BrdU incorporation, vessel-like network formation, vessel dropout, neovascular area, and branching were compared by two-way ANOVA with Tukey's post hoc test for multiple comparisons. Analysis was performed using GraphPad Prism version 6.0h (La Jolla, CA, USA). $P < 0.05$ was considered significant.

Results

Neurofibromin Regulates VEGF Signaling in EC

Activation of the RTK VEGFR2 leads to phosphorylation of the Ras kinases, Erk and Akt; however, the role of neurofibromin in regulating VEGF/VEGFR2 signaling is poorly understood. Incubation of human ECFC (Fig. 1A) with VEGF reduced neurofibromin protein expression in confluent and subconfluent (60%–70%) ECFC (Figs. 1B, 1C). These observations corresponded with enhanced phosphorylation of Akt and Erk kinases. Expression of total Erk and Akt were unchanged (data not shown). A similar molecular signature was observed in HMVEC (Fig. 1D). In both cell types, neurofibromin expression was decreased transiently in response to VEGF and neurofibromin expression was fully restored by 30 minutes after VEGF treatment, which corresponded with blunting of Erk and Akt phosphorylation (data not shown).

Nf1 Knockdown Activates Ras and Enhances EC Proliferation and Vessel-Like Network Formation

Using two shRNA constructs targeting the *Nf1* gene, we show that decreased neurofibromin expression in ECFC (*NF1*KD) does not enhance Erk or Akt phosphorylation in the absence of growth factor stimulation (Fig. 2A). For subsequent experiments, we elected to use shNF1 (*NF1*KD). In response to VEGF, *NF1KD* ECFC exhibit enhanced Erk phosphorylation as compared with shCtr ECFC. On the other hand, phosphorylation of Akt appears to be similar between shCtr and *NF1*KD ECFC, which is consistent with preferential activation of canonical Ras-Erk signaling in neurofibromin-deficient cells. Next, we treated *Nf1*KD ECFC with VEGF and examined EC proliferation using BrdU incorporation. *NF1*KD ECFC exhibited a time-dependent increase in BrdU incorporation when compared with shCtr ECFC (Figs. 2B, 2C). Similarly, vessel-like network formation was enhanced in *NF1*KD ECFC when compared with shCtr ECFC, which is completely blocked by treatment of *NF1*KD ECFC with the PI3-K-Akt inhibitor wortmannin (Figs. 2D, 2E).

Hypoxia and VEGF Exert Additive Effects on *NF1*KD ECFC Proliferation

Ischemic retinopathy is the pathologic consequence of perturbations in VEGF expression and activity, coupled with a relative oxygen gradient, leading to disruptions in EC proliferation and capillary formation. Because VEGF markedly increased proliferation and vessel-like network formation in *NF1*KD ECFC, we used BrdU incorporation to assess ECFC proliferation in response to hypoxia and/or VEGF. *NF1*KD ECFC exhibits a modest, but nonsignificant proliferative advantage over shCtr ECFC (Fig. 3). However, hypoxia (1%) exposure and VEGF amplified proliferation in *NF1*KD ECFC when compared with Scr ECFC. Together, VEGF and hypoxia synergistically enhance proliferation in *NF1*KD ECFC. A similar, but more modest trend, was observed in shCtr ECFC.

$Nf1^{+/-}$ EC Angiogenic Sprouting is Enhanced by VEGF

Based on our observation that VEGF suppresses neurofibromin expression and that *NF1*KD ECFC proliferation and vessel-like network formation is significantly increased in *NF1*KD ECFC when compared with shCtr ECFC, we isolated thoracic aortic rings to examine EC outgrowth in response to VEGF. EC outgrowth was significantly higher in $Nf1^{+/-}$ aortic rings stimulated with VEGF when compared with WT aortic rings stimulated with VEGF (Figs. 4A, 4B). Suppression of Akt phosphorylation with wortmannin effectively blocked EC outgrowth from $Nf1^{+/-}$ aortic rings (Figs. 4A, 4B). Next, we used the Matrigel plug assay to confirm these observations. Matrigel supplemented with VEGF (100 ng/mL) were implanted into the subcutaneous layer of $Nf1^{+/-}$ and WT mice. In response to VEGF, Matrigel plugs harvested from $Nf1^{+/-}$ mice

Investigative Ophthalmology & Visual Science

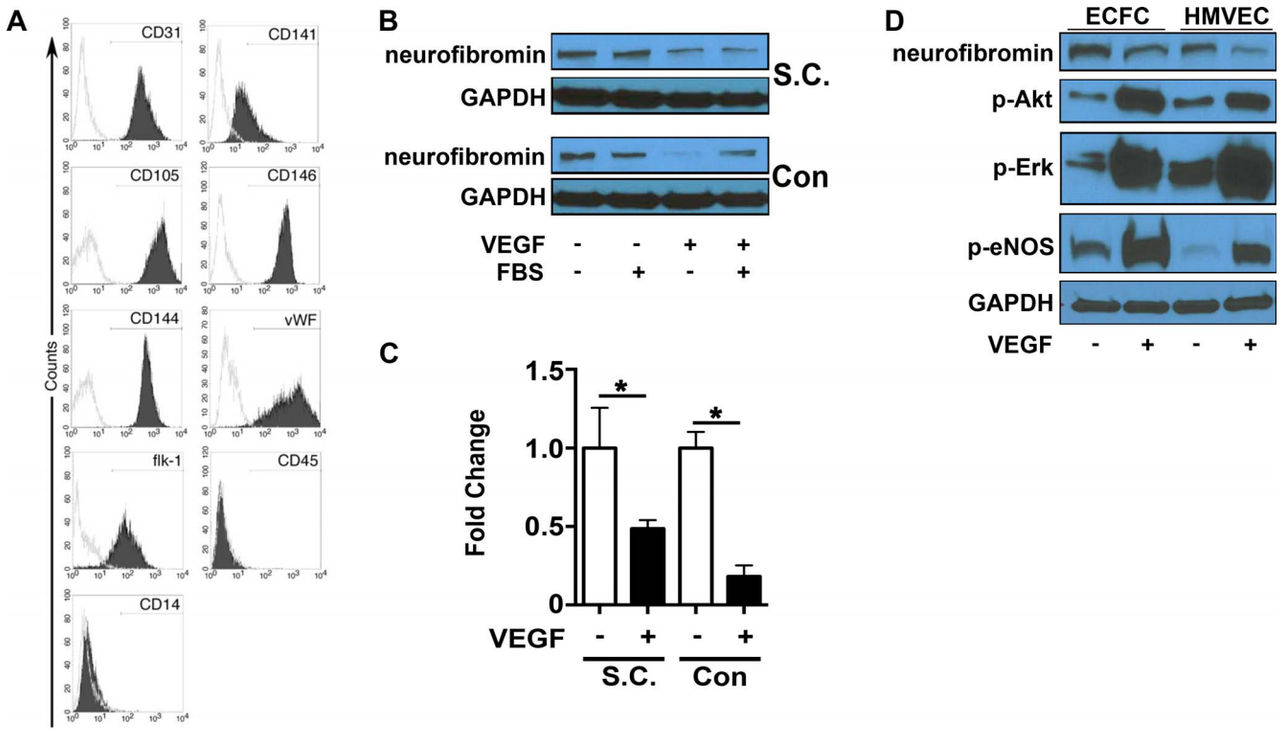

Figure 1. Neurofibromin is a negative regulator of VEGF signaling in endothelial cells. (**A**) Phenotypic characterization of ECFC showing positive and negative selection markers consistent with classification as EC. (**B**, **C**) Representative Western blots (**B**) and quantitative densitometry (**C**) showing neurofibromin expression in response to VEGF (25 ng/mL) in subconfluent and confluent ECFC and HMVEC, $n = 3$. (**D**) Representative Western blots showing neurofibromin expression and phosphorylation of Akt, Erk, and eNOS (1177) in response to VEGF in ECFC and HMVEC, $n = 3$.

were invested with more CD31-positive vessel-like networks when compared with Matrigel plugs harvested from WT mice (Fig. 4C).

Vessel Dropout and Neovascularization are Increased in *Nf1*$^{+/-}$ Mice

Human studies strongly suggest that NF1 patients exhibit pathologic retinal vasculature, endothelial cell overgrowth, and neovascularization. A preclinical model of NF1 retinopathy has not been developed. Therefore, we used the oxygen-induced retinopathy model to assess retinal neovascularization and vessel dropout in *Nf1*$^{+/-}$ and WT mice. Examination of P9 retinas from *Nf1*$^{+/-}$ and WT mice raised in normoxia (21%) revealed a complete network of superficial retinal vessels in both genotypes (data not shown). However, exposure to hyperoxia from P7 to P12 increased central vessel dropout area and enhanced neovascularization in *Nf1*$^{+/-}$ mice at P17 when compared with WT mice (Figs. 5A–C). Neovascular tufts were noted to be approximate to the line of demarcation between the vascular and avascular retina in WT mice. In contrast, neovascularization appeared more diffuse in *Nf1*$^{+/-}$ retinas. The number of branching capillaries adjacent to the avascular retina was increased in *Nf1*$^{+/-}$ mice when compared with WT mice (Figs. 6A, 6B).

Deletion of *Nf1* in Tie2^{+} Cells Enhances Neovascularization and Reduces Vessel Dropout

Based on our observation that *Nf1*$^{+/-}$ retinas have increased vessel dropout and neovascularization, features that are seen in NF1 patients, we used *Cre/lox* technology to delete *Nf1* in Tie2+ EC and examine retinal vasculature in the OIR model. ?10 Similar to previous published reports, homozygous deletion of *Nf1* in Tie2^{+} cells results in midgestation lethality. Therefore, we used *Nf1*$^{flox/+}$;Tie2cre animals, which express a single *Nf1* mutation in Tie2^{+} EC and monocytes/macrophages. Similar to *Nf1*$^{+/-}$ and WT mice, a complete network of superficial retinal vessels was observed in *Nf1*$^{flox/+}$;Tie2cre at P9 (data not shown). In response to hyperoxia/hypoxia, *Nf1*$^{flox/+}$;Tie2cre retinas exhibited increased neovascularization, which was similar qualitatively and quantitatively to *Nf1*$^{+/-}$ retinas (Figs. 7A–C). In contrast to *Nf1*$^{+/-}$ retinas, central vessel dropout was markedly reduced in *Nf1*$^{flox/+}$;Tie2cre and more closely resembled WT retinas (Figs. 7A, 7B).

Deletion of *Nf1* in VE Cadherin^{+} Cells Recapitulates *Nf1*$^{+/-}$ Phenotype

Based on the observation that *Nf1* deletion in Tie2^{+} cells did not fully recapitulate the phenotype observed in *Nf1*$^{+/-}$ retinas, we intercrossed *Nf1*$^{flox/flox}$ and VEcre animals to generate *Nf1*$^{flox/+}$;VEcre offspring and subjected pups to OIR. In response to OIR, *Nf1*$^{flox/+}$;VEcre retinas exhibited increased neovascularization and vessel dropout, which closely resembled our observations in *Nf1*$^{+/-}$ animals (Figs. 8A, 8B).

Discussion

A growing body of evidence supports the hypothesis that Ras activation is crucial for retinal neovascularization and targeting Ras kinases directly or indirectly has proven efficacious in animal models of oxygen-induced retinopathy.[21–24] Erk and Akt, the principal downstream kinases that mediate Ras

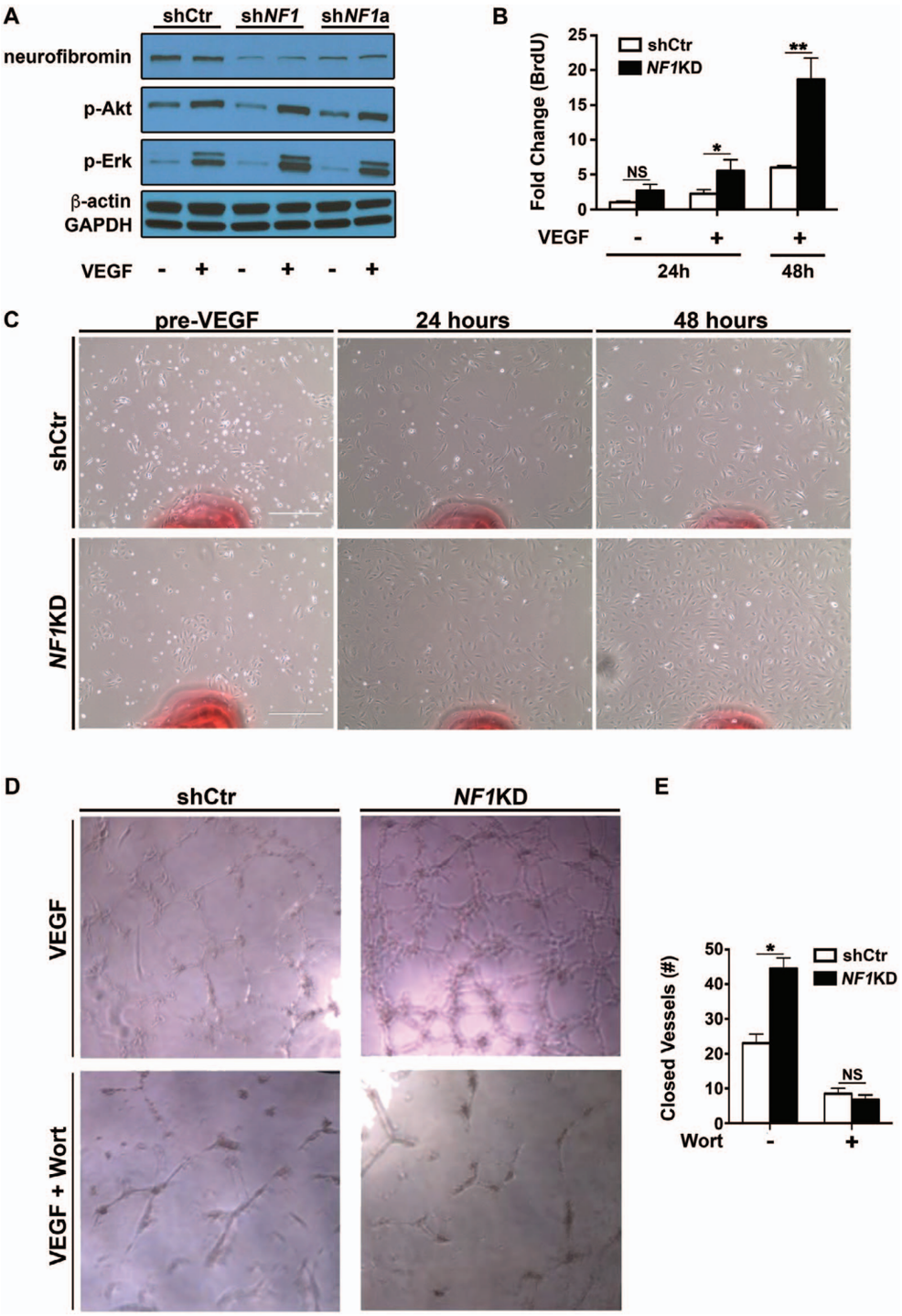

Figure 2. *NF1* silencing enhances Ras signaling endothelial cell function. (**A**) Representative Western blot confirming *NF1* gene silencing (*NF1*KD) and Akt and Erk activation in the presence or absence of VEGF (25 ng/mL). (**B**, **C**) BrdU incorporation (**B**) and photomicrographs (**C**) of control (*white bars*) and *NF1*KD (*black bars*) ECFC in response to VEGF (25 ng/mL) over 48 hours. Data represent mean ± SEM, $^{*}P < 0.01$, $^{**}P < 0.001$, $n = 3$. (**D**, **E**) VEGF-induced vessel-like network formation (**D**) and quantification (**E**) at 12 hours in control and *NF1*KD ECFC in the presence or absence of wortmannin (10 nM), $n = 3$ in triplicate.

signaling, are activated in retinal and nonretinal EC in response to VEGF and their activation is essential for VEGF-induced EC proliferation, migration, and vessel-like network formation.[25–28] Further, phosphorylated Erk colocalizes with VEGFR2 in sprouting endothelial cells during retinal neovascularization and pharmacologic inhibition of Erk kinase and the Akt-mTOR pathway suppresses retinal neovascularization during oxygen-induced retinopathy.[22,25,29,30] Thus, Ras signal-

Investigative Ophthalmology & Visual Science

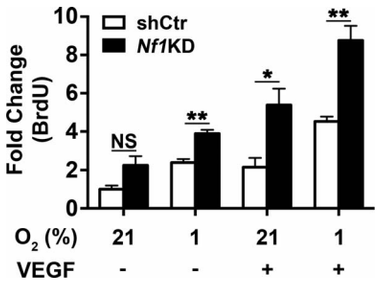

FIGURE 3. Hypoxia and VEGF exert additive effect on *NF1*KD ECFC proliferation. BrdU incorporation in control (*white bars*) and *NF1*KD (*black bars*) ECFC in response to VEGF (25 ng/mL) in ambient (21%) and hypoxic (1%) environment. Data represent mean ± SEM, $^{*}P < 0.05$, $^{**}P < 0.01$, $n = 3$.

ing mediates the effects of VEGF during the neovascular phase of OIR when VEGF expression is rapidly upregulated and Ras activation is essential for sprouting angiogenesis.

Neurofibromin interacts with WT H-, N-, and K-Ras via its GTP-ase regulatory domain (GRD) and serves as a molecular switch for Ras by stabilizing Ras in its diphosphate (inactive) conformation. Thus, neurofibromin suppresses Ras signaling in response to extracellular growth factors, including VEGF, and loss of neurofibromin permits Ras signaling to proceed unchecked. In the present study, we provide the first direct evidence that suppression of neurofibromin is an intermediate step in VEGF activation of the Ras kinases Erk and Akt in circulating and microvascular EC. The transient nature of decreased neurofibromin expression and temporal relationship with the active conformations of Erk and Akt suggests that VEGF-induced Ras activation is tightly regulated by neurofibromin. Growth factor–induced suppression of neurofibromin is the result of protein kinase C (PKC)-mediated ubiquitination and proteasomal degradation.[31] Interestingly, PKC overexpression, which enhances neurofibromin degradation, increases retinal neovascularization while genetic deletion or pharmacologic inhibition of PKC prevents retinal neovascularization in OIR.[32,33] Suppression of neurofibromin permits VEGF-mediated Ras activation and restoration of neurofibromin expression is necessary to turn off VEGF signaling. These relationships are perturbed in persons with NF1 who fail to express full length, active neurofibromin as evidenced by the enhanced proliferation observed in *NF1*KD ECFC in response to VEGF and/or hypoxia. The inability to turn off VEGF-Ras signaling in the setting of neurofibromin-deficiency contributes to uncontrolled EC proliferation and angiogenesis and likely contributes to retinal neovascularization, which is highly prevalent in persons with NF1.

Molecular targeting of Ras kinase activity is particularly attractive in the prevention or treatment of neovascularization with emerging evidence suggesting this approach is both plausible and efficacious.[30,34–37] Ras is active in sprouting retinal EC and appears to be suppressed in quiescent retinal EC during neovascularization.[22] Interestingly, expression of p120RasGAP, a protein that suppresses Ras activity, is poorly expressed in VEGFR2-expressing tip EC during neovascular tuft formation, but is readily expressed after peak tuft formation, which suggests that Ras is tightly regulated during retinal neovascularization.[22] Our observation that VEGF suppresses neurofibromin expression and this suppression corresponds closely with Erk and Akt activation as well as EC proliferation lends support to this hypothesis because vitreoretinal VEGF expression surges during the neovascular phase of OIR. While pharmacologic inhibition of canonical Ras-Erk signaling impairs neurofibromin-deficient EC proliferation, noncanonical activation PI3-K-Akt signaling in these cells is completely unexplored. Similar to increased Erk kinase activity in proliferating retinal EC, Akt expression is upregulated in the hypoxic phase of OIR and administration of an Akt inhibitor during this phase suppresses retinal neovascularization.[38] Additionally, Akt phosphorylates eNOS and eNOS expression and activity is temporally related to hyperoxia and hypoxia in the formation of retinal neovascular tufts.[39–41] Our observation that the PI3-K-Akt inhibitor wortmannin suppresses vessel-like network formation and prevents EC sprouting from $Nf1^{+/-}$ aortic rings suggests that Akt activation is a critical step for neurofibromin-deficient EC proliferation, migration, and capillary formation. However, Erk is also activated in *NF1*KD ECFC and previous studies by our group and others have suggested that pharmacologic inhibition of canonical Ras-Erk signaling impairs neurofibromin-deficient EC proliferation and migration.[27,42] Interestingly, Ismat et al.[43] showed that canonical Ras-Erk signaling is constitutively active and Ras-Akt signaling is suppressed in *Nf1* knockout EC. Expression of the GRD in *Nf1* knockout EC suppressed Erk activity and, conversely, enhanced Akt phosphorylation, which demonstrates the close and sometimes opposing relationship between these two pathways.

While our data demonstrate that *NF1*KD ECFC are highly proliferative and exhibit enhanced angiogenic capacity, we also recognize that stromal cells may influence neurofibromin-deficient EC proliferation and neovascularization in $Nf1^{+/-}$ mice. *NF1* gene silencing in Schwann cells, the principal cells

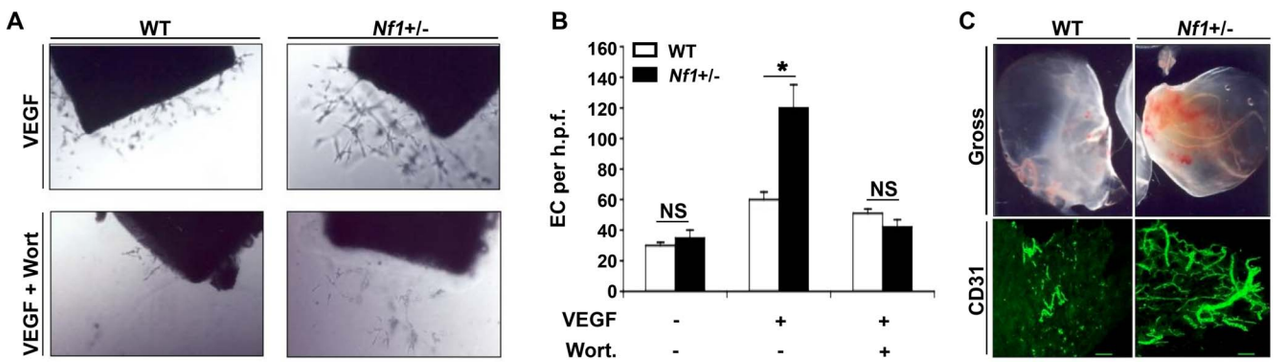

FIGURE 4. VEGF enhances vascular sprouting in $Nf1^{+/-}$ mice and aortas via the Ras-PI-3kinase pathway. (**A**, **B**) Photomicrographs (**A**) and quantification (**B**) of EC outgrowth from aortic rings isolated from WT (*white bars*) and $Nf1^{+/-}$ (*black bars*) mice in response to VEGF in the presence/absence of wortmannin (10 nM). Data represent mean ± SEM, $^{*}P < 0.01$, $n = 3$ in triplicate. (**C**) Photograph and confocal imaging of anti-CD31 staining of Matrigel plugs containing VEGF inserted into WT and $Nf1^{+/-}$ mice.

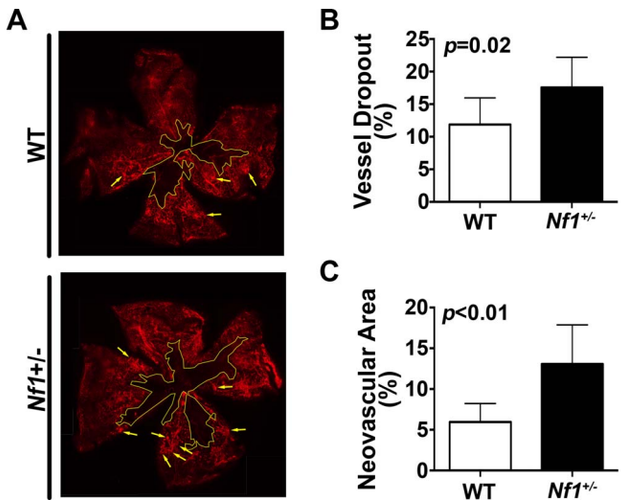

FIGURE 5. Vessel dropout and neovascular area are increased in $Nf1^{+/-}$ retinas. (**A**) Representative photomicrograph of P17 retinal flat mounts isolated from WT and $Nf1^{+/-}$ mice. Central vessel dropout is outlined in *yellow*. *Yellow arrows* indicate neovascular tufts. (**B**, **C**) Quantification of percent vessel dropout (**A**) and neovascular area (**B**) in WT (*white bars*) and $Nf1^{+/-}$ (*black bars*) retinas. Data represent mean ± SD, $n = 10–12$ per group.

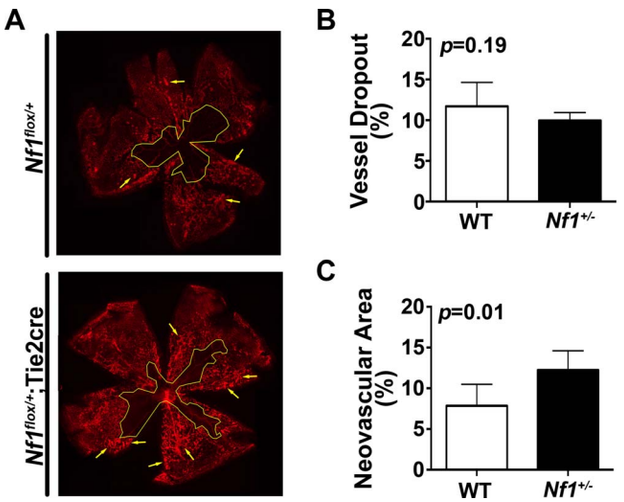

FIGURE 7. Heterozygous deletion of *Nf1* in Tie2+ cells promotes retinal neovascularization. (**A**) Representative photomicrograph of P17 retinal flat mounts isolated from $Nf1^{flox/+}$ and $Nf1^{flox/+}$;Tie2cre mice. Central vessel dropout is outlined in *yellow*. *Yellow arrows* indicate neovascular tufts. (**B**, **C**) Quantification of percent vessel dropout (**A**) and neovascular area (**B**) in $Nf1^{flox/+}$ (white bars) and $Nf1^{flox/+}$;Tie2cre (*black bars*) retinas. Data represent mean ± SD, $n = 10–12$ per group.

in neurofibromas (pathognomonic tumor of NF1), increases VEGF secretion and promotes angiogenesis in $Nf1^{+/-}$ mice27.[44–46] These vascular tumors are characterized by high expression of VEGF and VEGFR2, which provides a clinical rationale for the use of anti-VEGF antibodies and VEGFR2 inhibitors for neurofibromas. Our own observations may suggest that loss of neurofibromin in stromal cells enhances angiogenesis and neovascularization. EC sprouting is increased in aortic explants from $Nf1^{+/-}$ mice and capillary formation was enhanced in Matrigel plugs implanted into $Nf1^{+/-}$ mice, which may be the result of cues from $Nf1^{+/-}$ stromal cells and circulating hematopoietic cells to induce $Nf1^{+/-}$ EC proliferation. In this regard, monocytes and macrophages are intriguing support cells for angiogenic EC and retinal neovascularization. Macrophages are abundant in the retina during the hypoxia phase of OIR and are critical for pathologic neovascularization.[47–49] Nonselective depletion of macrophages has a protective effect against neovascular tuft formation.[50] This line of thinking is intriguing because we recently demonstrated that neurofibromin is a master regulator of macrophage differentiation and neurofibromin-deficient macrophages exhibit a prosurvival phenotype characterized by enhanced proliferation, migration, adhesion, and secretion of growth factors and reactive oxygen species.[51–54] Further, the similarities/differences in neovascular tuft formation between $Nf1^{+/-}$ and $Nf1^{flox/+}$;Tie2cre retinas in response to hyperoxia/hypoxia may be explained by the presence of the Tie2 promoter in both EC and macrophages.[55–57] Deletion of *Nf1* in macrophages increases ROS production and growth factor secretion, which may lead to excessive proliferation of neurofibromin-deficient retinal EC.[52,53] Thus, the neovascular phenotype observed in $Nf1^{+/-}$ and $Nf1^{flox/+}$;Tie2cre retinas may be explained by a cooperation between infiltrating neurofibromin-deficient macrophages and/or resident microglia and angiogenic EC to promote pathologic angiogenesis at the expense of retinal revascularization. Based on the overlapping expression of Tie2 in both EC and hematopoietic cells, we intercrossed the $Nf1^{flox/flox}$ mice with mice expressing Cre under the VE cadherin promoter (VECre). These mice are generally accepted to be highly EC-specific; however, close examination of the

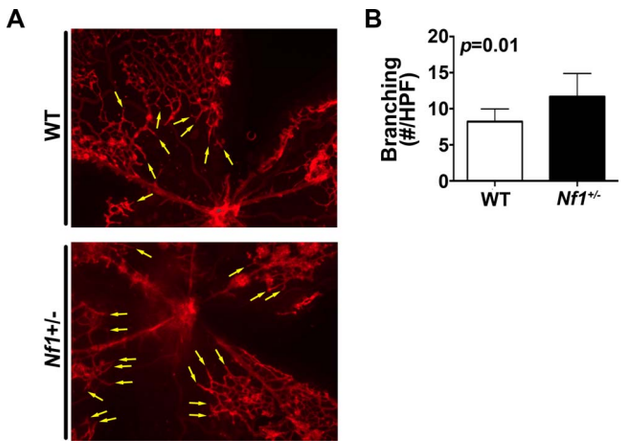

FIGURE 6. Branching is enhanced in $Nf1^{+/-}$ retinas. (**A**) Representative high-power photomicrograph of P17 retinal flat mounts isolated from WT and $Nf1^{+/-}$ mice. *Yellow arrows* indicate angiogenic sprouts. (**B**) Quantification of branching in WT (*white bar*) and $Nf1^{+/-}$ (*black bar*) retinas. Data represent mean ± SD, $n = 10–12$ per group.

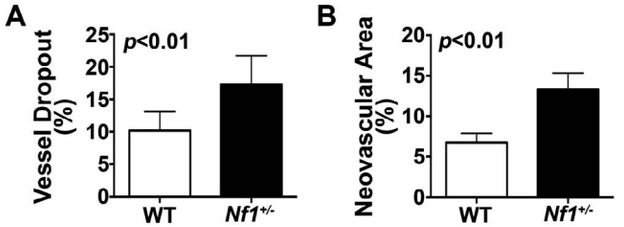

FIGURE 8. Heterozygous deletion of *Nf1* in VE cadherin^{+} cells recapitulates $Nf1^{+/-}$ phenotype. (**A**, **B**) Quantification of percent vessel dropout (**A**) and neovascular area (**B**) in $Nf1^{flox/+}$ (white bars) and $Nf1^{flox/+}$; VECre (*black bars*) retinas. Data represent mean ± SD, $n = 7–8$ per group.

expression pattern of VE cadherin (also known as, Cdh5) in both commercially available Cre lines demonstrates that 50% to 95% of circulating hematopoietic cells in adult mice arise from progenitor cells that at one time expressed VE cadherin.[58,59] Thus, while $Nf1^{flox/+}$;VECre mice completely recapitulate the retina phenotype observed in $Nf1^{+/-}$ mice, cautious interpretation of these results must be taken because *Cre* expression is occurring in EC and circulating hematopoietic cells. Ongoing studies in our laboratory are focused on exploring the relationship between EC and various hematopoietic cells in the pathogenesis of OIR.

Here, we demonstrate that neurofibromin functions as a negative regulator of VEGF signaling in EC. Inactivating mutations in the *NF1* gene confer a proliferative EC phenotype and impair their ability to turn off extracellular cues leading to retinal neovascularization and impaired revascularization. Our findings provide a framework for interrogating VEGF signaling in the retinal vasculature and an in vivo platform for the rational design of antiangiogenic compounds that promote or maintain neurofibromin expression.

Acknowledgments

Supported by grants from the American Heart Association (15SDG25500005, BKS; City, State, Country), Department of Defense (NF140031, BKS; City, State, Country), National Institutes of Health (5R01EY011766, RBC; City, State, Country), and The James and Jean Culver Vision Discovery Institute at Augusta University (City, State, Country).

?11

Disclosure: **H. Zhang**, None; **F.Z. Hudson**, None; **Z. Xu**, None; **R. Tritz**, None; **M. Rojas**, None; **C. Patel**, None; **S.B. Haigh**, None; **Z. Bordán**, None; **D. A. Ingram**, None; **D.J. Fulton**, None; **N.L. Weintraub**, None; **R.B. Caldwell**, None; **B.K. Stanfield**, None

References

1. Hirbe AC, Gutmann DH. Neurofibromatosis type 1: a multidisciplinary approach to care. *Lancet Neurol*. 2014;13:834–843.
2. Riccardi VM. Neurofibromatosis: past, present, and future. *N Engl J Med*. 1991;324:1283–1285.
3. Lubs ML, Bauer MS, Formas ME, Djokic B. Lisch nodules in neurofibromatosis type 1. *N Engl J Med*. 1991;324:1264–1266.
4. Listernick R, Ferner RE, Liu GT, Gutmann DH. Optic pathway gliomas in neurofibromatosis-1: controversies and recommendations. *Ann Neurol*. 2007;61:189–198.
5. Muci-Mendoza R, Ramella M, Fuenmayor-Rivera D. Corkscrew retinal vessels in neurofibromatosis type 1: report of 12 cases. *Br J Ophthalmol*. 2002;86:282–184.
6. Parrozzani R, Pilotto E, Clementi M, et al. Retinal vascular abnormalities in a large cohort of patients affected by neurofibromatosis type 1: a study using optical coherence tomography angiography. *Retina*. 2017;38:585–593.
7. Abdolrahimzadeh S, Felli L, Piraino DC, Mollo R, Calvieri S, Recupero SM. Retinal microvascular abnormalities overlying choroidal nodules in neurofibromatosis type 1. *BMC Ophthalmol*. 2014;14:146.
8. Abdolrahimzadeh S, Felli L, Plateroti R, et al. Morphologic and vasculature features of the choroid and associated choroid-retinal thickness alterations in neurofibromatosis type 1. *Br J Ophthalmol*. 2015;99:789–793.
9. Abdolrahimzadeh S, Plateroti AM, Recupero SM, Lambiase A. An Update on the ophthalmologic features in the phakomatoses. *J Ophthalmol*. 2016;2016:3043026.
10. Yasunari T, Shiraki K, Hattori H, Miki T. Frequency of choroidal abnormalities in neurofibromatosis type 1. *Lancet*. 2000;356:988–992.
11. Viola F, Villani E, Natacci F, et al. Choroidal abnormalities detected by near-infrared reflectance imaging as a new diagnostic criterion for neurofibromatosis 1. *Ophthalmology*. 2012;119:369–375.
12. Shields JA, Pellegrini M, Kaliki S, Mashayekhi A, Shields, CL. Retinal vasoproliferative tumors in 6 patients with neurofibromatosis type 1. *JAMA Ophthalmol*. 2014;132:190–196.
13. Shields JA, Reichstein D, Mashayekhi A, Shields CL. Retinal vasoproliferative tumors in ocular conditions of childhood. *J AAPOS*. 2012;16:6–9.
14. Shields CL, Kaliki S, Al-Dahmash S, et al. Retinal vasoproliferative tumors: comparative clinical features of primary vs secondary tumors in 334 cases. *JAMA Ophthalmol*. 2013;131:328–334.
15. Mund JA, Estes ML, Yoder MC, Ingram DA Jr, Case J. Flow cytometric identification and functional characterization of immature and mature circulating endothelial cells. *Arterioscler Thromb Vasc Biol*. 2012;32:1045–1053.
16. Ingram DA, Mead LE, Tanaka H, et al. Identification of a novel hierarchy of endothelial progenitor cells using human peripheral and umbilical cord blood. *Blood*. 2004;104:2752–2760.
17. Stansfield BK, Bessler WK, Mali R, et al. Heterozygous inactivation of the Nf1 gene in myeloid cells enhances neointima formation via a rosuvastatin-sensitive cellular pathway. *Hum Mol Genet*. 2013;22:977–988.
18. Malinda KM. In vivo matrigel migration and angiogenesis assay. *Methods Mol Biol*. 2009;467:287–294.
19. Smith LE, Wesolowski E, McLellan A, et al. Oxygen-induced retinopathy in the mouse. *Invest Ophthalmol Vis Sci*. 1994;35:101–111.
20. Stahl A, Connor KM, Sapieha P, et al. Computer-aided quantification of retinal neovascularization. *Angiogenesis*. 2009;12:297–301.
21. Pan H, Nguyen NQ, Yoshida H, et al. Molecular targeting of antiangiogenic factor 16K hPRL inhibits oxygen-induced retinopathy in mice. *Invest Ophthalmol Vis Sci*. 2004;45:2413–2419.
22. Westenskow PD, Kurihara T, Aguilar E, et al. Ras pathway inhibition prevents neovascularization by repressing endothelial cell sprouting. *J Clin Invest*. 2013;123:4900–4908.
23. Wu M, Wallace MR, Muir D. Nf1 haploinsufficiency augments angiogenesis. *Oncogene*. 2006;25:2297–2303.
24. Wollen EJ, Kwinta P, Bik-Multanowski M, et al. Hypoxia-reoxygenation affects whole-genome expression in the newborn eye. *Invest Ophthalmol Vis Sci*. 2014;55:1393–1401.
25. Bullard LE, Qi X, Penn JS. Role for extracellular signal-responsive kinase-1 and -2 in retinal angiogenesis. *Invest Ophthalmol Vis Sci*. 2003;44:1722–1731.
26. Grant MB, Davis MI, Caballero S, Feoktistov I, Biaggioni I, Belardinelli, L. Proliferation, migration, and ERK activation in human retinal endothelial cells through A(2B) adenosine receptor stimulation. *Invest Ophthalmol Vis Sci*. 2001;42:2068–2073.
27. Munchhof AM, Li F, White HA, et al. Neurofibroma-associated growth factors activate a distinct signaling network to alter the function of neurofibromin-deficient endothelial cells. *Hum Mol Genet*. 2006;15:1858–1869.
28. Di Y, Zhang Y, Nie Q, Chen X. CCN1/Cyr61-PI3K/AKT signaling promotes retinal neovascularization in oxygen-induced retinopathy. *Int J Mol Med*. 2015;36:1507–1518.
29. Anand S, Majeti BK, Acevedo LM, et al. MicroRNA-132-mediated loss of p120RasGAP activates the endothelium to facilitate pathological angiogenesis. *Nat Med*. 2010;16:909–914.

30. Yagasaki R, Nakahara T, Ushikubo H, Mor A, Sakamoto K, Ishi K. Anti-angiogenic effects of mammalian target of rapamycin inhibitors in a mouse model of oxygen-induced retinopathy. *Biol Pharm Bull*. 2014;37:1838–1842.
31. Hollstein PE, Cichowski K. Identifying the ubiquitin ligase complex that regulates the NF1 tumor suppressor and Ras. *Cancer Discov*. 2013;3:880–893.
32. Suzuma K, Takahara N, Suzuma I, et al. Characterization of protein kinase C beta isoform's action on retinoblastoma protein phosphorylation, vascular endothelial growth factor-induced endothelial cell proliferation, and retinal neovascularization. *Proc Natl Acad Sci U S A*. 2002;99:721–726.
33. Danis RP, Bingaman DP, Jirousek M, Yang Y. Inhibition of intraocular neovascularization caused by retinal ischemia in pigs by PKCbeta inhibition with LY333531. *Invest Ophthalmol Vis Sci*. 1998;39:171–179.
34. Sasore T, Kennedy B. Deciphering combinations of PI3K/AKT/mTOR pathway drugs augmenting anti-angiogenic efficacy in vivo. *PLoS One*. 2014;9:e105280.
35. Jacot JL, Sherris D. Potential therapeutic roles for inhibition of the PI3K/Akt/mTOR pathway in the pathophysiology of diabetic retinopathy. *J Ophthalmol*. 2011;2011:589813.
36. Zhu T, Sennlaub F, Beauchamp MH, et al. Proangiogenic effects of protease-activated receptor 2 are tumor necrosis factor-alpha and consecutively Tie2 dependent. *Arterioscler Thromb Vasc Biol*. 2006;26:744–750.
37. Yang XM, Wang YS, Zhang J, et al. Role of PI3K/Akt and MEK/ERK in mediating hypoxia-induced expression of HIF-1alpha and VEGF in laser-induced rat choroidal neovascularization. *Invest Ophthalmol Vis Sci*. 2009;50:1873–1879.
38. Wang P, Tian XF, Rong JB, Liu D, Yi GG, Tan Q. Protein kinase B (akt) promotes pathological angiogenesis in murine model of oxygen-induced retinopathy. *Acta Histochem Cytochem*. 2011;44:103–111.
39. Ando A, Yang A, Mori K, et al. Nitric oxide is proangiogenic in the retina and choroid. *J Cell Physiol*. 2002;191:116–124.
40. Ando A, Yang A, Nambu H, Campochiaro PA. Blockade of nitric-oxide synthase reduces choroidal neovascularization. *Mol Pharmacol*. 2002;62:539–544.
41. Fulton D, Gratton JP, McCabe TJ, et al. Regulation of endothelium-derived nitric oxide production by the protein kinase Akt. *Nature*. 1999;399:597–601.
42. Bajaj A, Li, QF Zheng Q, Pumiglia K. Loss of NF1 expression in human endothelial cells promotes autonomous proliferation and altered vascular morphogenesis. *PLoS One*. 2012;7:e49222.
43. Ismat FA, Xu J, Lu MM, Epstein JA. The neurofibromin GAP-related domain rescues endothelial but not neural crest development in Nf1 mice. *J Clin Invest*. 2006;116:2378–2384.
44. Kawachi Y, Xu X, Ichikawa E, Imakado S, Otsuka F. Expression of angiogenic factors in neurofibromas. *Exp Dermatol*. 2003;12:412–417.
45. Kotsuji-Maruyama T, Imakado S, Kawachi Y, Otsuka F. PDGF-BB induces MAP kinase phosphorylation and VEGF expression in neurofibroma-derived cultured cells from patients with neurofibromatosis 1. *J Dermatol*. 2002;29:713–717.
46. Kawachi Y, Maruyama H, Ishitsuka Y, et al. NF1 gene silencing induces upregulation of vascular endothelial growth factor expression in both Schwann and non-Schwann cells. *Exp Dermatol*. 2013;22:262–265.
47. Zhou Y, Yoshida S, Nakao S, et al. M2 macrophages enhance pathological neovascularization in the mouse model of oxygen-induced retinopathy. *Invest Ophthalmol Vis Sci*. 2015;56:4767–4777.
48. Sennlaub F, Courtois Y, Goureau O. Inducible nitric oxide synthase mediates the change from retinal to vitreal neovascularization in ischemic retinopathy. *J Clin Invest*. 2001;107:717–725.
49. Gao S, Li C, Zhu Y, et al. PEDF mediates pathological neovascularization by regulating macrophage recruitment and polarization in the mouse model of oxygen-induced retinopathy. *Sci Rep*. 2017;7:42846.
50. Gao X, Wang YS, Li XQ, et al. Macrophages promote vasculogenesis of retinal neovascularization in an oxygen-induced retinopathy model in mice. *Cell Tissue Res*. 2016;364:599–610.
51. Stansfield BK, Bessler WK, Mali R, et al. Ras-mek-erk signaling regulates nf1 heterozygous neointima formation. *Am J Pathol*. 2014;184:79–85.
52. Bessler WK, Kim G, Hudson FZ, et al. Nf1+/- monocytes/macrophages induce neointima formation via CCR2 activation. *Hum Mol Genet*. 2016;25:1129–1139.
53. Bessler WK, Hudson FZ, Zhang H, et al. Neurofibromin is a novel regulator of ras-induced reactive oxygen species production in mice and humans. *Free Radic Biol Med*. 2016;97:212–222.
54. Li F, Downing BD, Smiley LC, et al. Neurofibromin-deficient myeloid cells are critical mediators of aneurysm formation in vivo. *Circulation*. 2014;129:1213–1224.
55. De Palma M, Venneri MA, Galli R, et al. Tie2 identifies a hematopoietic lineage of proangiogenic monocytes required for tumor vessel formation and a mesenchymal population of pericyte progenitors. *Cancer cell*. 2005;8:211–226.
56. De Palma M, Murdoch C, Venneri MA, Naldini L, Lewis CE. Tie2-expressing monocytes: regulation of tumor angiogenesis and therapeutic implications. *Trends Immunol*. 2007;28:519–524.
57. Gomez Perdiguero E, Klapproth K, Schulz C, et al. Tissue-resident macrophages originate from yolk-sac-derived erythro-myeloid progenitors. *Nature*. 2015;518:547–551.
58. Chen MJ, Yokomizo T, Zeigler BM, Dzierzak E, Speck NA. Runx1 is required for the endothelial to haematopoietic cell transition but not thereafter. *Nature*. 2009;457:887–891.
59. Alva JA, Zovein AC, Monvoisin A, et al. VE-Cadherin-Cre-recombinase transgenic mouse: a tool for lineage analysis and gene deletion in endothelial cells. *Dev Dyn*. 2006;235:759–767.

Investigative Ophthalmology & Visual Science

Queries for iovs-59-06-12

Author: This article has been lightly edited for grammar, style, and usage. Please compare against your original document and make changes on these pages. Please limit your corrections to substantive changes that affect meaning. If no change is required in response to a question, please write "OK as set" in the margin. Copy editor

Author: Carefully check the spelling and order of the author names and check the affiliations for all of the authors.

Author: Make sure that ALL funding/financial support is listed in the information following the Acknowledgments.

Author: Check the bottom of the first page to make sure the license shown is the license you prefer. (The two options are the Creative Commons Attribution-NonCommercial-NoDerivatives license and the Creative Commons Attribution license.)

1. Author: Please provide a short title for the running head. Must be 50 characters or fewer (spaces do not count toward the total). Copy editor
2. Author: In the Human Endothelial Cell Culture section, please include location information for Lonza and Hyclone. Copy editor
3. Author: In the NF1 Gene Silencing section, please include location information for Sigma and Invitrogen and include manufacturer information for DMEM, polybrene, and puromycin. Also, please define FT Copy editor
4. Author: In the Regents section, please include location information for all manufacturers. Copy editor
5. Author: In the BrdU Incorporation section, please include location information for Millipore and BioSpherix, and full manufacturer information for the spectrophotometer. Copy editor
6. Author: in the Vessel-Like Network Formation section, please include location and full manufacturer information for Corning and the inverted microscope. Copy editor
7. Author: In the Animals section, sentence 4, please include location information for Jackson Laboratory. Copy editor
8. Author: in the Matrigel Plug Assay section, please include location and full manufacturer information for Zeiss and the digital camera. Also, per journal style, the use of the word "sacrificed" is not preferred and has been changed to "killed" or "euthanized." Copy editor
9. Author: In the Analysis of Vessel Dropout and Neovascularization section, please include location and full manufacturer information for Fisher and Vector Labs Copy editor
10. Author: In the Deletion of *Nf1* in Tie2+ Cells Enhances Neovascularization and Reduces Vessel Dropout section, sentence 1, please define OIR. Copy editor
11. Author: please include location information for all grant funders. Copy editor

Molecular and Cellular Endocrinology xxx (2018) 1–10

Contents lists available at ScienceDirect

Molecular and Cellular Endocrinology

journal homepage: www.elsevier.com/locate/mce

Deletion of the Duffy antigen receptor for chemokines (DARC) promotes insulin resistance and adipose tissue inflammation during high fat feeding

Tyler W. Benson [a], Daniel S. Weintraub [a], Matthew Crowe [a], Nicole K.H. Yiew [a, b], Orishebawo Popoola [a], Ajay Pillai [a], Joel Joseph [a], Krystal Archer [a], Charlotte Greenway [a], Tapan K. Chatterjee [a], James Mintz [a], David W. Stepp [a, c], Brian K. Stansfield [a, d], Weiqin Chen [c], Julia Brittain [a, e], Vladimir Y. Bogdanov [g], Yan Gao [h], James G. Wilson [h], Yaoliang Tang [a, f], Ha Won Kim [a, f, *, 1], Neal L. Weintraub [a, f, **, 1]

[a] Vascular Biology Center, Medical College of Georgia at Augusta University, United States
[b] Departments of Pharmacology and Toxicology, Medical College of Georgia at Augusta University, United States
[c] Physiology, Medical College of Georgia at Augusta University, United States
[d] Pediatrics, Medical College of Georgia at Augusta University, United States
[e] Cellular Biology and Anatomy, Medical College of Georgia at Augusta University, United States
[f] Medicine, Medical College of Georgia at Augusta University, United States
[g] Department of Medicine, University of Cincinnati College of Medicine, United States
[h] Department of Physiology and Biophysics, University of Mississippi Medical Center, United States

ARTICLE INFO

Article history:
Received 21 November 2017
Received in revised form
11 January 2018
Accepted 12 January 2018
Available online xxx

Keywords:
DARC
High fat diet
Obesity
Insulin resistance
Inflammation

ABSTRACT

Objective: Inflammation in adipose tissues in obesity promotes insulin resistance and metabolic disease. The Duffy antigen receptor for chemokines (DARC) is a promiscuous non-signaling receptor expressed on erythrocytes and other cell types that modulates tissue inflammation by binding chemokines such as monocyte chemoattractant protein-1 (MCP-1) and by acting as a chemokine reservoir. DARC allelic variants are common in humans, but the role of DARC in modulating obesity-related metabolic disease is unknown.

Methods: We examined body weight gain, tissue adiposity, metabolic parameters and inflammatory marker expression in wild-type and DARC knockout mice fed a chow diet (CD) and high fat diet (HFD).

Results: Compared to wild-type mice, HFD-fed DARC knockout mice developed glucose intolerance and insulin resistance independent of increases in body weight or adiposity. Interestingly, insulin sensitivity was also diminished in lean male DARC knockout mice fed a chow diet. Insulin production was not reduced by DARC gene deletion, and plasma leptin levels were similar in HFD fed wild-type and DARC knockout mice. MCP-1 levels in plasma rose significantly in the HFD fed wild-type mice, but not in the DARC knockout mice. Conversely, adipose tissue MCP-1 levels were higher, and more macrophage crown-like structures were detected, in the HFD fed DARC knockout mice as compared with the wild-type mice, consistent with augmented adipose tissue inflammation that is not accurately reflected by plasma levels of DARC-bound MCP-1 in these mice.

Abbreviations: DARC, Duffy antigen receptor for chemokines; ACKR1, atypical chemokine receptor 1; CCL, C-C motif chemokine ligand; MCP-1, monocyte chemoattractant protein-1; TNF-α, tissue necrosis factor alpha; HFD, high fat diet; CD, chow diet; IP, intraperitoneal; NMR, nuclear magnetic resonance; CLAMS, comprehensive laboratory animal monitoring system; IL, interleukin; qPCR, quantitative polymerase chain reaction; ELISA, enzyme-linked immunosorbent assay; GTT, glucose tolerance test; ITT, insulin tolerance test.

* Corresponding author. Department of Medicine, Division of Cardiology, Vascular Biology Center, Medical College of Georgia at Augusta University, 1459 Laney Walker Blvd, Augusta, GA 30912, United States.
** Corresponding author. Department of Medicine, Division of Cardiology, Vascular Biology Center, Medical College of Georgia at Augusta University, 1459 Laney Walker Blvd, Augusta, GA 30912, United States
E-mail addresses: hkim3@augusta.edu (H.W. Kim), nweintraub@augusta.edu (N.L. Weintraub).
[1] Drs. Kim and Weintraub contributed equally to this manuscript.

https://doi.org/10.1016/j.mce.2018.01.006

Conclusions: These findings suggest that DARC regulates metabolic function and adipose tissue inflammation, which may impact obesity-related disease in ethnic populations with high frequencies of DARC allelic variants.

1. Introduction

Obesity, which afflicts approximately one-third of the US population, is associated with increased risk for the development of the metabolic syndrome characterized by insulin resistance, abnormal blood glucose, hypertension, and dyslipidemia (Flegal et al., 2012). Diseases associated with obesity and the metabolic syndrome include diabetes, cardiovascular disease, stroke, and certain cancers. The health care costs related to obesity impose an economic burden of up to $190 billion annually (Cawley and Meyerhoefer, 2012) that is projected to increase by $48–66 billion each year by 2030 (Wang et al., 2011).

Obesity is accompanied by chronic low grade inflammation that originates from increased production of pro-inflammatory cytokines and chemokines in adipose tissues. The accumulating chemokines recruit additional immune cells, most notably macrophages, which in turn produce more chemokines in a viscous cycle of chronic inflammation. Certain adipocytokines and chemokines, such as tissue necrosis factor alpha (TNF-α) and monocyte chemoattractant protein-1 (MCP-1), have been causally linked to the development of insulin resistance, a key feature of the metabolic syndrome, and type 2 diabetes (Xu et al., 2003; Kwon and Pessin, 2013). Indeed, genetic deletion or pharmacological inhibition of TNF-α (Hotamisligil et al., 1993; Uysal et al., 1997) or MCP-1 (Weisberg et al., 2006; Kanda et al., 2006) was shown to improve insulin sensitivity in mice in the setting of obesity. MCP-1 levels were also reported to be elevated in plasma of obese patients (Huber et al., 2008), correlating with the degree of insulin resistance (Kim et al., 2006). Conversely, in other studies, MCP-1 deficiency in mice failed to restrain macrophage recruitment to adipose tissues or ameliorate insulin resistance during diet-induced obesity (Kirk et al., 2008). These disparate findings suggest that unidentified biological variables modulate the function of individual chemokines in obesity-related metabolic disease.

Chemokines bind not only to their respective signaling receptors, but also to several non-signaling receptors, the most noteworthy of which is the atypical chemokine receptor 1 (ACKR1), also known as the Duffy antigen receptor for chemokines (DARC). DARC is a promiscuous chemokine receptor with the unique ability to bind both C-C and C-X-C class chemokines. In humans, DARC is expressed on erythrocytes, capillary and post-capillary endothelial cells, lymphatic endothelial cells, littoral cells of splenic sinusoids, lung epithelium, kidney collecting ducts, and cerebellar Purkinje cells (Hansell et al., 2011). Lacking the triplet sequence Asp-Arg-Tyr (DRY motif) in its second intracellular loop, DARC cannot activate G-protein coupled signaling pathways (de Brevern et al., 2005) and is thought to act primarily as a chemokine modulator by sequestering chemokines (i.e., 'buffer-sink' function) or by regulating their local concentration at sites of inflammation. Among various chemokines, DARC has strong binding affinity for C-C motif chemokine ligand 2 (CCL2)/MCP-1 (Hansell et al., 2011), and humans that lack functional DARC expression are more sensitive to MCP-1-induced monocyte mobilization (Mayr et al., 2009). Indeed, chemokines such as MCP-1 depend upon erythrocyte DARC to maintain plasma concentrations, and loss of functional DARC correlated with decreased levels of DARC-bound chemokines in the serum in both humans and mice (Schnabel et al., 2010; Lentsch, 2002). Erythrocyte DARC binds and clears chemokines from sites of inflammation to buffer inflammation while at the same time reducing receptor desensitization to counterbalance the buffering effect (Hansell et al., 2011). These findings illustrate the complex mechanisms whereby DARC regulates chemokine function.

The human population is characterized by three common alleles of the DARC gene: the ancestral FYB and the derived FYA and FYO alleles. The FYB and FYA alleles differ by a single amino acid (Asp42Gly), while the FYO allele is characterized by the lack of expression of DARC on erythrocytes (McManus et al., 2017). Blood donors carrying the FYO and FYA alleles exhibit reduced serum MCP-1 levels compared to FYB donors linked to reduced erythrocyte DARC binding affinity, suggesting that chemokine regulation is altered in these cohorts (Schnabel et al., 2010). Given the role of DARC in regulating chemokines that are thought to mediate obesity-related metabolic disease, and given the existence of common polymorphisms in the human population associated with differences in circulating chemokine levels, the role of the DARC in the development of obesity-related metabolic disease merits investigation.

Here, we investigated the impact of global DARC gene deletion on diet-induced obesity and insulin resistance in mice fed a high fat diet (HFD). DARC knockout mice fed a HFD exhibited marked impairments in glucose tolerance and insulin sensitivity compared to corresponding wild-type mice. Circulating levels of DARC-bound MCP-1 did not increase with HFD in DARC knockout mice as seen in wild-type controls; however, adipose tissue MCP-1 levels were higher in DARC knockout mice than in the wild-type mice, suggesting incongruence of plasma and adipose tissue levels of DARC-bound chemokines in DARC knockout mice. Surprisingly, moderate insulin resistance was also seen in male DARC knockout mice maintained on chow diet (CD) despite the lack of adipose tissue inflammation. Taken together, these data suggests that DARC regulates metabolic function and diet-induced obesity in mice.

2. Materials and methods

2.1. Mice

Male and female DARC knockout mice in the C57BL/6J background were obtained from Jackson Laboratories and bred in house to obtain littermates. Mice were housed in cages of 4–5 maintained on CD after weaning. At 8 weeks of age, mice were either maintained on CD (Harlan Teklad, LM-485) or switched to HFD (Research Diet, D12492, with 60% calories from fat) for up to 42 weeks. In a separate study, a weight-matched experiment in male non-littermate wild-type and DARC knockout mice was performed to control for body weight. Weight matched non-littermate wild-type mice (C57BL/6J) were either maintained on CD or switched to HFD for up to 26 weeks. Thereafter, mice were euthanized, blood was collected via cardiocentesis, and tissues were harvested following perfusion with ice-cold saline as previously described (Chatterjee et al., 2014). All animal studies were conducted using a protocol approved by the Institutional Animal Care and Use Committee of Augusta University, following appropriate guidelines.

Please cite this article in press as: Benson, T.W., et al., Deletion of the Duffy antigen receptor for chemokines (DARC) promotes insulin resistance and adipose tissue inflammation during high fat feeding, Molecular and Cellular Endocrinology (2018), https://doi.org/10.1016/j.mce.2018.01.006

2.2. Body fat and food intake measurements

Body weights were obtained weekly for mice fed CD or HFD. Body fat mass was measured in conscious mice fed CD or HFD one week prior to sacrifice using nuclear magnetic resonance (NMR) spectroscopy (Bruker Minispec LF90II) as described previously (Zhou et al., 2016). Food intake and metabolic energy expenditure were determined after 25 weeks on CD or HFD using a comprehensive laboratory animal monitoring system (CLAMS, Columbus Instruments, Columbus, OH) for 4 days (2 days of acclimation, followed by 2 days of measurement) as previously described (Zhou et al., 2016).

2.3. Examination of insulin and glucose tolerance

Glucose tolerance testing (GTT) was performed between 16 and 17 weeks (weight-matched cohort and female cohort) or 36 weeks (littermate cohort) on CD or HFD. Glucose levels were measured from tail veins immediately prior to and 30, 60, 90 and 120 min after intraperitoneal (IP) injection of glucose at 2 g/kg body weight in mice fasted for 12 h using glucose strips. Insulin sensitivity evaluated by insulin tolerance testing (ITT) was assessed at 20 weeks (weight-matched cohort and female cohort) or 38 weeks (littermate cohort) on CD or HFD by measurement of plasma glucose from tail veins at 0, 30, 60 and 90 min after IP injection of 0.75 U/kg body weight of porcine insulin in 6 hr-fasted mice.

2.4. Enzyme-linked immunosorbent assay (ELISA)

Plasma levels of adiponectin, leptin, and insulin were measured in mice after overnight fasting, utilizing commercially available ELISA kits (R&D Systems) as described previously (Unruh et al., 2015). Plasma levels of MCP-1 were quantified using mouse CCL2/JE/MCP-1 antibody (R&D Systems) according to the manufacturer's protocol.

2.5. Histology

Pancreas, liver and adipose tissues were fixed by immersion in neutral buffered formalin (10%), dehydrated in ethanol and then transferred to xylene solution for embedding in paraffin. Five μm sections were stained with hematoxylin-eosin (H&E) or incubated with anti-insulin (Abcam, 1:100 dilution, to detect beta cells) or anti-F4/80 antibodies (Sigma-Aldrich, 1:100 dilution, to detect macrophages) for 4 h at 37 °C, and then processed with HistoMouse-SP kit (Invitrogen) or DAB Substrate kits (Vector Labs) according to the manufacturers' protocols. The number of F4/80-positive crown-like structures were counted in 5 randomly selected high-power fields and normalized to mm^2 for quantification.

2.6. RNA isolation, quantitative polymerase chain reaction (qPCR), and Western blotting

RNA was isolated utilizing RNeasy lipid mini kit (Qiagen), and qPCR quantification of mRNA levels was performed as described previously (Chatterjee et al., 2011) using Syber-green qPCR kit (Agilent). Arbp (acidic ribosomal phosphoprotein P0) mRNA was selected as a reference for normalization of transcripts under investigation. The primer sequences used in the qPCR assay are provided in Supplementary Table 1. Western blot analysis was performed as described previously (Chatterjee et al., 2011).

2.7. Statistical analysis

Data are expressed as mean ± SEM except for weight data (expressed as mean ± SD). Analysis was accomplished by one way ANOVA followed by Tukey or Bonferroni post-hoc analysis. *P* values less than 0.05 were considered statistically significant.

3. Results

3.1. Increased adiposity and weight gain in male DARC knockout mice

Baseline weights did not differ amongst male wild-type and DARC knockout littermate mice. Over the course of the experiment, the CD-fed DARC knockout mice tended to gain more weight than their littermate counterparts, although the difference did not achieve statistical significance. HFD feeding resulted in progressive weight gain in both groups of mice (Fig. 1A), and under these conditions, the DARC knockout mice gained significantly more weight than did their wild-type littermates (Fig. 1A). Body composition by NMR spectroscopy showed that the CD-fed DARC knockout mice exhibited greater fat mass, and less lean mass, compared with their CD wild-type littermates (Fig. 1B). These differences were abolished by HFD feeding, during which both DARC knockout and wild-type mice exhibited dramatic increases in fat mass, and commensurate reductions in lean mass (Fig. 1B). Quantification of adipose depot weights (normalized to body weight) demonstrated that CD-fed DARC knockout mice possessed significantly more visceral adipose tissue, and a trend towards more subcutaneous adipose tissue, compared to their CD-fed wild-type littermates; however, following HFD feeding, percentage body fat and subcutaneous adipose mass increased proportionately in both groups of mice (Fig. 1B-C). The DARC knockout mice developed more liver enlargement during HFD feeding as compared with wild-type mice (Fig. 1D); percentage liver fat (quantified by NMR spectroscopy) tended to be higher in HFD-fed DARC knockout mice versus their littermate controls, although the difference was not statistically significant (Supplemental Fig. S1). Skeletal muscle mass was similar in DARC knockout and wild-type mice fed a CD or HFD, respectively (data not shown). Also, quantification of food consumption demonstrated no differences between wild-type and DARC knockout mice fed a CD or HFD, respectively (Fig. 1E).

3.2. Impaired glucose tolerance and insulin sensitivity in HFD-fed DARC knockout mice

Next, we examined metabolic status in these mice by performing glucose and insulin tolerance testing. Glucose tolerance was similar in CD-fed wild-type and DARC knockout mice (Fig. 1F). Basal fasting glucose levels were elevated in the HFD-fed DARC knockout mice, and glucose levels rose significantly higher at all time points after glucose administration in these mice as compared with the wild-type mice (Fig. 1F). Interestingly, as compared to wild-type mice, CD-fed DARC knockout mice also exhibited a strong trend towards diminished insulin sensitivity (Fig. 1G). As expected, the HFD obese wild-type mice exhibited insulin resistance, the degree of which was amplified in the DARC knockout mice. Plasma insulin levels were similar in CD-fed wild-type and DARC knockout mice and were significantly but similarly elevated in both HFD groups (Fig. 1H). Likewise, we detected a similar degree of positive immunostaining for beta cells in pancreatic tissues from both groups of HFD-fed mice (Fig. 1I). These findings suggest that the impaired glucose tolerance and insulin resistance observed in the HFD-fed DARC knockout mice did not result from diminished capacity to produce insulin.

Please cite this article in press as: Benson, T.W., et al., Deletion of the Duffy antigen receptor for chemokines (DARC) promotes insulin resistance and adipose tissue inflammation during high fat feeding, Molecular and Cellular Endocrinology (2018), https://doi.org/10.1016/j.mce.2018.01.006

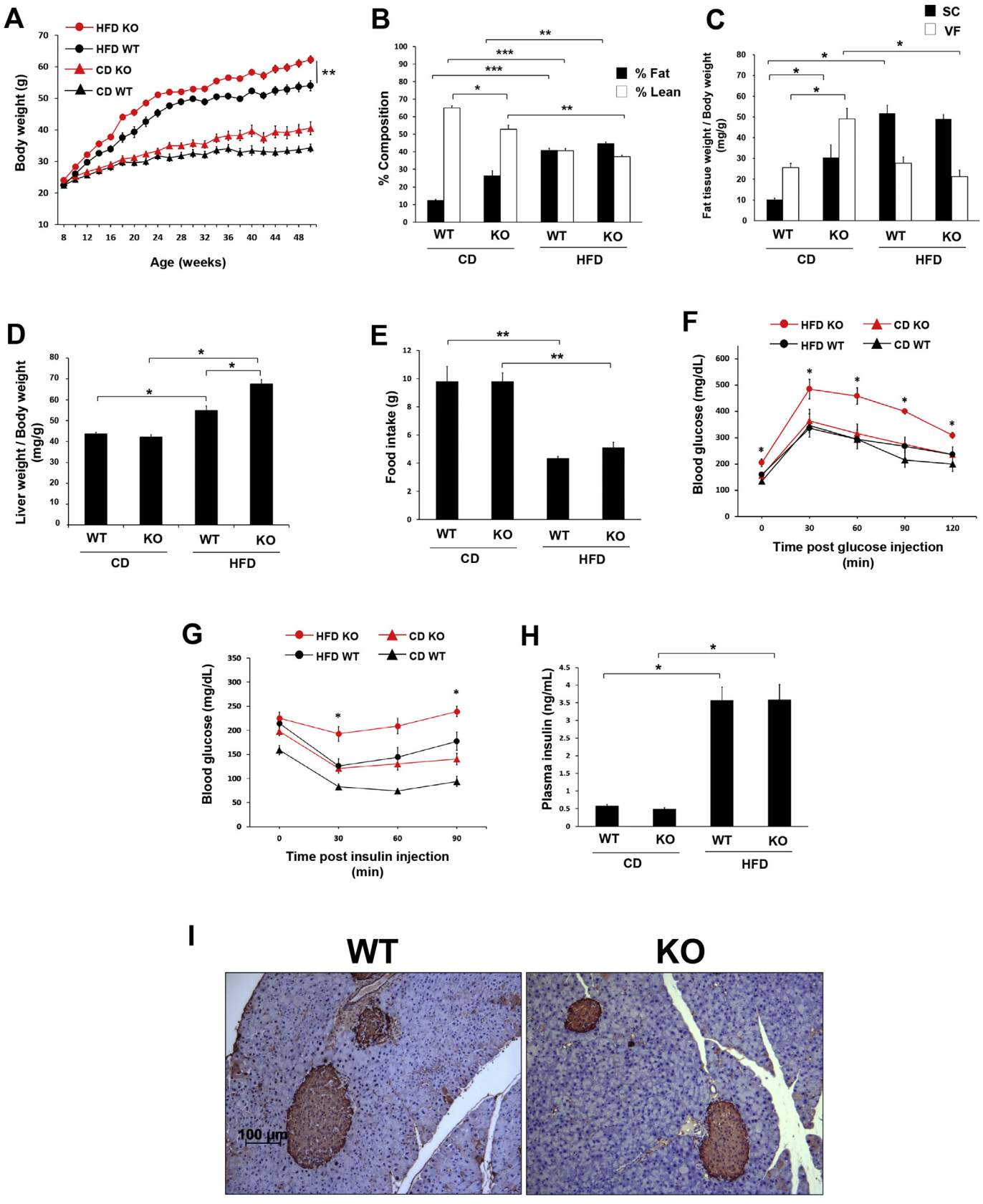

Fig. 1. Increased adiposity, weight gain with impaired glucose tolerance, insulin sensitivity in male DARC knockout mice. (A) Growth curves of male littermate DARC knockout (KO, red symbols) and wild-type (WT, black symbols) mice fed either HFD (open circles) or CD (closed circles) ($^{**}p < .01$ vs HFD WT). (B) Lean mass (black bars) and fat mass (white bars) measured by whole body composition by nuclear magnetic resonance ($^{*}p < .05$, $^{**}p < .01$, $^{***}p < .001$, n = 5). (C) Inguinal (SC) and epididymal (VF) fat pad weight normalized to body weight ($^{*}p < .05$, n = 5). (D) Liver weight normalized to body weight ($^{*}p < .05$, n = 5). (E) Food intake presented as g/mouse in WT and DARC knockout mice fed a CD or HFD ($^{**}p < .01$, n = 4). (F) Glucose tolerance test after 32 weeks of CD or HFD ($^{*}p < .05$ vs HFD WT, n = 5). (G) Insulin tolerance test after 36 weeks of CD or HFD ($^{*}p < .05$ vs HFD WT, $^{\#}p < .05$ vs CD WT, n = 5). (H) Fasting plasma insulin levels measured by ELISA in the CD and HFD groups ($^{*}p < .05$, n = 5). (I) Immunostaining for pancreatic beta cells in the HFD WT and KO groups. Representative images are shown (n = 3). (For interpretation of the references to colour in this figure legend, the reader is referred to the Web version of this article.)

Please cite this article in press as: Benson, T.W., et al., Deletion of the Duffy antigen receptor for chemokines (DARC) promotes insulin resistance and adipose tissue inflammation during high fat feeding, Molecular and Cellular Endocrinology (2018), https://doi.org/10.1016/j.mce.2018.01.006

3.3. Controlling for body weight did not normalize the metabolic phenotype of HFD-fed male DARC knockout mice

The metabolic phenotype observed in the DARC knockout mice could have been explained, at least in part, by differences in body weight as compared to their wild-type littermates. Thus, we performed a weight-matched study in non-littermate wild-type and DARC knockout mice to control for this variable. As expected, during the course of the study, body weights did not differ amongst wild-type and DARC knockout mice fed a CD or HFD, respectively (Fig. 2A), nor were there differences in food intake (Supplemental Fig. S2A), locomotor activity (Supplemental Fig. S3A) or metabolic energy expenditure (Supplemental Fig. S3B). Likewise, fat mass and adipose tissue weights were similar in the weight-matched wild-type and DARC knockout mice (Fig. 2B and C). However, as was observed in the littermate study, liver enlargement was noted in the HFD-fed DARC knockout mice (Fig. 2D), and hepatic steatosis was detected in both wild-type and DARC knockout mice fed a HFD (Fig. 2E). Despite the similar weights and adiposity, the HFD fed DARC knockout mice exhibited impaired glucose tolerance as compared to the wild-type mice (Fig. 2F). Moreover, insulin sensitivity was significantly impaired in both CD-fed and HFD-fed DARC knockout mice as compared to their respective wild-type counterparts (Fig. 2G).

Next, we examined adipokine expression in the weight-matched cohort. Plasma leptin levels were slightly but significantly higher in the CD-fed DARC knockout mice than in wild-type mice (Fig. 2H) and tended to be higher in DARC knockout mice in response to HFD, although the differences were not statistically significant (Fig. 2H). Plasma adiponectin levels were similar in wild-type and DARC knockout mice in the CD and HFD groups (Fig. 2I). In adipose tissues, leptin mRNA levels were significantly increased in HFD-fed DARC knockout mice as compared to wild-type mice (Fig. 2J).

3.4. Increased adipose tissue inflammation in HFD-fed DARC knockout mice

DARC can bind and regulate the activity of MCP-1, a chemokine reported to promote adipose inflammation in obesity. Thus, we assayed MCP-1 in plasma of our weight-matched wild-type and DARC knockout mice. As expected, MCP-1 in plasma rose significantly during HFD feeding in the wild-type mice. However, the DARC knockout mice tended to exhibit lower plasma MCP-1 levels at baseline, and no significant increase was noted following HFD feeding (Fig. 3A). In contrast to the plasma MCP-1 findings, adipose MCP-1 (assayed by Western blotting) was significantly higher in HFD-fed DARC knockout mice as compared with wild-type mice (Fig. 3B). mRNA expression of TNFα and MCP-1 was likewise higher in visceral adipose tissues from HFD-fed DARC knockout mice as compared to wild-type (Fig. 2C&D), while interleukin (IL)-6 and CCL5 expression was similar in both groups of mice (Figure E&F). Adipose tissue immunostaining demonstrated few infiltrating F4/80 positive macrophages in visceral adipose tissues of CD-fed wild-type or DARC knockout mice (Fig. 3G&H). Following HFD feeding, increased macrophage staining was detected in adipose tissues of both wild-type and DARC knockout mice. However, significantly more crown-like structures were detected in the HFD-fed DARC knockout mice, consistent with increased adipose tissue inflammation (Fig. 3G&H).

3.5. Impaired glucose tolerance and insulin sensitivity in HFD-fed female DARC knockout mice

Finally, we studied female wild-type and DARC knockout mice fed a CD or HFD. As was observed in the male mice, female DARC knockout mice gained more weight during the course of HFD feeding as compared to wild-type mice (Fig. 4A). However, we did not detect differences in body composition (Fig. 4B) or subcutaneous fat mass (Fig. 4C) between female DARC knockout and wild-type mice fed a CD or HFD, respectively. Also, unlike the male mice, female DARC knockout mice did not develop liver enlargement during HFD feeding (Fig. 4D). However, glucose tolerance (Fig. 4E) and insulin sensitivity (Fig. 4F) were significantly worse in the HFD-fed female DARC knockout mice as compared to the wild-type controls. Plasma insulin levels were similar in CD-fed wild-type and DARC knockout mice but were significantly higher in HFD-fed DARC knockout mice (Fig. 4G).

4. Discussion

Here, we investigated the impact of global DARC gene deletion on metabolic function and inflammation in diet-induced obesity. After HFD feeding, both male and female DARC knockout mice gained more weight and exhibited diminished glucose tolerance and insulin sensitivity compared to wild-type mice. In a weight-matched cohort, similar impairments in glucose tolerance and insulin sensitivity were observed, indicating body mass-independent metabolic dysfunction in the DARC knockout mice. While male DARC knockout mice displayed lower plasma levels of MCP-1, their visceral adipose tissues contained more MCP-1 protein and macrophage crown-like structures compared to the wild-type mice, consistent with heightened inflammation. Interestingly, male DARC knockout mice on CD also exhibited decreased insulin sensitivity despite the absence of tissue inflammation. Taken together, these data suggest that DARC plays a complex role in regulating systemic metabolism as well as adipose tissue inflammation during HFD feeding.

Because DARC acts as a chemokine regulator, its role has been investigated in a variety of pathological states. After lipopolysaccharide (LPS) challenge, DARC knockout mice exhibited increases in tissue inflammation compared to wild-type controls, suggesting a primary role for DARC as a buffer-sink in this acute inflammatory model (Hansell et al., 2011). Interestingly, blood monocytes in DARC knockout mice expressed significantly less tissue factor in response to intraperitoneally administered LPS (Østerud et al., 2015). Studies in DARC knockout mice and human cohorts lacking erythrocyte DARC expression have demonstrated increased incidence/severity of prostate cancer, attributed to the loss of DARC's buffer-sink functionality to regulate tissue levels of angiogenic chemokines such as CXCl1 (Lentsch, 2002). The role of DARC in atherosclerosis has also been investigated by crossing DARC knockout mice with apolipoprotein E knockout mice. In this model, the loss of DARC conferred protection against atherosclerosis, presumably due to the lack of chemokines bound to erythrocytes that extravasated into atheromatous plaques (Wan et al., 2015). Thus, DARC appears able to play both pro- and anti-inflammatory roles depending on the specific disease. The role of DARC in regulating chronic low grade inflammation associated with diet-induced obesity, however, has not been previously investigated.

Weight gain leading to obesity induces a state of chronic inflammation that is associated with the development of metabolic syndrome and type 2 diabetes (Xu et al., 2003). As expected in the pro-inflammatory setting of obesity, male wild-type mice fed a HFD displayed a marked increase in circulating MCP-1 levels, concomitant with increased adipose tissue MCP-1 protein and macrophage infiltration. However, circulating MCP-1 levels remained low in the male DARC knockout mice following consumption of the HFD, despite the fact that their adipose tissues contained even more MCP-1 and macrophage crown-like structures than did the WT

Please cite this article in press as: Benson, T.W., et al., Deletion of the Duffy antigen receptor for chemokines (DARC) promotes insulin resistance and adipose tissue inflammation during high fat feeding, Molecular and Cellular Endocrinology (2018), https://doi.org/10.1016/j.mce.2018.01.006

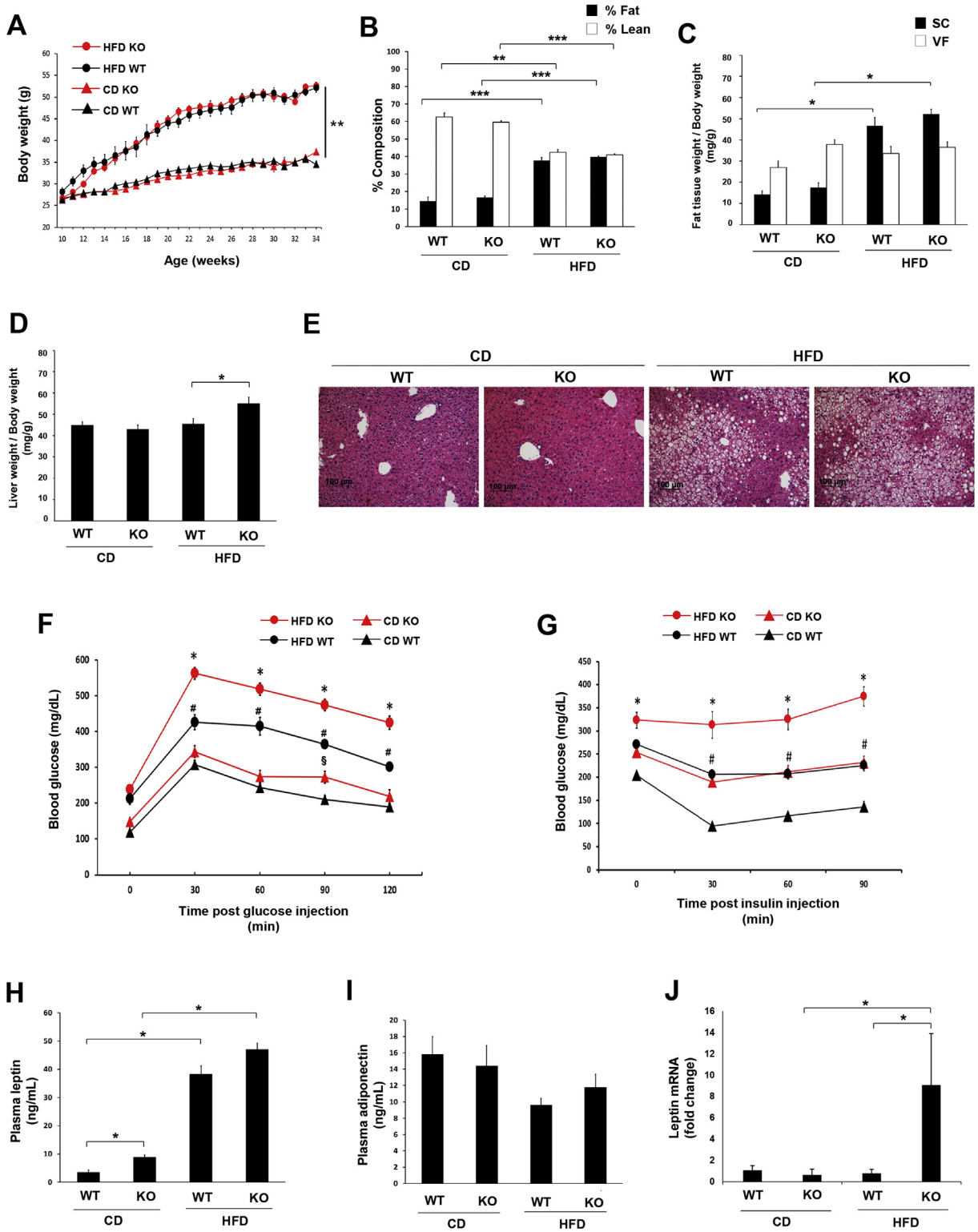

Fig. 2. Controlling for body weight did not normalize the metabolic phenotype of HFD fed male DARC knockout mice. (A) Growth curves of male weight-matched DARC knockout mice (red symbols) and WT mice (black symbols) fed either HFD (open circles) or CD (closed circles) ($^{**}p < .01$ vs CD WT and CD KO). (B) Lean mass (white bars) and fat mass (black bars) measured by whole body composition by NMR spectroscopy ($^{***}p < .001$, $^{**}p < .01$, n = 10). (C) Inguinal (SC) and epididymal (VF) fat pad weight normalized to body weight ($^{*}p < .05$, n = 10). (D) Liver weight normalized to body weight ($^{*}p < .05$, n = 10). (E) Representative H&E staining images of liver tissues (n = 3). Glucose tolerance test (F) after 17 weeks on diet and insulin tolerance test (G) after 20 weeks on diet ($^{\S}p < .05$ vs CD WT, $^{*}p < .05$ vs HFD WT, $^{\#}p < .05$ vs CD WT, n = 10). Plasma leptin (H) and adiponectin (I) from weight-matched male mice fed on diet for 24 weeks assayed by ELISA ($^{*}p < .05$, n = 5). (J) Leptin mRNA expression in adipose tissues quantified by real-time PCR ($^{*}p < .05$, n = 4). (For interpretation of the references to colour in this figure legend, the reader is referred to the Web version of this article.)

Please cite this article in press as: Benson, T.W., et al., Deletion of the Duffy antigen receptor for chemokines (DARC) promotes insulin resistance and adipose tissue inflammation during high fat feeding, Molecular and Cellular Endocrinology (2018), https://doi.org/10.1016/j.mce.2018.01.006

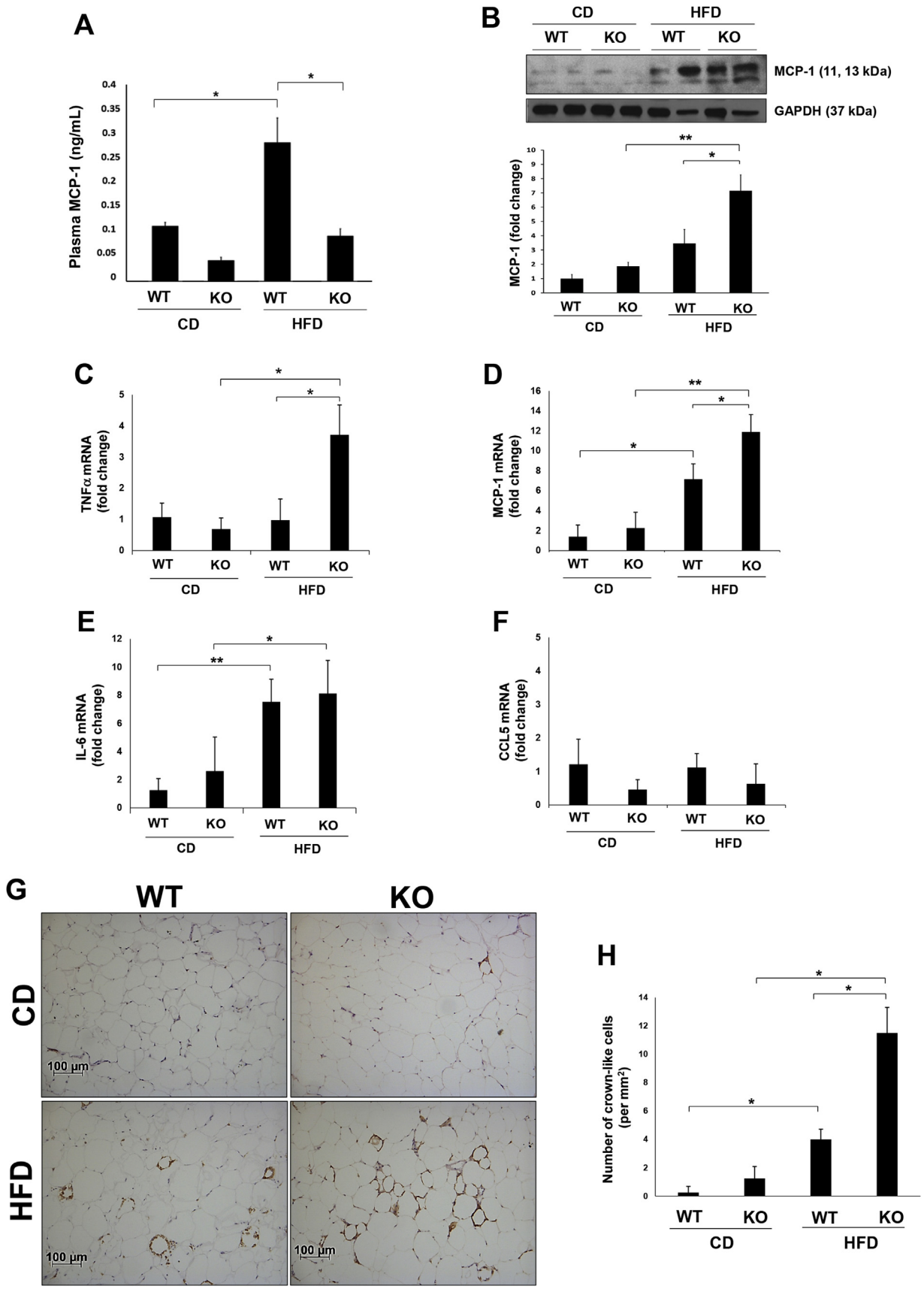

Fig. 3. Increased adipose tissue inflammation in HFD fed DARC knockout mice. (A) Plasma MCP-1 concentration measured by ELISA following treatment of whole blood with heparin from weight-matched male mice on diet for 24 weeks ($^{*}p < .05$, n = 4). (B) Representative Western blot and quantitated data showing MCP-1 protein in epididymal adipose tissue homogenates of WT and DARC knockout mice ($^{*}p < .05$, $^{**}p < .01$, n = 5). Adipose mRNA expression of TNFα (C), MCP-1 (D), IL-6 (E) and CCL5 (F) as examined by real time PCR ($^{*}p < .05$, $^{**}p < .01$, n = 4). (G) Representative images of F4/80 positive macrophage immunostaining in epididymal adipose tissue. Quantification of crown-like structures is shown in (H) ($^{*}p < .05$, n = 4).

Please cite this article in press as: Benson, T.W., et al., Deletion of the Duffy antigen receptor for chemokines (DARC) promotes insulin resistance and adipose tissue inflammation during high fat feeding, Molecular and Cellular Endocrinology (2018), https://doi.org/10.1016/j.mce.2018.01.006

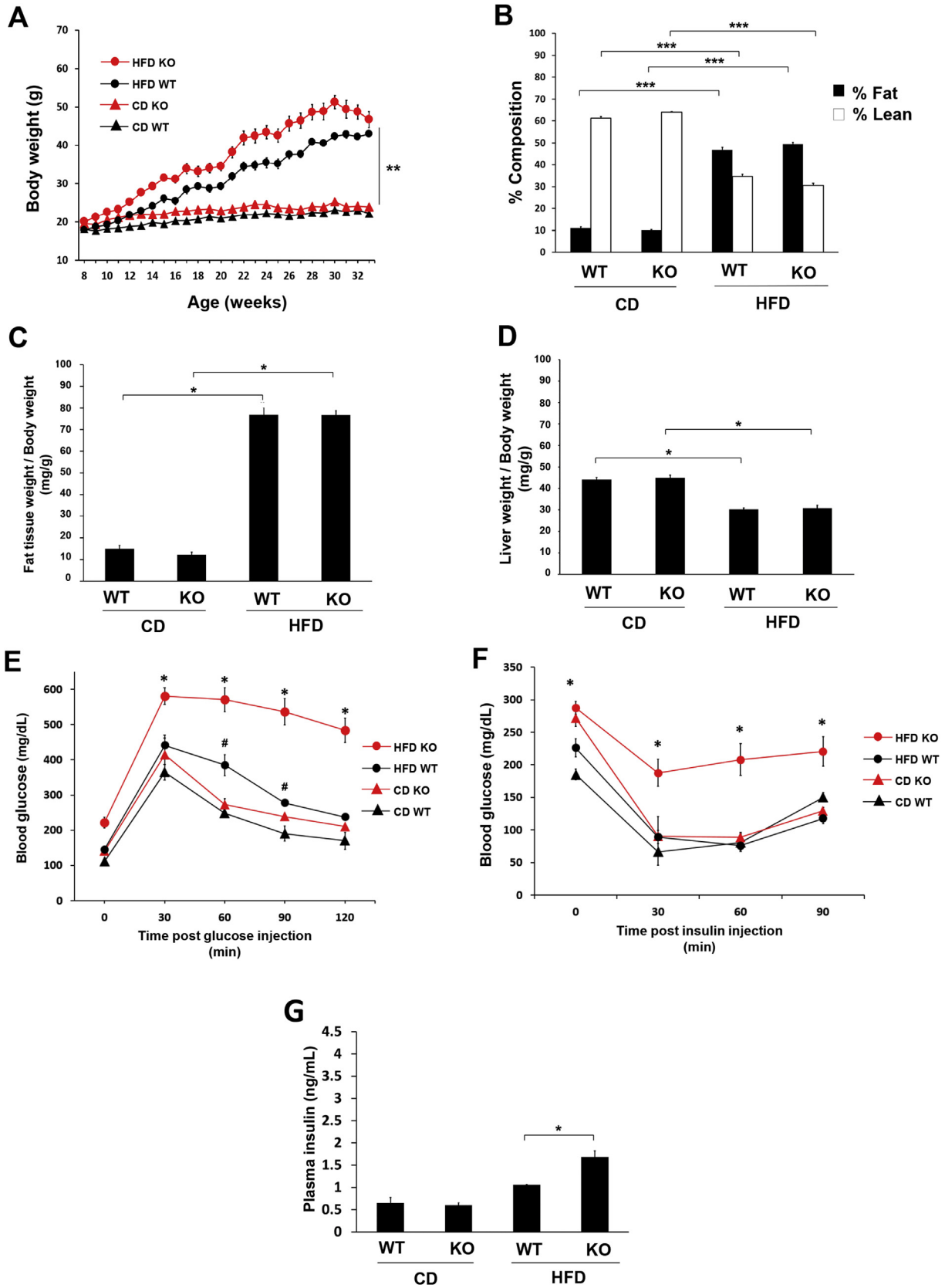

Fig. 4. Impaired glucose tolerance and insulin sensitivity in HFD-fed female DARC knockout mice. (A) Growth curves of female DARC knockout mice (red symbols) and WT mice (black symbols) fed either HFD (open circles) or CD (closed circles) ($^{**}p < .01$ vs CD WT and CD KO). (B) Lean mass (white bars) and fat mass (black bars) measured by whole body composition by NMR spectroscopy ($^{***}p < .001$, n = 5). (C) Inguinal (SC) fat pad weight normalized to body weight ($^{*}p < .05$, n = 4). (D) Liver weight normalized to body weight ($^{*}p < .05$, n = 5). Glucose tolerance test (E) at 17 weeks on diet and insulin tolerance test (F) at 20 weeks on diet ($^{*}p < .05$ vs HFD WT, $^{\#}p < .05$ vs CD WT, n = 4). (G) Fasting plasma insulin levels measured by ELISA in the CD and HFD groups ($^{*}p < .05$, n = 4). (For interpretation of the references to colour in this figure legend, the reader is referred to the Web version of this article.)

Please cite this article in press as: Benson, T.W., et al., Deletion of the Duffy antigen receptor for chemokines (DARC) promotes insulin resistance and adipose tissue inflammation during high fat feeding, Molecular and Cellular Endocrinology (2018), https://doi.org/10.1016/j.mce.2018.01.006

mice, indicative of enhanced adipose tissue inflammation. This phenotype of the DARC knockout mice could not be explained by differences in body weight or adiposity. Interestingly, male DARC knockout mice fed CD displayed insulin resistance comparable to that of HFD-fed WT mice despite a lack of adipose tissue inflammation. DARC gene deletion did not diminish fasting plasma insulin, and no gross changes in pancreatic beta cell expression were observed in the male DARC knockout mice, indicating that the ability to produce insulin was not impaired. Thus, the role of DARC in regulating insulin sensitivity is likely to be complex, extending beyond adipose tissue inflammation perhaps to insulin signaling. Further studies are required to determine whether DARC is expressed on insulin-sensitive cells, and if so what its function may be.

During metabolic testing in the CLAMS unit, both wild type and DARC knockout mice on HFD consumed less food (total grams or Kcal) when compared to their counterparts on CD (Supplemental Fig. S2A). This may be partially explained by the fact that the diets must be ground up to load into the CLAMS unit feeders, which turns the HFD into a dense, sticky paste that is harder for mice to consume compared to the powder-like CD. Second, it is possible that obese mice have a more difficult time accessing the CLAMS feeder due to their body habitus. These explanations are supported by a trend toward a higher percentage of body weight loss by both groups of mice on HFD during the CLAMS testing (Supplemental Fig. S2B).

One of the interesting findings in this study is the liver enlargement of male DARC knockout mice fed a HFD compared to wild-type control. We observed a strong trend toward increased percentage of liver fat in the DARC knockout mice compared to wild-type, suggesting the enlargement could in part be attributed to excess hepatic lipid accumulation in these mice. In contrast, liver enlargement was not seen in female DARC knockout mice during HFD feeding, despite their increased weight gain and insulin resistance, suggesting that female sex hormones and/or the estrous cycle could potentially modulate hepatic lipid flux in these mice. Future in-depth studies would be required to address this possibility.

Three main alleles of the DARC gene are present in the human population: FYB, FYA and FYO, the prevalence of which varies by region and ancestry (Howes et al., 2011). FYA is the most common allele globally and is most prevalent in those of Asian descent, FYB predominates in those of European descent, while FYO is most prevalent in those of African descent. The distribution of the DARC alleles is thought to result from selection pressure imposed by *Plasmodium vivax* malaria. *P. vivax* engages DARC to penetrate erythrocytes, and the absence of DARC on FYO-expressing erythrocytes blocks the entrance of *P. vivax* and thereby confers resistance to the parasite (Miller et al., 1976). Notably, *P. vivax* is largely absent from equatorial Africa, where the FYO allele is nearly fixed. FYA may have also emerged as an adaptation directed against *P. vivax* (King et al., 2011), and natural selection also appears to have acted on the FYA allele in India (Chittoria et al., 2012).

Evolutionary adaptations often carry fitness trade-offs. Indeed, the FYO allele has been associated with apparently maladaptive phenotypes, including increased risk of prostate cancer (Shen et al., 2006). Interestingly, neutrophil levels are also lower in carriers of the FYO allele (Reich et al., 2009). The present study found that DARC gene deletion exacerbated metabolic dysfunction in both male and female mice fed a HFD. Coincidentally, populations of African and Asian descent, respectively dominated by the FYO and FYA alleles, are at increased risk of metabolic disease compared to those of European ancestry (McNeely and Boyko, 2004; Brancati et al., 2000). Moreover, FYO and FYA human cohorts exhibit lower circulating MCP-1 levels (Schnabel et al., 2010), as was detected in DARC knockout mice in the present study, although it is unknown whether adipose tissue levels of MCP-1 in obese human FYO and FYA cohorts are disproportionately elevated. Given the results of this study, it is worth considering whether circulating MCP-1 levels provide an accurate representation of adipose inflammation in FYA and FYO populations. The extent to which our findings apply to human populations, however, remains unclear. The DARC knockout genotype does not equate to FYA or FYO carriers, and numerous environmental and genetic factors can impact circulating chemokine levels and metabolic disease risk in humans.

5. Conclusions

This study is the first to investigate the impact of DARC gene deletion on metabolic function during diet-induced obesity. Both male and female DARC knockout mice fed a HFD exhibited impaired glucose tolerance and insulin sensitivity, and increased adipose tissue inflammation, compared to HFD-fed wild-type mice. Increased adipose tissue inflammation alone does not appear to explain the observed phenotype, however, as male DARC knockout mice on CD also displayed moderate insulin resistance despite a lack of adipose tissue inflammation, suggesting a more complex role for DARC in metabolism beyond its role in regulating chemokines. Our study also reveals a disconnect between circulating and adipose tissue levels of DARC-bound chemokines in the DARC knockout mice which potentially may be relevant to human populations expressing common DARC allelic variants. Focused studies are needed to elucidate the potential impact of DARC polymorphisms on adipose tissue inflammation and metabolic disease in human populations.

Conflicts of interest

The authors declare no conflict of interest.

Acknowledgments

This study was supported by NIH grants HL126949 and HL112640 (N.L.W.), HL134354 and AR070029 (Y.T. and N.L.W.), and Department of Defense grant NF140031 (B.K.S.).

Appendix A. Supplementary data

Supplementary data related to this article can be found at https://doi.org/10.1016/j.mce.2018.01.006.

References

Brancati, F.L., Kao, W.H., Folsom, A.R., Watson, R.L., Szklo, M., 2000. Incident type 2 diabetes mellitus in African American and white adults: the atherosclerosis risk in communities study. J. Am. Med. Assoc. 283 (17), 2253–2259.

Cawley, J., Meyerhoefer, C., 2012. The medical care costs of obesity: an instrumental variables approach. J. Health Econ. 31, 219–230.

Chatterjee, T.K., Idelman, G., Blanco, V., Blomkalns, A.L., Piegore Jr., M.G., Weintraub, D.S., Kumar, S., Rajsheker, S., Manka, D., Rudich, S.M., Tang, Y., Hui, D.Y., Bassel-Duby, R., Olson, E.N., Lingrel, J.B., Ho, S.M., Weintraub, N.L., 2011. Histone deacetylase 9 is a negative regulator of adipogenic differentiation. J. Biol. Chem. 286 (31), 27836–27847.

Chatterjee, T.K., Basford, J.E., Knoll, E., Tong, W.S., Blanco, V., Blomkalns, A.L., Rudich, S., Lentsch, A.B., Hui, D.Y., Weintraub, N.L., 2014. HDAC9 knockout mice are protected from adipose tissue dysfunction and systemic metabolic disease during high-fat feeding. Diabetes 63 (1), 176–187.

Chittoria, A., Mohanty, S., Jaiswal, Y.K., Das, A., 2012. Natural selection mediated association of the Duffy (FY) gene polymorphisms with Plasmodium vivax malaria in India. PLoS One 7 (9), e45219.

de Brevern, A.G., Wong, H., Tournamille, C., Colin, Y., Le Van Kim, C., Etchebest, C., 2005. A structural model of a seven-transmembrane helix receptor: the Duffy antigen/receptor for chemokine (DARC). Biochim. Biophys. Acta 1724 (3), 288–306.

Flegal, K.M., Carroll, M.D., Kit, B.K., Ogden, C.L., 2012. Prevalence of obesity and

trends in the distribution of body mass index among US adults, 1999–2010. J. Am. Med. Assoc. 307 (5), 491–497.
Hansell, C.A., Hurson, C.E., Nibbs, R.J., 2011. DARC and D6: silent partners in chemokine regulation? Immunol. Cell Biol. 89 (2), 197–206.
Hotamisligil, G.S., Narinder, S.S., Spiegelman, B.M., 1993. Adipose expression of tumor necrosis factor-alpha: direct role in obesity-linked insulin resistance. Science 259 (5091), 87–91.
Howes, R.E., Patil, A.P., Piel, F.B., Nyangiri, O.A., Kabaria, C.W., Gething, P.W., Zimmerman, P.A., Barnadas, C., Beall, C.M., Gebremedhin, A., Ménard, D., Williams, T.N., Weatherall, D.J., Hay, S.I., 2011. The global distribution of the Duffy blood group. Nat. Commun. 2, 266.
Huber, J., Kiefer, F.W., Zeyda, M., Ludvik, B., Silberhumer, G.R., Prager, G., Zlabinger, G.J., Stulnig, T.M., 2008. CC chemokine and CC chemokine receptor profiles in visceral and subcutaneous adipose tissue are altered in human obesity. J. Clin. Endocrinol. Metab. 93 (8), 3215–3221.
Kanda, H., Tateya, S., Tamori, Y., Kotani, K., Hiasa, K., Kitazawa, R., Kitazawa, S., Miyachi, H., Maeda, S., Egashira, K., Kasuga, M., 2006. MCP-1 contributes to macrophage infiltration into adipose tissue, insulin resistance, and hepatic steatosis in obesity. J. Clin. Invest. 116 (6), 1494–1505.
Kim, C.S., Park, H.S., Kawada, T., Kim, J.H., Lim, D., Hubbard, N.E., Kwon, B.S., Erickson, K.L., Yu, R., 2006. Circulating levels of MCP-1 and IL-8 are elevated in human obese subjects and associated with obesity-related parameters. Int. J. Obes. 30, 1347–1355.
King, C.L., Adams, J.H., Xianli, J., Grimberg, B.T., McHenry, A.M., Greenberg, L.J., Siddiqui, A., Howes, R.E., da Silva-Nunes, M., Ferreira, M.U., Zimmerman, P.A., 2011. Fya/Fyb antigen polymorphism in human erythrocyte Duffy antigen affects susceptibility to Plasmodium vivax malaria. Proc. Natl. Acad. Sci. U. S. A 108 (50), 20113–20118.
Kirk, E.A., Sagawa, Z.K., McDonald, T.O., O'Brien, K.D., Heinecke, J.W., 2008. Monocyte chemoattractant protein-1 deficiency fails to restrain macrophage infiltration into adipose tissue. Diabetes 57 (5), 1254–1261.
Kwon, H., Pessin, J.E., 2013. Adipokines mediate inflammation and insulin resistance. Front. Endocrinol. 4, 71.
Lentsch, A.B., 2002. The Duffy antigen/receptor for chemokines (DARC) and prostate cancer. A role as clear as black and white? Faseb. J. 16 (9), 1093–1095.
Mayr, F.B., Spiel, A.O., Leitner, J.M., Firbas, C., Schnee, J., Hilbert, J., Derendorf, H., Jilma, B., 2009. Influence of the Duffy antigen on pharmacokinetics and pharmacodynamics of recombinant monocyte chemoattractant protein (MCP-1, CCL-2) in vivo. Int. J. Immunopathol. Pharmacol. 22, 615–625.
McManus, K.F., Taravella, A.M., Henn, B.M., Bustamante, C.D., Sikora, M., Cornejo, O.E., 2017. Population genetic analysis of the DARC locus (Duffy) reveals adaptation from standing variation associated with malaria resistance in humans. PLoS Genet. 13 (3), e1006560.
McNeely, M.J., Boyko, E.J., 2004. Type 2 diabetes prevalence in Asian Americans. Diabetes Care 27 (1), 66–69.
Miller, L.H., Mason, S.J., Clyde, D.F., McGinniss, M.H., 1976. The resistance factor to Plasmodium vivax in blacks: the Duffy-blood-group genotype. FyFy. N. Engl. J. Med 295 (6), 302–304.
Østerud, B., Unruh, D., Olsen, J.O., Kirchhofer, D., Owens 3rd, A.P., Bogdanov, V.Y., 2015. Procoagulant and proinflammatory effects of red blood cells on lipopolysaccharide-stimulated monocytes. J. Thromb. Haemostasis 13 (9), 1676–1682.
Reich, D., Nalls, M.A., Kao, W.H., Akylbekova, E.L., Tandon, A., Patterson, N., Mullikin, J., Hsueh, W.C., Cheng, C.Y., Coresh, J., Boerwinkle, E., Li, M., Waliszewska, A., Neubauer, J., Li, R., Leak, T.S., Ekunwe, L., Files, J.C., Hardy, C.L., Zmuda, J.M., Taylor, H.A., Ziv, E., Harris, T.B., Wilson, J.G., 2009. Reduced neutrophil count in people of African descent is due to a regulatory variant in the Duffy antigen receptor for chemokines gene. PLoS Genet. 5 (1), e1000360.
Schnabel, R.B., Baumert, J., Barbalic, M., Dupuis, J., Ellinor, P.T., Durda, P., Dehghan, A., Bis, J.C., Illig, T., Morrison, A.C., Jenny, N.S., Keaney Jr., J.F., Gieger, C., Tilley, C., Yamamoto, J.F., Khuseyinova, N., Heiss, G., Doyle, M., Blankenberg, S., Herder, C., Walston, J.D., Zhu, Y., Vasan, R.S., Klopp, N., Boerwinkle, E., Larson, M.G., Psaty, B.M., Peters, A., Ballantyne, C.M., Witteman, J.C., Hoogeveen, R.C., Benjamin, E.J., Koenig, W., Tracy, R.P., 2010. Duffy antigen receptor for chemokines (Darc) polymorphism regulates circulating concentrations of monocyte chemoattractant protein-1 and other inflammatory mediators. Blood 115 (26), 5289–5299.
Shen, H., Schuster, R., Stringer, K.F., Waltz, S.E., Lentsch, A.B., 2006. The Duffy antigen/receptor for chemokines (DARC) regulates prostate tumor growth. Faseb. J. 20 (1), 59–64.
Unruh, D., Srinivasan, R., Benson, T., Haigh, S., Coyle, D., Batra, N., Keil, R., Sturm, R., Blanco, V., Palascak, M., Franco, R.S., Tong, W., Chatterjee, T., Hui, D.Y., Davidson, W.S., Aronow, B.J., Kalfa, T., Manka, D., Peairs, A., Blomkalns, A., Fulton, D.J., Brittain, J.E., Weintraub, N.L., Bogdanov, V.Y., 2015. Red blood cell dysfunction induced by high-fat diet: potential implications for obesity-related atherosclerosis. Circulation 132 (20), 1898–1908.
Uysal, K.T., Wiesbrock, S.M., Marino, M.W., Hotamisligil, G.S., 1997. Protection from obesity-induced insulin resistance in mice lacking TNF-alpha function. Nature 389 (6651), 610–614.
Wan, W., Liu, Q., Lionakis, M.S., Marino, A.P., Anderson, S.A., Swamydas, M., Murphy, P.M., 2015. Atypical chemokine receptor 1 deficiency reduces atherogenesis in ApoE-knockout mice. Cardiovasc. Res. 106 (3), 478–487.
Wang, Y., McPherson, K., Marsh, T., Gortmaker, S.L., Brown, M., 2011. Health and economic burden of the projected obesity trends in the USA and the UK. Lancet 378 (9793), 815–825.
Weisberg, S.P., Hunter, D., Huber, R., Lemieux, J., Slaymaker, S., Vaddi, K., Charo, I., Leibel, R.L., Ferrante Jr., A.W., 2006. CCR2 modulates inflammatory and metabolic effects of high-fat feeding. J. Clin. Invest. 116 (1), 115–124.
Xu, H., Barnes, G.T., Yang, Q., Tan, G., Yang, D., Chou, C.J., Sole, J., Nichols, A., Ross, J.S., Tartaglia, L.A., Chen, H., 2003. Chronic inflammation in fat plays a crucial role in the development of obesity-related insulin resistance. J. Clin. Invest. 112 (12), 1821–1830.
Zhou, H., Black, S.M., Benson, T.W., Weintraub, N.L., Chen, W., 2016. Berardinelli-Seip congenital lipodystrophy 2/seipin is not required for brown adipogenesis but regulates brown adipose tissue development and function. Mol. Cell Biol. 36 (15), 2027–2038.

Please cite this article in press as: Benson, T.W., et al., Deletion of the Duffy antigen receptor for chemokines (DARC) promotes insulin resistance and adipose tissue inflammation during high fat feeding, Molecular and Cellular Endocrinology (2018), https://doi.org/10.1016/j.mce.2018.01.006

Figure 1

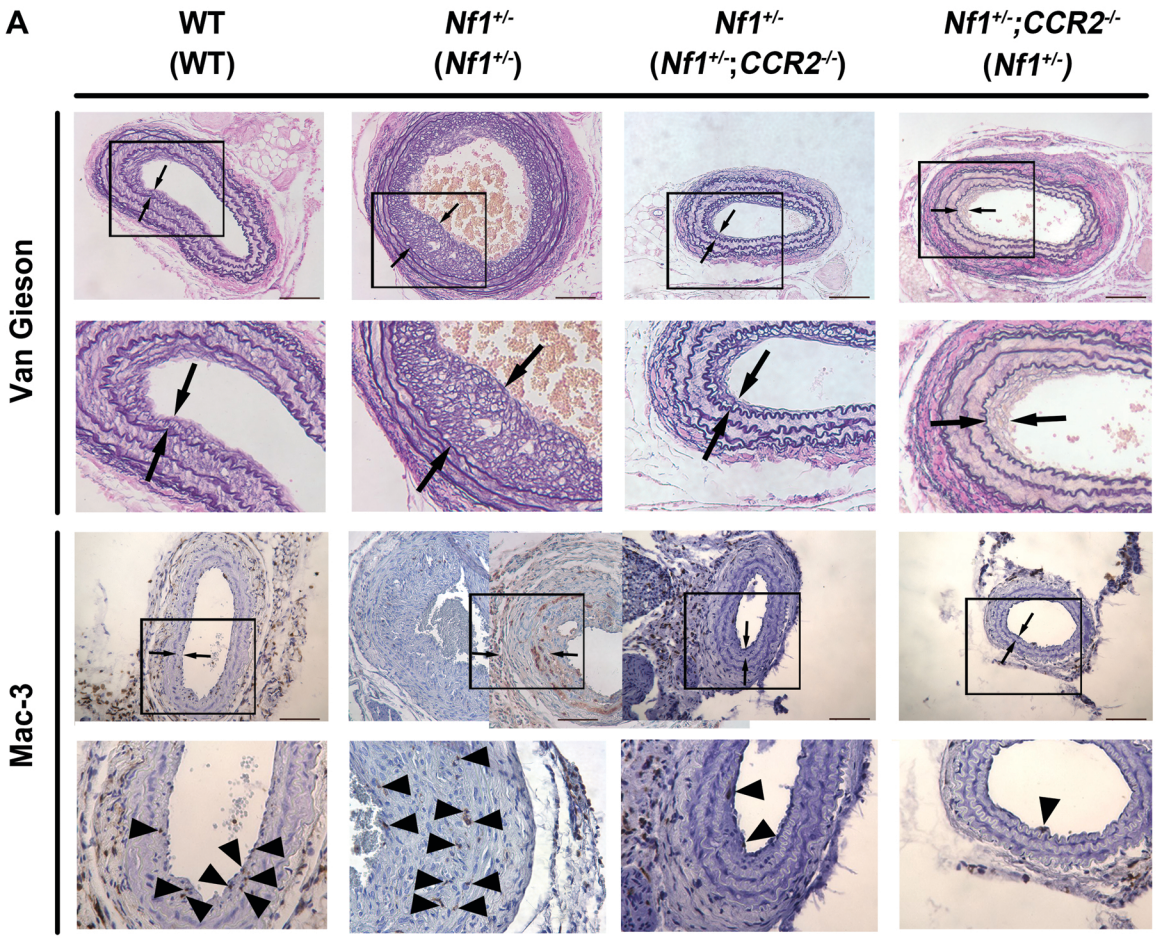
A
WT
(WT)
Nf1+/-
(Nf1+/-)
Nf1+/-
(Nf1+/-;CCR2-/-)
Nf1+/-;CCR2-/-
(Nf1+/-)
Van Gieson
Mac-3

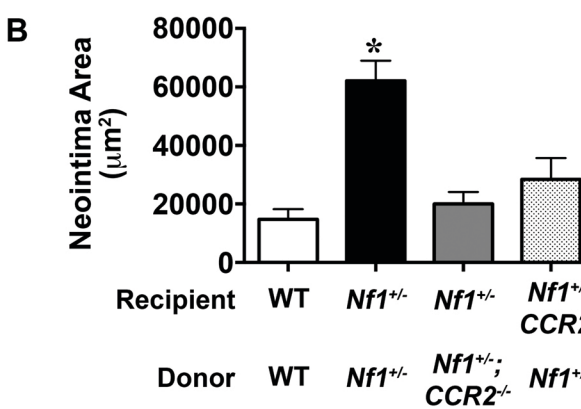
B
Neointima Area
(μm2)
80000
60000
40000
20000
0
*
Recipient
WT
Nf1+/-
Nf1+/-
Nf1+/-;
CCR2-/-
Donor
WT
Nf1+/-
Nf1+/-;
CCR2-/-
Nf1+/-

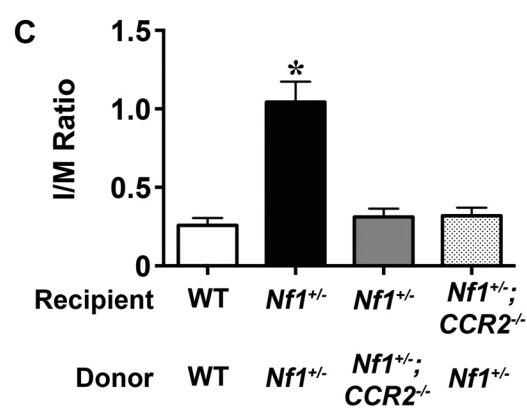
C
I/M Ratio
1.5
1.0
0.5
0
*
Recipient
WT
Nf1+/-
Nf1+/-
Nf1+/-;
CCR2-/-
Donor
WT
Nf1+/-
Nf1+/-;
CCR2-/-
Nf1+/-

Figure 2

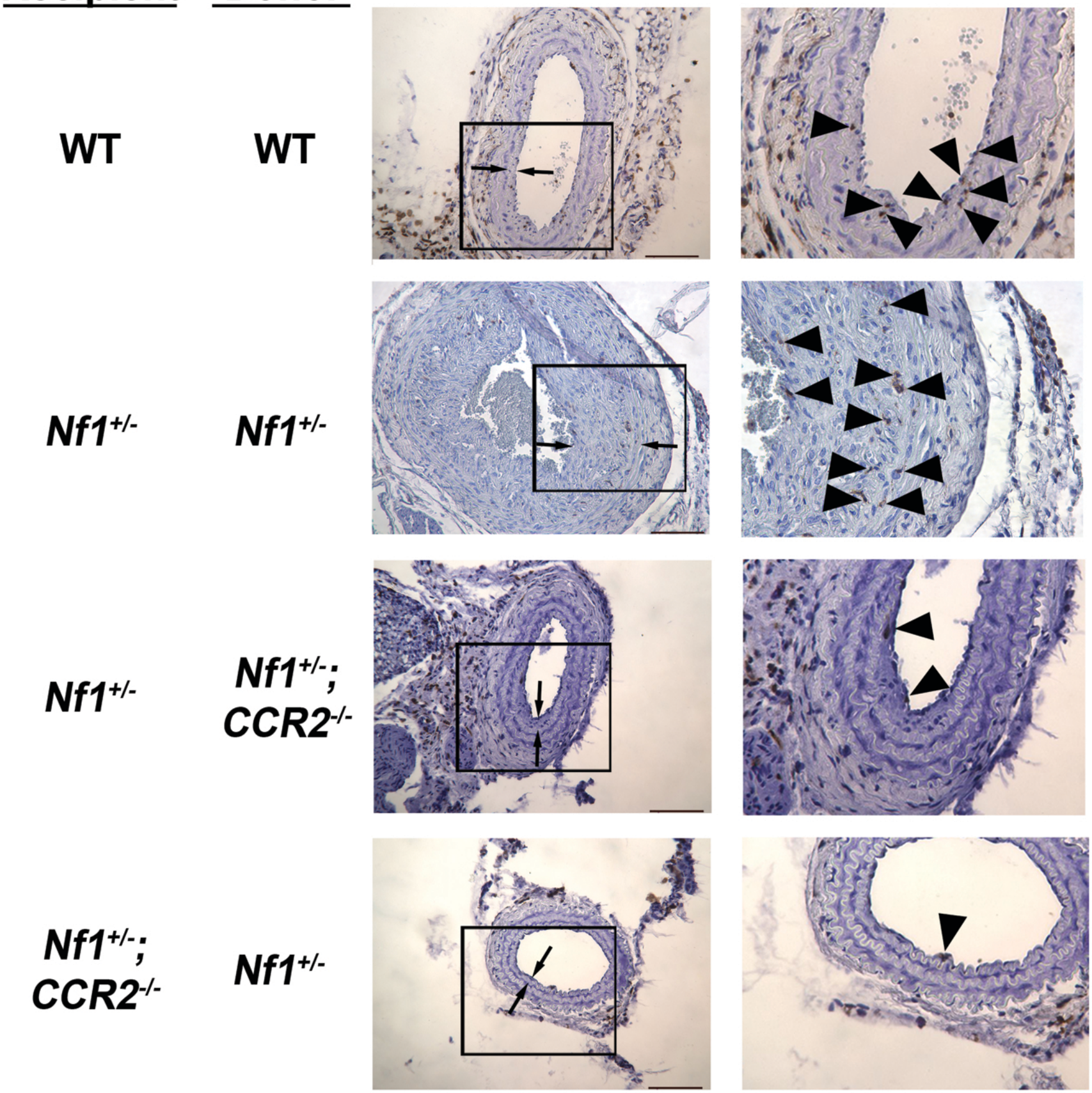

Figure 3

A

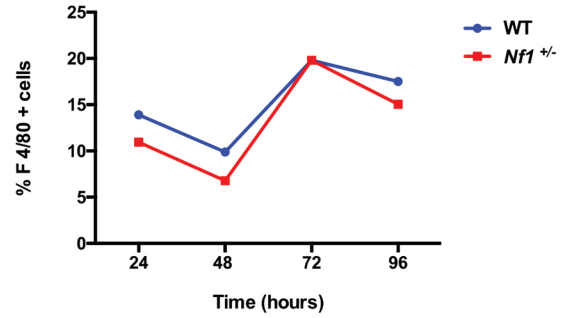
% F 4/80 + cells
25
20
15
10
5
0
24
48
72
96
Time (hours)
WT
Nf1 +/-

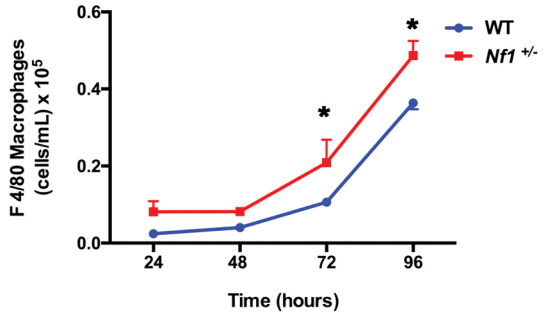
F 4/80 Macrophages (cells/mL) x 10^5
0.6
0.4
0.2
0.0
*
*
24
48
72
96
Time (hours)
WT
Nf1 +/-

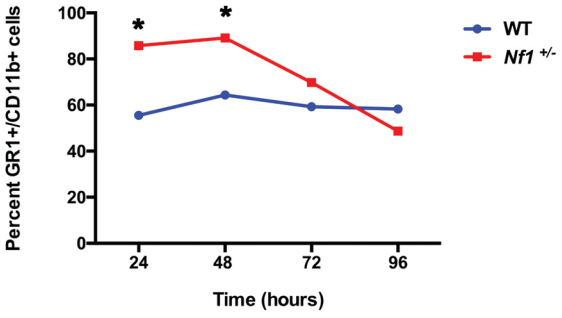
Percent GR1+/CD11b+ cells
100
80
60
40
20
0
*
*
24
48
72
96
Time (hours)
WT
Nf1 +/-

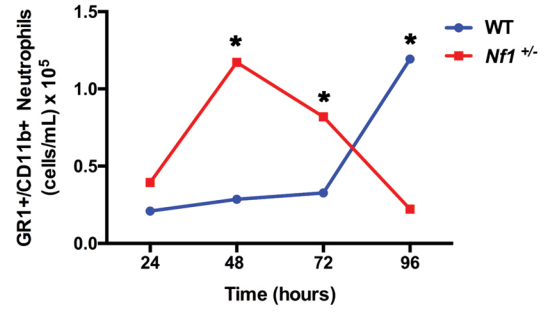
GR1+/CD11b+ Neutrophils (cells/mL) x 10^5
1.5
1.0
0.5
0.0
*
*
*
24
48
72
96
Time (hours)
WT
Nf1 +/-

Figure 4

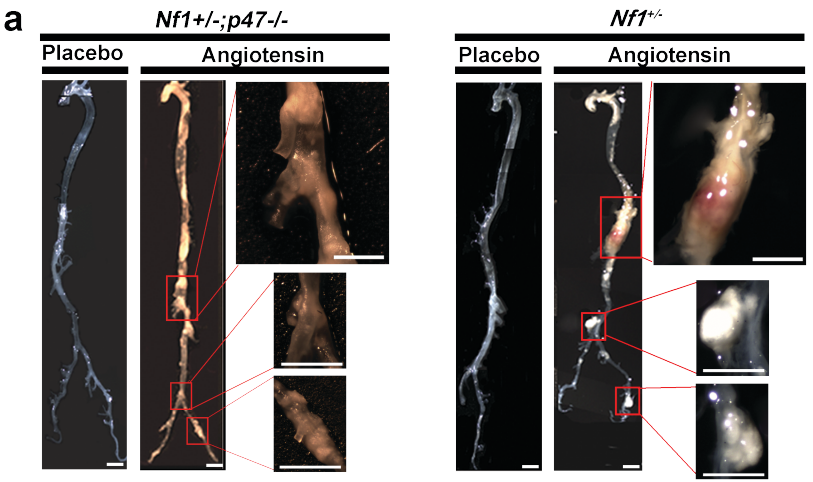
a
Nf1+/-;p47-/-
Placebo
Angiotensin
Nf1+/-
Placebo
Angiotensin

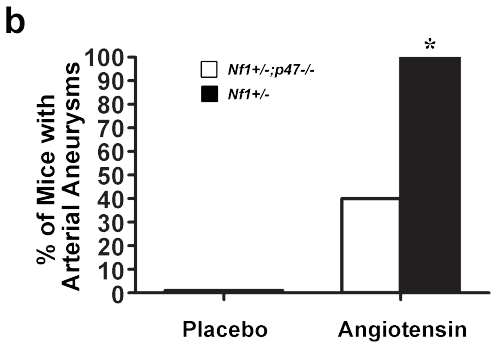
b
% of Mice with Arterial Aneurysms
Nf1+/-;p47-/-
Nf1+/-
*
Placebo
Angiotensin

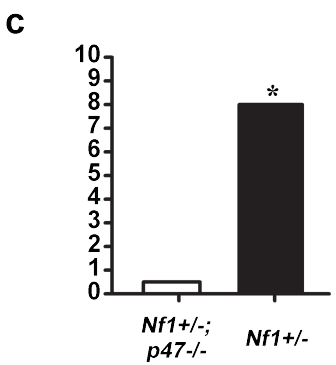
c
*
Nf1+/-; p47-/-
Nf1+/-

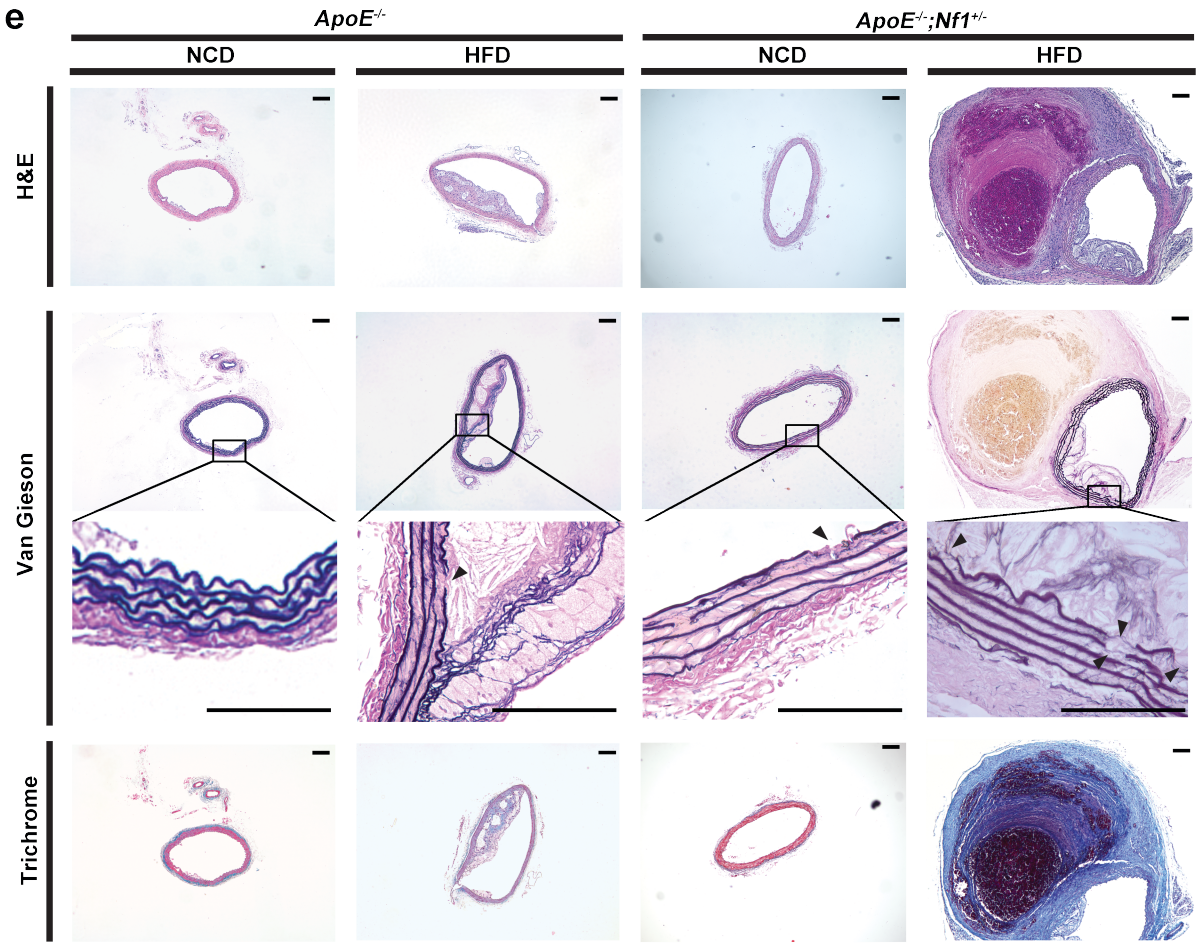
e
ApoE-/-
ApoE-/-;Nf1+/-
NCD
HFD
NCD
HFD
H&E
Van Gieson
Trichrome

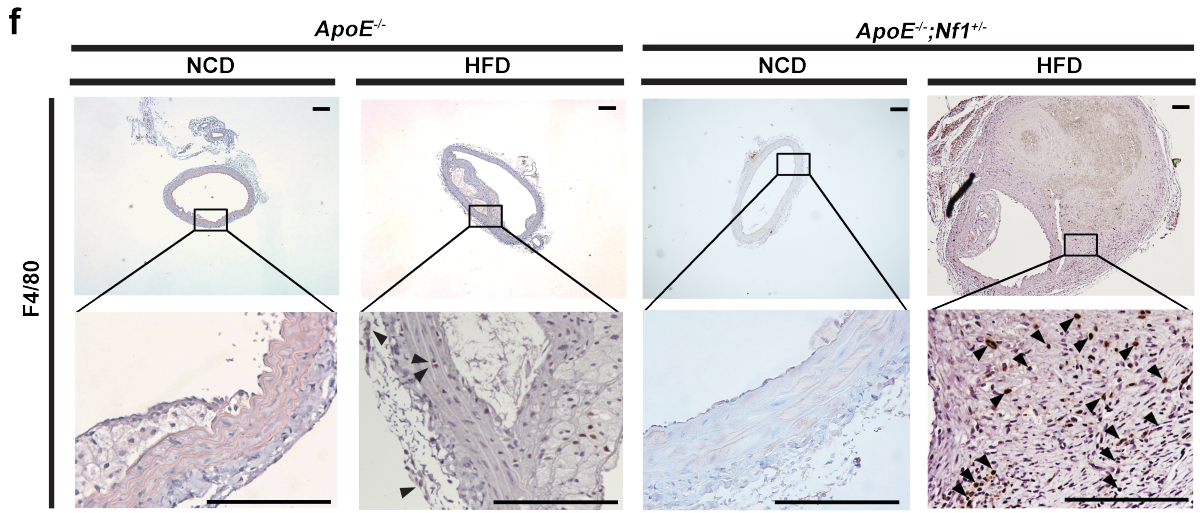
f
ApoE-/-
ApoE-/-;Nf1+/-
NCD
HFD
NCD
HFD
F4/80

Figure 5

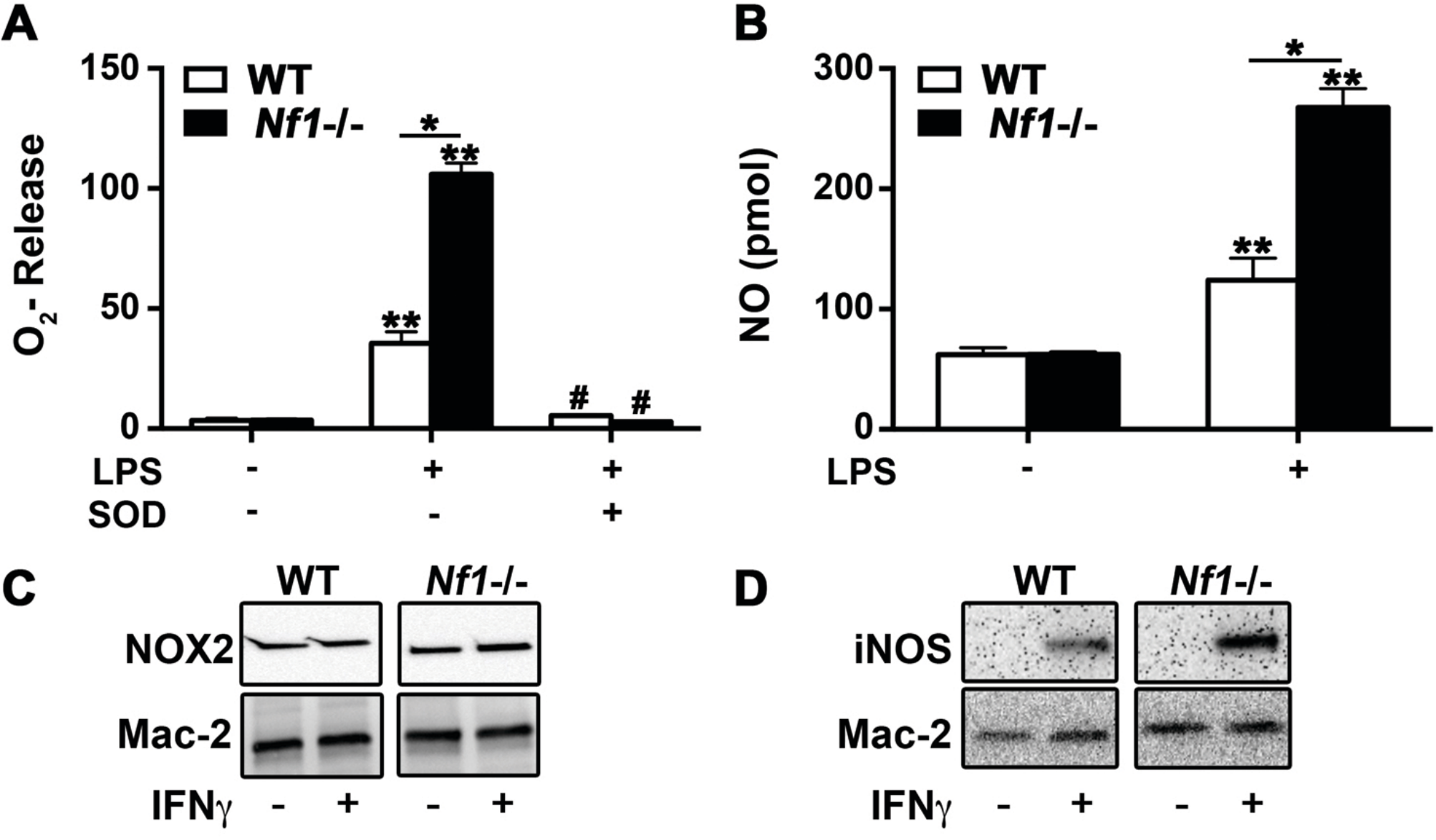
A
150
100
50
0
WT
Nf1-/-
*
**
**
#
#
O2- Release
LPS - + +
SOD - - +
B
300
200
100
0
WT
Nf1-/-
*
**
**
NO (pmol)
LPS - +
C
WT
Nf1-/-
NOX2
Mac-2
IFNγ - + - +
D
WT
Nf1-/-
iNOS
Mac-2
IFNγ - + - +

Figure 6

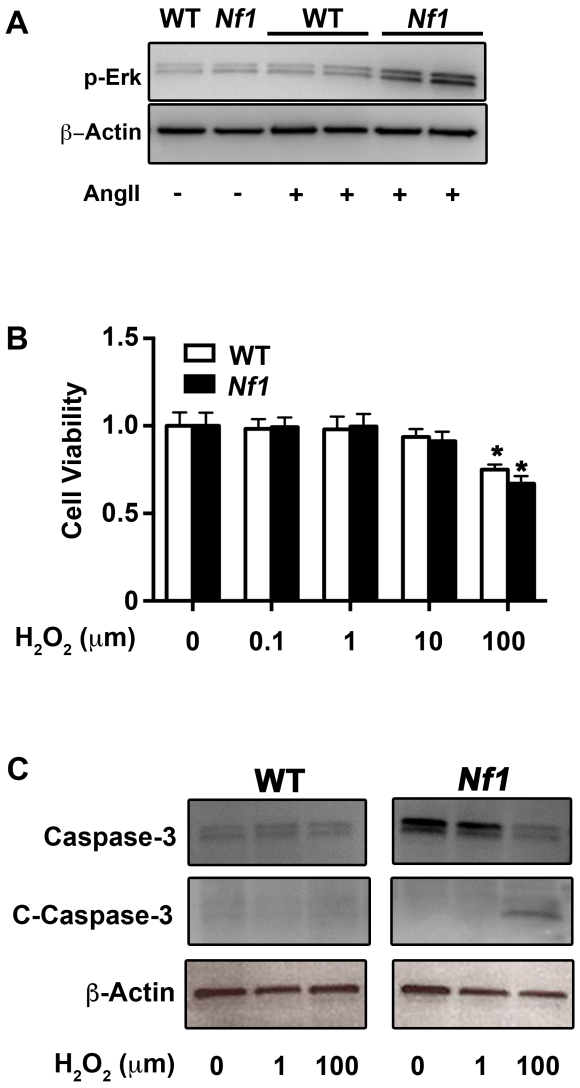
A
WT
Nf1
WT
Nf1
p-Erk
β–Actin
AngII - - + + + +
B
1.5
1.0
0.5
0
Cell Viability
WT
Nf1
*
*
H2O2 (μm) 0 0.1 1 10 100
C
WT
Nf1
Caspase-3
C-Caspase-3
β-Actin
H2O2 (μm) 0 1 100 0 1 100

CURRICULUM VITAE

NAME: Brian Kevin Stansfield, M.D.

CONTACT: Division of Neonatology
1120 15th St, BIW 6033
Augusta, GA 30912

EDUCATION:

UNDERGRADUATE:

1996-2000	Georgia Southern University, Statesboro, GA	B.S. Chemistry

GRADUATE:

2000-2004	Medical College of Georgia, Augusta, GA	M.D.

POSTDOCTORAL:

2004-2007	Resident Physician in Pediatrics	Medical College of Georgia
2009-2011	Fellow in Neonatal/Perinatal Medicine	Indiana University S.O.M.
2011-2013	NIH Fellow in Pediatric Scientist Development Program	Indiana University S.O.M.

ACADEMIC APPOINTMENTS:

2007-2009	Instructor of Clinical Pediatrics, Medical College of Georgia
2013-2018	Assistant Professor of Pediatrics, Augusta University
2015-present	College of Graduate Studies, Augusta University
2019-present	Associate Professor of Pediatrics, Augusta University

HOSPITAL APPOINTMENTS:

2007-2009	Attending Physician, University Hospital Emergency Department, Augusta, GA
2013-present	Attending Physician, Augusta University Hospital, Augusta, GA

SPECIALTY BOARD STATUS:

2007	American Board of Pediatrics – General Pediatrics
2014	American Board of Pediatrics – Neonatal/Perinatal Medicine

LICENSURE AND CERTIFICATION:

2007—2011	South Carolina Medical License
2009-2013	Indiana Medical License
2007-present	Georgia Medical License

PROFESSIONAL ORGANIZATIONS:

2004-present Member, American Academy of Pediatrics
2007-present Member, American Medical Association
2009-present Member, AAP section on Perinatal Pediatrics
2009-2013 Member, AAP section on Medical Student, Resident and Fellowship Trainees
2009-2013 Member, Indiana Medical Society
2010-present Member, American Society of Hematology
2010-present Member, American Heart Association
2014-present Member, Southern Society for Pediatric Research
2016-present Member, Society for Pediatric Research

HONORS AND AWARDS:

2000 Magna Cum Laude, Georgia Southern University
2000 American Chemical Society Undergraduate Research Award
2007 William P. Kanto Resident Research Award, Medical College of Georgia
2010 Red Shoes Award for compassionate care at Riley Hospital for Children
2011 Pediatric Scientist Development Program Award
2012 Riley Scholar's Day Award
2012 Jack Metcoff Award for Outstanding Fellow Presentation by MWSPR
2013 NIH Loan Repayment Award
2015 "Caught in the Act of Great Teaching", Augusta University
2015 Basic Science Young Investigator Award by SSPR
2015 Basic Science Poster Award, Children's Tumor Foundation
2015 NIH Loan Repayment Competitive Renewal
2015 MCG Exemplary Teaching Award, Augusta University
2016 Clinical Science Young Investigator Award by SSPR
2016 Jag20 Emerging Alumni Leader Award, Augusta University
2017 SSPR Young Faculty Award
2018 SSPR Young Faculty Award
2018 Outstanding Young Clinical Science Faculty Award, MCG at Augusta University
2019 *Pediatric Research* Young Travel Award for Early Career Investigators

TEACHING ASSIGNMENTS:

COURSES:

2014-2017 PEDS 5037, Advanced Pediatric Elective, AU
2015-present COGS 8060, Intro to Research II, AU
2017 VBI 8130, Modern Drug Discovery and Development, AU
2017-present VBIO 9210, Investigation of a Problem, AU

MEDICAL FELLOWS:

2013-2015 Pinkal Patel, Neonatology, Augusta University
2015-2018 Emily Masoumy, Neonatology, Augusta University
2017-2018 Dusit Adstamongkonkul, Pediatric Neurology, Augusta University
2018-2021 Alexander Eason, Neonatology, Augusta University

MEDICAL RESIDENTS:

2011 Hilary White, Indiana University S.O.M.

2015-2016 Meredith Johnston, Augusta University M.C.G.
2016-2018 Kate McCutcheon, Augusta University M.C.G.
2016-2019 Stephanie Komic, Augusta University M.C.G.
2016-2019 Claire Jones, Augusta University M.C.G.

GRADUATE STUDENTS:
2016-2020 Rebekah Tritz, PhD Candidate, Augusta University
AHA Pre-doctoral Fellowship (01/01/2019 – 12/31/2020)
2019-2023 Chris Truelove, PhD Candidate, Augusta University

MEDICAL STUDENTS:
2012 Jacob Capito, Indiana University S.O.M.
2014 Christopher Walker, Augusta University M.C.G.
2016 Stephanie Ryals, Augusta University M.C.G.
2016-2019 Alexandra Sawyer, Augusta University M.C.G.
2017-2018 Jenny Patel, Augusta University M.C.G.
2017 Folasade Aderibigbe, Augusta University M.C.G.
2018 Jack Hortenstine, Augusta University M.C.G.
2018 Chederli Ga Belongilot, Augusta University M.C.G.
2018 Selena Soviravong, Augusta University, M.C.G.
2019 Jordan Mattern, Augusta University, M.C.G.
2019 Rilee Racine, Augusta University, M.C.G.
2019 Nadiya Zafar, Augusta University, M.C.G.
2019 Avirale Sharma, Augusta University, M.C.G.

UNDERGRADUATE STUDENTS:
2010 James Wodoka, Case Western University (MD/PhD at Indiana University)
2013-2014 Grace Kim, Vanderbilt (MS at Georgetown/NIH, MD at U. South Florida)
2015-2016 Sanah Aslam (B.S./M.D. program), Augusta University (MD at AU)
2016-2017 Alexandra Cetatoiu, Augusta University

UNIVERSITY SERVICE:
2010-2012 Wells Center for Pediatric Research summer intern program, IU S.O.M.
2013-present PEDS 5000, Junior core rotation in Pediatrics, AU
2013-present PEDS 5001, Sub-internship in Neonatology, AU
2013-present Neonatal Fellowship Lecture Series, AU
2013-present Children's Summer Scholars Program, AU
2014-present Neonatology Fellowship Clinical Competency Committee, AU
2015-2016 LCME Site Visit Representative, AU
2015-2017 Pediatric Fellows 1st Year Curriculum, AU
2015-2017 Dean's Research Committee of the MCG Faculty Senate, AU
2015-present Pediatric Residency Program Evaluation Committee, AU
2015-present Pediatric Resident Mentor, AU
2015-present Pediatric Residency Clinical Competency Committee, AU
2016-present MD/PhD Admissions Committee Member, AU
2017-2018 Pediatric Chairman Search Committee, AU
2017-present Assistant Director of Neonatal ECMO, AU
2018-present Pediatric Grand Rounds and Lectureships Oversight Committee, AU

OTHER PROFESSIONAL ACTIVITIES:

INVITED LECTURES:

2013 "Understanding the Pathogenesis of Vascular Disease in Neurofibromatosis Type 1 Patients: Insights from Mouse Models" Perinatal Grand Rounds. University of Alabama at Birmingham

2016 "Zika Virus in the Continental United States" Family Medicine Grand Rounds. Augusta University

2017 "The Lifelong Effects of Early Life" Perinatal Grand Rounds. MUSC

2018 "Neurofibromin Deficiency Induces Endothelial Cell Proliferation and Retinal Neovascularization", 10th Annual Culver Vision Discovery Institute Retreat

AD HOC REVIEW

ATVB
BMJ Open
Cellular and Molecular Life Sciences
Cellular Physiology and Biochemistry
Clinical Epidemiology
Clinical Epigenetics
Circulation Research
International Journal of Obesity
Journal of Maternal-Fetal & Neonatal Medicine
Journal of Molecular and Cellular Medicine
Journal of Perinatology
Nutrition in Clinical Practice
Pediatric Research
PLOS One

GRANTS AND FELLOWSHIPS:

CURRENT SUPPORT:

"Responsive Parenting, Sleep, and Rapid Weight Gain among African American Infants", National Institutes of Health
09/1/2017-08/31/2021 Total Costs
Birch, Lavner, Principal Investigator, B. Stansfield, Co-Investigator

"Mechanisms of Myeloperoxidase and NOX4 Interactions in Abdominal Aortic Aneurysm" National Institutes of Health
01/01/2018 – 12/31/2023 Total Costs
Weintraub, Principal Investigator, B. Stansfield, Co-Investigator

"Leveraging Macrophage Bioenergetics in NF1"
Augusta University
06/01/2018 – 05/31/2019 Total Costs
B. Stansfield, Principal Investigator

"Inflammation and Retinopathy of Prematurity"
National Institutes of Health
04/01/2019 – 03/30/2024 Total Costs

B. Stansfield, Principal Investigator
"Inflammatory Macrophages and Retinal Neovascularization"
American Heart Association (pre-doctoral fellowship)
01/01/2019 – 12/31/2020 Total Costs
Tritz, Principal Investigator, B. Stansfield, Mentor

PRIOR SUPPORT:
"Myeloid Cells and NF1 Vasculopathy"
Pediatric Scientist Development Program/NIH-NICHD
07/01/11-06/30/14, Total Cost
B. Stansfield, Principal Investigator

"Cardiovascular Abnormalities in Pediatric Patients with Neurofibromatosis Type 1"
Texas Neurofibromatosis Foundation
05/01/2016 – 05/01/2017 Total Costs
Klesse, Principal Investigator, B. Stansfield, Co-Investigator

"Interrogating NF1 Arterial Stenosis"
American Heart Association
07/01/2015-06/30/2018 Total Costs
B. Stansfield, Principal Investigator

"Characterizing Myeloid Cell Activation in NF1 Vasculopathy"
Department of Defense/CDMRP
07/01/2015-06/30/2018 Total Costs
B. Stansfield, Principal Investigator

GRANTS UNDER REVIEW:
''Inflammatory Macrophages and NF1-tumor Angiogenesis"
Department of Defense
04/01/2019 – 03/30/2022 Total Costs
B. Stansfield, Principal Investigator

"Responsive Parenting to Reduce Rapid Weight Gain among Late Preterm African American Infants: A Randomized Pilot Study"
National Institutes of Health
07/01/2019 – 06/30/2021 Total Costs
Birch, Lavner, Principal Investigator, B. Stansfield, Co-Investigator

PRINT AND ELECTRONIC PUBLICATIONS:

I. TEACHING AND CURRICULUM DEVELOPMENT

1. Pediatric Fellows Education Curriculum, Indiana University (2011-2013)
   Co-chaired committee to develop and implement new educational curriculum for pediatric fellows including professional development, scholarship, and quality improvement
2. PEDS 5037, Advanced Pediatrics Elective, Augusta University
   Developed curriculum and facilitated 3-day lecture series to introduce "Evidence Based Medicine" and literature searches to senior students in graduate medical education
3. VBI 8130, Modern Drug Discovery and Development, Augusta University
   Lecturer
4. Neonatal/Perinatal Medicine, Augusta University

Developed and implemented new curriculum for graduate students, medical residents, and fellows in the Division of Neonatal/Perinatal Medicine (10 lectures/year)

5. Pediatric Resident Research Program, Chair, Augusta University
   Revised and implemented curriculum for pediatric resident research
6. Pediatric Fellow Research Program, co-leader of 1st year curriculum
   Helped develop formal didactic sessions on clinical trial design, IRB approval, protection of human subjects, statistical analysis, and manuscript preparation

II. RESEARCH, SCHOLARSHIP, OR CREATIVE ACTIVITIES (Refereed Journals)

1. Timoney PJ, **Stansfield BK**, Whitehead R, Lee HB, Nunery WR. Eyelid Lacerations Secondary to Caesarean Section Delivery. *Ophthal Plast Reconstr Surg.* 2012 Jul-Aug;28(4):e90-2.
2. **Stansfield BK**, Bessler WK, Mund JA, Downing B, Mali RS, Sarchet KN, Li F, Distasi MR, Conway SJ, Kapur R, Ingram DA. Heterozygous Inactivation of the *Nf1* Gene in Myeloid Cells Enhances Neointima Formation via a Rosuvastatin-Sensitive Cellular Pathway. *Hum Mol Genet*. 2013 Mar 1;22(5):977-88.
3. **Stansfield BK**, Bessler WK, Mali RS, Mund JA, Downing B, Kapur R, Ingram DA. Ras-Mek-Erk Signaling Regulates *Nf1* Heterozygous Neointima Formation. *Am J Pathol*. 2014 Jan;184(1):79-85.
4. Downing B, Li F, Mund JA, Bessler WB, Smiley LC, Sarchet KN, Distasi MR, Conway SJ, Clapp DW, **Stansfield BK***, Ingram DA. "Neurofibromin-deficient Myeloid Cells are Critical Mediators of Aneurysm Formation *In Vivo*". *Circulation*. 2014 Mar 129:1213-1224. ***Corresponding Author**
5. Ham PB, Patel P, Wise LJ, Walters C, **Stansfield BK**. "Severe Myocardial Injury and Extracorporeal Membrane Oxygenation in Perinatal Asphyxia" *J Pediatr Surg*. 2015, doi: 10.1016/j.epsc.2015.03.010
6. Ham PB, Wise LJ, Wang EJ, **Stansfield BK**, Hatley RM, Walters KC, Pipkin WL, Bhatia J. "Venovenous Extracorporeal Membrane Oxygenation for Cardiorespiratory Failure due to Congenital Diaphragmatic Hernia and Ebstein's Anomaly". *Amer Surg.* 2015 Aug 81:9
7. **Stansfield BK***, Ingram DA. "Clinical Significance of Monocyte Heterogeneity". *Clin Transl Med*. 2015 Nov 4(1): 5 ***Corresponding Author**
8. Bessler WK, Kim G, Hudson FZ, Mund JA, Mali R, Menon K, Kapur R, Clapp DW, Ingram DA, **Stansfield BK**. "Nf1+/- Monocytes/Macrophages Induced Neointima Formation via CCR2 Activation". *Hum Mol Genet*. 2016 Mar 1:25(6):1129-1139.
9. Bessler WK, Hudson FZ, Zhang H, Harris V, Wang Y, Mund JA, Downing B, Ingram DA, Case J, Fulton DJ, **Stansfield BK**. "Neurofibromin Regulates Reactive Oxygen Species Production and Arterial Remodeling". *Free Radic Biol Med*. 2016 Jun 3;97:212-222.
10. **Stansfield BK***, Fain ME, Bhatia J, Gutin B, Nguyen JT, Pollock NK. "Nonlinear Relationship between Birthweight and Visceral Fat in Adolescents". *J Pediatr*. 2016 Jul;174:185-92. ***Corresponding Author**
11. Lalani A, Ham PB, Wise LJ, McDaniel JM, Walters CK, Pipkin WL, **Stansfield BK**, Hatley R, Bhatia J. "Management of Patients with Gastroschisis Requiring ECMO for Concurrent Respiratory Failure" *Amer Surg.* 2016 Sep;82(9):768-72.
12. Christou H, Dizon MLV, Farrow K, Jadcherla SR, Leeman KT, Maheshwari A, Rubin LP, **Stansfield BK**, Rowitch DH. "Sustaining Careers of Physician-Scientists in Neonatology and Pediatric Critical Care Medicine: Formulating Supportive Departmental Policies".

Pediatr Res. 2016 Nov;80(5):635-640.

13. Masoumy EP, **Stansfield BK**. "Breakthrough in the Prevention of Mother-to-Child Hepatitis B Transmission?" *J Perinatol*. 2017 **37,** 333–334.

14. **Stansfield BK***, Wise LJ, Ham PB, Patel P, Parman M, Jin C, Mathur S, Harshfield G, Bhatia J. "Outcomes Following Routine Antithrombin III Replacement during Neonatal Extracorporeal Membrane Oxygenation". *J Pediatr Surg*. 2017 Apr;52(4):609-613 ***Corresponding Author**

15. Kim HW, **Stansfield BK**. "Genetic and Epigenetic Regulation of Aortic Aneurysms". *Biomed Res Int.* 2017;2017(12)

16. Sawyer A, Wise LJ, Ghosh S, Bhatia J, **Stansfield BK**. "Comparison of transfusion thresholds during neonatal extracorporeal membrane oxygenation". *Transfusion*. 2017. Sep;57(9):2115-2120. **Cover Article, Editorial, and Letter to Editor**

17. Yiew KH, Chatterjee TK, Tang YL, Pellenberg R, **Stansfield BK**, Bagi Z, Fulton DJ, Stepp DW, Chen W, Patel V, Kamath VM, Litwin SE, Hui DY, Rudich SM, Kim HW, Weintraub NL. "Novel role for Wnt inhibitor APCDD1 in adipocyte differentiation: implications for diet-induced obesity". *J Biol Chemist.* Apr 14;292(15):6312-6324.

18. Kim HW, Blomkalns AL, Ogbi M, Thomas M, Gavrila D, Neltner BS, Cassis LA, Thompson RW, Weiss RW, Lindower PD, Blanco VM, McCormick ML, Daugherty A,Fu X, Hazen SL, **Stansfield BK**, Huo Y, Fulton, DJ, Chatterjee T, Weintraub NL. Role of myeloperoxidase in abdominal aortic aneurysm formation: mitigation by taurine. *Am J Physiol - Heart Circ Physiol.* 2017 Dec 1;313(6):H1168-H1179.

19. Zhang H, Hudson FZ, Xu Z, Tritz R, Rojas M, Patel C, Haigh SB, Bordan Z, Ingram DA, Fulton DJ, Weintraub NL, Caldwell RB, **Stansfield BK**. "Neurofibromin Deficiency Induces Endothelial Cell Proliferation and Retinal Neovascularization". *Invest Ophthalmol Vis Sci*. 2018. May; 59(6): 2520-2528

20. Sawyer A, Wise LJ, Ghosh S, Bhatia J, **Stansfield BK**. "Response to Letter by Lohmann *et al*". *Transfusion*. 2018. May:48(5) 1327-1328.

21. Kim HW, Benson TW, Weintraub DS, Crowe M, Yiew KH, Popoola O, Pillai A, Joseph J, Archer K, Greenway C, Chatterjee C, Mintz J, Stepp DW, **Stansfield BK**, Chen W, Brittain J, Bogdanov V, Gao Y, Williams J, Weintraub NL. "Deletion of the Duffy Antigen Receptor for chemokines (DARC) promotes insulin resistance and adipose tissue inflammation during high fat feeding." *Mol Cell Endocrinol*. 2018. Sep 15;473:79-88.

22. Masoumy E, Thompson JT, Sawyer AA, Sharma S, Gordon PMK, Regnault TRH, Matushewski B, Weintraub NL, Richardson B, **Stansfield BK**. "The Lifelong Impact of Fetal Growth Restriction on Cardiac Development". *Pediatr Res*. 2018. Oct;84(4):537-44.

23. Safarulla A, Kuhn W, Lyon M, Etheridge RJ, **Stansfield BK**, Best G, Thompson A, Masoumy EP, Bhatia J. "RANS Scan: Rapid Assessment of the Neonate with Sonography Scan". *J Ultras Med*. 2018: 1-11.

24. Fouda AY, Xu Z, Shosha EF, Lemtalsi T, Chen J, Toque H, Tritz R, Cui R, **Stansfield BK**, Huo Y, Rodriguez PC, Smith SB, Caldwell RW, Narayanan SP, Caldwell RB. "Arginase 1 Promotes Retinal Neurovascular Protection from Ischemia Through Suppression of Macrophage Inflammatory Responses". *Cell Death Dis*. 2018. Sep 25;9(10).

25. Eriksen BJ, Savage NM, **Stansfield BK**, Mann PC. "A Novel Mutation in *PTPN11* in an Extremely Preterm Infant with Suspected Juvenile Mylelomonocytic Leukemia". *J Clinic Neonatal*. 2018. Oct 7(4): 269-72.

26. Horimatsu T, Patel A, Prasad R, Reid L, Benson T, Zarzour A, Ogbi M, Bruder do Nascimento T, Belin de Cantemele E, **Stansfield BK**, Lu X, Kim HW, Weintraub NL. "Systemic Effects of Transplanted Perivascular Adipose Tissue on Endothelial Function and Atherosclerosis". *Cardiovasc Drugs Ther*. 2018. Oct 32(5): 503-510.

27. Zou J, Ma W, Littlejohn R, **Stansfield BK**, Kim I, Liu J, Zhou J, Weintraub NL, Su H. "Transient Inhibition of Neddylation at the Neonatal Stage Evokes Reversible Cardiomyopathy and Predisposes the Heart to Isoproterenol-induced Heart Failure." *Am J Physiol - Heart Circ Physiol.* 2019. Mar 29.

28. Sawyer AA, Pollock NK, Gutin B, Weintraub NL, **Stansfield BK**. "Proportionality at Birth and Left Ventricular Mass in Healthy Adolescents". *Early Hum Develop*. 2019. Apr 3;132:24-29

29. Lavner JA, **Stansfield BK**, Beach SRH, Brody GH, Birch LL. Sleep SAAF: A Responsive Parenting Intervention to Prevent Excessive Weight Gain and Obesity among African American Infants. *BMC Pediatrics*. Editorial Review.

30. Horimatsu T, Blomkaln AL, Ogbi M, Patel S, Gilreath N, Reid L, Benson TW, Pye J, Ahmadieh S, Thompson A, Robbins N, Mann A, Edgell A, Benjamin S, **Stansfield BK**, Huo Y, Fulton DJ, Agarwal G, Singh N, Offermanns S, Weintraub NL, Kim HW. "Niacin Protects Against Abdominal Aortic Aneurysm Formation via GPR109A Independent Mechanisms: Role of NAD+/Nicotinamide". *JCI-Insight*. Editorial Review.

31. Keene SD, Patel RM, **Stansfield BK**, Davis J, Josephson CD, Winkler A. "Blood Product Transfusion and Mortality in Neonatal ECMO". *Ped Crit Car Med.* Editorial Review.

32. Ghoshal P, Singla B, Lin H, Cherian-Shaw M, Hudson FZ, Zhang H, Tritz R, **Stansfield BK**, Csanyi G. "Loss of GTPase Activating Protein Neurofibromin Stimulates Paracrine Cell Communication via Macropinocytosis". *Redox Biol.* Editorial Review

33. Sawyer AA, Wise L, Bhatia J, **Stansfield BK**. "Vitamin K and ECMO for Neonatal Hypoxic Respiratory Failure". *ASAIO*. Editorial Review.

34. McCutcheon KC, Wise L, Lewis K, Gilbert B, Bhatia J, **Stansfield BK**. "The Utility of Cranial Ultrasound as a Screening Tool for Neonatal ECMO". *Pediatr Radiol.* Editorial Review

35. Tritz R, Zhang H, Hudson FZ, Harris V, Weintraub NL, Fulton DJ, **Stansfield BK**. "Neurofibromin-deficiency Enhances Insulin Signaling and Lean Body Mass". *Hum Mol Genet.* Editorial Review.

BOOK CHAPTERS:

1. **Stansfield BK**, Conway SJ, Ingram DA, Friedman JA. "Molecular Basis of Cardiovascular Abnormalities in NF1", in Upadhyay, M (ed): Neurofibromatosis Type 1. Springer-Verlag Berlin Heidelberg. 2013

ABSTRACTS PRESENTED (*PLATFORM PRESENTATION):

2000 **Stansfield BK***, Deal ST. *Regio-selective reduction of a benzylidene acetal group on a derivatized glucose,* Georgia Academy of Sciences, Valdosta, GA

2007 **Stansfield BK**, Hanevold C, Caldwell A. *Prenatal predictors of vesicoureteral reflux,* Medical College of Georgia Research Symposium, Augusta, GA

2010 **Stansfield BK**, Bessler WK, Mund JA, Ingram DA. *Nf1* heterozygous macrophages are the primary effectors of *Nf1*$^{+/-}$ neointima formation, Riley Research Symposium Indianapolis, IN

2010 **Stansfield BK***, Bessler WK, Mund JA, Sarchet KN, Downing B, Distasi M, Smiley LC, Li F, Ingram DA. *Lineage restricted studies of monocytes in Nf1*$^{+/-}$ *vaso-occlusive disease*, Midwest Section of Perinatal Medicine, Cincinnati, OH

2011 **Stansfield BK**, Bessler WK, Mund JA, Sarchet KN, Downing B, Distasi M, Li F, Ingram DA. *Nf1 heterozygous macrophages are the primary effectors of Nf1*$^{+/-}$ *neointima formation*, Riley Research Symposium, Indianapolis, IN

2011 **Stansfield BK***, Bessler WK, Mund JA, Sarchet KN, Downing B, Distasi M, Smiley LC, Li F, Ingram DA. *Heterozygous inactivation of Nf1 in monocytes/macrophages alone is necessary and sufficient for enhanced neointima formation in vivo*, Children's Tumor Foundation, Jackson Hole, WY

2012 **Stansfield BK**,* Bessler WK, Mund JA, Sarchet KN, Downing B, Distasi M, Smiley LC, Li F, Conway SJ, Kapur R, Ingram DA. *Heterozygous Inactivation of the Nf1 Gene in Myeloid Cells Enhances Neointima Formation via a Rosuvastatin-Sensitive Cellular Pathway*, Riley Research Symposium, Indianapolis, IN

2012 Downing B, Li F, Bessler WK, **Stansfield BK**, Mund JA, Sarchet KN, Distasi MC, Ingram DA. *Myeloid cells induce Nf1*$^{+/-}$ *aneurysms via activation of NADPH oxidase,* National Clinical and Translational Sciences Predoctoral Programs Meeting. Rochester, MN

2012 Downing B, Li F, Bessler WK, **Stansfield BK,** Mund JA, Distasi MC, Smiley LC, Ingram DA. *Monocyte/macrophages are the primary effectors of Nf1*$^{+/-}$ *aneurysm formation via increased activation of the NADPH oxidase system*, Gordon Research Conference and Symposium: NOX Family NADPH Oxidases, Waterville Valley, NH

2012 **Stansfield BK***, Bessler WK, Mund JA, Downing B, Li F, Kapur R, Ingram DA. *Heterozygous Inactivation of the Nf1 Gene in Myeloid Cells Enhances Neointima Formation via a Rosuvastatin-Sensitive Cellular Pathway*, Midwest Society for Pediatric Research, Columbus, OH

2014 Bessler WK, Mali RM, Kapur R, Ingram DA, **Stansfield BK***. *MCP-1/CCR2 Signaling Mediates Nf1*$^{+/-}$ *Neointima Formation*, Society for Pediatric Research, Vancouver, BC

2015 **Stansfield BK***, Ingram DA. *CCR2 Signaling is Necessary for Nf1*$^{+/-}$ *Neointima Formation*, Southern Society for Pediatric Research, New Orleans, LA

2015 Benson TW, Chatterjee TK, Weintraub DS, Popoola O, **Stansfield BK**, Crowe M, Pillai A, Mintz J, Stepp D, Brittain J, Bogdanov V, Weintraub NL. *Duffy Antigen Receptor for Chemokines Modulates Adipose Inflammation in Obesity Related Metabolic Disease*, American Diabetes Association, Boston, MA

2015 Bessler,WK, Hudson FZ, Fulton DJ, Ingram DA, **Stansfield BK***. *Neurofibromin Regulates Oxidative Stress and Arterial Remodeling*, Children's Tumor Foundation,

Monterey, CA. **Award for Basic Science Poster**

2015 **Stansfield BK**, Wise L, Patel P, Parman M, Wall D, Bhatia J. *Single Center Review of Outcomes Following Administration of Antithrombin III during Extracorporeal Membrane Oxygenation,* ELSO, Atlanta, GA

2016 **Stansfield BK**, Wise L, Patel P, Parman M, Wall D, Bhatia J. *Outcomes Following Routine Antithrombin III Replacement during Neonatal Extracorporeal Membrane Oxygenation,* Southern Society for Pediatric Research, New Orleans, LA

2016 **Stansfield BK***, Fain ME, Bhatia J, Gutin B, Nguyen JT, Pollock NK. *Nonlinear Relationship between Birthweight and Visceral Fat in Adolescents.* Southern Society for Pediatric Research, New Orleans, LA

2016 Benson TW*, Chatterjee TK, Weintraub DS, Popoola O, Joseph J, **Stansfield BK**, Crowe M, Yiew N, Unruh D, Pillai A, Williams j, Mintz J, Stepp D, Brittain J, Bogdanov V, Weintraub NL. *The Role of the Duffy Antigen Receptor for Chemokines in Metabolic Disease*, Experimental Biology, San Diego, CA

2016 Thompson J*, Mintz J, **Stansfield BK**. *Cardiometabolic Risk in the Offspring of Het_{db} Pregnancy*, Perinatal Biology Symposium, Aspen, CO ***Perinatal Biology Travel Award**

2016 Johnston M*, Sharma N, Mathur S, **Stansfield BK**. *Addressing Childhood Obesity: One Variable at a Time*, MCG Pediatric Scholars' Day, Augusta, GA ***William P. Kanto Resident Research Award.**

2016 Sawyer A, Wise LJ, Ghosh S, Bhatia J, **Stansfield BK**. "Transfusion Threshold for Neonatal ECMO". ELSO, San Diego, CA

2016 Johnston M, Sharma N, Mathur S, **Stansfield BK**. *Addressing Childhood Obesity: One Variable at a Time*, American Academy of Pediatrics National Conference & Exhibition, San Francisco, CA

2016 Masoumy E*, **Stansfield BK.** *Fetal Growth Restriction Reduces Cardiomyocyte Number and Alters Cardiac Development.* Perinatal Pediatrics, Marco Is, FL

2017 Masoumy E*, Thompson JE, Richardson BS, **Stansfield BK**. *Maternal Nutrient Restriction Programs Offspring Cardiomyocyte Fate in Guinea Pigs and Humans*. Southern Society for Pediatric Research, New Orleans, LA
***Basic Science Young Investigator Award Finalist**

2017 Tritz R, Zhang H, Fulton DJ, **Stansfield BK**. *Metabolic Characterization of Circulating Human Endothelial Colony Forming Cells*. Southern Society for Pediatric Research, New Orleans, LA

2017 Sawyer A, Wise LJ, Bhatia J, **Stansfield BK**. *Comparison of Transfusion Thresholds for Neonatal ECMO*. Southern Society for Pediatric Research, New Orleans, LA

2017 Thompson JA*, Larion S, Mintz JD, **Stansfield BK**. *Impact of Gestational Diabetes on Metabolic Risk in the Offspring*. Pediatric Academic Societies, San Francisco, CA

2017 Masoumy E*, Thompson JE, Richardson BS, Sharma S, **Stansfield BK.** *Fetal Growth Restriction Impairs Cardiomyocyte Development in Guinea Pigs and Humans.* Pediatric Academic Societies Meeting, San Francisco, CA
***Perinatal Travel Award**

2017 Tritz R, Zhang HB, Hudson FZ, Benson TW, Kim HW, Fulton DJ, Weintraub NL, **Stansfield BK.** *Neurofibromin is a Novel Regulator of Macrophage Polarization via PFKFB3 Activation.* Children's Tumor Foundation, Washington D.C.

2017 Sawyer AA, Pollock N, **Stansfield BK**. "Birth BMI and Growth Trajectory Predict Cardiometabolic Risk in Adolescents". National Conference and Exhibition of American Academy of Pediatrics, Chicago, IL

2017 Masoumy E, Thompson JE, Richardson BS, **Stansfield BK*.** "The Lifelong Effects of Fetal Growth Restriction on Cardiac Development" Neonatal Cardiopulmonary Biology Young Investigators Forum, Chicago, IL

2018 Zhang H, Hudson FZ, Caldwell RB, **Stansfield BK*.** "Neurofibromin is a novel regulator of endothelial cell proliferation and retinal neovascularization" Southern Society for Pediatric Research, New Orleans, LA. ***Young Faculty Travel Award**

2018 Keene SD Patel RM, **Stansfield BK**, Josephson CD, Winkler AM. "Transfusion and Mortality in Neonatal ECMO" Keystone ECMO Meeting, Keystone, CO

2018 Eason AJ*, Crethers D, Ghosh S, **Stansfield BK**, Polimenokas AC. "Vascular thrombotic events in neonates with congenital heart disease: Risk assessment and Outcome analysis in the Neonatal Intensive Care Unit" Cardiovascular and Thoracic Critical Care Conference, Washington D.C.

2019 Komic SR*, Aderibigbe F, Rao A, **Stansfield BK**. "Predictors of Length of Stay in Gastroschisis" Southern Society for Pediatric Research, New Orleans, LA. ***Trainee Travel Award**

2019 **Stansfield BK***. "Inflammatory Monocytes are Mobilized in Infants with Type 1 Retinopathy of Prematurity" Southern Society for Pediatric Research, New Orleans, LA.

2019 Masoumy E, **Stansfield BK*.** "The Lifelong Impact of Fetal Growth Restriction on Cardiac Development. What's Next". Pediatric Academic Societies Meeting, Baltimore, MD

2019 **Stansfield BK**. "Inflammatory Monocytes are Mobilized in Infants with Type 1 Retinopathy of Prematurity" Pediatric Academic Societies, Baltimore, MD.

III. PROFESSIONAL SERVICE:

2015-2016 Southern Society for Pediatric Research, Institutional Representative

2016-2018 Southern Society for Pediatric Research, Council Member

2019-2020 Southern Society for Pediatric Research, President

IV. INTEGRATION OF TWO OR MORE ASPECTS OF FACULTY WORK:

2014-present Chair, Pediatric Resident Research Committee

2018-present Chair, Pediatric Grand Rounds and Lectureships Oversight Committee

Date: _____ Signature: _____